

Universität
Rostock



Traditio et Innovatio

Hydrogen Bonding in Mixtures of Protic Ionic Liquids: Influence on Structure and Thermodynamic Properties

Cumulative Dissertation

to obtain the academic degree

doctor rerum naturalium (Dr. rer. nat.)

of the Faculty of Mathematics and Natural Sciences

at the University of Rostock

Submitted by

M.Sc. Benjamin Golub

born on 22/06/1990 in Oranienburg

ORCID: 0000-0003-4374-909X

Rostock, November 2022

https://doi.org/10.18453/rosdok_id00004297



Dieses Werk ist lizenziert unter einer
Creative Commons Namensnennung-Nicht kommerziell 4.0 International
Lizenz.

First Reviewer:

Prof. Dr. Ralf Ludwig
Universität Rostock, Institut für Chemie
Physikalische und Theoretische Chemie
Rostock, Germany

Second Reviewer:

Prof. Dr. Abenacer Idrissi
Université de Lille, Faculté des sciences et technologies
Département chimie
Lille, France

Year of submission: 2022

Year of oral defence: 2023

*All models are wrong,
but some are useful.*

George E. P. Box

Contents

Declaration of Authorship	IV
List of Abbreviations	V
Acknowledgments	VII
Abstract	IX
1 Introduction	1
1.1 Motivation	1
1.2 Protic Ionic Liquids	2
1.3 Molecular Dynamics Simulations	4
2 Research Overview	7
2.1 Remarks	7
2.2 Mixtures of Protic Ionic Liquids	7
2.3 Protic Ionic Liquids in Water	18
2.4 Force Field Development and Conversion	22
2.4.1 Optimizing a Force Field	22
2.4.2 A Force Field Conversion Tool Based on XML - ForConX	25
3 Perspective	29
4 Publications	37
4.1 Overview	37
4.2 Publication I	40
4.3 Publication II	69
4.4 Publication III	80
4.5 Publication IV	105
4.6 Publication V	137
4.7 Publication VI	167
4.8 Publication VII	178

Declaration of Authorship

I hereby declare under oath that I have completed the work submitted here independently and have composed it without outside assistance. Furthermore, I have not used anything other than the resources and sources stated. Where I have taken sections from these works in terms of content or text, I have identified this appropriately.

Benjamin Golub
Rostock, November 10, 2022

List of Abbreviations

APILs	aprotic ionic liquids
CIPs	contact ion pairs
CRedit	contributor roles taxonomy
DFT	density functional theory
DSILs	double salt ionic liquids
FIR	far-infrared
ILs	ionic liquids
IR	infrared
IUPAC	International Union of Pure and Applied Chemistry
KPL	force field by Köddermann, Paschek, Ludwig [1]
LJ	Lennard-Jones
MD	molecular dynamics
MIR	mid-infrared
NGOLP	force field by Neumann, Golub, Odebrecht, Ludwig, Paschek [2]
NMR	nuclear magnetic resonance
PILs	protic ionic liquids
QM	quantum mechanics
SIPs	solvent-separated ion pairs
SSIPs	solvent-shared ion pairs
XML	extensible markup language
<hr/>	
[EMIm][Cl]	1-ethyl-3-methylimidazolium chloride
NaCl	sodium chloride
[TEA][OTf]	triethylammonium triflate
[TEA][OMs]	triethylammonium methylsulfonate
[C_nMIIm][NTf₂]	1-alkyl-3-methylimidazolium bis(trifluoromethanesulfonyl)azanide

Acknowledgments

I would like to thank Prof. Dr. Ralf Ludwig for the opportunity to do my PhD thesis on this interesting topic in his working group, and also for having an open ear when I was struggling. Furthermore, I would like to thank him for the opportunities to visit conferences, meetings and summer schools.

A big "thank you" goes to my supervisor Dr. Dietmar Paschek for the help with scientific questions, the support during my whole research, the trust he put in me and the one time he let me borrow the office presentation medium.

I would like to thank Prof. Dr. Christian Schröder for the warm welcome in his research group during my research stay at the University of Vienna and his support with simulations that just wouldn't work. I learned a lot about science in these three months.

Likewise, I want to thank the whole working group of Prof. Dr. Ralf Ludwig as well as the Physical Chemistry Department at the University of Rostock. For me, working at this place was a blast. Thoughts of Bad Malente, the Stammtisch and other events will always make me smile. A warm and special thanks goes out to Jan, it was an honor to share office and hotel rooms with you. I also want to thank Elias, Johanna, Sebastian, Sille and Wigbert for a great office atmosphere. Andreas, thank you for taking care of all the software support and the great teamwork as the technical support team at different conferences. Furthermore, I would like to thank Anika for always having a helping hand. And a big shout-out to the real heroes: my proofreading team, you are the best.

And no, I haven't forgotten you: Lars, Anika, Nico, Suse, Anne, Marie, Meeri, Lisa, Raik, Björn, Joy, my D&D groups and the people from Block C, without you guys I wouldn't know the shocking twist in Sharknado 3, that you can drink more than 10 traffic lights or that I can sing like an angel. Even though some paths split, without you it wouldn't have been the same, thank you all.

Vivi, you make my life just so easy, and I am grateful to have you in it. Thank you for everything.

Ebenso möchte ich meiner Familie für die Unterstützung während meines gesamten Studiums danken. Ohne euch wäre die Anfertigung dieser Arbeit nicht möglich gewesen. Danke.

If I missed somebody, please forgive me, contact me and the next round is on me!

Abstract

In this work, the influence of hydrogen bonds on structure and thermodynamic properties of binary mixtures of two protic ionic liquids (PILs), sharing the same cation, are investigated.

The two PILs studied are triethylammonium triflate ([TEA][OTf]) and triethylammonium methylsulfonate ([TEA][OMs]). For binary mixtures of these two PILs non-ideal mixing behavior is observed, for example for the self-diffusion coefficients and energies of mixing. Results from infrared (IR) spectroscopy suggest that the reason for this observed non-ideality is due to the difference in the hydrogen bonding strength in [TEA][OTf] compared to [TEA][OMs]. For insight on a molecular level, molecular dynamics (MD) simulations of the PIL mixture as well as [TEA][OMs]/water mixtures are employed.

For the PIL mixture the assumption from IR spectroscopy is supported. The difference in the hydrogen bonding strength leads to the formation of complex hydrogen-bonded clusters. These clusters are responsible for the observed non-ideal behavior. These findings are supported and better understood with a newly developed simple lattice model. The model also shows that the mixing process is enthalpy-driven and not entropy-driven, as one would expect.

On the example of [TEA][OMs]/water mixtures, the formation of ion pairs is presented. It is shown that it takes four water molecules per ion pair to break the hydrogen bond between the anion and cation. Moreover, the simple lattice model is extended to also describe these PIL/water mixtures.

The last part of this work takes a closer look at force fields used in MD simulations and proves that a thorough evaluation of force fields, even well established ones, is necessary. Furthermore, a tool is presented that supports researchers with the conversion of force fields between different MD programs.

1 Introduction

1.1 Motivation

It is well known that mixing two liquids, which are able to form hydrogen bonds, can lead to interesting and, at first glance, astonishing observations. The most famous one is probably the volume contraction, which is observed when alcohols and water are mixed [3]. So, it comes with no surprise that mixtures of ionic liquids (ILs), a substance class that can show strong Coulomb interactions as well as hydrogen bonding [4, 5], sparked the interest of many researchers [6–8]. This work focuses on mixtures of ILs and the interactions of Coulomb forces with hydrogen bonding. It will go into detail why these mixtures are intriguing and how they can help us to better understand hydrogen bonding in general.

The substance class of ILs is not well-defined, but in general the scientific community has agreed on the following: ILs are substances that consist only of ions and have a melting point “around or below 100 °C” [9]. There is some debate about the arbitrary cutoff of 100 °C and who established it [10]. To better understand what ILs are, it is helpful to compare them to another substance class that is solely built up of ions: salts, like sodium chloride (NaCl). Most salts consist of small inorganic ions, leading to strong Coulomb interactions. These strong Coulomb interactions result in a high lattice energy, which leads to a high melting point. The melting point of NaCl is $T_m(\text{NaCl}) = 800.7^\circ\text{C}$ [11]. In ILs the ions, or at least one ion, is a larger organic ion, for example 1-ethyl-3-methylimidazolium chloride [EMIm][Cl] (figure 1.1). Due to the size of the [EMIm]-cation, the charge centers of an- and cation are further apart. Furthermore, the positive charge is distributed over the whole cation. Both effects lead to a lower melting point in comparison to NaCl ($T_m([\text{EMIm}][\text{Cl}]) = 85^\circ\text{C}$ [12]).

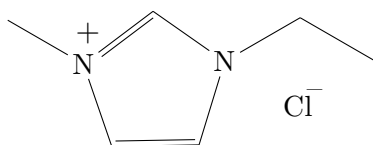


Figure 1.1: Structural formula of 1-ethyl-3-methylimidazolium chloride [EMIm][Cl].

The field of ILs is relatively new but fast-growing. Providing an overview over the whole research of the last 30 years is beyond the scope of this work. Nevertheless, some important review articles to the general field of ILs are given here. Foremost, mentioning the seminal introductory paper “Ionic Liquids — A Brief History” by Welton from 2018 [10]. Welton gives an overview over the development of the field of ILs and points out essential works. Hayes et al. discuss the structure of ILs in more detail [13], whereas Watanabe et al. review the application of ILs for energy storage [14]. The already mentioned review articles by Marsh et al., Niedermeyer et al., and Chatel et al. are dealing with mixtures of ILs [6–8].

For researchers it is important to take a closer look at the mixing behaviors of these liquids, because of their potential uses. From the beginning, ILs were considered to replace organic solvents in industrial processes, due to the possibility to *tune* their properties by choosing the *right* anion and cation [15–20]. Rodgers and Seddon estimated, that there are “at least one million” ILs by combining one anion with one cation, by mixing those ILs they estimated 10^{18} possible ILs mixtures [9]. If an ideal mixing behavior is observed, it would be possible to further optimize a given property to better fit those industrial processes. It gets even more exciting if a non-ideal mixing is observed. In that case, the properties of the mixture cannot be described by the characteristics of the pure liquids and a new substance has been formed [8].

The three review articles mentioned before mostly report ideal mixing behavior. The same could be observed by Stoppa et al. and Lepre et al. [21, 22]. The aim of this work is to show that non-ideal mixing behavior in ILs can be accomplished by choosing the *right* anion-cation combination.

Before going into more detail about the ILs investigated and methods used, a word about the motivation and scope of this work, which can be best expressed in the words of Welton [10]:

“While many came to work with ionic liquids due to their exciting applications, others sought a deeper understanding of their behaviours, structures and how these arise.”

The following work definitely belongs to the second category, showing how molecular dynamics (MD) simulations help to get a better understanding of hydrogen bonding in ILs, and how the hydrogen bonding is responsible for some observed non-ideal mixing behaviors.

1.2 Protic Ionic Liquids

In this work, the non-ideal mixing behavior is accomplished by using the two ILs triethylammonium triflate, [TEA][OTf], (figure 1.2) and triethylammonium methylsulfonate,

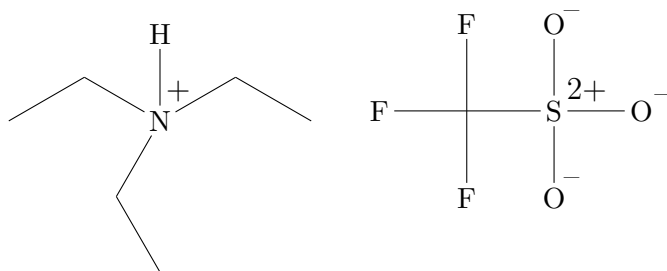


Figure 1.2: Structural formula of [TEA][OTf]. The [TEA]-cation is shown on the left side, the [OTf]-anion on the right side.

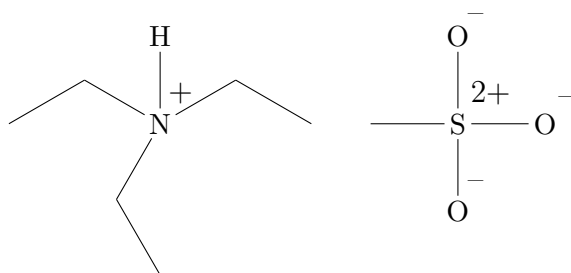


Figure 1.3: Structural formula of [TEA][OMs]. The [TEA]-cation is shown on the left side, the [OMs]-anion on the right side.

[TEA][OMs], (figure 1.3). Both liquids belong to a subclass of ILs called protic ionic liquids (PILs). PILs are formed by a proton transfer from the acid to the base. Consequently, they can build strong hydrogen bonds between the an- and cation [23–25]. In comparison to aprotic ionic liquids (APILs), PILs have been investigated to a lesser extent. Greaves et al. provide in their two review articles from 2008 and 2015 insights into the field of PILs, their applications as well as open research topics [24, 26].

The two studied PILs were chosen with great care. They are structurally very similar, but experimental infrared (IR) spectroscopy studies indicate that the hydrogen bond strength in [TEA][OTf] and [TEA][OMs] is different [27, 28]. It is shown that the hydrogen bond between the [TEA]-cation and the [OMs]-anion is stronger than the hydrogen bond between the [TEA]-cation and the [OTf]-anion. These observations are supported by density functional theory (DFT) calculations by Fedorova et al. [29]. This is due to the electron-withdrawing inductive effect of the fluorine atoms in the [OTf]-anion. The electron withdrawing decreases the electron density on the oxygen atoms, thus leading to a diminished hydrogen bond acceptor ability and weakening the hydrogen bond in comparison to the [TEA][OMs]. A mixture of these two PILs is a promising candidate to learn more about hydrogen bonding and its effects on the mixing behavior.

In **Publication I**, a combined effort of several methods was used to investigate the non-ideal mixing behavior of the PILs mentioned. **Publication II** is a MD study on the observed properties. Furthermore, a simple lattice model to describe the observed hydrogen-bonded clusters is established. A step further is taken in **Publication III** where the enthalpy of mixing is calculated and experimentally measured. Additionally, the simple lattice model presented in **Publication II** is used to get more information about the influence of hydrogen bonding on the enthalpy of mixing. In **Publication IV** the simple lattice model is used to describe the entropy of mixing and investigate the reason these two PILs are mixing.

To gain further information about the hydrogen-bonded clusters, in **Publication V** [TEA][OMs] is mixed with water. The influence of water on the hydrogen bonded structures is investigated and a closer look at ion pairing is taken.

1.3 Molecular Dynamics Simulations

In MD simulations, each molecule is described by a set of parameters. These parameters include atom charges, atom masses, information about bond, bond angle and dihedral angle potentials as well as non-bonding information like Lennard-Jones (LJ) parameters. A set of these parameters is called force field. With the help of these force fields it is possible to calculate the forces which affect a particle i

$$\vec{F}_i = -\nabla_i V, \quad (1.1)$$

where V is the potential. This potential can be divided into an intermolecular and an intramolecular part

$$V = V_{\text{inter}} + V_{\text{intra}}. \quad (1.2)$$

The intermolecular potential is the sum of the LJ potential and the Coulomb potential,

$$V_{\text{inter}} = V_{\text{LJ}} + V_{\text{Coulomb}} \quad (1.3)$$

with

$$V_{\text{Coulomb}} = \frac{1}{4\pi\epsilon_0} \sum_{i=1}^{n-1} \sum_{j=i+1}^n \frac{q_i q_j}{r_{ij}}, \quad (1.4)$$

where ϵ_0 is the vacuum permittivity, q_i/j is the charge of the particle i/j and r_{ij} is the distance between the particles i and j . The LJ potential is given by [30]

$$V_{\text{LJ}} = \sum_{i=1}^{n-1} \sum_{j=i+1}^n 4\epsilon_{ij} \left[\left(\frac{\sigma_{ij}}{r_{ij}} \right)^{12} - \left(\frac{\sigma_{ij}}{r_{ij}} \right)^6 \right], \quad (1.5)$$

with ϵ being the depth of the potential minima, and σ being the distance where the potential is zero. The parameters ϵ and σ are called LJ parameters. In the force field the LJ parameters

are only given for interactions of identical atom types (σ_{ii} and ϵ_{ii}), the LJ parameters for interactions of different atom types are calculated using the Lorentz-Berthelot mixing rules:

$$\epsilon_{ij} = \sqrt{\epsilon_{ii}\epsilon_{jj}} \quad (1.6)$$

and

$$\sigma_{ij} = (\sigma_{ii} + \sigma_{jj})/2. \quad (1.7)$$

The intramolecular potential V_{intra} describes the molecule, containing the already mentioned Coulomb and LJ potentials, as well as additional potentials for bonds, bond angles, and dihedral angles

$$\begin{aligned} V_{\text{intra}} = & V_{\text{LJ}} + V_{\text{Coulomb}} + V_{\text{bond}} + V_{\text{bond angle}} \\ & + V_{\text{dihedral angle, harm}} + V_{\text{dihedral angle}} \end{aligned} \quad (1.8)$$

with

$$V_{\text{bond}} = \sum_{\text{b}} \frac{1}{2} k_{ij}^{\text{b}} (r_{ij} - r_{ij}^0)^2 \quad (1.9)$$

$$V_{\text{bond angle}} = \sum_{\text{a}} \frac{1}{2} k_{ijk}^{\text{a}} (\phi_{ijk} - \phi_{ijk}^0)^2 \quad (1.10)$$

$$V_{\text{dihedral angle, harm}} = \sum_{\text{dh}} \frac{1}{2} \cdot k_{ijkl}^{\text{dh}} (\psi_{ijkl} - \psi_{ijkl}^0)^2 \quad (1.11)$$

$$V_{\text{dihedral angle}} = \sum_{\text{d}} k_{ijkl}^{\text{d}} (1 + \cos(m_n \psi_{ijkl} - \psi_{ijkl}^0)), \quad (1.12)$$

where k_{ij}^{b} , k_{ijk}^{a} , k_{ijkl}^{dh} , k_{ijkl}^{d} are the force constants of the bonds, bond angles and dihedral angles, r_{ij}^0 , ϕ_{ijk}^0 and ψ_{ijkl}^0 are the equilibrium distances respectively the equilibrium angles and r_{ij} , ϕ_{ijk} as well as ψ_{ijkl} are the distances and angles between the atoms i , j , k and l .

The development of a good force field is a topic of its own. Especially in IL research it is a non-trivial task. The most important works in the field of ILs were done by Pádúa et al. Since 2004, they publish transferable force field parameters for ILs and are constantly improving them [31–40]. In 2007 Köddermann et al. optimized the force field from Pádúa et al. for $[\text{C}_n\text{MIm}][\text{NTf}_2]$ ILs, known as the KPL force field [1]. They focused on rescaling the LJ parameters to better describe experimental observations. It is stated that [1]:

“At this stage the change of LJ-parameters seems to be somewhat arbitrary.

The procedure is justified by the obtained results.”

That the authors were right, can be seen by the fact that the force field is still in use today [41, 42]. In 2009 Borodin wrote an article about force fields for ionic liquids, and he endorsed the work, by stating [43]:

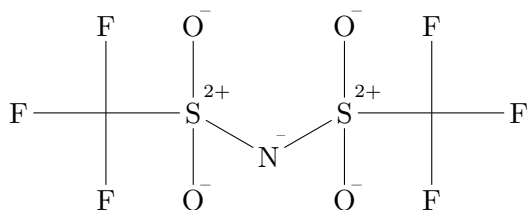


Figure 1.4: Structural formula of the bis(trifluoromethanesulfonyl)azanid anion.

“There are only a few instances when a developed IL force field has been shown to accurately describe IL density, heat of vaporization, ion transport, and viscosity. Loddermann [sic], Paschek, and Ludwig’s force field for [alkylimidazolium]-[NTf₂] ILs is a clear example of such a success.”

As part of this thesis, the force field by Köddermann et al. was further optimized since it was observed that there is a misrepresentation of the dihedral angles leading to conformations which are not in agreement with the experiment. This work is described in **Publication VI**. In 2020 Gehrke and Kirchner used this optimized force field (called NGOLP) and found [44]:

“The use of the NGOLP force field renders charge scaling in the [NTf₂]⁻-containing systems redundant.”

Due to the great success of the KPL force field and the structural similarities between the [NTf₂]-anion and the [OTf]-/[OMs]-anion (figures 1.2–1.4), the KPL force field parameters are used as basis for the force fields of the anions. The [TEA]-cation is based on the works from Krienke et al. [45] and Martin et al. [46]. The complete force field is described in **Publication II** as well as the supporting information of **Publication I**. For the simulation of mixtures with water, described in **Publication V**, the TIP4P/2005 water model by Abascal and Vega is used [47].

The described potentials in equations 1.1-1.12 are only valid for MD simulations done with GROMACS [48]. If a different MD simulation code is used, e.g. CHARMM [49], the potentials are differently written and a conversion of the force field is necessary. In **Publication VII** a conversion tool is described which was developed in cooperation with researchers from Germany, Austria, France, and Portugal under the aegis of Prof. Christian Schröder from the University of Vienna.

2 Research Overview

2.1 Remarks

During the process of releasing **Publications I–IV** the convention of naming the PILs and ions has changed. In the interest of a better readability, a consistent naming syntax is used in this work. Figures taken from publications are changed in the way, that the naming of the PILs fits the text. Furthermore, when properties of binary mixtures are discussed as a function of the mole fraction x , the notation of the mole fraction is written as x_{OMs} , for the mole fraction of [TEA][OMs], and x_{OTf} for the mole fraction of [TEA][OTf], respectively. If not differently stated, no additional modifications are done to the figures. This should avoid confusions between figures in publications and figures in this research overview.

2.2 Mixtures of Protic Ionic Liquids

Based on the works of Fumino et al. mentioned in section 1.2 [27, 50] mixtures of the two PILs [TEA][OTf] and [TEA][OMs] are studied. These mixtures are interesting objects of investigation, due to the structural similarities of the [OTf]- and [OMs]-anion, but the difference in the hydrogen bond strength to the [TEA]-cation. It allows the research of the influence of hydrogen bonding on structure and thermodynamic properties, in the hope of observing non-ideal mixing behavior. Up to this point, researchers were more focused on mixtures of APILs and found mostly ideal or nearly ideal mixing behavior [6–8].

In **Publication I** mixtures of these two PILs are first investigated with IR spectroscopy. It is possible to assign one vibrational band to the $\text{N-H} \cdots \text{O}=\text{S}$ interaction in [TEA][OTf], respectively [TEA][OMs]. For the pure PILs as well as three mixtures, the intensity of these vibrational bands is measured. It can be observed, that the intensity of these bands shows a non-ideal behavior as function of the mixture composition (figure 2.1).

The intensity of the vibrational band for the [TEA][OTf] is smaller, whereas the intensity of the [TEA][OMs] interaction is larger, in comparison to an ideal mixing behavior. To further support these findings, the density as well as the viscosity of the mixtures are measured. For the density of the mixtures, a near-ideal mixing behavior can be observed, whereas the viscosity shows clear non-ideality. This is in agreement with observations by Chatel et al., who proposed that the classification of the mixing behavior (ideal or non-ideal) depends on

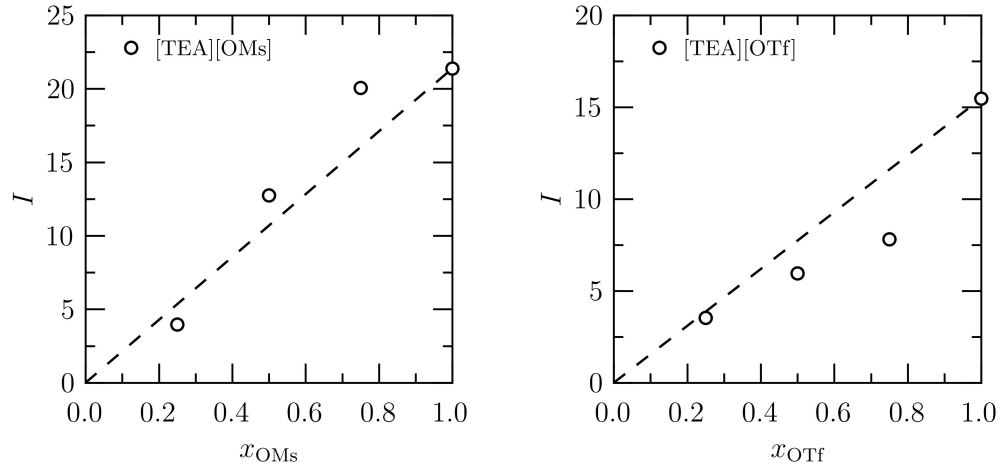


Figure 2.1: Intensities of the N-H \cdots O=S vibrational bands for [TEA][OMs] (left) and [TEA][OTf] (right) as function of the mole fraction. The dashed lines indicate an ideal mixing behavior. Original figure: **Publication I** figure 3.

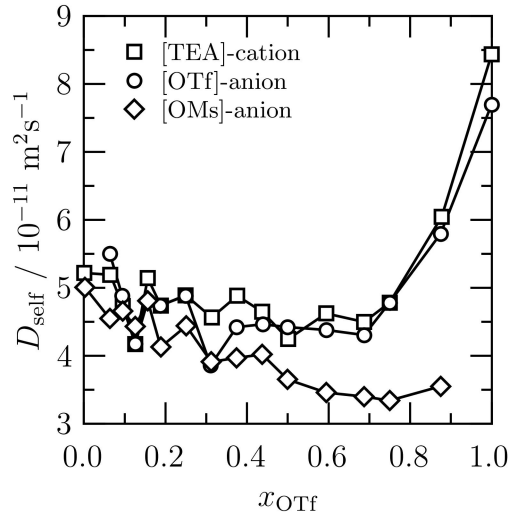


Figure 2.2: Self-diffusion coefficients calculated from MD simulations with equation 2.1 for the [TEA]-cation, as well as the [OTf]- and [OMs]-anion as function of the mole fraction of [TEA][OTf] at $T = 400 \text{ K}$. Original figure: **Publication I** figure 6 b.

the investigated properties [8]. The results from **Publication I–IV** are supporting their idea of “double salt ionic liquids” (DSILs). DSILs are mixtures of ILs that show unique properties which can not be understood simply by the attributes of the pure ILs alone.

Insights on a molecular level are given through MD simulations of mixtures of the two PILs. The pure PILs as well as 14 different mixture compositions are simulated and analyzed, at six temperatures in the range of $T = 300$ K to $T = 400$ K. Information about the force field parameters used are documented in section 1.3.

First, the self-diffusion coefficient is calculated using the Einstein-Kubo-Helfand relation [51, 52]

$$D_i = \lim_{t \rightarrow \infty} \frac{1}{6} \frac{\partial}{\partial \tau} \langle |\vec{r}_i(t) - \vec{r}_i(t + \tau)|^2 \rangle, \quad (2.1)$$

where the displacement of the center-of-mass coordinates \vec{r}_i of an ion species i is averaged over times t . A clearly non-ideal mixing behavior is observed (figure 2.2). Over the whole mixing range, the self-diffusion coefficient of the [OMs]-anion is below the self-diffusion coefficient in the pure PIL [TEA][OMs]. For mixtures with $x_{\text{OTf}} > 0.5$, a significant drop in the self-diffusion coefficient for the [TEA]-cation as well as the [OTf]-anion, in comparison to the pure PIL [TEA][OTf], is observed.

Since the difference in the hydrogen bond strength is assumed to be the reason for the observed non-ideal mixing behavior in IR spectroscopy, viscosity and self-diffusion coefficients, an extensive study of the hydrogen-bonded clusters is performed. Therefore, a definition of a hydrogen bond between a cation and an anion is needed. Defining a hydrogen bond can be quite challenging. The IUPAC technical reports by Arunan from 2011 give detailed inside into this topic [53, 54]. Worth reading is also the report to the occasion of 100 years of hydrogen bonding [55]. In MD simulations, it is common to define a hydrogen bond by the bond length and the bond angle.

As shown in **Publication II** and supported by DFT calculations [29, 56], the investigated PILs form strong linear hydrogen bonds. Therefore, a simple distance criterion ($r_{\text{cut}} < 0.24$ nm) without further usage of an additional bond angle criterion is sufficient.

This simple, but well-defined criterion for a hydrogen bond, allows to calculate the portion of cations involved in a hydrogen bond to one of the two anion types. For an ideal mixture, the portion of cations involved in a hydrogen bond to a [OTf]-anion linearly decreases with an increase of the mole fraction of [TEA][OMs], the opposite is true for the [OMs]-anion (figure 2.3, dotted lines). In contrast to the ideal behavior, the percentage of [TEA]-cations involved in a hydrogen bond to an [OTf]-anion decreases much faster (figure 2.3). As indicated from IR spectroscopy, the interaction between the [TEA]-cation and the [OMs]-anion seems to be favored over the interaction to the [OTf]-anion. It is important to note, that over the whole mixing range, the [TEA]-cation always forms a hydrogen bond to one of the anions.

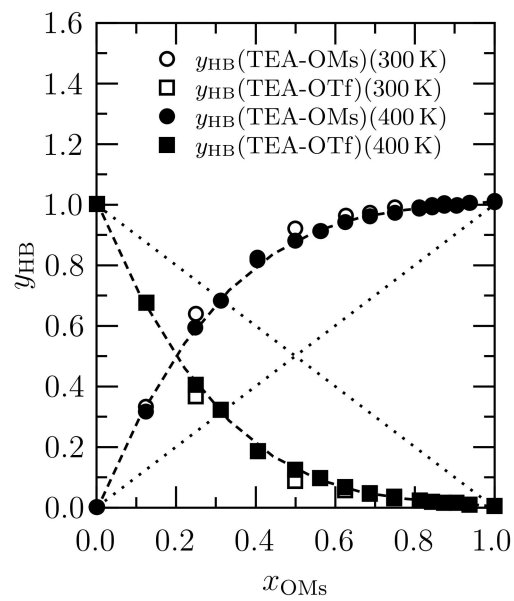


Figure 2.3: Percentage of [TEA]-cations involved in a hydrogen bond to a [OTf]-anion (squares) or a [OMs]-anion (circles) as function of the mole fraction of [TEA][OMs] at $T = 300 \text{ K}$ (open symbols) and $T = 400 \text{ K}$ (closed symbols). Original figure: **Publication II** figure 11.

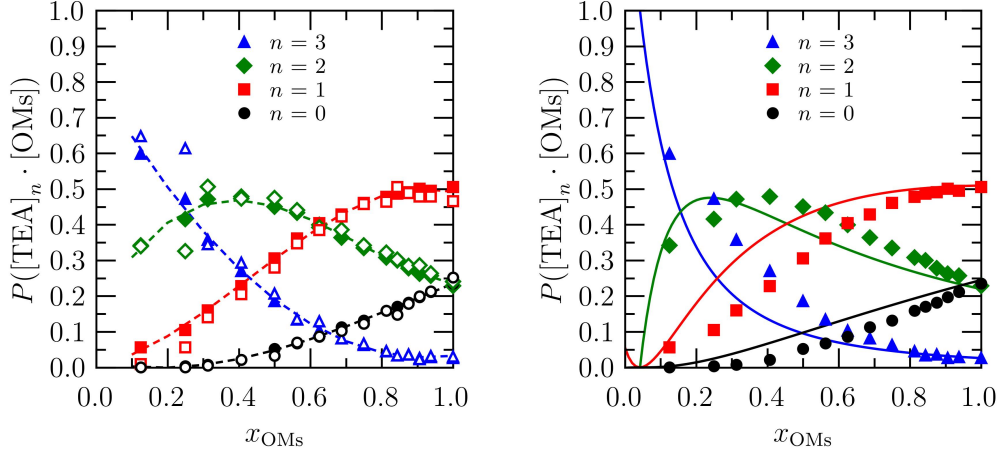


Figure 2.4: Probability of [OMs]-anions hydrogen-bonded n [TEA]-cations as a function of the mole fraction of [TEA][OMs] at $T = 300$ K (open symbols) and $T = 400$ K (closed symbols). The dashed lines on the left are guides for the eyes and the solid lines on the right are calculated from the simple lattice model. Original figures: **Publication II** left: figure 13 top; right: figure 17 left ¹.

For the anions, the hydrogen bond situation is more complex, due to the three oxygen atoms. Each anion has the possibility to accept up to three hydrogen bonds at the time. It is worth mentioning here, that the possibility for branched hydrogen bonds is well below 0.1 %. Branched hydrogen bonds are hydrogen bonds, where one oxygen atom accepts two hydrogens.

With the increase of the mole fraction x_{OMs} the probability of an [OMs]-anion involved in three hydrogen bonds ($n = 3$) decreases, whereas the probability for no hydrogen bonds ($n = 0$) and one hydrogen bond ($n = 1$) increases (figure 2.4). The probability of clusters with two hydrogen bonds ($n = 2$) first increases until a mole fraction of $x_{\text{OMs}} = 0.4$ and then decreases. This distribution of hydrogen-bonded clusters as function of the mixture helps to better understand the observed strong decrease in the self-diffusion coefficient shown before (figure 2.2). Due to the formation of larger hydrogen-bonded clusters, $n = 3$, the self-diffusion coefficient significantly decreases and the viscosity increases. Increasing the amount of [OMs]-anions in the mixture leads to a decrease in the probability of clusters with the size $n = 3$, and thus leads to an increase in the self-diffusion coefficient again.

¹In **Publication II**, open symbols were used for figure 17, for an easier readability it is changed here to closed symbols.

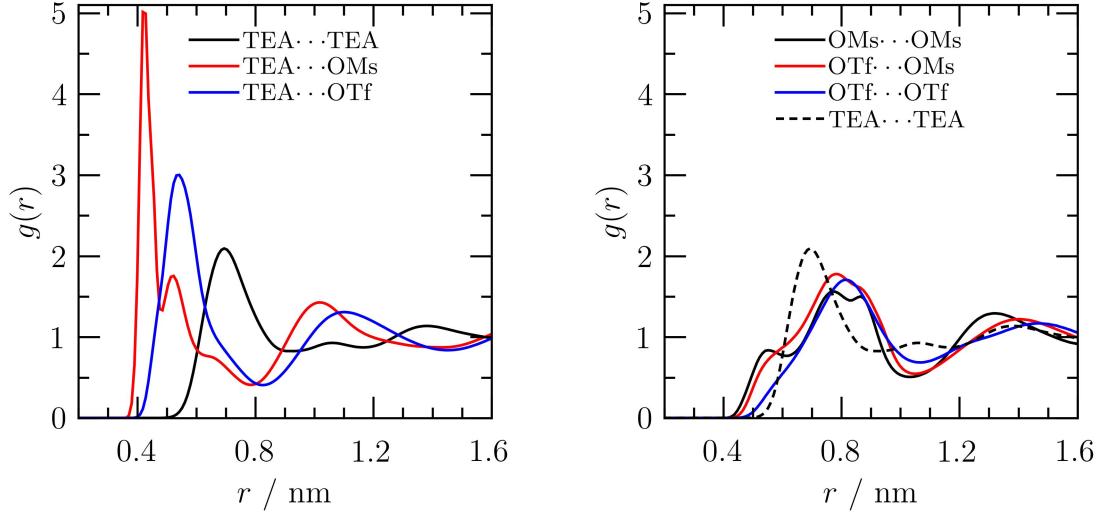


Figure 2.5: Ion-ion center of mass pair distribution functions $g(r)$ for the 50:50 mixture of [TEA][OTf]:[TEA][OMs] at $T = 300$ K. Original figure: **Publication II** figure 3.

For the pure PILs a very characteristic distribution of hydrogen-bonded clusters is observed. In both PILs, 50 % of the anions are involved in one hydrogen bond, 25 % in two and 23 % are not involved in a hydrogen bond to a cation. The other 2 % correspond to anions which build three hydrogen bonds to three different cations (figure 2.4 left for [TEA][OMs]). This is in good agreement with simulations by Cardozo et al. [57]. There 50 % of the [OTf]-anions form one hydrogen bond with the [TEA]-cation, 30 % two, 18 % none and 2 % three hydrogen bonds to the cation. Furthermore, they also find no significant temperature dependence (for a temperature range of $T = 300$ K to $T = 400$ K). The differences in the probability for no and two hydrogen bonds can arise from the different force fields used. However, it should be noted that Cardozo et al. build their simulation box with 125 ion pairs, while in **Publication II** 256 ion pairs were used. Since they used production runs of $t = 100$ ns the smaller box size should not have a significant impact on the results. According to Schröder et al., 50 ion pairs seem to be enough to describe the structure of an ionic liquid [58], but they also recommend to use 500 ion pairs, especially when dynamics are investigated. To test and further improve the results, in **Publication III** and **Publication IV** simulation boxes with 500 ion pairs are used. The findings from **Publication I–II** are confirmed, thus it appears that the simulation size has no further influence on the results, obviously the statistics improve significantly.

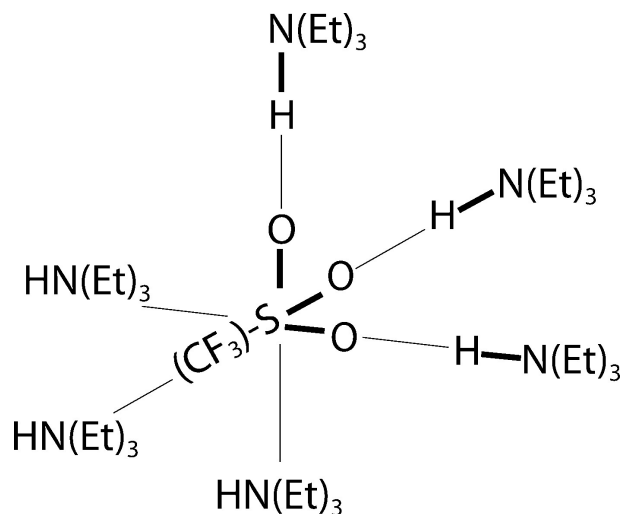


Figure 2.6: Schema of the simple lattice model for $c = 6$. The anion, here the [OTf]-anion, is surrounded by c cations, with the possibility to accept up to three hydrogen bonds from three different [TEA]-cations. Original figure: **Publication II** figure 14.

Even though a non-ideal mixing behavior as well as hydrogen-bonded cluster formation are observed, a well-defined structure is preserved. By analyzing the center of mass pair distribution functions (figure 2.5), it becomes clear that in the first solvation shell each ion is surrounded only by counter ions. This observation sparked the idea that the hydrogen bond distribution could possibly be described by a simple lattice model. The model assumes that each anion is placed on a lattice and is surrounded by c cations (figure 2.6, example for $c = 6$). In addition, information on the probability of a hydrogen bond between one [TEA]-cation and the two anions (y_{OTf} and y_{OMs} , figure 2.4), as well as the hydrogen-bonded cluster distribution for the pure PILs is taken from MD simulations. With these information, the model can describe the distribution quite accurately (figure 2.4 right, solid lines). An in-depth description of the model can be found in **Publication II**. In **Publication III–V** the simple lattice model is refined, and it is shown that this model can help to get a better understanding of the mixing process.

Until now, only qualitative information was given for the difference in the hydrogen bond strength. In **Publication III**, the difference was quantified for the first time. Using a van't-Hoff plot, the difference in the hydrogen bond strength can be calculated from the equilibrium constant K between the two hydrogen-bonded states, it is given by:

$$K = \frac{y_{\text{OMs}}}{y_{\text{OTf}}}, \quad (2.2)$$

where y_{OMs} and y_{OTf} are the fractions of the cations with a hydrogen bond to the [OMs]- or [OTf]-anion. From the slopes of the van't-Hoff plots, a standard enthalpy $\Delta H^\circ = -10.5 \text{ kJ mol}^{-1}$ is calculated. Since the anions have a comparable size, the difference in the volume of the two bonded states can be neglected and thus the standard enthalpy and the standard energy are approximately identical:

$$\Delta U^\circ \approx \Delta H^\circ = -10.5 \text{ kJ mol}^{-1}. \quad (2.3)$$

The difference in the hydrogen bond strength is also accessible by another method. Since the mixtures of the two PILs have a well-defined structure, as shown before, it is possible to calculate the difference in the hydrogen bond strength from the energies of mixing. By employing the already briefly discussed simple lattice model, the energies of mixing are directly calculated from MD simulations using:

$$\Delta U_{\text{mix}}(x_{\text{OMs}}) = U(x_{\text{OMs}}) - x_{\text{OMs}} \cdot U_{[\text{TEA}][\text{OMs}]} - (1 - x_{\text{OMs}}) \cdot U_{[\text{TEA}][\text{OTf}]}, \quad (2.4)$$

where x_{OMs} is the mole fraction of [TEA][OMs], $U(x_{\text{OMs}})$ is the energy of the mixture at a given mole fraction of [TEA][OMs], $U_{[\text{TEA}][\text{OMs}]}$ and $U_{[\text{TEA}][\text{OTf}]}$ are the energies of the pure PILs [TEA][OMs] and [TEA][OTf]. The energy of mixing shows a strong negative deviation from an ideal mixing behavior (figure 2.7, left). The deviation from an ideal mixing behavior of the energy of mixing implies a "breaking and making" of interactions [8], and therefore a change in the liquid structure [59]. Lower absolute values are found with increasing temperature, and a temperature independent shift of the minima to $x_{\text{OMs}} = 0.4$ is observed. With the developed lattice model, the energy of mixing can be described by:

$$\Delta U_{\text{mix}}(x_{\text{OMs}}) = N_{\text{TEA}}(y_{\text{OMs}} - x_{\text{OMs}}) \cdot \Delta \epsilon_{\text{HB}}, \quad (2.5)$$

where N_{TEA} is the number of cations, y_{OMs} the fraction of hydrogen bonds from the [TEA]-cation to the [OMs]-anion, x_{OMs} is the mole fraction of [TEA][OMs] and $\Delta \epsilon_{\text{HB}}$ is the difference in the hydrogen bond strength, which is defined as:

$$\Delta \epsilon_{\text{HB}} = \epsilon_{\text{HB:TEA-OMs}} - \epsilon_{\text{HB:TEA-OTf}}. \quad (2.6)$$

For more details on the lattice model see **Publication III**.

Equation 2.5 is used to fit the data from MD simulations (figure 2.7, left). The model perfectly reproduces the results from the MD simulation, even though it only describes the first solvation shell of an ion. The so calculated $\Delta \epsilon_{\text{HB}}$ is averaged over all temperatures and a $\Delta \epsilon_{\text{HB}} = (-10.6 \pm 0.5) \text{ kJ mol}^{-1}$ is calculated. Which is, again, in excellent agreement with results from MD simulations.

Furthermore, it is possible to determine $\Delta \epsilon_{\text{HB}}$ with a combination of titration calorimetry and NMR experiments. The calculation is analogously done to the way described before, with

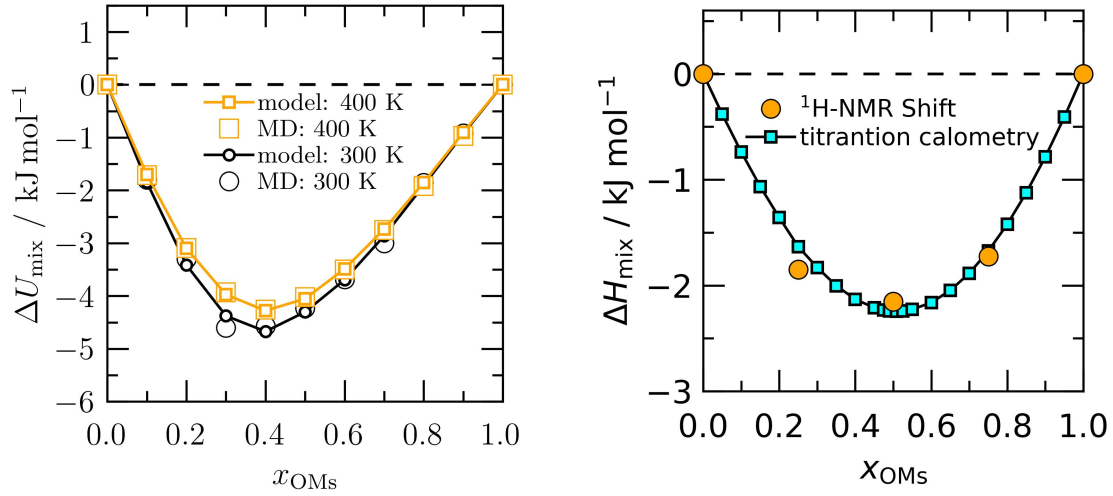


Figure 2.7: Left: Mixing energies as function of the mole fraction of [TEA][OMs] at $T = 300 \text{ K}$ and $T = 400 \text{ K}$. The big open symbols show the results directly taken from MD simulations, the lines with small symbols show the calculated values from the described model. Right: Experimental mixing enthalpies at $T = 298 \text{ K}$ determined from calorimetric titration data (cyan squares) and $^1\text{H-NMR}$ chemical shifts (yellow circles). Original figures: **Publication III** left: figure 6; right: figure 8 left.

the knowledge of the enthalpy of mixing and the fraction of hydrogen bonds to the different anions (equation 2.5). The enthalpy of mixing is calculated from the titration calorimetry experiments using the Redlich-Kister approach [60]. The probability of a hydrogen bond to a [OMs]-anion y_{OMs} , is computed from ^1H -NMR chemical shifts, following:

$$y_{\text{OMs}} = \frac{\delta(^1\text{H}, x_{\text{OMs}}) - \delta(^1\text{H}, [\text{TEA}][\text{OTf}])}{\delta(^1\text{H}, [\text{TEA}][\text{OMs}]) - \delta(^1\text{H}, [\text{TEA}][\text{OTf}])}. \quad (2.7)$$

It is important to note that under these conditions ΔH_{mix} and ΔU_{mix} are approximately identical. The enthalpy of mixing determined from titration calorimetry shows smaller absolute values, and no shifting of the location of the minima is observed (figure 2.7, right). A difference in the hydrogen bond strength of $\Delta\epsilon_{\text{HB}} = -13 \text{ kJ mol}^{-1}$ is calculated, being in good agreement with the results from MD simulations as well as the simple lattice model.

With the simple lattice model, different parameters can be tweaked. In this way it is possible to investigate where the difference between the experimental data and the MD simulations originates. As it is shown in **Publication III** the difference in the location of the minima in the energy of mixing as well as the higher absolute values can solely be attributed to the equilibrium of $y_{\text{OMs}}/y_{\text{OTf}}$. The MD simulations seem to overestimate the interaction between the [TEA]-cation and the [OMs]-anion, while the data from the experimental measurements suggest a more even distribution between the hydrogen bonds.

In **Publication IV** the driving force behind the mixing process is investigated. It is shown that, with a slightly modified lattice model, it is possible to determine the Helmholtz free energy ΔA_{mix} as well as the entropy of mixing ΔS_{mix} (figure 2.8). Especially peculiar is the calculated negative entropy of mixing in the range of $0.1 \leq x_{\text{OMs}} \leq 0.6$. This effect is caused by a large negative excess entropy ΔS_{E} , overcompensating the ideal contribution $\Delta S_{\text{mix-id}}$ to the entropy of mixing (figure 2.9). The reason for the negative excess enthalpy is that in the mixture the orientational configuration space of the [TEA]-cation is limited in comparison to the pure PILs. In the pure PIL the interaction energy to all anions is the same, however, in the mixture the interaction to the [OMs]-anion is preferred due to a stronger interaction. This reduces the orientational configuration space of the cation. All investigations in **Publication IV** lead to the surprising conclusion that the mixing process of the PILs [TEA][OTf] and [TEA][OMs] is not entropy, but enthalpy driven.

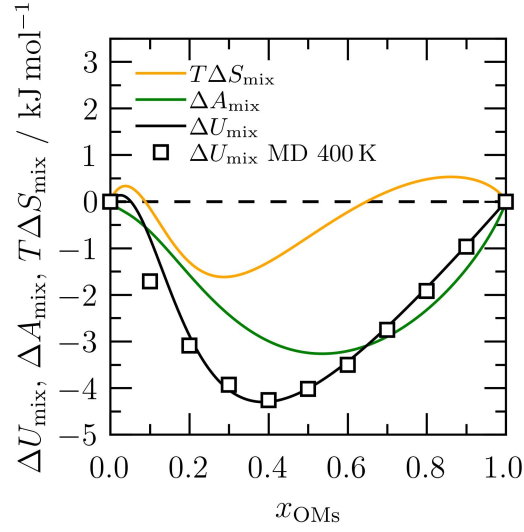


Figure 2.8: Thermodynamic properties as predicted from the model described in detail in **Publication IV** at $T = 400$ K (solid lines). $T\Delta S_{\text{mix}}$ is the entropy of mixing, ΔA_{mix} the Helmholtz energy of mixing and ΔU_{mix} is the energy of mixing. The open squares are results from MD simulations. Original figure: **Publication IV** figure 5 left.

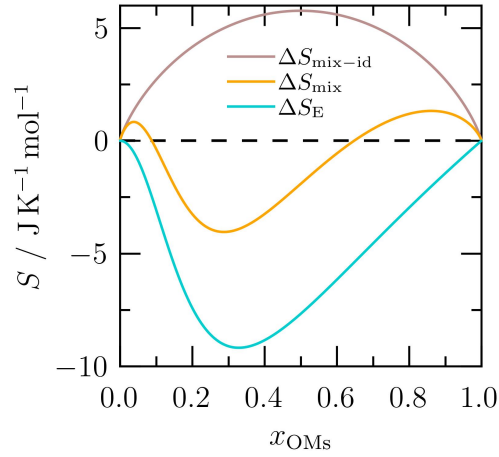


Figure 2.9: Contributions to the entropy of mixing ΔS_{mix} as predicted from the model described in detail in **Publication IV** at $T = 400$ K. Original figure: **Publication IV** figure 6.

2.3 Protic Ionic Liquids in Water

To further study the hydrogen-bonded clusters in PILs, mixtures of [TEA][OMs] with water are investigated in **Publication V**. A combination of IR spectroscopy, DFT calculations as well as MD simulations are employed. From earlier investigations by Ludwig et al. it is known that the hydrogen-bonded clusters can be disturbed by introducing solvents into the liquids [27, 50, 61]. Particularly interesting is the equilibrium between contact ion pairs (CIPs) and solvent-shared (SSIPs) respectively solvent-separated ion pairs (SIPs). A CIP is an ion pair where a direct hydrogen bond between anion and cation is present, for SSIPs and SIPs at least one solvent molecule, in this case water, must be between the two ions (figure 2.10).

One method to investigate the formation of ion pairs is the far-infrared (FIR) spectroscopy. In FIR spectroscopy the vibrational band around $\tilde{\nu} = 150\text{ cm}^{-1}$ can be assigned to the $\text{N}-\text{H} \cdots \text{O}=\text{S}$ interaction, thus the formation of ion pairs can directly be observed. The results show that for a mixture with more than 80 mol% water, this vibrational band is replaced by a new one at $\tilde{\nu} = 180\text{ cm}^{-1}$. This new band is assigned to interactions between water and the [TEA]-cation. Therefore, the hydrogen bond between the [OMs]-anion and the [TEA]-cation is broken. This leads to the conclusion that with a water content of above 80 mol%, the transformation from CIPs to SSIPs/SIPs is observed.

More insight on the transition from CIPs to SSIPs/SIPs is gained by employing DFT calculations for different ion pair/water aggregates with up to nine water molecules. It is observed that aggregates with less than four water molecules are only stable if a direct hydrogen bond between the cation and the anion is present (formation of CIPs is favored).

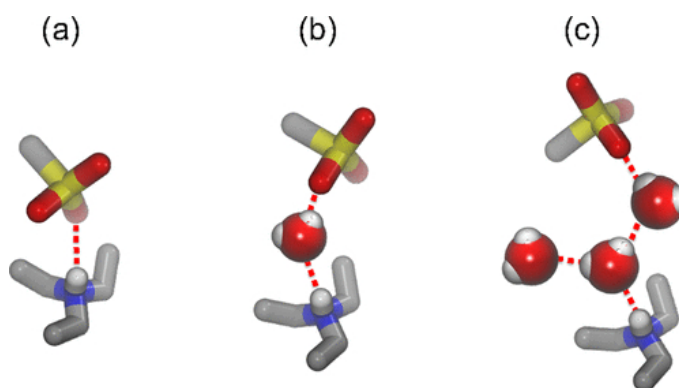


Figure 2.10: Visualization of three different types of ion pairs: (a) contact ion pair (CIP), (b) solvent-shared ion pair (SSIP), and (c) solvent-separated ion pair (SIP). Color code: red - O, yellow - S, grey - CH_x , blue - N, white - H. Taken from **Publication V** scheme 1.

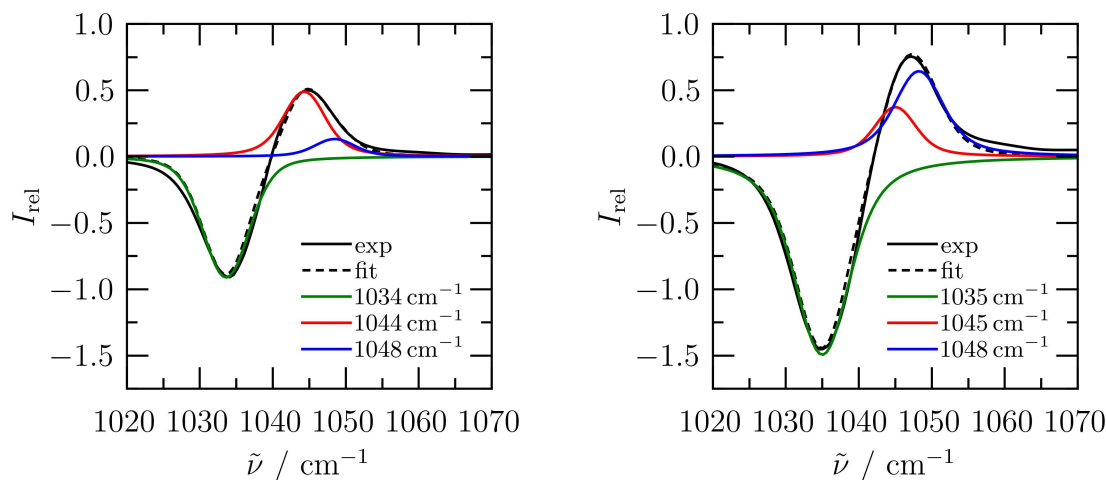


Figure 2.11: Difference MIR spectra and the deconvoluted contributions of [TEA][OMs]/water mixtures at $T = 298$ K, left: 50 mol% water, right: 80 mol% water. The solid black line is the experimental spectra, the colored solid lines are results of the deconvolution of the spectra with three contributions. The dashed line is the fit resulting from the deconvoluted contributions. Original figure: **Publication V** figure 10.

For aggregates with four and more water molecules, CIPs as well as SIPs are stable, but the formation of SIPs is enthalpically favored. Of course in SIPs there is an entropic penalty, due to the *trapped* water molecule between the [OMs]-anion and the [TEA]-cation, which suggests that the equilibrium between CIP/SIP is temperature dependent. Four water molecules per ion pair correspond to a mixture composition of 80 mol% water. Thus the DFT calculations support the results from FIR spectroscopy.

To obtain quantitative information about the ion pair formation, mid-infrared (MIR) spectroscopy is used. In MIR spectroscopy, the frequency range of $\tilde{\nu} = 1020 \text{ cm}^{-1}$ to $\tilde{\nu} = 1250 \text{ cm}^{-1}$ can be assigned to the S–O stretching motion of the anion. The oxygen atoms of the anion are the hydrogen bond acceptors, therefore measuring this motion is a direct sensor for the hydrogen bond between the anion and the cation. By deconvolution of the difference spectra, three contributions can be differentiated (figure 2.11). The negative intensity at 1035 cm^{-1} belongs to vibrational modes of the [OMs]-anion in the pure CIP configuration. The positive intensity at higher frequencies can be split into two contributions. The contribution at lower frequencies is assigned to interactions of CIPs with water, and the

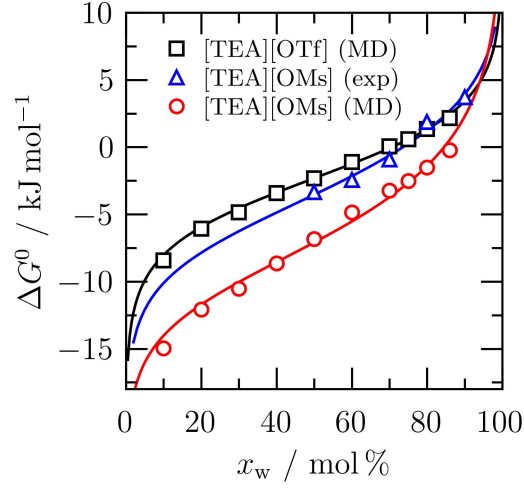


Figure 2.12: Standard Gibbs free energy differences for the interconversion of CIP and SIP for [TEA][OMs]/water mixtures as a function of the water content: from MD simulations at $T = 300$ K (red circles), from experiment at $T = 298$ K (blue triangles) as well as for [TEA][OTf]/water mixtures from MD simulations at $T = 300$ K (black squares). Predictions from the simplified lattice model are shown as solid lines. Original figure: **Publication V** figure 12.

one at higher frequencies to interactions of SIPs with water. For a mixture with 50 mol% water, the contribution of CIPs is dominating (figure 2.11, left), where in mixtures with 80 mol% water content, the contribution of the SIPs gets more and more important (figure 2.11, right).

Assuming that the absorption of the CIP/water and SIP/water interactions is approximately the same, it is possible to calculate the equilibrium constant K for the transition between the two bonding states. The equilibrium constant is defined as:

$$K = \frac{I_{\text{CIP}}}{I_{\text{SIP}}}, \quad (2.8)$$

where $I_{\text{CIP/SIP}}$ is the intensity of the respective bands. For mixtures with 80 to 90 mol% water, a significant amount of SSIP/SIP can be observed. From the equilibrium constant K the standard Gibbs free energy can be calculated, following:

$$\Delta G^\circ = -RT \ln(K). \quad (2.9)$$

If ΔG° is negative, CIPs are dominating in the mixtures. If ΔG° is positive the SIPs are more significant (figure 2.12). The MIR investigations support the results from FIR as well

as DFT calculations and help to quantify the equilibrium between CIPs and SIPs for the first time.

To conclude the investigations, MD simulations of [TEA][OMs]/water mixtures as well as [TEA][OTf]/water mixtures are employed. Since the two PILs are structural similar but differ in the strength of the hydrogen bond between the anion and the cation (section 2.2), MD simulations of [TEA][OTf]/water mixtures are a perfect completion of the [TEA][OMs]/water studies.

In the MD simulations, a linear hydrogen bond between the [TEA]-cation and a water molecule is observed. So, when analyzing the hydrogen bonds a distance cutoff is sufficient. Analogous to the PILs, no angle criterion is needed to define a hydrogen bond. The standard Gibbs free energy can be calculated using equation 2.9, analogous to the MIR experiment. Here the equilibrium constant K is given by

$$K = \frac{y_{\text{anion}}}{y_{\text{water}}}, \quad (2.10)$$

where y_{anion} is the fraction of cations involved in a hydrogen bond to an anion and y_{water} is the fraction of cations involved in a hydrogen bond to a water molecule.

The MD simulations can reproduce the qualitative observations from the MIR experiments, with increasing water content, the standard Gibbs free energy is increasing (figure 2.12). However, the data from MD simulations are significantly shifted to lower values. The simulations of [TEA][OTf] are in better agreement with the experimental data. It seems, that the TIP4P/2005 water model in combination with the [TEA][OTf] force field matches better than with the [TEA][OMs] force field. The hydrogen bond acceptor site in the water model cannot compete with the acceptor site in the [OMs]-anion, and therefore it is not able to break the hydrogen bond between the anion and the cation.

To test the lattice model from **Publication II**, a modified version is used to describe the mixtures with water. It is shown that the relatively simple description of the first solvation shell is enough to predict the concentration dependence of the standard Gibbs free energy (figure 2.12, solid lines).

With this multi-method approach, it is possible to get a better understanding of the hydrogen bonding, the ion pair formation and the conversion from CIPs to SSIP/SIP. All three methods (IR spectroscopy, DFT calculations and MD simulations), yield qualitatively the same result and even quantitatively findings are in good agreement. For mixtures with a water content of above 80 mol%, SSIPs/SIPs are the favored configurations. The simple lattice mixing model proves again to predict thermodynamic properties.

2.4 Force Field Development and Conversion

In **Publication I–V** it is shown that experimental methods like IR spectroscopy or titration calorimetry, and MD simulations can complement each other. However, this is only possible if the used force field, is valid for the described substance. A brief introduction into force fields was already given in section 1.3. In the next two sections, two important topics concerning force fields are discussed. Firstly, a well-established force field is optimized, which shows that the development of a force field is never really finished, and it needs to be reevaluated regularly. Secondly, the problem of different MD codes using different force field syntax is tackled by presenting a tool which helps researchers with the conversion of force field parameters.

2.4.1 Optimizing a Force Field

In **Publication VI** the $[\text{NTf}_2]$ -anion parameters from the well-established KPL force field by Köddermann et al.[1] are refined. Even though the force field describes diffusion coefficients, densities and other properties in good agreement with experimental measurements, a mismatch between the conformation using the KPL force field (figure 2.13) and structures described by quantum mechanics (QM) calculations as well as Raman experiments (figure 2.14) is found [62, 63]. This difference can lead to errors, when investigating the formation of hydrogen bonds in ILs. The accessibility of the oxygen atoms is critical for the formation of hydrogen bonds, because they are the primary hydrogen bond acceptor sites, and the access to these sites depends on the conformation of the anion.

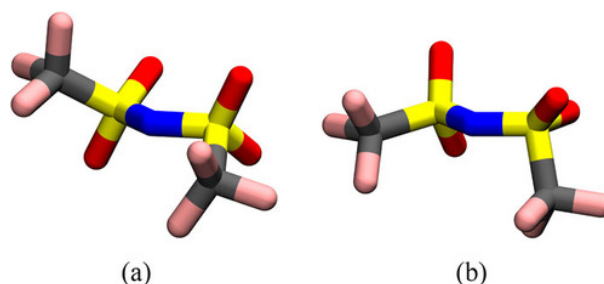


Figure 2.13: Snapshot of the global minimum (a) and local minimum (b) energy conformation of the $[\text{NTf}_2]$ -anion from MD simulations with the KPL force field, as indicated by the plus-sign and asterisk in figure 2.16. Color code: red - O, blue - N, yellow - S, grey - C, rose - F. Taken from **Publication VI** figure 1.

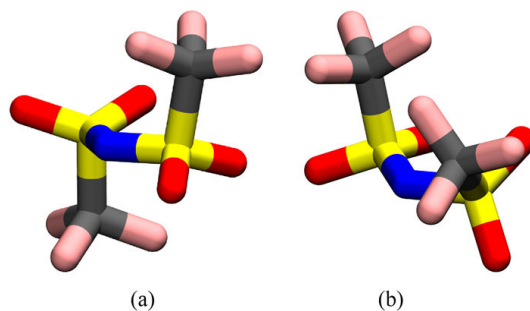


Figure 2.14: Ab initio calculated global minimum (a) and local minimum (b) energy conformation of the $[\text{NTf}_2]$ -anion. These conformations are supported by earlier QM calculations from Lopes et al. [63] as well as Raman experiments by Fujii et al. [62]. Color code: red - O, blue - N, yellow - S, grey - C, rose - F. Taken from **Publication VI** figure 2.

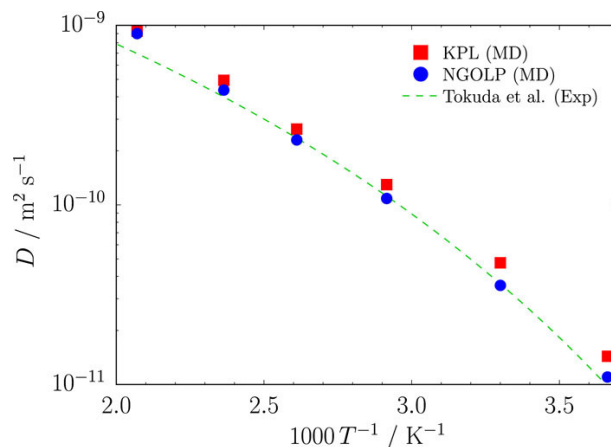


Figure 2.15: Self-diffusion coefficients calculated from MD simulations with equation 2.1 employing the KPL force field (red squares) and the NGOLP force field (blue dots) as function of the temperature in $[\text{C}_2\text{MIm}][\text{NTf}_2]$ in comparison to experimental values by Tokuda et al. (green dashed line) [64]. Original figure: **Publication VI** figure 12.

A closer look at the conformational energy landscape of the $[\text{NTf}_2]$ -anion offers more insight into the problem. For the KPL force field, one global minimum structure and two local minimum structures are observed (figure 2.16, top). However, due to the symmetry of the anion, two global minimum conformations as well as four local minimum structures are expected. In **Publication VI**, it is shown that the misrepresentation of the conformational space is caused by ill-fitted dihedral angles along the main bonding axis. With a new fitting scheme, it is possible to fit the dihedral angles S-N-S-C as well as F-C-S-N to QM calculations,

which are in agreement with experimental observations. To differentiate the new parameters from the KPL force field, they are collected in a new [NTf₂]-anion force field called NGOLP. The conformational energy landscape of the [NTf₂]-anion for the NGOLP force field shows the expected two global and four local minima conformations (figure 2.16, bottom).

The NGOLP force field model not only describes the structural features of the IL better than the KPL force field, but it also describes other properties, as good as the KPL model or even better. As an example, the diffusion coefficient of the [NTf₂]-anion in [C₂MIm][NTf₂] is calculated as function of the temperature (figure 2.15): The results of the KPL model are already in good agreement with the experiment, however, using the new dihedral optimized model, the agreement between experiment and MD simulations is even better.

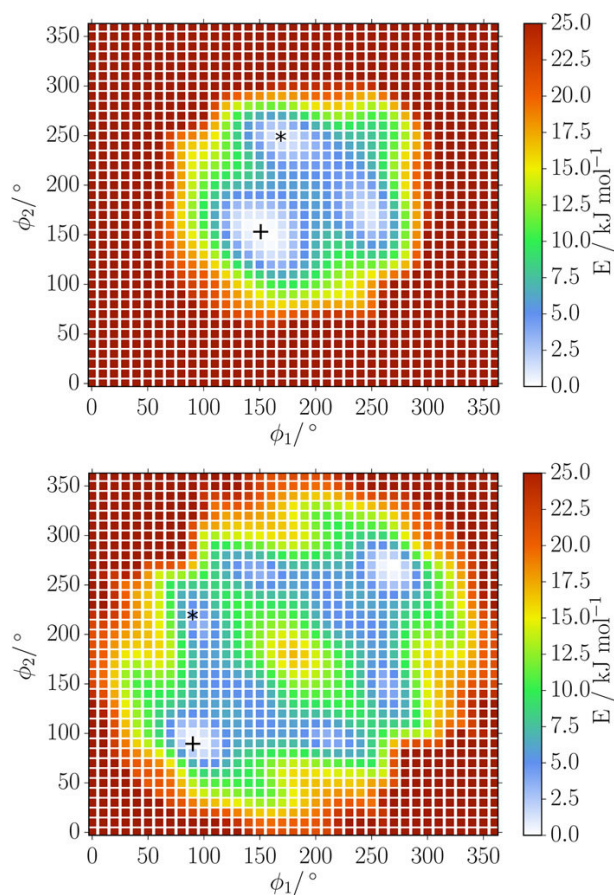


Figure 2.16: Comparison of the potential energy surfaces for the [NTf₂]-anion calculated with the KPL force field (top panel) and the NGOLP force field (bottom panel). Only the NGOLP force field shows the expected symmetry. Global minima are marked with a plus-sign, local minima with an asterisk. Taken from **Publication VI** figure 4.

2.4.2 A Force Field Conversion Tool Based on XML - ForConX

The development and optimization of a force field, which is able to represent the experimentally observed properties, is essential. But it is also important to take a look at how accessible the new model is and how other researchers can use it. Since everything described to this point was done with the MD simulations program GROMACS, only researchers who are working with GROMACS can directly use the presented force fields. If a different MD code is used, a careful conversion of the given force field is needed. This is challenging, since there are numerous pitfalls to keep in mind when converting force fields between different MD codes. In **Publication VI**, in order to make this process easier and help scientists to reliably convert force fields, Prof. Christian Schröder (University of Vienna) assembled researchers from Germany, Austria, France and Portugal, who use different MD codes in their research. In collaboration, a Python tool called ForConX (*A Forcefield conversion tool based on XML*) was developed. During the development of the tool five different MD codes were used, AMBER[65, 66], CHARMM [49], GROMACS [48], LAMMPS [67] and DL Poly [68].

Since the conversion is done in a two-step process it is easy to add more MD codes (figure 2.17). The first step is a conversion of the force field into a standardized XML format. In a second step the force field in the XML format can be converted into force fields for other MD codes. This allows each researcher to work on their part of the code, conversion into XML and conversion from XML can be done without knowledge of the other MD codes. It is only necessary to know the XML norm, which is explained in the publication.

In the following section some examples for difficulties in the conversion of force field parameters between GROMACS and CHARMM are given. First of all, GROMACS and CHARMM work with different units. Where GROMACS is using kJ and nm, CHARMM is using kcal and Å. Furthermore, both codes use different ways to calculate the bonding between two atoms. In GROMACS, as shown in equation 1.9, the bond is calculated with:

$$V_{\text{bond,GROMACS}} = \sum_b \frac{1}{2} k_{ij,\text{GROMACS}}^b (r_{ij} - r_{ij}^0)^2, \quad (2.11)$$

whereas in CHARMM the same potential is described with:

$$V_{\text{bond,CHARMM}} = \sum_b k_{ij,\text{CHARMM}}^b (r_{ij} - r_{ij}^0)^2. \quad (2.12)$$

For a conversion of a force field between the two codes, one must keep the factor of 1/2 in mind,

$$k_{ij,\text{CHARMM}}^b = \frac{1}{2} k_{ij,\text{GROMACS}}^b. \quad (2.13)$$

This is true for the bond and angle potentials, but not for the dihedral potentials, since GROMACS does not use the factor of 1/2 for the constant of the dihedral angle (equation

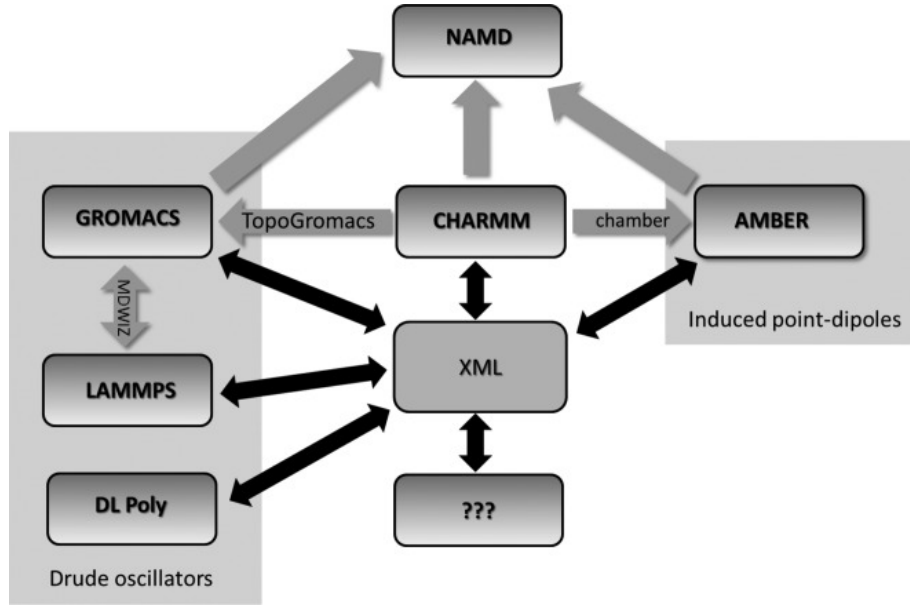


Figure 2.17: Overview of MD codes include in ForConX at the moment, as well as conversion possibilities and used methods for including polarizability. Taken from **Publication VII** figure 1.

1.12). Another example is the described LJ potential (equation 1.5): GROMACS directly uses the LJ parameters σ and ϵ , where CHARM is using r_{\min} and $-\epsilon$. The LJ parameter σ and r_{\min} are connected via

$$r_{\min} = \sqrt[6]{2}\sigma. \quad (2.14)$$

These are just some pitfalls which need to be navigated when successfully converting a force field between the various MD codes. Units and factors of $1/2$ are easily overlooked. But ForConX was not only developed for the conversion of classical MD simulation parameters, it also deals with parameters from polarizable force fields.

The field of polarizable simulations is broad and beyond the scope of this thesis, but in general, in polarizable simulations it is possible to explicitly consider the polarizability of atoms. There are different methods how the polarizability can be included. GROMACS, LAMMPS, DL-Poly and CHARM use Drude oscillators, whereas AMBER employs induced point-dipoles. Especially for ILs these kinds of simulation are very promising, a very good overview over polarizable simulation in the field of ILs and electrolytes is given by Bderov et al. [69].

To prove that the conversion of the force fields is working as intended, different MD simulations were done. To compare the results from the simulations, energy differences between the MD-codes are calculated. The energy differences between the different MD

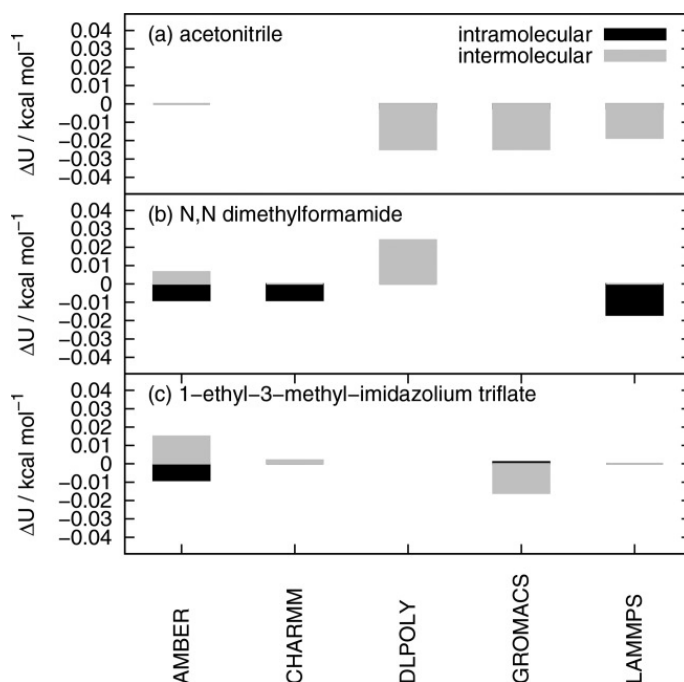


Figure 2.18: Three examples of energy discrepancies after conversion of a force field using ForConX: (a) the conversion of a CHARMM force field for acetonitrile, (b) the conversion of a GROMACS force field for N,N-dimethylformamide and (c) the conversion of a DL-Poly force field for 1-ethyl-3-methylimidazolium triflate. Taken from **Publication VII** figure 8.

codes are quite small (figure 2.18), suggesting that the conversion of the force fields is successful. A small difference in these energies is expected, since different MD codes can use different algorithms to solve the equations shown in section 1.3. Scientists should keep in mind that no conversion of a force field will be perfect. Nevertheless, ForConX is a useful tool to avoid human errors in the conversion.

3 Perspective

From **Publications I–V** the hydrogen bonding in PILs can be better understood. These studies can be expanded to other PILs. It would be very interesting to investigate mixtures of PILs where the cation offers two hydrogen bond donors, leading to a 3D-structured hydrogen bond network. Furthermore, it could be exciting to add a third anion to the mixture by adding for example [TEA][NTf₂] to the mixture.

The simple lattice model, which has proven to be very useful, should be expanded to other ILs and be further investigated. It is an intriguing model and the limits should be thoroughly tested.

From the MD simulations point, there are a few very interesting possibilities for the future. Firstly, the interaction of the [OMs]-anion with the [TEA]-cation seems to be overestimated in the present force field, it could be worthwhile redefining these parameters. But even more interesting are probably the uses of polarizable force fields. As briefly mentioned in section 2.4, polarizable simulations will be important in the future. The reason why polarizable MD simulations are so critical is simple: it is well known that classical MD simulations of ILs tend to underestimate the dynamic properties of the ions [70–74], which could also be shown for [TEA][OTf] and [TEA][OMs] [75–77].

There are different methods to deal with this problem, charge scaling [72, 78–80] or the more sophisticated polarizable simulations [81–84]. Charge scaling is simple and cheap but has its problems, where polarizable simulations are more complicated and expensive [85, 86]. First simulations with charge scaling were already done, and they look promising, this should be further investigated. It was also tried to run polarizable simulations with the force fields described in this work, unfortunately this is quite difficult, as described in section 1.3. The force fields of the anions are based on the [NTf₂]-anion parameters of the KPL force field. In this force field, the LJ parameters are highly optimized, and significantly changed in comparison to the original force field. Therefore, the polarization is in a way already considered. Adding polarizability leads to instable MD simulations. For future research with polarizable simulation, the force field should be changed, a starting point could be the new parameters by Pádua et al. [40].

As for ForConX, it was developed in the working group of Prof. Christian Schröder because it was needed. At that time, Prof. Christian Schröder who is an expert on polarizable

simulations, worked with the MD code CHARMM. He had many visiting students, who wanted to learn about polarizable simulation and use them with their substances. Most of the time the students did not use CHARMM, but a different MD code, so a conversion was necessary. This leads to the general question: How are force fields published? Is it necessary to have a standardized way of publishing force fields? It would be thinkable, that a force field can be published as before but in addition, it must be published in a standardized format, a XML format as used by ForConX. Maybe ForConX could even become a central part of the future of publishing force fields. These thoughts belong to the ambition of the NFDI4Chem [87, 88] which strives to establish FAIR data [89], good research data management and standards. Starting the conversation by explaining ForConX to the *Task Area 4 — Standards* of the NFDI4Chem is a promising next step.

Bibliography

- (1) T. Köddermann, D. Paschek and R. Ludwig, *ChemPhysChem*, 2007, **8**, 2464–2470.
- (2) J. Neumann, B. Golub, L.-M. Odebrecht, R. Ludwig and D. Paschek, *J. Chem. Phys.*, 2018, **148**, 193828/1–9.
- (3) F. Franks and D. J. G. Ives, *Quart. Rev.*, 1966, **20**, 1–44.
- (4) P. A. Hunt, C. R. Ashworth and R. P. Matthew, *Chem. Soc. Rev.*, 2015, **44**, 1257–1288.
- (5) B. Kirchner, *J. Phys.: Condens. Matter*, 2015, **27**, 463002/1–15.
- (6) K. N. Mars, J. A. Boxall and R. Lichtenthaler, *Fluid Phase Equilib.*, 2004, **219**, 93–98.
- (7) H. Niedermeyer, J. P. Hallett, I. J. Villar-Garcia, P. A. Hunt and T. Welton, *Chem. Soc. Rev.*, 2012, **42**, 7780–7802.
- (8) G. Chatel, J. F. B. Pereira, V. Debbeti, H. Wang and R. D. Rogers, *Green Chem.*, 2014, **16**, 2051–2083.
- (9) R. D. Rogers and K. R. Seddon, *Science*, 2003, **302**, 792–793.
- (10) T. Welton, *Biophys. Rev.*, 2018, **10**, 691–706.
- (11) *CRC Handbook of Chemistry and Physics*, ed. W. M. Haynes, CRC Press, 95th edn., 2014, pp. 4–89.
- (12) *CRC Handbook of Chemistry and Physics*, ed. W. M. Haynes, CRC Press, 95th edn., 2014, pp. 6–175.
- (13) R. Hayes, G. G. Warr and R. Atkin, *Chem. Rev.*, 2015, **115**, 6357–6426.
- (14) M. Watanabe, M. L. Thomas, S. Zhang, K. Ueno, T. Yasuda and K. Dokko, *Chem. Rev.*, 2017, **117**, 7190–7239.
- (15) J. G. Huddleston, H. D. Willauer, R. P. Swatloski, A. E. Visser and R. D. Rogers, *Chem. Commun.*, 1998, **16**, 2399–2407.
- (16) T. Welton, *Chem. Rev.*, 1999, **99**, 2071–2083.
- (17) M. J. Earle and K. R. Seddon, *Pure Appl. Chem.*, 2000, **72**, 1391–1398.
- (18) K. R. Seddon, *Chem. Commun.*, 2001, **23**, 2399–2407.

- (19) N. V. Plechkova and K. R. Seddon, *Chem. Soc. Rev.*, 2008, **37**, 123–150.
- (20) J. P. Hallett and T. Welton, *Chem. Rev.*, 2011, **111**, 3508–3576.
- (21) A. Stoppa, R. Buchner and G. Hefter, *J. Mol. Liq.*, 2010, **153**, 46–51.
- (22) L. F. Lepre, M. Costa Gomes, A. A. H. Pádua, R. A. Ando and M. C. C. Ribeiro, *J. Phys. Chem. B*, 2019, **123**, 6579–6587.
- (23) R. Hayes, S. Imberti, G. G. Warr and R. Atkin, *Angew. Chem. Int. Ed.*, 2013, **52**, 4623–4627.
- (24) T. L. Greaves and C. J. Drummond, *Chem. Rev.*, 2015, **115**, 11379–11448.
- (25) K. Dong, S. Zhang and J. Wang, *Chem. Commun.*, 2016, **52**, 6744–6764.
- (26) T. L. Greaves and C. J. Drummond, *Chem. Rev.*, 2008, **108**, 206–237.
- (27) K. Fumino, V. Fossog, K. Wittler, R. Hempelmann and R. Ludwig, *Angew. Chem.*, 2013, **125**, 2425–2429.
- (28) K. Fumino, S. Reimann and R. Ludwig, *Phys. Chem. Chem. Phys.*, 2014, **16**, 21903–21929.
- (29) I. V. Fedorova and L. P. Safonova, *J. Phys. Chem. A*, 2019, **123**, 293–300.
- (30) J. E. Lennard-Jones, *Math. Proc. Camb. Philos. Soc.*, 1931, **27**, 469–480.
- (31) J. N. Canongia Lopes, J. Deschamps and A. A. H. Pádua, *J. Phys. Chem. B*, 2004, **108**, 2038–2047.
- (32) J. N. Canongia Lopes and A. A. H. Pádua, *J. Phys. Chem. B*, 2004, **108**, 16893–16898.
- (33) J. N. Canongia Lopes and A. A. H. Pádua, *J. Phys. Chem. B*, 2006, **110**, 19586–19592.
- (34) J. N. Canongia Lopes, A. A. H. Pádua and K. Shimizu, *J. Phys. Chem. B*, 2008, **112**, 5039–5046.
- (35) K. Shimizu, D. Almantariotis, M. F. Costa Gomes, A. A. H. Pádua and J. N. Canongia Lopes, *J. Phys. Chem. B*, 2010, **114**, 3592–3600.
- (36) J. N. Canongia Lopes and A. A. H. Pádua, *Theor. Chem. Acc.*, 2012, **131**, 1129/1–11.
- (37) C. E. S. Bernardes and J. N. Canongia Lopes, *J. Chem. Theory Comput.*, 2017, **13**, 6167–6176.
- (38) A. S. L. Gouveia, C. E. S. Bernardes, L. I. N. Tomé, E. I. Lozinskaya, Y. S. Vygodskii, A. S. Shaplov, J. N. Canongia Lopes and I. M. Marrucho, *Phys. Chem. Chem. Phys.*, 2017, **19**, 29617–29624.
- (39) K. Goloviznina, J. N. Canongia Lopes, M. Costa Gomes and A. A. H. Pádua, *J. Chem. Theory Comput.*, 2019, **15**, 5858–5871.

-
- (40) K. Goloviznina, Z. Gong, M. F. Costa Gomes and A. A. H. Pádua, *J. Chem. Theory Comput.*, 2021, **17**, 1606–1617.
- (41) K. Ishione, G. Ori and M. Boero, *Phys. Chem. Chem. Phys.*, 2022, **24**, 9597–9607.
- (42) T. Mangin, R. Schurhammer and G. Wipff, *J. Phys. Chem. B*, 2022, **126**, 2876–2890.
- (43) O. Borodin, *J. Phys. Chem. B*, 2009, **113**, 11463–11478.
- (44) S. Gehrke and B. Kirchner, *J. Chem. Eng. Data*, 2020, **65**, 1146–1158.
- (45) H. Krienke, V. Vlachy, G. Ahn-Ercan and I. Bakó, *J. Phys. Chem. B*, 2009, **113**, 4360–4371.
- (46) M. G. Martin and J. I. Siepmann, *J. Phys. Chem. B*, 1998, **102**, 2569–2577.
- (47) J. L. F. Abascal and C. Vega, *J. Chem. Phys.*, 2005, **123**, 234505/1–12.
- (48) M. J. Abraham, T. Murtola, R. Schulz, S. Páll, J. C. Smith, B. Hess and E. Lindahl, *SoftwareX*, 2015, **1-2**, 19–25.
- (49) B. R. Brooks, C. L. Brooks III, A. D. MacKerell, L. Nilsson, R. J. Petrella, B. Roux, Y. Won, G. Archontis, C. Bartels, S. Boresch, A. Caffisch, L. Caves, Q. Cui, A. R. Dinner, M. Feig, S. Fischer, J. Gao, M. Hodoscek, W. Im, K. Kuczera, T. Lazaridis, J. Ma, V. Ovchinnikov, E. Paci, R. W. Pastor, C. B. Post, J. Z. Pu, M. Schaefer, B. Tidor, R. M. Benable, H. L. Woodcock, X. Wu, W. Yang, D. M. York and M. Karplus, *J. Comp. Chem.*, 2009, **30**, 1545–1615.
- (50) K. Fumino, V. Fossog, P. Stange, K. Wittler, W. Polet, R. Hempelmann and R. Ludwig, *ChemPhysChem*, 2014, **15**, 2604–2609.
- (51) R. Kubo, *J. Phys. Soc. Jpn.*, 1957, **12**, 570–586.
- (52) E. Helfand, *Phys. Rev.*, 1960, **119**, 1–9.
- (53) E. Arunan, G. R. Desiraju, R. A. Klein, J. Sadlej, I. Scheiner, S. Alkorta, D. C. Clary, R. H. Crabtree, J. J. Dannenberg, P. Hobza, H. G. Kjaergaard, A. C. Legon, B. Mennucci and D. J. Nesbitt, *Pure Appl. Chem.*, 2011, **83**, 1619–1636.
- (54) E. Arunan, G. R. Desiraju, R. A. Klein, J. Sadlej, I. Scheiner, S. Alkorta, D. C. Clary, R. H. Crabtree, J. J. Dannenberg, P. Hobza, H. G. Kjaergaard, A. C. Legon, B. Mennucci and D. J. Nesbitt, *Pure Appl. Chem.*, 2011, **83**, 1637–1641.
- (55) E. Arunan, *J. Indian Inst. Sci.*, 2020, **100:1**, 249–255.
- (56) L. E. Shmukler, I. V. Fedorova, M. S. Gruzdev and L. P. Safonova, *J. Phys. Chem. B*, 2019, **123**, 10794–10806.
- (57) J. F. Mora Cardozo, T. Burankova, J. P. Embs, A. Benedetto and P. Ballone, *J. Phys. Chem. B*, 2017, **121**, 11410–11423.

- (58) C. Schröder and O. Steinhauser, *J. Chem. Phys.*, 2012, **137**, 094501/1–12.
- (59) *The Structure of Ionic Liquids*, ed. R. Caminiti and L. Gontrani, Springer Cham, 2014.
- (60) O. Redlich and A. T. Kister, *Ind. Eng. Chem.*, 1948, **40**, 345–348.
- (61) P. Stange, K. Fumino and R. Ludwig, *Angew. Chem.*, 2013, **125**, 3064–3068.
- (62) K. Fujii, T. Fujiimori, T. Takamuku, R. Kanzaki, Y. Umebayashi and S. Ishiguro, *J. Phys. Chem. B*, 2006, **110**, 8179–8183.
- (63) J. N. Canongia Lopes, K. Shimizu, A. A. H. Pádua, Y. Umebayashi, S. Fukuda, K. Fujii and S. Ishiguro, *J. Phys. Chem. B*, 2008, **112**, 1465–1472.
- (64) H. Tokuda, K. Hayamizu, K. Ishii, M. A. B. H. Susan and M. Watanabe, *J. Phys. Chem. B*, 2005, **109**, 6103–6110.
- (65) D. A. Case, T. E. Cheatham, T. Darden, H. Gohlke, R. Luo, K. M. Merz, J. A. Onufriev, C. Simmerling, B. Wang and R. Woods, *J. Computat. Chem.*, 2005, **26**, 1668–1688.
- (66) R. Salomon-Ferrer, D. A. Case and R. C. Walker, *WIREs Comput. Mol. Sci.*, 2013, **3**, 198–210.
- (67) A. P. Thompson, H. M. Aktulga, R. Berger, D. S. Bolintineanu, W. M. Brown, P. S. Crozier, P. J. in 't Veld, A. Kohlmeyer, S. G. Moore, T. D. Nguyen, R. Shan, M. J. Stevens, J. Tranchida, C. Trott and S. J. Plimpton, *Comp. Phys. Comm.*, 2022, **271**, 108171/1–34.
- (68) https://www.scd.stfc.ac.uk/Pages/DL_POLY.aspx accessed 03/10/2022.
- (69) D. Bedrov, J.-P. Piquemal, O. Borodin, A. D. MacKerell, J. B. Roux and C. Schröder, *Chem. Rev.*, 2019, **119**, 7940–7995.
- (70) T. Yan, C. J. Burnham, M. G. Del Pópolo and G. A. Voth, *J. Phys. Chem. B*, 2004, **108**, 11877–11881.
- (71) A. Bagno, F. D'Ámico and G. Saielli, *J. Mol. Liq.*, 2007, **131-134**, 17–23.
- (72) B. L. Bhargava and S. Balasubramanian, *J. Chem. Phys.*, 2005, **123**, 144505/1–8.
- (73) D. Bedrov, O. Borodin, Z. Li and G. D. Smith, *J. Phys. Chem. B*, 2010, **114**, 4984–4997.
- (74) A. de Oliveira Cavalcante, M. C. C. Ribeiro and M. S. Skaf, *J. Chem. Phys.*, 2014, **140**, 144108/1–10.
- (75) M. Strauch, A.-M. Bonsa, B. Golub, V. Overbeck, D. Michalik, D. Paschek and R. Ludwig, *Phys. Chem. Chem. Phys.*, 2016, **18**, 17788–17794.

-
- (76) A. E. Khudozhitkov, P. Stange, B. Golub, D. Paschek, A. G. Stepanov, D. I. Kolokolov and R. Ludwig, *Angew. Chem.*, 2017, **129**, 14500–1505.
- (77) V. Overbeck, B. Golub, H. Schröder, A. Appellhagen, D. Paschek, K. Neymeyer and R. Ludwig, *J. Mol. Liq.*, 2020, **319**, 114207.
- (78) M. H. Ghatee, A. R. Zolghadr, F. Moosavi and Y. Ansari, *J. Chem. Phys.*, 2012, **136**, 124706/1–14.
- (79) R. Ishizuka and N. Matubayasi, *J. Chem. Theory Comput.*, 2016, **12**, 804–811.
- (80) R. Ishizuka and N. Matubayasi, *J. Comp. Chem.*, 2017, **38**, 2559–2569.
- (81) G. Lamoureux and B. Roux, *J. Chem. Phys.*, 2003, **119**, 3025–3039.
- (82) C. Schröder and O. Steinhauser, *J. Chem. Phys.*, 2010, **133**, 154511/1–13.
- (83) J. A. Lemkul, B. Roux, D. van der Spoel and D. J. MacKerell, *J. Comp. Chem.*, 2015, **36**, 1473–1479.
- (84) J. A. Lemkul, J. Huang, B. Roux and D. J. MacKerell, *Chem. Rev.*, 2016, **116**, 4983–5013.
- (85) C. Schröder, *Phys. Chem. Chem. Phys.*, 2012, **14**, 3089–3102.
- (86) F. Dommert, K. Wendler, R. Berger, L. D. Site and C. Holm, *ChemPhysChem*, 2012, **13**, 1625–1637.
- (87) S. Herres-Pawlis, O. Koepler and C. Steinbeck, *Angew. Chem.*, 2019, **58**, 10766–10768.
- (88) C. Steinbeck, O. Koepler, F. Bach, S. Herres-Pawlis, N. Jung, J. C. Liermann, S. Neumann, M. Razum, C. Baldauf, F. Biedermann, T. W. Bocklitz, F. Boehm, F. Broda, P. Czodrowski, T. Engel, M. G. Hicks, S. M. Kast, C. Kettner, W. Koch, G. Lanza, A. Link, R. A. Mata, W. E. Nagel, A. Porzel, N. Schlörer, T. Schulze, H.-G. Weinig, W. Wenzel, L. A. Wessjohann and S. Wulle, *Res. Ideas Outcomes*, 2020, **6**, e55852/1–100.
- (89) M. D. Wilkinson, M. Dumontier, I. J. Aalbersberg, G. Appleton, M. Axton, A. Baak, N. Blomberg, J.-W. Boiten, L. B. da Silva Santos, P. E. Bourne, J. Bouwman, A. J. Brookes, T. Clark, M. Crosas, I. Dillo, O. Dumon, S. Edmunds, C. T. Evelo, R. Finkers, A. Gonzales-Beltran, A. J. G. Gray, P. Groth, C. Goble, J. S. Grethe, J. Heringa, P. A. C. Hoen, R. Hooft, T. Kuhn, R. Kok, J. Kok, S. J. Lusher, M. E. Martone, A. Mons, A. L. Packer, P. Persson, B. Rocca-Serra, M. Roos, R. van Schaik, S.-A. Sansone, E. Schultes, T. Sengstag, T. Slater, G. Strawn, M. A. Swertz, M. Thompson, J. van der Lei, E. van Mulligen, H. Velterop, P. Waagmeester, A. Wittenburg, K. Wolstencroft, J. Zhao and B. Mons, *Sci. Data*, 2016, **3**, 160018/1–9.
- (90) <https://credit.niso.org/contributor-roles-defined/> accessed 03/10/2022.

- (91) A. O. Holcombe, *Publications*, 2019, **7**, 1–11.
- (92) L. Allen, A. O’Connell and V. Kiermer, *Lern. Publ.*, 2019, **32**, 71–74.

4 Publications

The contribution to the publication is given by naming the contribution roles according to Contributor Roles Taxonomy (CRediT) [90–92].

4.1 Overview

Publication I

Non-Ideal Mixing Behavior of Hydrogen Bonding in Mixtures of Protic Ionic Liquids

K. Fumino, A.-M. Bónsa, B. Golub, D. Paschek and R. Ludwig
ChemPhysChem, 2015, **15**, 299-304

CRediT roles: Formal analysis (MD simulations), Investigation (MD simulations), Visualization (MD simulations)

Approximated contribution to the publication in percent: 20 %

Publication II

Hydrogen Bonding in a Mixture of Protic Ionic Liquids: A Molecular Dynamics Simulation Study

D. Paschek, B. Golub and R. Ludwig
Phys. Chem. Chem. Phys., 2015, **17**, 8431-8440

CRediT roles: Formal analysis, Investigation, Visualization

Approximated contribution to the publication in percent: 40 %

Publication III

Hydrogen Bond Redistribution Effects in Mixtures of Protic Ionic Liquids Sharing the Same Cation: Nonideal Mixing with Large Negative Mixing Enthalpies

B. Golub, D. Ondo, V. Overbeck, R. Ludwig and D. Paschek

Phys. Chem. Chem. Phys., 2022, **24**, 14740-14750

CRedit roles: Data curation (MD simulations), Formal analysis (MD simulations), Investigation (MD simulations), Visualization, Writing - original draft
Approximated contribution to the publication in present: 50 %

Publication IV

Why Do Liquids Mix? The Mixing of Protic Ionic Liquids Sharing the Same Cation is Apparently Driven by Enthalpy, not Entropy

B. Golub, D. Ondo, R. Ludwig and D. Paschek

J. Phys. Chem. Lett., 2022, **13**, 3556-3561

CRedit roles: Formal analysis (MD simulations), Investigation (MD simulations), Visualization, Writing - review & editing
Approximated contribution to the publication in present: 40 %

Publication V

Balance Between Contact and Solvent-Separated Ion Pairs in Mixtures of the Protic Ionic Liquid [Et₃NH][MeSO₃] with Water Controlled by Water Content and Temperature

B. Golub, K. Fumino, P. Stange, V. Fossog, R. Hempelmann, D. Ondo, D. Paschek, R. Ludwig

J. Phys. Chem. B, 2021, **125**, 4476-4488

CRedit roles: Formal analysis (MD simulations), Investigation (MD simulations), Visualization (MD simulations), Writing - review & editing
Approximated contribution to the publication in present: 30 %

Publication VI

Revisiting Imidazolium Based Ionic Liquids: Effect of the Conformation Bias of the [NTf₂] Anion Studied by Molecular Dynamics Simulations

J. Neumann, B. Golub, L.-M. Odebrecht, R. Ludwig and D. Paschek

J. Chem. Phys., 2018, **148**, 193828/1-9

CRedit roles: Formal analysis, Investigation, Visualization, Methodology, Writing - original draft (equal)

Approximated contribution to the publication in percent: 30 %

Publication VII

ForConX: A Forcefield Conversion Tool Based on XML

V. Lesch, D. Diddens, C. E. S. Bernardes, B. Golub, A. Dequidt, V. Zeindlhofer, M. Sega
and C. Schröder

J. Comp. Chem., 2017, **28**, 629-638

CRedit roles: Software (Gromacs part, equal), Writing - review & editing

Approximated contribution to the publication in percent: 20 %

4.2 Publication I

Non-Ideal Mixing Behavior of Hydrogen Bonding in Mixtures of Protic Ionic Liquids

K. Fumino, A.-M. Bonga, B. Golub, D. Paschek and R. Ludwig
ChemPhysChem, 2015, **15**, 299-304

CRedit roles: Formal analysis (MD simulations), Investigation (MD simulations), Visualization (MD simulations)

Approximated contribution to the publication in percent: 20 %

Reprinted from K. Fumino, A.-M. Bonga, B. Golub, D. Paschek and R. Ludwig, *ChemPhysChem*, 2015, **15**, 299-304, with the permission of John Wiley and Sons.

Non-Ideal Mixing Behaviour of Hydrogen Bonding in Mixtures of Protic Ionic Liquids

Koichi Fumino,^[a] Anne-Marie Bonsa,^[a] Benjamin Golub,^[a] Dietmar Paschek,^[a, b] and Ralf Ludwig^{*[a, b]}

Ionic liquids (ILs) attract interest in science and technology as a result of their unique properties. Binary and ternary mixtures of ILs significantly increase the number of possible cation/anion combinations, resulting in targeted physical and chemical properties. In this work, we study the mixing behaviour of two protic ILs: triethyl ammonium methylsulfonate [Et₃NH][CH₃SO₃] and triethylammonium triflate [Et₃NH][CF₃SO₃]. We find a characteristic deviation from ideal mixing by means of low-frequency infrared spectroscopy. By using molecular dynamics simulations, we explain this behaviour as being the result of different strengths of anion/cation hydrogen bonding. This non-ideality of non-random H-bond mixing is also reflected in macroscopic properties such as the viscosity. Mixing suitable ILs may, thus, result in new ILs with targeted physical properties.

Since the beginning of this century, ionic liquids (ILs) have been receiving increasing interest from science and technology.^[1–4] To expand the ability of designing ILs by selection of cations and anions, binary and ternary mixtures of these coulombic fluids came into the focus of research.^[5,6] The subtle balance between Coulomb forces, hydrogen bonds and dispersion forces determines the interaction between the constituents of an IL and may result in targeted physical and chemical properties. The mixing behaviour of ILs has been reported for a number of thermodynamic and transport properties of mainly aprotic ILs.^[5–11] Physical properties such as the density and viscosity have been found to show near-ideal mixing behaviour and, therefore, vary almost linearly with the composition. Also, molar enthalpies and entropies of mixing indicated only a small deviation from ideality.^[8,9] Subtle deviations from ideal mixing behaviour for ILs were recently reported from spectroscopy studies. Quitevis and co-workers analysed optical Kerr effect (OKE) spectra for mixtures of ILs and found different behaviour for diverse mixtures.^[11] The OKE spectra result from

intermolecular vibrational modes and resemble Raman spectra. For the 1:1 mixture of [C₅C₁mim][PF₆]/[C₅C₁mim][CF₃CO₂], non-additivity was reported. The authors assumed new interactions between the mixed species, which are not present in the pure components. However, the phenomena of mixing could not be explained precisely in any of the given studies on the basis of interactions between the charged constituents. Thus, a molecular understanding of the structural and dynamical features of IL mixtures is still lacking. Recently, IL–IL mixtures received additional interest. Welton and co-workers reviewed the ideality and non-ideality of IL–IL mixtures with a focus on property changes and new opportunities for applications.^[6,7] Despite instances of non-ideal behaviour, these are still regarded as simple mixtures of two compounds. In contrast, Rogers et al. argued that IL compositions do not retain their individual nature and supported the concept of double-salt ILs (DSILs).^[5] DSILs are defined as ILs containing more than one cation or anion and presenting different physicochemical properties than that of the single ILs.

It is the purpose of this communication to understand the mixing behaviour of ILs at a molecular level. For a well-chosen binary mixture of protic ILs (PILs), we show that non-ideality can be explained by changing interaction strength between particular ions. In PILs, this interaction is considerably governed by hydrogen bonding. This goal could be achieved by using a combination of experimental and theoretical methods that provide detailed information for hydrogen-bonding characteristics upon mixing. Far-infrared (FIR) spectroscopy and molecular dynamics (MD) simulations allow molecular insight for the interaction characteristics in binary mixtures of PILs. At the end, we show that the non-ideal H-bond mixing behaviour in PIL–PIL mixtures is reflected in physical properties such as viscosity. Moreover, it can be used to accelerate or slow down anions for supporting or suppressing solvation and reaction.

Recently, we could show for pure PILs of [Et₃NH][anion] type that the ⁺N–H⁺⋯A[−] interaction results in a distinct low vibrational band observed in FIR or THz spectra. This spectral feature could be related to hydrogen bonding and was observed in the frequency range from 100 to 180 cm^{−1}, depending on the interaction strength of the anion. For [Et₃NH][CH₃SO₃] (TEAMS) and [Et₃NH][CF₃SO₃] (TEATF) PILs, these characteristic vibrational bands were observed at 149 and 129 cm^{−1}, respectively.^[12–15] Owing to the inductive effect of the fluorine atoms within the anion, the cation–anion interaction is significantly lowered indicated by a 20 cm^{−1} shift to lower wavenumbers for TEATF.^[13] The location and absorbance of this vibrational band is sensitive for the interaction strength between the PIL

[a] Dr. K. Fumino, A.-M. Bonsa, B. Golub, Dr. D. Paschek, Prof. Dr. R. Ludwig
Universität Rostock, Institut für Chemie
Abteilung für Physikalische Chemie
Dr.-Lorenz-Weg 1, 18059, Rostock (Germany)
Tel: (+ 49) 381-498-6517
E-mail: ralf.ludwig@uni-rostock.de

[b] Dr. D. Paschek, Prof. Dr. R. Ludwig
Leibniz-Institut für Katalyse
an der Universität Rostock e.V.
Albert-Einstein-Str. 29a, 18059 Rostock (Germany)

Supporting Information for this article is available on the WWW under <http://dx.doi.org/10.1002/cphc.201402760>.

constituents. But, what happens if these two PILs are mixed? Do both PILs retain their H-bond characteristics from the pure states? Is the H-bond mixing ideal? If not, can the non-ideal behaviour be detected experimentally? Can we draw some conclusion for the number and strength of H-bonding in these PIL mixtures? Is there a way to control the H-bond characteristics for assorted mixtures? And finally, is there any influence on macroscopic properties such as viscosity? All these issues are addressed in the present study.

Firstly, we would like to discuss the FIR spectra of pure TEAMS as well as its mixtures with a hydrophobic organic sol-

characteristics of the pure PILs are preserved when diluting them with CDCl_3 . This finding is in agreement with earlier results on ion speciation.^[14–16] For both PILs, the apolar solvent molecule was not able to penetrate between the cation and anion, leaving the PIL bonding characteristics untouched. Obviously, the intensities of selected vibrational bands can be used as a probe for measuring molecular interactions in particular hydrogen bonding in solution.

Secondly, we prepared molar mixtures of TEAMS and TEATF with $x=0.75$, 0.50 and 0.25 mole fraction. Following the nomenclature suggested by Niedermeyer et al.,^[6] we mixed two pure PILs, each describing one component including two constituents, resulting in two component mixtures $[\text{Et}_3\text{NH}][\text{CH}_3\text{SO}_3]_x[\text{CF}_3\text{SO}_3]_{(1-x)}$ comprising three constituents. Then, we measured the FIR spectra between 10 and 300 cm^{-1} . We obtained the mixture spectra for TEAMS and TEATF by subtracting the corresponding mole fraction of TEATF in the first and TEAMS in the latter case of the related spectra of the pure ma-

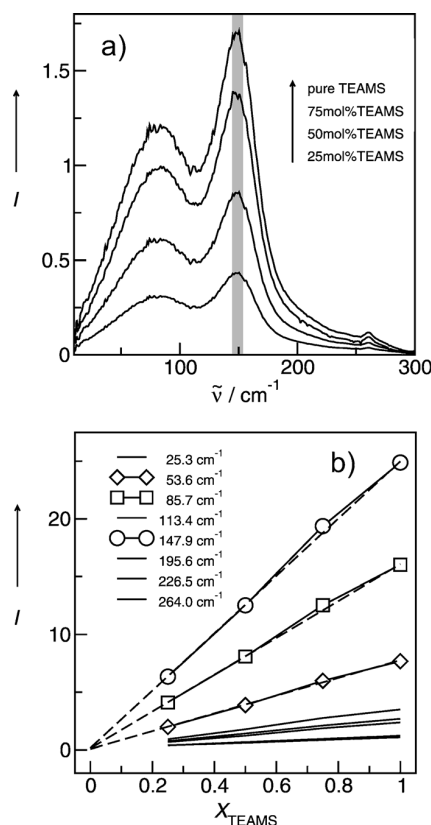


Figure 1. FIR spectra of TEAMS in mixtures with chloroform (CDCl_3). a) The intensity of the targeting vibrational band at 149 cm^{-1} decreases with increasing concentration of the solvent. b) The intensities of the deconvoluted vibrational bands decrease linearly and go through zero, indicating that the H-bond characteristics remain upon dilution in the hydrophobic environment.

vent: deuterated chloroform, CDCl_3 . In Figures 1a and 1b, it is shown that the absorbance of the distinct vibrational band at 149 cm^{-1} decreases continuously with increasing solvent concentration. If we plot the intensities of the vibrational bands versus the composition, a straight line is obtained, starting with the pure PIL absorbance and ending at zero for zero PIL concentration. This is what we would expect from an ideal mixture of TEAMS with the organic solvent. A similar behaviour is also observed for TEATF in mixtures with chloroform (see SI1–2 in the Supporting Information). Apparently, the H-bond

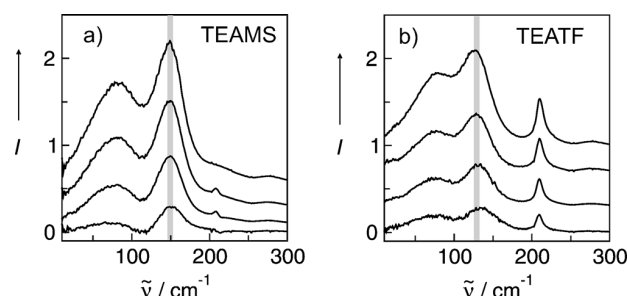


Figure 2. a) FIR spectra of the pure TEAMS and the difference spectra of the TEAMS/TEATF mixtures measured versus TEATF. b) FIR spectra of the pure TEATF and the difference spectra of the TEATF/TEAMS mixtures measured versus TEAMS. The vibrational bands at 149 and 129 cm^{-1} indicate the $^+\text{N}-\text{H}\cdots\text{A}^-$ cation–anion interaction. The intensities of these vibrational bands are used to study the mixing behaviour.

terials (see Figures 2a and 2b). As the background spectra, as well as the sample spectra, are referred to the absorption of the pure PILs in the filled IR cell, the mole-fraction-weighted results had to be corrected for the different molar volumes of TEAMS and TEATF, respectively. The deconvoluted spectra are shown in SI3–5 in the Supporting Information.

If we now plot the corrected absorbance of the distinct vibrational band $^+\text{N}-\text{H}\cdots\text{A}^-$ against the mole fraction, we find characteristic deviations from linear, and thus ideal, mixing behaviour, as shown in Figures 3a and 3b. For TEATF, including the weaker interacting triflate anion, we observe lower intensities than expected for ideal random mixing (Figure 3b). Apparently, the triflate anion forms fewer H-bonds with the triethylammonium cation in the mixtures compared to the situation in the pure PIL. It is plausible that the cations prefer to interact with the stronger H-bond acceptor anion in TEAMS and tend to replace the triflate for the methyl sulfonate anion. If this interpretation is correct, we should perhaps also observe an increased absorbance for TEAMS. Indeed, applying the same procedure results in higher intensities with increasing TEATF con-

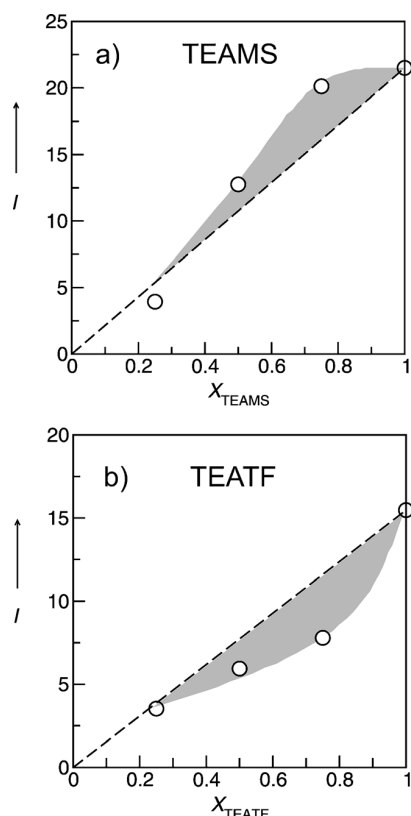


Figure 3. Non-ideal mixing behaviour in the PIL mixtures of TEAMS and TEATF. For TEAMS, we observe enhanced intensity at 149 cm^{-1} , whereas for TEATF the intensity at 129 cm^{-1} is weakened compared to the expected ideal behaviour, as indicated by the dotted line.

centration (Figure 3a). However, we would like to point out that the observation of positive deviations for the methyl sulfonate ions is perhaps not as obvious as the negative ones for the triflate ion. For TEATF, a decreasing number or strength of H-bonds should result in negative absorbance. For the positive deviation of TEAMS, however, it is necessary to consider that the methylsulfonate anion can form one, two or even three H-bonds with surrounding ethylammonium cations at the same time through the three oxygen atoms of the SO_3 group. This could explain the enhanced intensity, indicating increasing H-bond capacity. To support our experimental findings and for a more detailed interpretation, we performed MD simulations for the pure PILs and their mixtures (see SI7 in the Supporting Information).

From corresponding pair correlation functions, we could derive the distribution of the number of hydrogen bonds formed between the triflate and/or methylsulfonate anions and the ethyl ammonium cation in the mixtures. We would like to add that the probability of finding a N–H hydrogen-bond donor that is not involved in a hydrogen bond is very low, and well below 1%. In Figures 4a and 4b, it is shown whether the anions form zero, one, two or even three hydrogen bonds to the N–H bond of the cation. The hydrogen-bonding situation of the anion is similar in both pure ILs, that

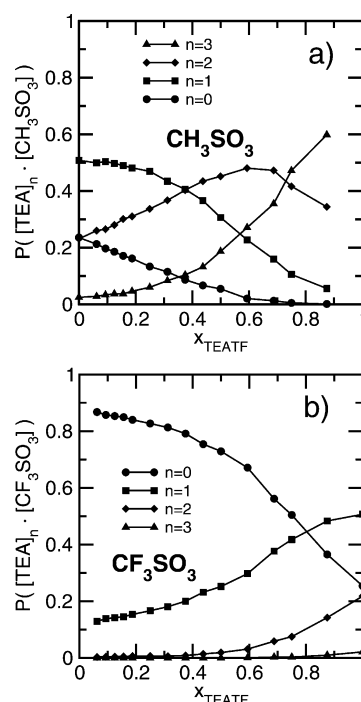


Figure 4. Probability of finding a certain number n of TEA cations attached to one type of anion through a hydrogen bond as a function of the mixture composition according to the MD simulations for a) methylsulfonate and b) triflate.

is, just over 50% of the anions form one hydrogen bond, about 25% form two hydrogen bonds and 25% are not H-bonded at all.

In the mixture, the anions compete with each other; hence, the H-bond distribution changes systematically as a function of mixture composition. For the triflate anion, with increasing TEAMS concentration the doubly bound species ($n=2$) disappear almost completely above a 1:1 mixture. Also, the fraction of single H-bonded species ($n=1$) decreases significantly. Both are replaced by non-hydrogen-bonded triflate anions ($n=0$), as shown in Figure 4b. The reverse situation is observed for TEAMS. Here, the number of non-H-bonded and single H-bonded methylsulfonate anions drastically decreases in favour of double and triple H-bonded species. As shown in Figure 4a, at a composition of $x_{\text{TEATF}}=0.9$ (the highest TEATF concentration studied), the methylsulfonate anions bind mostly two and three triethylammonium cations, whereas methylsulfonate anions with $n=0$ fully disappear and those with $n=1$ contribute only 5% of the overall number of species at this concentration.

The H-bond characteristics of both PILs in the mixtures can be summarized by an increased H bonding for TEAMS and decreased H bonding for TEATF in the TEATF/TEAMS mixtures compared to an ideal random distribution. The positive and negative deviations for the fraction of hydrogen bonds of the TEA cation to each of the anion species in the TETF/TEAMS mixtures are shown in Figure 5. For TEAMS, this fraction increases and for TEATF it decreases, indicating enhanced and

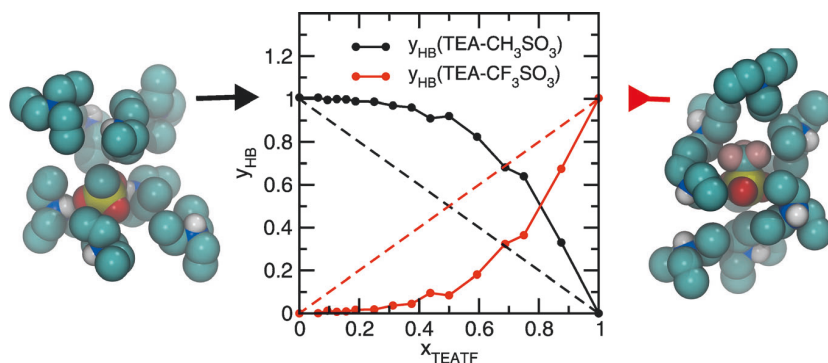


Figure 5. Fraction of hydrogen bonds of the TEA cation to one particular anion species according to MD data. The TEA cation prefers to interact with the methylsulfonate anion, as illustrated by the snapshots from the MD simulations: Two cations H-bonded to $CH_3SO_3^-$ (left) and zero cations H-bonded to $CF_3SO_3^-$.

weakened H bonding, respectively. This behaviour explains our experimental findings of increased and decreased infrared intensities compared to those expected for ideal mixing.

In addition, the effect of unequal hydrogen-bond strength is also reflected in the transport properties, such as the MD-simulated self-diffusion coefficients of the TEA cation, the triflate anion and the methylsulfonate anion in the PIL mixtures. As shown in Figure 6a, the average number of multiple H-bonded methylsulfonate anions increases with increasing TEATF concentration. On average, this number ranges from one H bond

each other for TEA, which is reducing the average size of the hydrogen-bonded aggregates, and is leading to a concerted increase of the self-diffusion coefficient of all ion species.

Now, is non-ideal H-bond mixing in the TEAMS/TEATF mixtures also reflected in physical properties, which are presently experimentally available to us? In Figure 7, the measured densities and viscosities of the pure PILs and their mixtures are shown as a function of temperature (see also SI6 in the Sup-

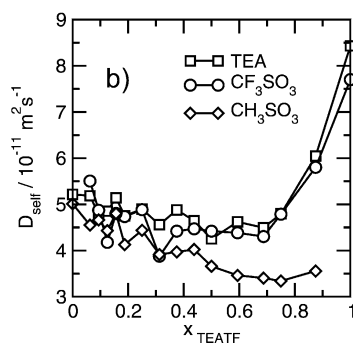
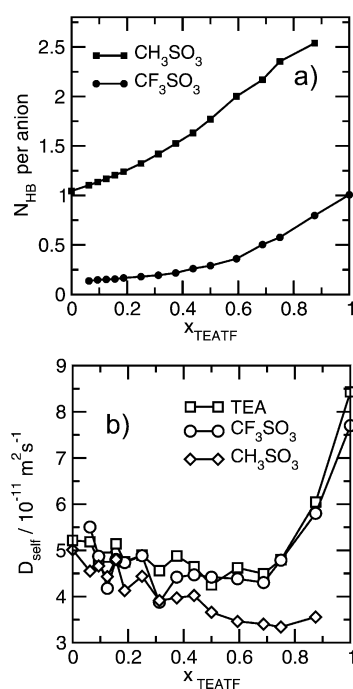


Figure 6. a) Average total number of hydrogen bonds for each of the anions to the neighbouring TEA cations as a function of composition in the TEA-triflate/TEA-methylsulfonate mixture at 400 K. b) Self-diffusion coefficients of the TEA cation, the triflate anion and the methylsulfonate anion in the TEA-triflate/TEA-methylsulfonate mixture at 400 K obtained from MD simulations.

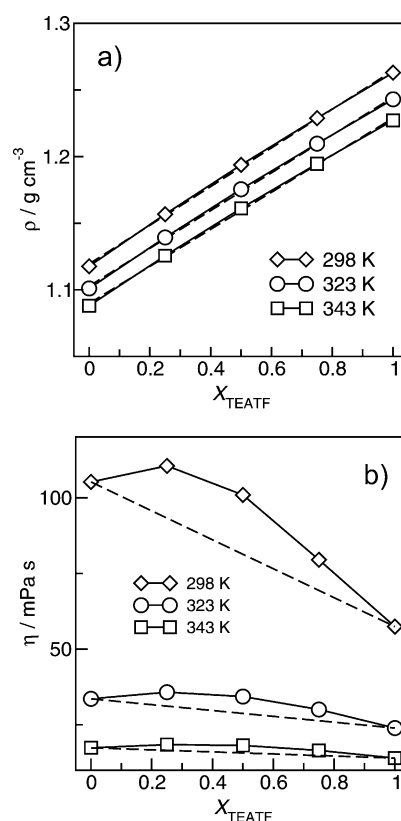


Figure 7. Measured densities (a) and viscosities (b) of the TEAMS/TEATF mixtures at three different temperatures. Whereas the densities show almost ideal mixing behaviour, the viscosities exhibit positive deviations from ideality, owing to enhanced H bonding of the MS anion.

porting Information). The densities show mainly linear behaviour with mixing. There is an almost straight line connecting the densities of the pure PILs. Obviously, the H-bond characteristic does not have any influence on the density of the mixtures in the Coulombic system. A completely different behaviour is found for the viscosities. For all PIL mixtures, the viscosity is larger than expected for ideal behaviour. However, this behaviour is in accord with our FIR spectra and can be understood from the H-bond statistics derived from our MD simulations. Starting with the pure TEAMS, we find an increase in viscosity, owing to enhanced hydrogen bonding. Here, the weak anion–cation interaction in TEATF is increasingly replaced by stronger multiple anion–cation interactions in TEAMS, leading to the formation of larger hydrogen-bonded aggregates with higher viscosity. This statement is not in contradiction to our earlier work with aprotic imidazolium-based ILs, where we claimed that hydrogen bonding can fluidise rather than toughen these Coulomb systems. In aprotic ILs with unique interaction sites, hydrogen bonds lead to the preformation of ion pairs, resulting in lower viscosities and enthalpies of vaporization.^[18–21] Instead, in PILs and their mixtures, as discussed here, the formation of multiple H bonds lead to larger H-bonded complexes, which enhance the stiffness of the coulombic fluid.

Another important aspect of this non-ideal H-bond mixing behaviour is the nearly complete H-bond stripping of the triflate anion, which can be then regarded as a ‘quasi-free anion’. Such species will be available for supporting chemical reactions or improving conductivity. In this sense, our results support the DSIL concept by Rogers and co-workers.^[5] The ions apparently change their identity in the mixture, resulting in a new liquid. We now have one pure liquid rather than two separate ILs. Our study also provides some hints for expanding the ability to design ILs by smart selection of cations and anions in binary or even ternary mixtures of ILs.

Experimental Section

The water content of the two PILs, TEAMS and TEATF was below 100 ppm, as detected by using the Karl–Fischer titration method. The PIL mixtures were prepared under an argon atmosphere and put in an ultrasonic bath until they reached homogeneity.

The FTIR measurements were performed with a Bruker Vertex 70 FTIR spectrometer equipped with an extension for measurements in the FIR region that consists a multilayer mylar beam splitter and a room-temperature DLATGS detector with preamplifier. Polyethylene (PE) windows with an internal optical path of 0.1 mm were used. Further improvement could be achieved by using a high-pressure mercury lamp and a silica beam splitter. The accessible spectral region for this configuration now lies between 10 and 680 cm^{−1} (0.3 and 20.3 THz). The spectra were deconvoluted simultaneously as well as separately into a number of Voigt profiles (convolution of Lorentzian and Gaussian functions) following the Levenberg–Marquardt procedure. The Voigt profile has four parameters: the intensity, the frequency, the half-width of the Lorentzian and the half-width of the Gaussian. The deconvolution procedure is described in detail in SI2–5 in the Supporting Information.

Temperature-dependent measurements of the density of the different mixtures were performed by using the oscillating tube densi-

tometer DSA 5000 m (Anton Paar/Austria) with internal viscosity correction. The density was determined in the range of 10–70 °C with intervals of 5 K (see SI6).

Temperature-dependent dynamic viscosities were measured with the Lovis 2000 ME (Anton Paar/Austria) microviscometer based on the rolling-ball principle. The viscosity was determined in the range of 10–70 °C with intervals of 5 K (see SI6).

We performed constant-pressure (NPT) MD simulations for 16 different mixtures of TEATF and TEAMS at a pressure of 1 bar and temperatures of 300 and 400 K. All simulated systems were composed of 256 ion pairs. A detailed description of the employed force-field parameters is provided in the Supporting Information. All simulations reported herein were performed with the GROMACS 4.5 simulation program.^[17] Simulation runs of 100 ns length with time steps of 2 fs were analysed for $T = 300$ K (24 ns for $T = 400$ K). Based on computed radial pair distribution functions, hydrogen-bonded ion pairs were identified by a $S=O \cdots H-N$ cut-off distance of 0.24 nm. For MD simulations details see SI7 in the Supporting Information.

Acknowledgements

This work was supported by the Deutsche Forschungsgemeinschaft (DFG) Priority Programme SPP 1191 “Ionic Liquids” and by the DFG Collaborative Research Centre SFB 652 “Strong correlations and collective effects in radiation fields: Coulomb systems, clusters and particles”.

Keywords: ionic liquids • IR spectroscopy • mixing behaviour • molecular dynamics • solvation chemistry

- [1] P. Wasserscheid, T. Welton, *Ionic Liquids in Synthesis*, 2nd ed., Wiley-VCH, Weinheim, **2008**.
- [2] F. Endres, S. Z. El Abedin, *Phys. Chem. Chem. Phys.* **2006**, *8*, 2101–2116.
- [3] H. Weingärtner, *Angew. Chem. Int. Ed.* **2008**, *47*, 654–670; *Angew. Chem.* **2008**, *120*, 664–682.
- [4] N. V. Plechkova, K. R. Seddon, *Chem. Soc. Rev.* **2008**, *37*, 123–150.
- [5] G. Chatel, J. F. B. Pereira, V. Debbeti, H. Wang, R. D. Rogers, *Green Chem.* **2014**, *16*, 2051–2083.
- [6] H. Niedermeyer, J. P. Hallett, I. J. Villar-Garcia, P. A. Hunt, T. Welton, *Chem. Soc. Rev.* **2012**, *41*, 7780–7802.
- [7] M. Y. Lui, L. Crowhurst, J. P. Hallett, P. A. Hunt, H. Niedermeyer, T. Welton, *Chem. Sci.* **2011**, *2*, 1491–1496.
- [8] P. Navia, J. Trouscoso, L. Romani, *J. Chem. Eng. Data* **2007**, *52*, 1369–1374.
- [9] A. Arce, M. J. Earle, S. P. Katdare, H. Rodriguez, K. R. Seddon, *Chem. Commun.* **2006**, 2548–2550.
- [10] J. N. Canongia Lopes, T. C. Cordeiro, J. M. S. S. Esperanca, H. J. R. Guedes, S. Huq, L. P. N. Rebelo, K. R. Seddon, *J. Phys. Chem. B* **2005**, *109*, 3519–3525.
- [11] D. Xiao, J. R. Rajian, L. G. Hines, Jr., S. Li, R. A. Bartsch, E. L. Quitevis, *J. Phys. Chem. B* **2008**, *112*, 13316–13325.
- [12] K. Fumino, E. Reichert, K. Wittler, R. Hempelmann, R. Ludwig, *Angew. Chem. Int. Ed.* **2012**, *51*, 6236–6240; *Angew. Chem.* **2012**, *124*, 6340–6344.
- [13] K. Fumino, V. Fossog, K. Wittler, R. Hempelmann, R. Ludwig, *Angew. Chem. Int. Ed.* **2013**, *52*, 2368–2372; *Angew. Chem.* **2013**, *125*, 2425–2429.
- [14] P. Stange, K. Fumino, R. Ludwig, *Angew. Chem. Int. Ed.* **2013**, *52*, 2990–2994; *Angew. Chem.* **2013**, *125*, 3064–3068.
- [15] K. Fumino, P. Stange, V. Fossog, R. Hempelmann, R. Ludwig, *Angew. Chem. Int. Ed.* **2013**, *52*, 12439–12442; *Angew. Chem.* **2013**, *125*, 12667–12670.

- [16] K. Fumino, V. Fossog, P. Stange, K. Wittler, W. Polet, R. Hempelmann, R. Ludwig, *ChemPhysChem* **2014**, *15*, 2604–2609.
- [17] E. Lindahl, B. Hess, D. van der Spoel, *J. Mol. Model.* **2001**, *7*, 306–317.
- [18] K. Fumino, A. Wulf, R. Ludwig, *Angew. Chem. Int. Ed.* **2008**, *47*, 8731–8734; *Angew. Chem.* **2008**, *120*, 8859–8863.
- [19] A. Wulf, K. Fumino, R. Ludwig, *Angew. Chem. Int. Ed.* **2010**, *49*, 449–453; *Angew. Chem.* **2010**, *122*, 459–463.
- [20] T. Peppel, C. Roth, K. Fumino, D. Paschek, M. Köckerling, R. Ludwig, *Angew. Chem. Int. Ed.* **2011**, *50*, 6661–6665; *Angew. Chem.* **2011**, *123*, 6791–6795.
- [21] K. Fumino, T. Peppel, M. Geppert-Rybczynska, D. H. Zaitsau, J. K. Lehmann, S. P. Verevkin, M. Köckerling, R. Ludwig, *Phys. Chem. Chem. Phys.* **2011**, *13*, 14064–14075.

Received: October 27, 2014

Published online on November 20, 2014

Supporting Information

© Copyright Wiley-VCH Verlag GmbH & Co. KGaA, 69451 Weinheim, 2015

Non-Ideal Mixing Behaviour of Hydrogen Bonding in Mixtures of Protic Ionic Liquids

Koichi Fumino,^[a] Anne-Marie Bensa,^[a] Benjamin Golub,^[a] Dietmar Paschek,^[a, b] and Ralf Ludwig^{*[a, b]}

cphc_201402760_sm_miscellaneous_information.pdf

Non-ideal mixing behavior of hydrogen bonding in mixtures of protic ionic liquids*

Koichi Fumino,^a Anne-Marie Bonsa,^a Benjamin Golub,^a Dietmar Paschek,^{a,b} and Ralf Ludwig^{a,b,}*

[*] Dr. Koichi Fumino, Dipl.-Chem. Anne-Marie Bonsa, B. Sc. Benjamin Golub, Dr. Dietmar Paschek, Prof. Dr. R. Ludwig
Universität Rostock, Institut für Chemie, Abteilung für Physikalische Chemie
Dr.-Lorenz-Weg 1, 18059, Rostock (Germany)
Tel: (+49) 381-498-6517
E-mail: ralf.ludwig@uni-rostock.de

Prof. Dr. R. Ludwig
Leibniz-Institut für Katalyse
an der Universität Rostock e.V.
Albert-Einstein-Str. 29a, 18059 Rostock (Germany)

Supporting Information

Contents

- SI1 Deconvoluted far infrared (FIR) difference spectra of TEAMS/CDCl₃ mixtures versus CDCl₃**
- SI2 Deconvoluted far infrared (FIR) difference spectra of TEATF/CDCl₃ mixtures versus CDCl₃**
- SI3 Deconvoluted far infrared (FIR) difference spectra of TEAMS/TEATF mixtures versus TEATF**

- S14 Deconvoluted far infrared (FIR) difference spectra for TEAMS/TEATF mixtures versus TEAMS**
- S15 Corrected intensities for the vibrational modes N-H ... anion in the TEAMS/TEATF mixtures for the different molar volumes of TEAMS and TEAF**
- S16 Densities and viscosities of TEAMS and TEATF and their mixtures**
- S17 Molecular dynamics (MD) simulations**

SI1 Deconvoluted far infrared (FIR) of TEAMS and TEAMS/ CDCl_3 mixtures measured versus CDCl_3 .

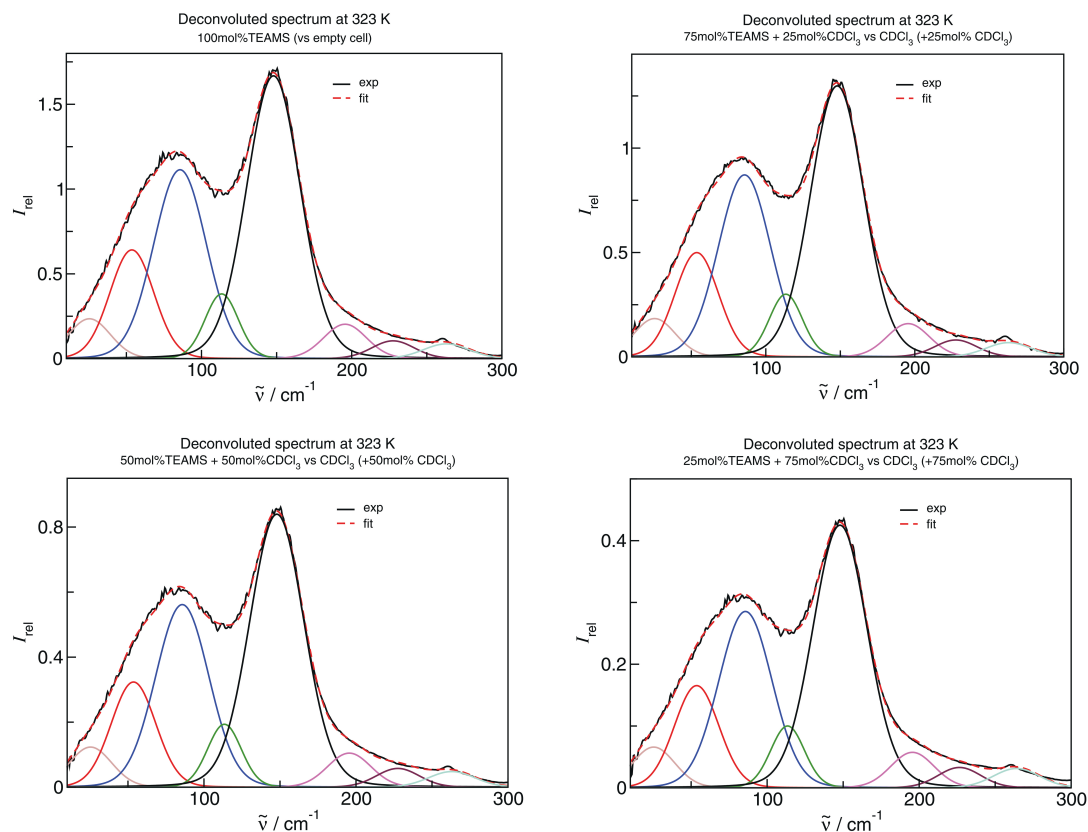


FIG1-SI Deconvoluted far infrared (FIR) difference spectra of pure triethylammonium methylsulfonate $[\text{Et}_3\text{NH}][\text{CH}_3\text{SO}_3]$ and triethylammonium methylsulfonate $[\text{Et}_3\text{NH}][\text{CH}_3\text{SO}_3]$ in mixtures with chloroform (CDCl_3) subtracting the corresponding fraction of CDCl_3 in the frequency range between 10 and 300 cm^{-1} .

SI2 Deconvoluted far infrared (FIR) of TEATF and TEATF/ CDCl_3 mixtures measured versus CDCl_3 .

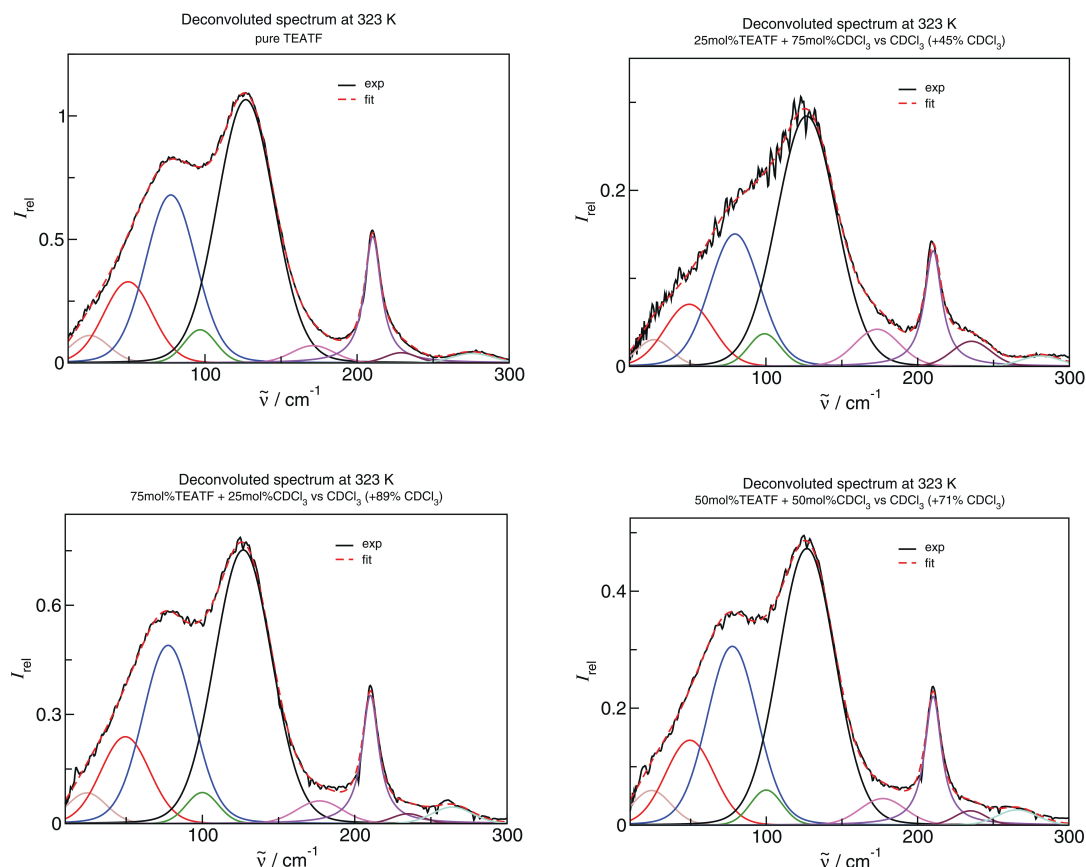


FIG2-SI Deconvoluted far infrared (FIR) difference spectra of pure triethylammonium triflate $[\text{Et}_3\text{NH}][\text{CF}_3\text{SO}_3]$ and triethylammonium triflate $[\text{Et}_3\text{NH}][\text{CF}_3\text{SO}_3]$ in mixtures with chloroform (CDCl_3) subtracting the corresponding fraction of CDCl_3 in the frequency range between 10 and 300 cm^{-1} .

SI3 Deconvoluted FIR spectra for the TEAMS/TEATF mixtures versus TEATF

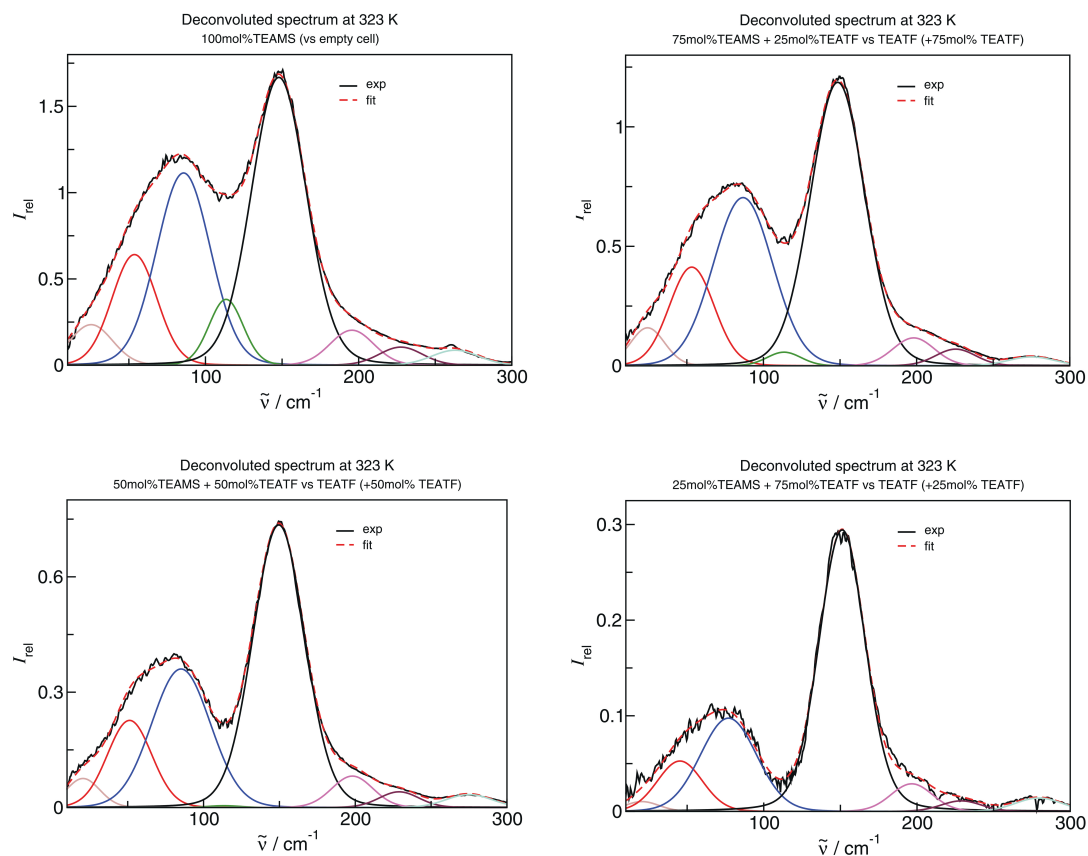


FIG3-SI Deconvoluted far infrared (FIR) difference spectra of pure triethylammonium methylsulfonate $[\text{Et}_3\text{NH}][\text{CH}_3\text{SO}_3]$ and triethylammonium methylsulfonate $[\text{Et}_3\text{NH}][\text{CH}_3\text{SO}_3]$ in mixtures with triethylammonium triflate $[\text{Et}_3\text{NH}][\text{CF}_3\text{SO}_3]$ subtracting the corresponding fraction of $[\text{Et}_3\text{NH}][\text{CF}_3\text{SO}_3]$ in the frequency range between 10 and 300 cm^{-1} ..

SI4 Deconvoluted FIR spectra for the TEATF/DMSO mixtures versus TEAMS

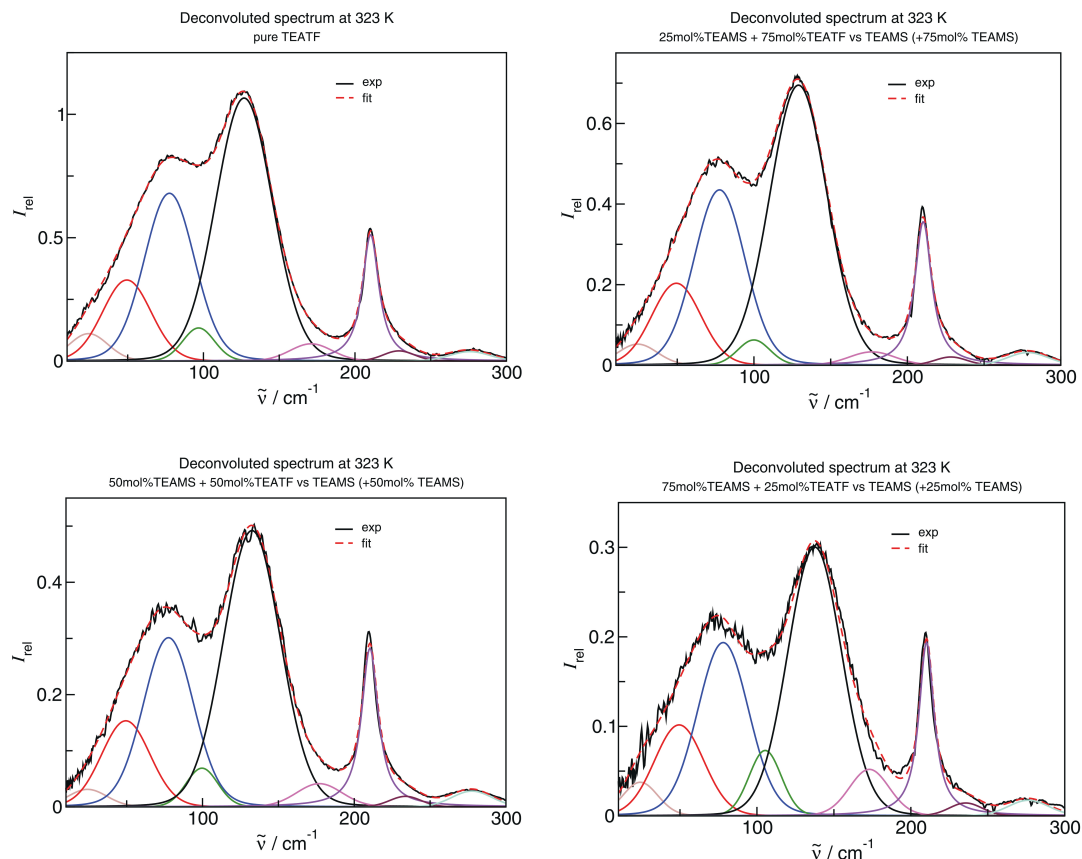


FIG4-SI Deconvoluted far infrared (FIR) difference spectra of pure triethylammonium triflate $[\text{Et}_3\text{NH}][\text{CF}_3\text{SO}_3]$ and triethylammonium triflate $[\text{Et}_3\text{NH}][\text{CF}_3\text{SO}_3]$ in mixtures with triethylammonium methylsulfonate $[\text{Et}_3\text{NH}][\text{CH}_3\text{SO}_3]$ subtracting the corresponding fraction of $[\text{Et}_3\text{NH}][\text{CH}_3\text{SO}_3]$ in the frequency range between 10 and 300 cm^{-1} .

All spectra were deconvoluted simultaneously as well as separately into a number of Voigt profiles (convolution of Lorentzian and Gaussian functions) following the Levenberg-Marquardt procedure. The Voigt profile has four parameters: the intensity, the frequency, the half-width of the Lorentzian, and the half-width of the Gaussian. The frequency and the half-widths of each Voigt function for all vibrational modes were kept fixed in the simultaneous fitting procedure. These parameters were known from the spectra of the pure PIL and the highly diluted PIL, where SIPs are the dominant ion pairs.

SI5 Corrected intensities for the vibrational modes N-H \cdots anion in the TEAMS/TEATF mixtures for the different molar volumes of TEATF and TEAMS, respectively.

PIL mixtures	I	I_{corr}
TEAMS	21.50	
TEAMS/TEATF x=0.75	17.89	20.12
TEAMS/TEATF x=0.50	11.25	12.67
TEAMS/TEATF x=0.25	3.5	3.94
TEATF	15.47	
TEAMS/TEATF x=0.75	9.25	7.79
TEAMS/TEATF x=0.50	6.65	5.94
TEAMS/TEATF x=0.25	3.95	3.53

SI6 Densities and viscosities of TEAMS and TEATF and their mixtures
(Here: MS=OMs and TF=OTf)

[HN(C₂H₅)₃][OMs]

<i>Dichte</i> g/cm ³	<i>Dichte</i> °C	<i>Tempe Lovis Dyn.</i> mPa·s	<i>Vis Lovis</i> °C	<i>Temperatur</i>
1,121053	19,993	140,9	20,00	
1,117665	24,998	105,2	25,00	
1,114294	30,003	80,63	30,00	
1,110946	35,007	63,21	35,00	
1,107614	40,009	50,54	40,00	
1,104299	45,005	40,85	45,00	
1,101010	50,005	33,59	50,00	
1,097734	55,005	28,06	55,00	
1,094474	60,005	23,65	60,00	
1,091230	65,006	20,15	65,00	
1,087999	70,006	17,41	70,00	

[HN(C₂H₅)₃][OTf]

<i>Dichte</i> g/cm ³	<i>Dichte</i> °C	<i>Tempe Lovis Dyn.</i> mPa·s	<i>Vis Lovis</i> °C	<i>Temperatur</i>
1,267029	19,994	70,60	20,00	
1,262980	24,997	57,43	25,00	
1,258945	30,003	47,20	30,00	
1,254929	35,007	39,23	35,00	
1,250929	40,009	32,93	40,00	
1,246942	45,005	27,92	45,00	
1,242970	50,005	23,94	50,00	
1,239010	55,005	20,69	55,00	
1,235059	60,005	18,05	60,00	
1,231124	65,006	15,81	65,00	
1,227203	70,005	14,02	70,00	

75 mol% [HN(C ₂ H ₅) ₃][OMs] 25 mol% [HN(C ₂ H ₅) ₃][OTf]

<i>Dichte</i> g/cm ³	<i>Dichte</i> °C	<i>Tempe Lovis Dyn.</i> mPa·s	<i>Vis Lovis Temperatur</i> °C
1,160272	19,993	147,6	20,00
1,156731	24,998	110,5	25,00
1,153201	30,003	85,10	30,00
1,149697	35,007	66,81	35,01
1,146210	40,005	53,51	40,00
1,142742	45,005	43,40	45,00
1,139286	50,005	35,76	50,00
1,135846	55,005	29,83	55,00
1,132420	60,007	25,18	60,00
1,129007	65,006	21,49	65,00
1,125608	70,005	18,48	70,00

50 mol% [HN(C ₂ H ₅) ₃][OMs] 50 mol% [HN(C ₂ H ₅) ₃][OTf]

<i>Dichte</i> g/cm ³	<i>Dichte</i> °C	<i>Tempe Lovis Dyn.</i> mPa·s	<i>Vis Lovis Temperatur</i> °C
1,197455	19,994	131,6	20,00
1,193735	24,999	100,9	25,00
1,190035	30,005	78,18	30,00
1,186359	35,007	62,25	35,00
1,182715	40,006	50,36	40,00
1,179091	45,005	41,40	45,00
1,175488	50,005	34,34	50,00
1,171888	55,005	28,83	55,00
1,168294	60,005	24,51	60,00
1,164712	65,006	21,04	65,00
1,161139	70,006	18,20	70,01

25 mol% [HN(C ₂ H ₅) ₃][OMs] 75 mol% [HN(C ₂ H ₅) ₃][OTf]

<i>Dichte</i> g/cm ³	<i>Dichte</i> °C	<i>Tempe</i> mPa·s	<i>Lovis Dyn. Vis</i> °C	<i>Lovis Temperat</i>
------------------------------------	---------------------	-----------------------	-----------------------------	-----------------------

1,232700	19,999	101,3	20,00	
1,228814	24,992	79,50	25,00	
1,224947	29,995	63,86	30,00	
1,221098	34,998	52,07	35,00	
1,217265	40,002	42,72	40,00	
1,213451	45,005	35,64	45,00	
1,209657	50,006	30,06	50,00	
1,205877	55,008	25,53	55,00	
1,202106	60,009	21,92	60,00	
1,198353	65,007	19,00	65,00	
1,194612	70,008	16,56	70,00	

SI7 Molecular Dynamics (MD) Simulations

This part of the supporting information summarizes all aspects of the performed molecular dynamics simulation, such as the forcefield model, details about the MD simulations, as well as the characterization of hydrogen bonded states.

The Forcefield-Model

For the description of the potential model, a classical forcefield approach has been used, similar to the OPLS approach of Jorgensen et al.[1]. All employed partial charges are atom-centered and were determined from ab-initio calculations of the individual ions by applying many body perturbation theory (MP2) and using the 6-311++G** basis set. All reported ab initio calculations were performed with the Gaussian 09 program [2]. The charges were fitted to the electrostatic potential surrounded by the atoms using the ESP [3] and RESP [4] methods. Due to the rather small size of the ions no significant changes were found between the ESP and RESP charges. CH₃- and CH₂-groups treated as united atoms and represented by a single interaction site. Nonbonded Lennard-Jones Parameters for the Triflate-ions were taken from the [NTF₂] forcefield model of Köddermann et al. [5], while the starting point for the nonbonded parameters for the Triethylammonium were the parameters used by Krienke et al. [6] for the ammonium group using essentially the TraPPE-parameters of Martin and Siepmann [7] for the united CH₃- and CH₂-atoms. The σ -parameter for the nitrogen atom needed to be resized to 3.25 Å in order to match the H...O distance of the hydrogen bonded ion pair in the gas-phase with the distance obtained for the energy minimized structure using ab initio calculations. Constant pressure simulations of the resulting model describes the density of Triethylammonium-Triflate quite satisfactorily. For the Methylsulfonate-ion the Lennard-Jones parameters of Köddermann were also used for the SO₃-group. The starting point for the Lennard-Jones parameters for the methyl-group was again the forcefield of Martin and Siepmann [7]. Here the Lennard-Jones σ of the methyl-group needed to be resized to match the density of the liquid phase of neat Triethylammonium-Methylsulfonate. Due to stronger bond-polarization of the S-O bond within the Methylsulfonate-ion compared to the same bond in the Triflate-ion, larger absolute charges on the oxygens are observed for the Methylsulfonate, leading to stronger hydrogen bonding with the Triethylammonium ion. In order to represent molecular configurations of the ions properly, the equilibrium bond distances and angles were adjusted to yield a minimum energy configuration close to the structure obtained from the ab initio calculations. All nonbonded Lennard-Jones parameters and partial charges are summarized in Table 1. The Bond-length and bond-bending parameters can be found in Tables 2 and 3. Dihedral potentials for intramolecular torsions around the N-C2-bond in the Triethylammonium ion and the S-C-bond in the triflate ions were fitted to ab initio calculation to represent the molecular configurations accurately. The values are summarized in Table 4. The full torsion potential also include nonbonded 1-4-interactions. Here both, the nonbonded Lennard Jones and Coulomb 1-4-interactions are scaled by a factor of 0.5.

Molecular Dynamics Simulations

We employ molecular dynamics (MD) simulations in the isobaric isothermal (*NPT*) ensemble using the Nosé-Hoover thermostat [8, 9] and the Rahman-Parrinello barostat [10, 11] with coupling times $\tau_T = 0.5$ ps and $\tau_p = 2$ ps (assuming the isothermal compressibility to be $\chi_T = 5 \cdot 10^{-5}$ bar⁻¹), respectively. The electrostatic interactions are treated in the “full potential” approach by the smooth particle mesh Ewald summation [12] with a real space cutoff of 1.0 nm and a mesh spacing of approximately 0.12 nm and 4th order interpolation. The Ewald convergence factor α was set to 3.38 nm⁻¹

(corresponding to a relative accuracy of the Ewald sum of 10^{-5}). A 2.0 fs timestep was used for all simulations and the constraints were solved using the SETTLE procedure [13]. During the simulations all bond-length were kept fixed. All simulations reported here were carried out using the GROMACS 4.6 program [14, 15]. Statistical errors in the analysis were computed using the method of Flyvbjerg and Petersen [16]. For all reported systems and different statepoints initial equilibration runs of 1 ns length were performed using the Berendsen weak coupling scheme for pressure and temperature control $\tau_T = \tau_p = 0.5$ ps [17]. A total of 16 different compositions were investigated with compositions of $x_{\text{CH}_3\text{SO}_3} = \{0.0, 0.125, 0.25, 0.3125, 0.40625, 0.5, 0.5625, 0.625, 0.6875, 0.75, 0.8125, 0.84375, 0.875, 0.90625, 0.9375, 1.0\}$. In each case the simulated system consisted of 256 ion pairs. As shown in Figure 1, the density of the model-system follows rather well the experimental density both as a function of temperature and composition. Production runs of 100 ns simulation-length were finally analyzed.

Hydrogen Bonding

Numerous geometrical procedures for the determination of hydrogen bonds have been proposed [18]. Mostly, they depend on distance criteria as well as some angular constraints [19]. In the case of protic ionic liquids discussed here, the use of angular constraints doesn't even seem to be necessary, since the distance distribution between the ammonium-hydrogen and the sulfonate-oxygen alone does very well discriminate between hydrogen bonded and non-hydrogen bonded states. As shown in Figure 2, the pair correlation function between an ammonium-hydrogen and the sulfonate-oxygen exhibits a very sharp narrow first peak which almost goes down to zero for both ionic liquids. The number of nearest oxygen-neighbors around an hydrogen atom as a function of distance has a very well defined step-like form with a plateau at 1, which indicates that an NH-group in both ionic liquid is always involved in a hydrogen bond. Here we use a distance criterion of $r_{H...O} \leq 0.24$ nm to define a hydrogen bond for both the Triflate and the Methylsulfonate. This fact remains true also for all of the investigated mixtures and does also depend only very weakly on the temperature. Hydrogen bonding also affects the center-of mass pair correlation function and is largely responsible for the pronounced splitted first peak structure of the anion-cation pair correlation function shown in Figure 3. In the mixture, the hydrogen-bond donated by the cation is not equally shared by the both anions. In fact, the hydrogen bond to the Methylsulfonate-ion is significantly stronger, shifting the equilibrium strongly towards the formation of hydrogen bonds with the Methylsulfonate-ion. In Figure 4, the average number of hydrogen bonds accepted by one of the anions in the mixture is depicted as a function of composition. In the pure liquids, each anion accepts on average one hydrogen bond. Since each sulfonate group can accept a total about three hydrogen-bonds, the Methylsulfonate accepts about up to 2.7 hydrogen bonds in the diluted solution. By increasing the Methylsulfonate-concentration this number drops steadily, since the Methylsulfonate-ions start to compete with each other. The Triflate-ion in the dilute Triflate-solution only receives about 0.1 Hydrogen bonds on average, and is hence almost completely stripped of hydrogen bonds.

Self-Diffusion of the Ions in the Mixture

Self diffusion coefficients were used as a means to characterize the individual mobilities of the ions due to their changing hydrogen bond environment as a function of the mixture composition. The self diffusion coefficients of the ions were determined as the slope of mean square displacement of the

center of mass coordinates $\vec{r}_c(t)$ for the individual ions according to the well-known Einstein-relation

$$D_{\text{self}} = \frac{1}{6} \frac{\partial}{\partial \tau} \left\langle |\vec{r}_c(t) - \vec{r}_c(t + \tau)|^2 \right\rangle . \quad (1)$$

Here the brackets $\langle \dots \rangle$ indicate averaging over times t , as well as over ions of the same type. Slopes of the mean square displacement shown here were recorded for a temperature of 400 K for a time-interval between 1 ns and 12 ns based on simulation lengths of 24 ns for each composition. The self obtained self diffusion coefficients as a function of mixture-composition are shown in Figure 5 and are given in Table 5. At low concentration the Methylsulfonate ions attract multiple hydrogen bonds to the TEA cations, which leads to accordingly to a slowing down of the Methylsulfonate. An increasing Methylsulfonate concentration quickly also affects the rest of the mixture, leading to a rapid decrease in mobility of the TEA and Triflate ions, also leading to a shallow minimum of their mobility at about $x(\text{CH}_3\text{SO}_3) \approx 0.45$. Further increase in Methylsulfonate composition leads to an increase in diffusivity since, the Methylsulfonate-ions increasingly compete with each other for hydrogen bonds to the cations.

Atom i	$\sigma_{ii}/\text{\AA}$	$\epsilon_{ii} \cdot k_{\text{B}}^{-1}/\text{K}$	$q_i/ e $
Triflate:			
S	4.08	37.3	-0.73
O	3.46	31.7	1.40
C	3.15	10.0	0.48
F	2.66	8.0	-0.23
Methylsulfonate:			
S	4.08	37.3	-0.825
O	3.46	31.7	1.620
C3	2.90	98.0	-0.145
Triethylammonium:			
H	0.0	0.0	0.37
N	3.25	75.0	-0.39
C2	3.95	46.0	0.28
C3	3.75	98.0	0.06

Table 1: Non-bonding Lennard-Jones interaction parameters with $V_{ij} = 4\epsilon_{ij} \left[(\sigma_{ij}/r_{ij})^{12} - (\sigma_{ij}/r_{ij})^6 \right]$ and partial charges used in the MD Simulations of the PIL-mixtures. Lorentz-Berthelot mixing-rules with $\sigma_{ij} = (\sigma_{ii} + \sigma_{jj})/2$ and $\epsilon_{ij} = (\epsilon_{ii} \cdot \epsilon_{jj})^{1/2}$ were applied for determining the cross-parameters.

Bond $i - j$	$r_{ij}^0 / \text{\AA}$	$k_{ij}^b / \text{kJ mol}^{-1} \text{\AA}^{-2}$
Triflate:		
C-F	1.347	3700.0
C-S	1.860	1850.0
O-S	1.469	5850.0
Methylsulfonate:		
C3-S	1.8040	1850.0
O-S	1.4816	5850.0
Triethylammonium:		
H-N	1.020	2500.0
C2-N	1.500	2500.0
C2-C3	1.540	2500.0

Table 2: Harmonic bond-stretching parameters employed in the forcefield model using $V_{ij}^b = (k_{ij}^b/2) \cdot (r_{ij} - r_{ij}^0)^2$.

Angle $i - j - k$	θ_{ijk}^0 / degrees	k_{ijk}^a / kJ mol ⁻¹ rad ⁻²
Triflate:		
F-C-F	108.4	650.0
F-C-S	110.5	420.0
C-S-O	102.6	620.0
O-S-O	119.5	850.0
Methylsulfonate:		
C3-S-O	104.26	620.0
O-S-O	114.14	850.0
Triethylammonium:		
H-N-C2	108.4	460.0
C2-N-C2	108.4	460.0
C3-C2-N	108.4	460.0

Table 3: Harmonic bond-bending parameters employed in the forcefield model using $V_{ijk}^a = (k_{ijk}^a/2) \cdot (\theta_{ijk} - \theta_{ijk}^0)^2$.

$m(i - j - k - l)$	n_m	k_m^d / kJ mol ⁻¹
Triflate F-C-S-O:		
1	3.0	0.8619
Triethylammonium H-N-C2-C3:		
1	1.0	8.734
2	2.0	3.224
3	3.0	5.514
4	4.0	-0.465
5	5.0	-0.481
6	6.0	0.756

Table 4: Dihedral-Potential for the rotation around the N-C2 bond in the Triethylammonium-ion and for the C-S bond in the Triflate-ion according to $V_{ijkl} = \sum_m k_m^d [1 + \cos(n_m \cdot \phi)]$.

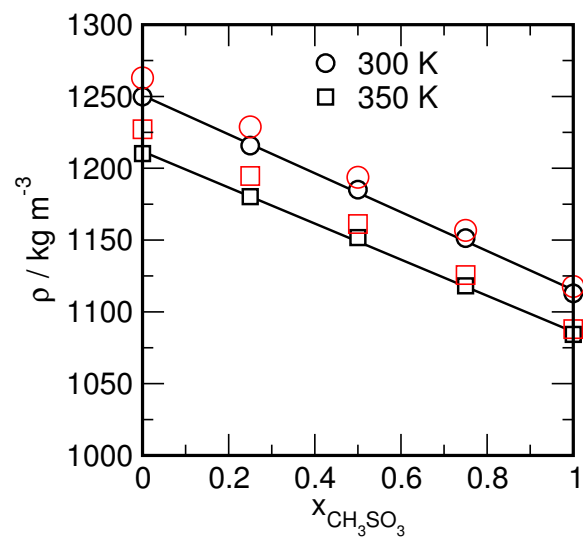


Figure 1: Densities of selected TEATF/TEAMS mixtures as a function of their composition as obtained from the molecular dynamics simulations at 300 K and 350 K, respectively. The red symbols refer to experimental densities obtained at 298 K and 343 K.

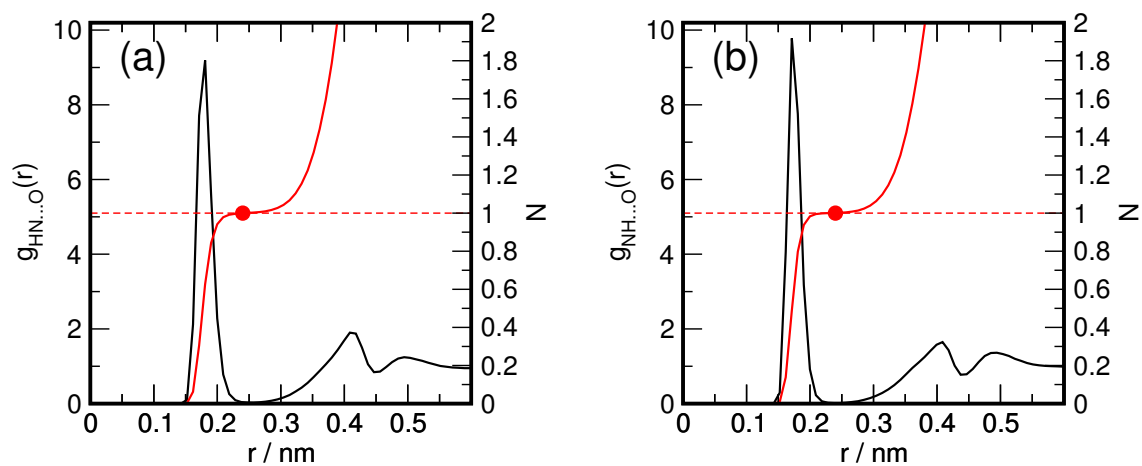


Figure 2: Intermolecular pair distribution functions between the ammonium hydrogen (NH) and the sulfonate-oxygen in the two pure ionic liquids as obtained by MD simulation. a) TEATF b) TEAMS. Also shown is the and integrated number of neighbors. All the data shown were obtained at $T = 300$ K.

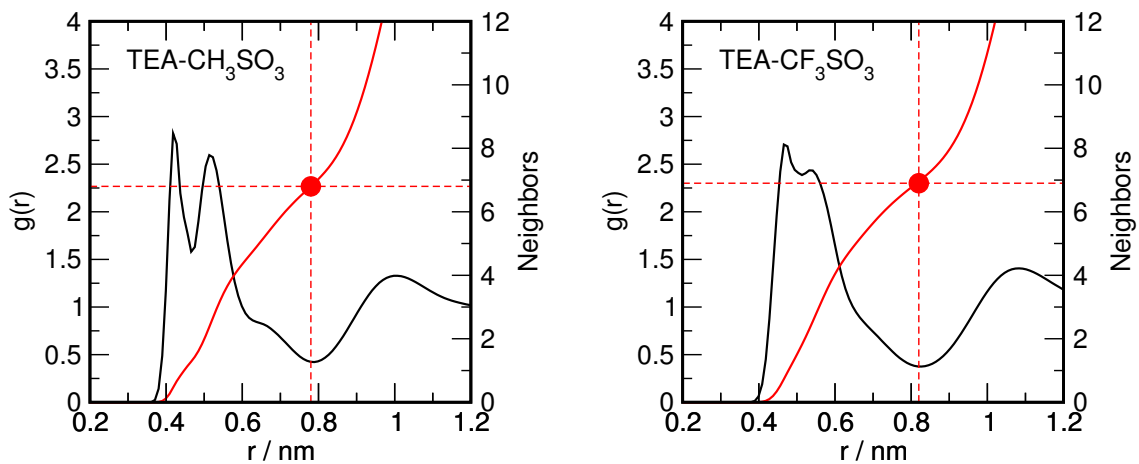


Figure 3: Cation-anion center of mass pair distribution functions and integrated number of neighbors obtained for the two pure ionic liquids at $T = 300$ K.

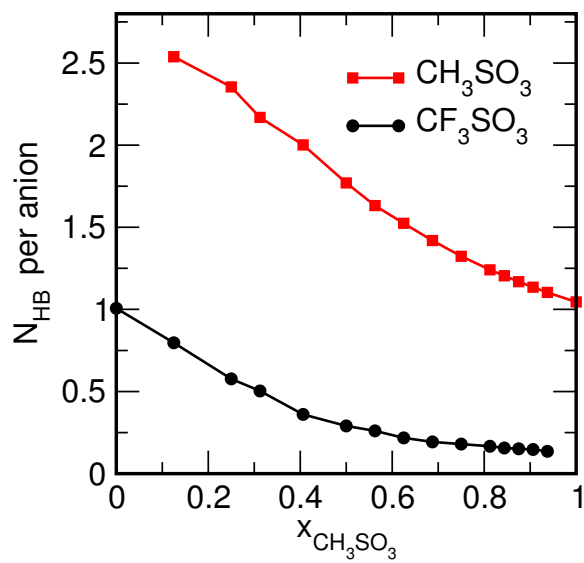


Figure 4: Average total number of hydrogen bonds for each of the anions to the neighboring TEA-cations as a function of composition in the TEA-Triflate/TEA-Methylsulfonate mixture at $T = 400$ K.

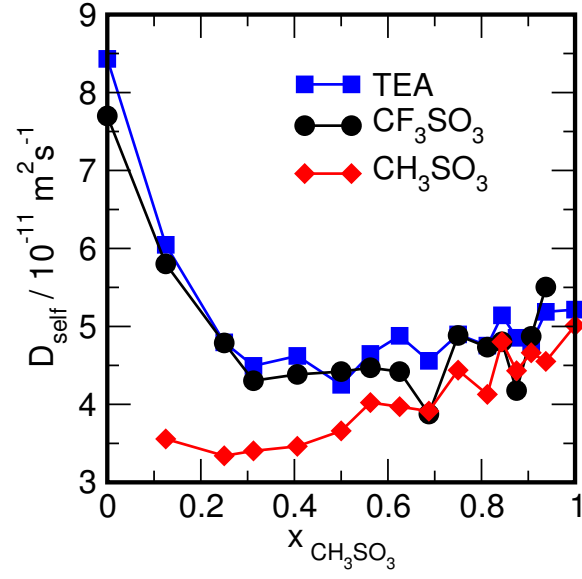


Figure 5: Self Diffusion Coefficients as a function of composition in the TEA-Triflate/TEA-Methylsulfonate mixture at $T = 400$ K.

$x(\text{CH}_3\text{SO}_3)$	$D_{\text{self}}(\text{TEA})$	$D_{\text{self}}/10^{-11} \text{ m}^2 \text{ s}^{-1}$	
		$D_{\text{self}}(\text{CF}_3\text{SO}_3)$	$D_{\text{self}}(\text{CH}_3\text{SO}_3)$
0	8.43	7.70	—
0.125	6.05	5.80	3.56
0.25	4.80	4.79	3.34
0.3125	4.49	4.30	3.40
0.40625	4.62	4.38	3.46
0.5	4.25	4.42	3.66
0.5625	4.65	4.47	4.02
0.625	4.88	4.42	3.97
0.6875	4.56	3.88	3.91
0.75	4.90	4.88	4.44
0.8125	4.75	4.73	4.13
0.84375	5.14	4.80	4.80
0.875	4.85	4.17	4.43
0.90625	4.78	4.87	4.66
0.9375	5.19	5.50	4.55
1	5.21	—	5.01

Table 5: Self Diffusion Coefficients as a function of composition in the TEA-Triflate/TEA-Methylsulfonate mixture at $T = 400$ K.

References

- [1] W. L. Jorgensen and M. Ibrahim. Structures and properties of organic liquids: n-alkyl ethers and their conformational equilibria. *J. Am. Chem. Soc.*, 103:3976–3985, 1981.
- [2] M. J. Frisch, G. W. Trucks, H. B. Schlegel, G. E. Scuseria, M. A. Robb, J. R. Cheeseman, G. Scalmani, V. Barone, B. Mennucci, G. A. Petersson, H. Nakatsuji, M. Caricato, X. Li, H. P. Hratchian, A. F. Izmaylov, J. Bloino, G. Zheng, J. L. Sonnenberg, M. Hada, M. Ehara, K. Toyota, R. Fukuda, J. Hasegawa, M. Ishida, T. Nakajima, Y. Honda, O. Kitao, H. Nakai, T. Vreven, J. A. Montgomery, Jr., J. E. Peralta, F. Ogliaro, M. Bearpark, J. J. Heyd, E. Brothers, K. N. Kudin, V. N. Staroverov, R. Kobayashi, J. Normand, K. Raghavachari, A. Rendell, J. C. Burant, S. S. Iyengar, J. Tomasi, M. Cossi, N. Rega, J. M. Millam, M. Klene, J. E. Knox, J. B. Cross, V. Bakken, C. Adamo, J. Jaramillo, R. Gomperts, R. E. Stratmann, O. Yazyev, A. J. Austin, R. Cammi, C. Pomelli, J. W. Ochterski, R. L. Martin, K. Morokuma, V. G. Zakrzewski, G. A. Voth, P. Salvador, J. J. Dannenberg, S. Dapprich, A. D. Daniels, J. Farkas, J. B. Foresman, J. V. Ortiz, J. Cioslowski, and D. J. Fox. Gaussian09 Revision D.01. Gaussian Inc. Wallingford CT 2009.
- [3] U.C.Singh and P.A. Kollman. An approach to computing electrostatic charges for molecules. *J. Comput. Chem.*, 5:129–145, 1984.
- [4] C. I. Bayly, P. Cieplak, W. D. Cornell, and P. A. Kollman. A well-behaved electrostatic potential based method using charge restraints for deriving atomic charges - the resp model. *J. Phys. Chem.*, 97:10269–10280, 1993.
- [5] Thorsten Ködderman, Dietmar Paschek, and Ralf Ludwig. Molecular dynamics simulations of ionic liquids: A reliable description of structure, thermodynamics and dynamics. *ChemPhysChem*, 8:2464–2470, 2007.
- [6] H. Krienke, V. Vlachy, G. Ahn-Ercan, and I. Bako. Modeling tetraalkylammonium halide salts in water: How hydrophobic and electrostatic interactions shape the thermodynamic properties. *J. Phys. Chem. B*, 113:4360–4371, 2009.
- [7] M. G. Martin and J. I. Siepmann. Transferable potentials for phase equilibria. 1. united-atom description of n-alkanes. *J. Phys. Chem. B*, 102:2569–2577, 1998.
- [8] S. Nosé. A molecular dynamics method for simulating in the canonical ensemble. *Mol. Phys.*, 52:255–268, 1984.
- [9] W. G. Hoover. Canonical dynamics: Equilibrium phase space distributions. *Phys. Rev. A*, 31, 1985.
- [10] M. Parrinello and A. Rahman. Polymorphic transitions in single crystals: A new molecular dynamics method. *J. Appl. Phys.*, 52:7182–7180, 1981.
- [11] S. Nosé and M. L. Klein. Constant pressure molecular dynamics for molecular systems. *Mol. Phys.*, 50:1055–1076, 1983.
- [12] U. Essmann, L. Perera, M. L. Berkowitz, T. A. Darden, H. Lee, and L. G. Pedersen. A smooth particle mesh ewald method. *J. Chem. Phys.*, 103:8577–8593, 1995.
- [13] S. Miyamoto and P. A. Kollman. Settle: An analytical version of the shake and rattle algorithms for rigid water models. *J. Comp. Chem.*, 13:952–962, 1992.

- [14] E. Lindahl, B. Hess, and D. van der Spoel. Gromacs 3.0: A package for molecular simulation and trajectory analysis. *J. Mol. Mod.*, 7:306–317, 2001.
- [15] Mark Abraham, Emile Apol, Rossen Apostolov, Herman J.C. Berendsen, Aldert van Buuren, Par Bjelkmar, Rudi van Drunen, Anton Feenstra, Sebastian Fritsch, Gerrit Groenhof, Christoph Junghans, Jochen Hub, Peter Kasson, Carsten Kutzner, Brad Lambeth, Per Larsson, Justin A. Lemkul, Erik Marklund, Peiter Meulenhoff, Teemu Murtola, Szilard Pall, Sander Pronk, Roland Schulz, Michael Shirts, Alfons Sijbers, Peter Tieleman, Maarten Wolf, Berk Hess and David van der Spoel, and Erik Lindahl. *GROMACS - Groningen Machine for Chemical Simulations User Manual Version 4.6.1*.
- [16] H. Flyvbjerg and H. G. Petersen. Error estimates on averages of correlated data. *J. Chem. Phys.*, 91:461–466, 1989.
- [17] H. J. C. Berendsen, J. P. M. Postma, W. F. van Gunsteren, A. DiNola, and J. R. Haak. Molecular dynamics with coupling to an external bath. *J. Chem. Phys.*, 81:3684–3690, 1984.
- [18] R. Kumar, J. R. Schmidt, and J. L. Skinner. Hydrogen bonding definitions and dynamics in liquid water. *J. Chem. Phys.*, 126:204107, 2007.
- [19] A. Luzar and D. Chandler. Hydrogen-bond kinetics in liquid water. *Nature*, 379:55–57, 1996.

4.3 Publication II

Hydrogen Bonding in a Mixture of Protic Ionic Liquids: A Molecular Dynamics Simulation Study

D. Paschek, B. Golub and R. Ludwig

Phys. Chem. Chem. Phys., 2015, **17**, 8431-8440

CRedit roles: Formal analysis, Investigation, Visualization

Approximated contribution to the publication in percent: 40 %

Reproduced from Ref.: D. Paschek, B. Golub, and R. Ludwig, *Phys. Chem. Chem. Phys.*, 2015, **17**, 8431-8440, DOI: 10.1039/C4CP05432F with permission from the Royal Society of Chemistry.



Cite this: *Phys. Chem. Chem. Phys.*,
2015, 17, 8431

Hydrogen bonding in a mixture of protic ionic liquids: a molecular dynamics simulation study

Dietmar Paschek,^{*a} Benjamin Golub^a and Ralf Ludwig^{*bc}

We report results of molecular dynamics (MD) simulations characterising the hydrogen bonding in mixtures of two different protic ionic liquids sharing the same cation: triethylammonium-methylsulfonate (TEAMS) and triethylammonium-triflate (TEATF). The triethylammonium-cation acts as a hydrogen-bond donor, being able to donate a single hydrogen-bond. Both, the methylsulfonate- and the triflate-anions can act as hydrogen-bond acceptors, which can accept multiple hydrogen bonds *via* their respective SO₃-groups. In addition, replacing a methyl-group in the methylsulfonate by a trifluoromethyl-group in the triflate significantly weakens the strength of a hydrogen bond from an adjacent triethylammonium cation to the oxygen-site in the SO₃-group of the anion. Our MD simulations show that these subtle differences in hydrogen bond strength significantly affect the formation of differently-sized hydrogen-bonded aggregates in these mixtures as a function of the mixture-composition. Moreover, the reported hydrogen-bonded cluster sizes can be predicted and explained by a simple combinatorial lattice model, based on the approximate coordination number of the ions, and using statistical weights that mostly account for the fact that each anion can only accept three hydrogen bonds.

Received 21st November 2014,
Accepted 20th January 2015

DOI: 10.1039/c4cp05432f

www.rsc.org/pccp

1 Introduction

During the past 15 years ionic liquids (ILs) have received great attention from the scientific community.^{1–4} More recently, also the ability to design targeted liquid properties by forming binary and ternary mixtures has become a focus of interest.^{5,6} In particular, it has been recognized that the balance between different competing interactions, such as Coulomb interactions, van der Waals interactions, and hydrogen bonds is of great importance. In a situation, where strong (Coulombic) forces compete with each other and partly cancel each other out, also weaker interactions, such as hydrogen-bonds, might be able to significantly affect the properties of the fluid.^{7,8} This is particularly important for mixtures of ionic liquids, where different constituents (ions) might compete with each other for specific interactions. The mixing behavior of several ionic liquids has been discussed recently with a focus on their thermodynamic and transport properties.^{5,6,9–13} However, mostly the behavior of aprotic ionic liquids has been considered so far. We would like to point out that physical properties

reported in these studies, such as the density and the viscosity, were mostly exhibiting ideal-like mixing behavior in the sense that the properties vary almost linearly with the mixture composition. In addition, also the molar mixing-enthalpies and -entropies indicated only a small deviation from the ideal mixture-behavior.^{10,11} Recently, Welton and co-workers have commented on the tendency for ideal-mixture behavior in mixtures of ionic liquids and reviewed IL mixtures with a focus on property design and opportunities for applications.^{5,9}

The situation seems to be different for protic ionic liquids, where strongly directional hydrogen-bonds (can) exist.^{14,15} We could show very recently, that for a mixture of triethylammonium-methylsulfonate (TEAMS) and triethylammonium-triflate (TEATF), which are both sharing the same cation, the two different anions compete with each other for a hydrogen bond to the triethylammonium-cation (TEA).¹⁶ Using far-infrared spectroscopy, we could assign signatures distinguishing between hydrogen-bonded aggregates of TEA to each of the two anions within the mixture.¹⁶ A population analysis as a function of mixture-composition is suggesting a favorable interaction of TEA with the methylsulfonate-ion. In addition, also the experimentally determined viscosity is showing a strongly non-linear mixture dependence, pointing at the changing size of aggregates in the liquid as a function of the mixture-composition.¹⁶ With the present study we would like to complement our earlier endeavour with an in-depth analysis of a detailed molecular model of the same binary TEATMS–TEATF mixture, focusing on the local solvation-structure of the ions, and, in particular,

^a Universität Rostock, Institut für Chemie, Abteilung Physikalische und Theoretische Chemie, Albert-Einstein-Str. 21, D-18059 Rostock, Germany.

E-mail: dietmar.paschek@uni-rostock.de; Fax: +49 381 498 6524

^b Universität Rostock, Institut für Chemie, Abteilung Physikalische und Theoretische Chemie, Dr.-Lorenz-Weg 1, D-18059 Rostock, Germany.

E-mail: ralf.ludwig@uni-rostock.de; Fax: +49 381 498 6524

^c Leibniz Institut für Katalyse an der Universität Rostock e.V., Albert-Einstein-Str. 29a, D-18059 Rostock, Germany



on the hydrogen-bonding. In addition, we will show that the size of the hydrogen-bonded aggregates can be predicted and explained by a simple combinatorial lattice model, which is based on an approximate coordination number of the ions, and is using statistical weights that mostly account for the fact that each anion can only accept up to three hydrogen bonds.

Finally, we would like to point out that Rogers and co-workers have argued recently that ions in a mixture of ILs do not seem to retain their individual nature and proposed to consider them as double salt ionic liquids.⁶ Double salts are salts containing more than one cation or anion, obtained by combination of two different salts which were crystallized in the same regular ionic lattice. Although this definition is not strictly applicable to the case of an amorphous state such as a liquid, we can provide evidence for double-salt-like behavior of the TEAMS-TEATF mixture.

2 Methods

2.1 Molecular dynamics simulations

We employ molecular dynamics (MD) simulations in the isobaric isothermal (NPT) ensemble using the Nosé-Hoover thermostat^{17,18} and the Rahman-Parrinello barostat^{19,20} with coupling-times $\tau_T = 0.5$ ps and $\tau_P = 2$ ps (assuming the isothermal compressibility to be $\chi_T = 5 \times 10^{-5} \text{ bar}^{-1}$), respectively. The electrostatic interactions are treated in the “full potential” approach by the smooth particle mesh Ewald summation²¹ with a real space cutoff of 1.0 nm and a mesh spacing of approximately 0.12 nm and 4th order interpolation. The Ewald convergence factor α was set to 3.38 nm^{-1} (corresponding to a relative accuracy of the Ewald sum of 10^{-5}). A 2.0 fs timestep was used for all simulations and the constraints were solved using the SETTLE procedure.²² During the simulations all bond-length were kept fixed. All simulations reported here were carried out using the GROMACS 4.6 program.^{23,24} Statistical errors in the analysis were computed using the method of Flyvbjerg and Petersen.²⁵ For all reported mixtures and temperatures initial equilibration runs of 1 ns length were performed using the Berendsen weak coupling scheme for pressure and temperature control $\tau_T = \tau_P = 0.5$ ps.²⁶ A total of 16 different compositions were investigated with compositions of $x = x_{\text{CH}_3\text{SO}_3} = \{0.0, 0.125, 0.25, 0.3125, 0.40625, 0.5, 0.5625, 0.625, 0.6875, 0.75, 0.8125, 0.84375, 0.875, 0.90625, 0.9375, 1.0\}$ at $T = 300 \text{ K}, 300 \text{ K}, 300 \text{ K}, 300 \text{ K}, 300 \text{ K}, 300 \text{ K}, 300 \text{ K}, 300 \text{ K}, 300 \text{ K}, 300 \text{ K}, 300 \text{ K}, 300 \text{ K}, 300 \text{ K}, 300 \text{ K}, 300 \text{ K}, 300 \text{ K}$. In each case the simulated system consisted of 256 ion pairs in a cubic box with periodic boundary conditions. As shown in Fig. 1, the density of the model-system follows rather well the experimental density, both as a function of temperature and composition. Production runs of 120 ns (300 K), 48 ns (350 K), and 24 ns (400 K) simulation-length were finally recorded and analyzed.

2.2 The molecular model

For the description of the potential model, a classical force-field approach has been used, similar to the OPLS-model of Jorgensen *et al.*²⁷ All employed partial charges are atom-centered and were determined from *ab initio* calculations of the individual

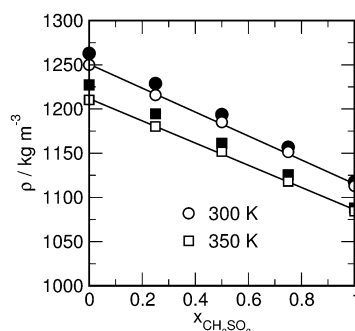


Fig. 1 Densities of selected TEATF-TEAMS mixtures as a function of their composition as obtained from the molecular dynamics simulations at 300 K and 350 K, respectively. The closed symbols refer to experimental densities obtained at 298 K and 343 K.¹⁶

ions by applying many body perturbation theory (MP2) and using the 6-311++G** basis set. All reported *ab initio* calculations were performed with the Gaussian 09 program.²⁸ The charges were fitted to the electrostatic potential surrounded by the atoms using the ESP²⁹ and RESP³⁰ methods. Due to the rather small size of the ions no significant changes were found between the ESP and RESP charges. CH_3^- and CH_2^- -groups treated as united atoms and represented by a single interaction site. Nonbonded Lennard-Jones parameters for the triflate-ions were taken from the [NTF₂] forcefield-model of Köddermann *et al.*,³¹ while the starting point for the nonbonded parameters for the triethylammonium were parameters reported by Krienke *et al.*³² for the ammonium group, in addition to the TraPPE-parameters of Martin and Siepmann³³ for the united-atom CH_3^- and CH_2^- -groups. The σ -parameter for the nitrogen atom needed to be resized to 3.25 Å in order to match the $\text{H} \cdots \text{O}$ distance of the hydrogen bonded ion pair in the gas-phase with the distance obtained for the energy minimized structure using *ab initio* calculations. Constant pressure simulations of the model describes the density of triethylammonium-triflate quite satisfactorily. For the methylsulfonate-ion, the Lennard-Jones parameters of Köddermann were also used for the SO_3^- -group. The starting point for the Lennard-Jones parameters for the methyl-group was again the forcefield of Martin and Siepmann.³³ In this case, the Lennard-Jones σ of the methyl-group needed to be resized to match the density of the liquid phase of neat triethylammonium-methylsulfonate. Due to a significantly stronger bond-polarization of the S-O bond within the methylsulfonate-ion, compared to the triflate-ion, larger partial charges on the oxygens were obtained for the methylsulfonate, leading to stronger hydrogen-bonding with the triethylammonium ion. In order to represent molecular configurations of the ions properly, the equilibrium bond distances and angles were adjusted in such a way that they lead to minimum energy configurations close to the structures obtained from the *ab initio* calculations. All nonbonded Lennard-Jones parameters and partial charges are summarized in Table 1. The bond-length and bond-bending parameters can be found in Tables 2 and 3. Dihedral potentials for intramolecular torsions around the N-C2-bond in the triethylammonium ion and the S-C-bond in



Table 1 Non-bonding Lennard-Jones interaction parameters with $V_{ij} = 4\epsilon_{ij}[(\sigma_{ij}/r_{ij})^{12} - (\sigma_{ij}/r_{ij})^6]$ and partial charges used in the MD Simulations of the PIL-mixtures. Lorentz–Berthelot mixing-rules with $\sigma_{ij} = (\sigma_{ii} + \sigma_{jj})/2$ and $\epsilon_{ij} = (\epsilon_{ii}\epsilon_{jj})^{1/2}$ were applied for determining the cross-parameters

Atom <i>i</i>	$\sigma_{ii}/\text{\AA}$	$\epsilon_{ii} \cdot k_B^{-1}/\text{K}$	$q_{ii}/ e $
Triflate			
S	4.08	37.3	1.40
O	3.46	31.7	−0.73
C	3.15	10.0	0.48
F	2.66	8.0	−0.23
Methylsulfonate			
S	4.08	37.3	1.620
O	3.46	31.7	−0.825
C3	2.90	98.0	−0.145
Triethylammonium			
H	0.0	0.0	0.37
N	3.25	75.0	−0.39
C2	3.95	46.0	0.28
C3	3.75	98.0	0.06

Table 2 Harmonic bond-stretching parameters employed in the force-field model using $V_{ij}^b = (k_{ij}^b/2) \cdot (r_{ij} - r_{ij}^0)^2$

Bond <i>i</i> – <i>j</i>	$r_{ij}^0/\text{\AA}$	$k_{ij}^b/\text{kJ mol}^{-1} \text{\AA}^{-2}$
Triflate		
C–F	1.347	3700.0
C–S	1.860	1850.0
O–S	1.469	5850.0
Methylsulfonate		
C3–S	1.8040	1850.0
O–S	1.4816	5850.0
Triethylammonium		
H–N	1.020	2500.0
C2–N	1.500	2500.0
C2–C3	1.540	2500.0

Table 3 Harmonic bond-bending parameters employed in the forcefield model using $V_{ijk}^a = (k_{ijk}^a/2) \cdot (\theta_{ijk} - \theta_{ijk}^0)^2$

Angle <i>i</i> – <i>j</i> – <i>k</i>	$\theta_{ijk}^0/\text{degrees}$	$k_{ijk}^a/\text{kJ mol}^{-1} \text{rad}^{-2}$
Triflate		
F–C–F	108.4	650.0
F–C–S	110.5	420.0
C–S–O	102.6	620.0
O–S–O	119.5	850.0
Methylsulfonate		
C3–S–O	104.26	620.0
O–S–O	114.14	850.0
Triethylammonium		
H–N–C2	108.4	460.0
C2–N–C2	108.4	460.0
C3–C2–N	108.4	460.0

the triflate ions were fitted to *ab initio* calculations to represent the molecular conformations accurately. The values are summarized in Table 4. The full torsion potential also include nonbonded 1–4-interactions. Here both, the nonbonded Lennard-Jones and Coulomb 1–4-interactions are scaled by a factor of 0.5.

Table 4 Dihedral-potential for the rotation around the N–C2 bond in the triethylammonium-ion and for the C–S bond in the triflate-ion according to $V_{ijkl} = \sum_m k_m^d [1 + \cos(n_m \cdot \phi)]$

<i>m</i> (<i>i</i> – <i>j</i> – <i>k</i> – <i>l</i>)	n_m	$k_m^d/\text{kJ mol}^{-1}$
Triflate F–C–S–O		
1	3.0	0.8619
Triethylammonium H–N–C2–C3		
1	1.0	8.734
2	2.0	3.224
3	3.0	5.514
4	4.0	−0.465
5	5.0	−0.481
6	6.0	0.756

3 Discussion

3.1 Structure of the ionic liquid mixture

To provide an impression of the structure of the discussed ionic liquid mixture, a snapshot of the 50:50 mixture of TEATF–TEMS at $T = 300$ K is given in Fig. 2. Indicated are the positions of the centers of mass of the ions, which can be identified *via* their respective colors. From visual inspection it is evident that the charge of the ions impose a long-range ion-alternating order, which is leading to a significant structural homogeneity of the ionic liquid. This behavior is typical for ionic liquids and has been pointed out earlier by Maroncelli and co-workers.³⁴ The ion-alternating order is a consequence of the fact that the ions are predominantly surrounded by a solvation shell of ions with opposite charge. This defining structural feature is well represented by the location of the first peak of the center-of-mass pair distribution functions of the ions: in Fig. 3a and b the center-of-mass pair distribution functions for all ion-pair combinations are shown for a 50:50 mixture obtained at 300 K. From Fig. 3a we can conclude that the first peak of the anion–cation pair correlation function is shifted to significantly lower values, with the dominant first peak of the TEA–MS-pair found at 0.41 nm, and the peak of the TEA–TF-pair at 0.54 nm. The first TEA–TEA-peak is found at a much larger distance of 0.70 nm. The anion–anion pair correlation functions are shown in Fig. 3b; here,

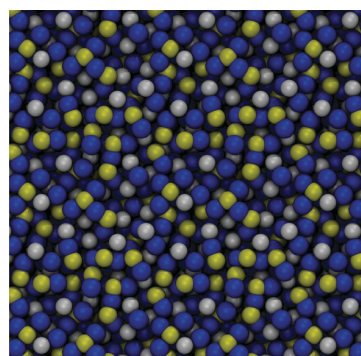


Fig. 2 Snapshot of a 50:50 mixture of TEATF–TEMS at $T = 300$ K. The spheres represent the centers of gravity of the ions. The TEA-positions are indicated by blue spheres. The triflate- and methylsulfonate-positions are color-coded in white and yellow, respectively.



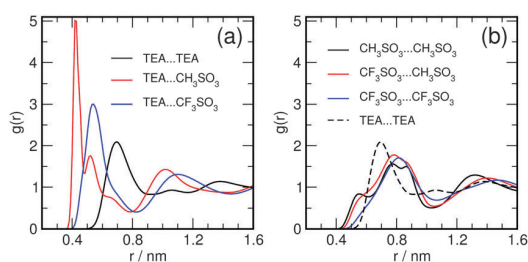


Fig. 3 Complete set of ion-ion center of mass pair distribution functions $g(r)$ obtained for the 50:50 mixture of TEATF-TEMS at $T = 300$ K.

we would like to point out that, besides the dominant main first peak around 0.8 nm, there also exists pre-peak at a distance of about 0.55 nm, which is most strongly pronounced for the correlation between the two methylsulfonate ions, and is only weakly pronounced in the pair-correlation of the triflate-ions. In addition, Fig. 3b also shows that this structural feature of the first peak is completely absent for the TEA-TEA correlations. The pre-peak in the anion-anion pair correlation function is indicating the existence of direct anion-anion contacts, whereas direct cation-cation contacts are apparently avoided. Moreover, also the snapshot in Fig. 2 reveals the presence of anion-anion-pairs in close proximity on many occasions.

The coordination number of the ion-solvation is deduced from the anion-cation pair correlation functions, shown in Fig. 4a and b for both pure ionic liquids. First, we would like to point at the characteristic three-sub-peak nature of peak of the first solvation-shell, which is present in both ionic liquids, although significantly more “structured” in the case of TEAMS. The integral over the pair correlation function reveals the number of neighbors as function of their distance

$$N(r) = 4\pi\rho \int_0^r g(r')r'^2 dr'. \quad (1)$$

Here ρ represents the number density of the selected ion-species. The data for $N(r)$ are also given in Fig. 4. Integrating over the entire first peak leads to a consistent number of nearest neighbors of about 6.8 to 6.9 counter-ions for both ionic liquids. Here, the first sub-peak corresponds in both cases to about one neighbor, strongly suggesting that this is indicative of a hydrogen-bonded ion-pair configuration. The second and third

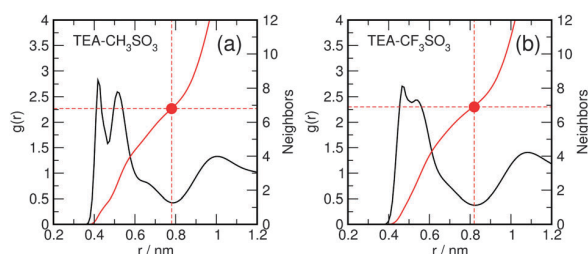


Fig. 4 Anion-cation center of mass pair distribution functions $g(r)$ obtained for (a) pure TEAMS and (b) pure TEATF at $T = 300$ K. The position of the first minimum is used as a cut-off distance for the nearest neighbor computation (TEA-MS: 0.78 nm, TEA-TF: 0.81 nm).

sub-peaks are contributing about three additional neighbors each. Both are apparently related to configurations with different orientational order. As shown in Fig. 5, the average first-shell counter-ion coordination number of about 6.8 to 6.9 remains constant over the entire mixture range.

At this point we would like to discuss apparent deviations from an ideal mixture-behavior in these ionic liquids: a significant structural difference between the pure liquids and the mixture is observed for first sub-peak of the anion-cation pair distribution functions for the 50:50 TEATF-TEAMS mixture, shown in Fig. 3a, compared to the pure liquids shown in Fig. 4. From Fig. 4 it is evident that the first sub-peak has about the same height for both pure ionic liquids. In the 50:50 mixture (Fig. 3a), however, the first peak is very strongly pronounced for the TEA-MS pair, and is almost completely absent for the TEA-TF pair, which is suggesting a preference for the formation of TEA-MS hydrogen bonded conformations. This preference is also evident from Fig. 2, where many of the supposedly hydrogen-bonded TEA-MS-pairs can be identified as dumbbell-like configurations, formed by a pair of blue and yellow spheres. This imbalance of the hydrogen-bond strengths has also a surprising consequence for the structure of solvation-shells of the ions in the mixture. In Fig. 5 the average coordination-number of the anions surrounding a central cation is depicted as a function of the mixture-composition. While the total number of anions varies only slightly between 6.8 and 6.9 as a function of mixture composition, the build-up of the individual solvation shells changes more strongly: as shown in Fig. 5, in a 50:50 mixture the average number of TF-anions ($N_{TF} = 3.82$) in the first solvation shell of a TEA-cation is significantly larger than the number of MS-anions ($N_{MS} = 3.08$). This imbalance is also represented in the solvation shell of the anions: Fig. 6 shows the distribution of the number of the TEA-cations in the first solvation shell around each anion. For the pure ionic liquids (given in Fig. 6a), the distribution functions are almost identical with a maximum at 7 neighbors. In the 50–50 mixture, however, the distribution for methylsulfonate is shifted to lower values, with a maximum at 6, whereas the distribution for triflate is shifted to larger values. Apparently, the triflate-ion is able to

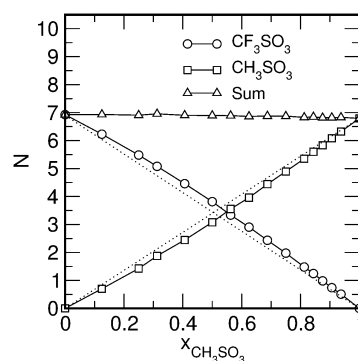


Fig. 5 Average number of both anion species N , as well as their sum, found in the first solvation shell of a TEA-cation as a function of mixture composition at $T = 300$ K.



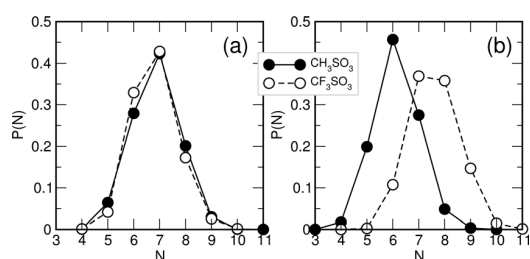


Fig. 6 Distribution of the number N of TEA-cations in the first solvation shell of the triflate- and methylsulfonate-anions at $T = 300$ K. (a) Pure ionic liquids (b) 50 : 50 mixture of TEATF–TEAMS.

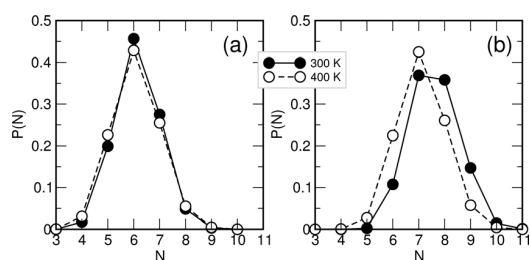


Fig. 7 Distribution of the number N of TEA-cations in the first solvation shell of the triflate- and methylsulfonate-anions in a 50 : 50 mixture of TEATF–TEAMS obtained for $T = 300$ K and $T = 400$ K. (a) Methylsulfonate–TEA (b) triflate–TEA.

“steal away” cations from the methylsulfonate in the mixture. This effect might be just due to the larger size of triflate-ion compared to the methylsulfonate. However, the reduced number of TEA-cations in the solvation shell of methylsulfonate leaves the methylsulfonate-ion prone to direct anion–anion contacts in the mixture as observed in Fig. 3. The number of TEA-cations attracted by the triflate- and methylsulfonate-ions is related with an average free energy of association, which has, of course, both entropic and an enthalpic contributions. The temperature dependence of the distribution functions shown in Fig. 7 indicates that the “binding” of TEA to the triflate-ion is significantly more temperature-sensitive than that of TEA to the methylsulfonate-ion and, hence, can be considered more weakly.

3.2 Hydrogen bonding

Numerous geometrical procedures for the determination of hydrogen bonds have been proposed³⁵ in the past. Mostly, they rely on distance criteria in addition to some angular constraints.^{35,36} We will see that for the case of protic ionic liquids discussed here, the use of angular constraints can even be omitted, since the distance distribution between the ammonium-hydrogen and the sulfonate-oxygen itself does very well discriminate between hydrogen bonded and non-hydrogen bonded states. As shown in Fig. 8, the pair correlation function between an ammonium-hydrogen and the sulfonate-oxygen exhibits a very sharp narrow first peak which goes almost down to zero for both, the pure ionic liquids, as well as for the mixtures. The number of nearest oxygen-neighbors around a hydrogen atom as a function of distance has a very well defined

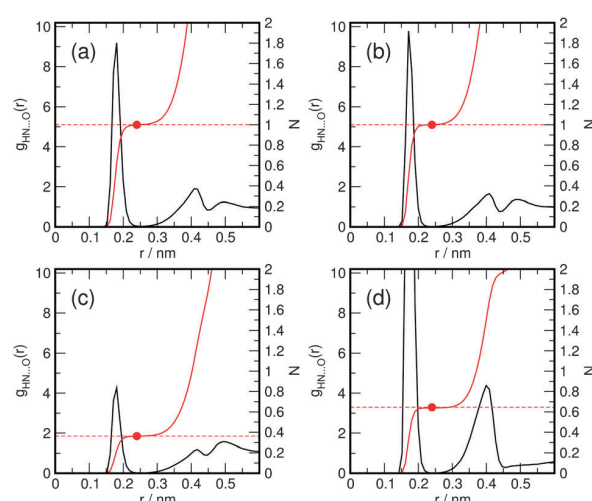


Fig. 8 H–O intermolecular site–site radial pair distribution functions $g(r)$ obtained for pure TEATF and TEAMS ionic liquids and their 50 : 50 mixture at 300 K. Also shown are the number of nearest neighbors as a function of distance $N(r)$. (a) pure TEATF (b) pure TEAMS (c) H–O correlation between TEA and TF in the $x_{\text{MS}} = 0.25$ mixture (d) H–O correlation between TEA and MS in the $x_{\text{MS}} = 0.25$ mixture.

step-like form with a plateau at 1 for the pure liquids, which indicates that an N–H-group in both ionic liquids stays practically always involved in a hydrogen-bond. Here we use a distance criterion of $r_{\text{H-O}} \leq 0.24$ nm to define a hydrogen bond for both, the triflate- and the methylsulfonate-ions. When applying this cutoff-distance of 0.24 nm, the sum of the computed number of oxygen-neighbors N for both anion-species add up to one with $\delta N < |\pm 0.01|$ for all investigated mixtures and temperatures. To further substantiate that the intermolecular H–O distance is a proper criterion for a hydrogen-bonded configuration, we have computed a probability density map of the distance $r_{\text{H-O}}$ and the cosine of the angle $\alpha_{\text{N-H/S-O}}$ between the N–H bond on the TEA and the respective S–O-bond on the methylsulfonate anion, depicted in Fig. 9. The density-plot in Fig. 9 shows that distances $r_{\text{H-O}} < 0.24$ nm correspond to an anti-parallel alignment, essentially confined to angles between 120 and 180 degrees. A second basin located at larger distances is well separated from the hydrogen-bonded basin by a free energy barrier at about $r_{\text{H-O}} \approx 0.24$ nm. The minimum of the second basin is located at a 60 degree angle, which is certainly incompatible with hydrogen bonded configurations. In fact, these configurations correspond to correlations with oxygen-sites adjacent to the oxygen involved in a hydrogen bond. An alternative representation is given in Fig. 10a, showing those angle-distributions for selected $r_{\text{H-O}}$ -distance intervals. Distances with $r_{\text{H-O}} > 0.44$ nm show almost no orientational bias with respect to the N–H and S–O bonds involved. For comparison, Fig. 10b shows the distribution of the cosine of the angle between the intermolecular N–O-vector and the N–H-bond $\alpha_{\text{N-H/N-O}}$, which has been used previously to identify linearly hydrogen-bonded configurations.³⁶ An angular cutoff of 30 degrees is suitable for hydrogen-bonds in liquid water.^{35,36} In the ionic



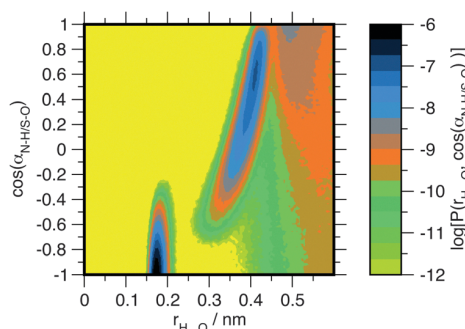


Fig. 9 Logarithmic representation of the probability-density of finding an intermolecular H-O distance $r_{H...O}$ and the cosine angle between the respective N-H and S-O vectors $\cos(\alpha_{N-H/S-O})$ obtained for the TEA-methylsulfonate pairs in a 50 : 50 TEAMS-TEATF-mixture at 300 K. The pairs were preselected with respect to their intermolecular N-O distance using $r_{N-O} < 0.8$ nm.

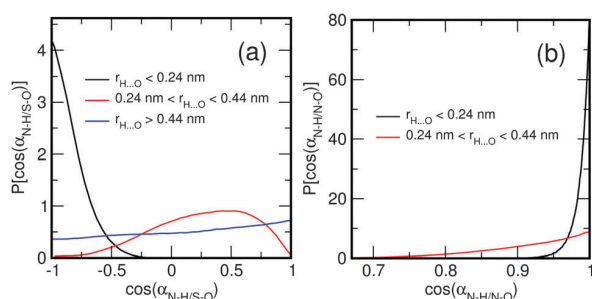


Fig. 10 Distribution of the cosine angles between two vectors for selected $r_{H...O}$ -distance ranges. (a) Cosine angle between the N-H-vector in TEA and S-O vector in methylsulfonate $\cos(\alpha_{N-H/S-O})$ (b) cosine angle between N-H-vector in TEA and intermolecular N-O vectors $\cos(\alpha_{N-H/N-O})$. Data is shown for TEA-methylsulfonate pairs in a 50 : 50 TEAMS-TEATF-mixture at 300 K. The pairs were preselected with respect to their intermolecular N-O distance using $r_{N-O} < 0.8$ nm.

liquid systems discussed here, the computed $\alpha_{N-H/N-O}$ fall well below this threshold. In fact, the computed $\alpha_{N-H/N-O}$ complies with a much narrower threshold-value of about 18 degrees, suggesting an even better defined linear hydrogen-bond configuration as in liquid water. We conclude that the O-H distance is a suitable measure to identify hydrogen bonds for the discussed systems. This has to be attributed to the peculiarities of the investigated IL, where we only have a single hydrogen-bond donor located on the cation, which is partially shielded by the ethyl-groups, in combination with an abundance of rather strong hydrogen-bond acceptor sites on the anions.

In the previous section we have seen that hydrogen bonding also affects the center-of-mass pair correlation functions and is assumed to be responsible for the splitted first peak of the anion-cation pair correlation function (shown in Fig. 4). As shown in Fig. 8c and d, the hydrogen-bond donated by the cation in the mixture is not shared by both anions according to their abundance in the mixture ($x_{MS} = 0.25$). In fact, the hydrogen bond to the methylsulfonate-ion appears to be formed in the majority of cases, shifting the equilibrium towards the

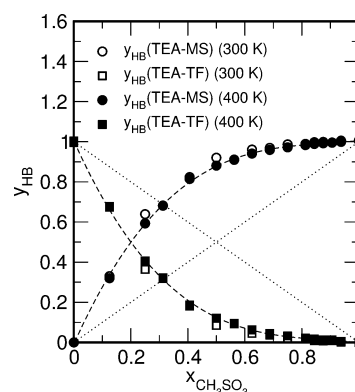


Fig. 11 Percentage of TEA-cations connected via a hydrogen bond to either a triflate- or a methylsulfonate-ion as a function of the mixture-composition at 300 K and 400 K, respectively.

formation of hydrogen bonds with the methylsulfonate-ion. This effect is not unexpected, given the larger negative partial charges on the methylsulfonate-oxygen sites. To quantify the shift, we have computed the percentage of TEA-cations involved in a hydrogen bond with respect to either anion (see Fig. 11). The data shown in Fig. 11 demonstrates the shift in equilibrium, and also indicates only a weak temperature dependence. Moreover, from the equimolar mixture we can directly estimate the difference in strength of the hydrogen-bond of a TEA-ion to either anion as a free-energy difference at 300 K according to $\Delta G_{HB}^0 = -RT \ln K_{HB} \approx 5 \text{ kJ mol}^{-1}$ with $K_{HB} = y_{HB,TF}/y_{HB,MS} \approx 0.13$.

The fact that both anions can accept up to three hydrogen bonds and that these hydrogen bonds are differently strong leads to a formation of hydrogen-bonded aggregates of varying size as a function of the composition of the mixture. First, we discuss the total number of hydrogen bonds accepted by each of the anions as a function of the mixture-composition shown in Fig. 12. In the pure liquids, each anion accepts on average one single hydrogen bond. Since each sulfonate group can accept up to three hydrogen-bonds, the strong TEA-MS hydrogen bonds causes the methylsulfonate-ion to accepting about up to ≈ 2.8 hydrogen bonds in the diluted solution ($x_{MS} \rightarrow 0$). By increasing the methylsulfonate-concentration, this number

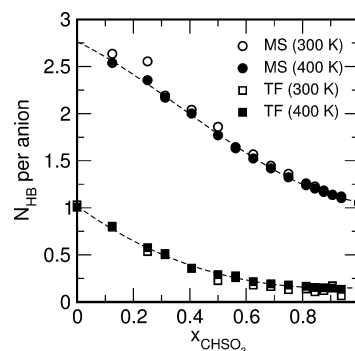


Fig. 12 Average number of hydrogen bonds accepted by the triflate- and methylsulfonate-ions at 300 K and 400 K, respectively.



drops monotonously, since the methylsulfonate-ions start to compete with each other for TEA hydrogen-bonds. The triflate-ion in the dilute triflate-solution ($x_{\text{MS}} \rightarrow 1$) only receives about ≈ 0.1 hydrogen-bonds on average, and is hence almost completely stripped of hydrogen bonds.

The distribution of the hydrogen-bonded aggregates are finally shown in Fig. 13. Indicated are the percentages of each of the anions connected to either no, one, two or three TEA-cations *via* hydrogen-bonding. Note that for both pure ionic liquids, the distribution of aggregate sizes is almost identical: single hydrogen-bonded ($n = 1$) aggregates contribute about $\approx 50\%$, whereas the configurations with no ($n = 0$) and two hydrogen bonds ($n = 2$) are both near at about $\approx 24\%$. Configurations with three hydrogen bonds ($n = 3$) are rare and contribute only to $\approx 2\text{--}3\%$. With increasing methylsulfonate-concentration, the population of triflate-ions with no hydrogen-bonds (“free” triflate-ions) is increasing strongly to a plateau value of about 85% to 90% for $x_{\text{MS}} \rightarrow 1$. At the same time the percentage of configurations with one hydrogen bond drops down to 10% to 15%. Configurations with more than one hydrogen bond are practically non-existent. With increasing triflate-concentration, on the other hand, the methylsulfate-ions attract more and more hydrogen-bonds, leading to an increasing percentage of MS-ions attached to two ($n = 2$) and three ($n = 3$) TEA-cations. Here the configurations with two hydrogen-bonds first increase, but are getting increasingly replaced by configurations with three hydrogen-bonds. For $x_{\text{MS}} \rightarrow 0$, finally,

the $n = 3$ -fraction represents the majority of configurations with $\approx 75\%$, and $n = 2$ representing the rest with $\approx 25\%$. Configurations with no or one hydrogen-bond have practically vanished.

We summarize that the exact size and distribution of the hydrogen-bonded aggregates is apparently determined by the strengths of the hydrogen-bonds, the number of hydrogen-bonded donors and acceptors on the ions, as well as their respective coordination-numbers. In the following section, we will introduce a “cartoon-like” representation of the ionic liquid, which is based on a minimal set of assumptions extracted from our MD-simulation, and can be used to compute the observed cluster-sizes as a function of the mixture-composition in a semi-quantitative fashion.

3.3 A “cartoon-like” model of hydrogen bonding in the IL mixture

For a better understanding of the hydrogen-bonded cluster-sizes in the IL mixtures, we would like to introduce a simplified description of the hydrogen bond equilibrium. For this purpose we construct a simplified model of the ionic liquid as outlined in Fig. 14. Here, the liquid is represented by a cubic lattice, where the anions and cation occupy sites in an alternating fashion, leading to a octahedral coordination of each ion with a coordination number of $c = 6$. In addition, we assume that each TEA-cation stays always involved in a hydrogen-bond, and is pointing with its N–H-bond towards one of the c surrounding anions. In a pure ionic liquid, the cation–anion hydrogen-bond is, of course, supposed to connect the TEA-cation randomly with one of its c anion neighbors. If each anion would be able to accept c hydrogen-bonds from the surrounding TEA-cations equally well, the probability of finding an anion accepting n hydrogen-bonds simultaneously $P_{c,n}$ would exactly follow a binomial distribution

$$P_{c,n} = \frac{c!}{n!(c-n)!} \cdot p^n \cdot (1-p)^{c-n}, \quad (2)$$

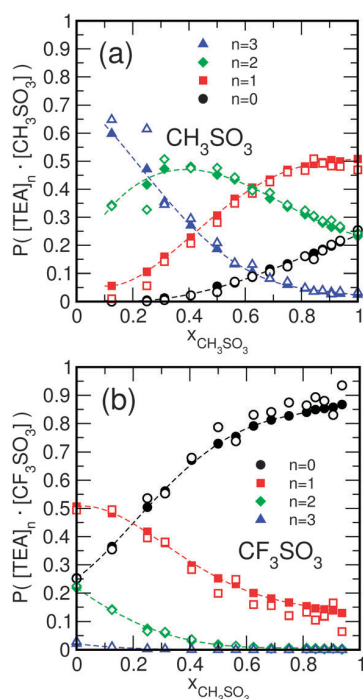


Fig. 13 Percentage of triflate- and methylsulfonate-ions hydrogen-bonded to zero, one, two, and three TEA-cations as a function of the mixture-composition. Open symbols: 300 K. Closed symbols: 400 K (a) methylsulfonate (b) triflate.

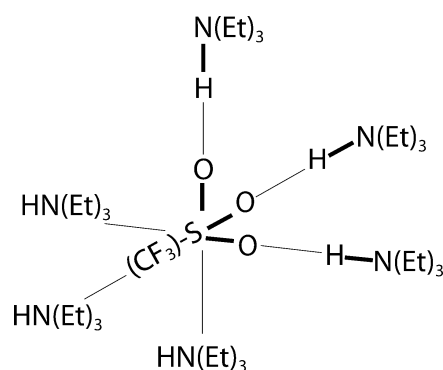


Fig. 14 “Cartoon-like” representation of the ionic liquid: the liquid is represented by a cubic lattice, where the anions and cations occupy sites in an alternating fashion. Each ion is octahedrally coordinated and surrounded by $c = 6$ counter-ions. Each anion (either triflate or methylsulfonate) can accept up to three hydrogen bonds. The N–H groups of each of the TEA-molecules are involved in a hydrogen-bond to one of their c surrounding neighbors.



where p represents the probability of a TEA-cation pointing with its N-H bond towards the central anion. Assuming a purely random orientation of the TEA-N-H-bond on the lattice, p corresponds to the inverse coordination number of the TEA-ion ($p = 1/c$). However, to account for the fact that the triflate and methylsulfonate-anions can each accept only up to three hydrogen-bonds, we have to modify the distribution function by introducing configuration-specific weights-factors $w_{c,n}$ with $w_{c,n} = 0$ for $n > 3$.

$$P_{c,n} = \frac{c!}{n!(c-n)!} \cdot Q^{-1} \cdot w_{c,n} \cdot p^n \cdot (1-p)^{c-n}. \quad (3)$$

To ensure proper normalisation, the modified weights are counter-balanced by a constant Q , which has to be computed numerically according to

$$Q = \sum_{n=0}^c \frac{c!}{n!(c-n)!} \cdot w_{c,n} \cdot p^n \cdot (1-p)^{c-n}. \quad (4)$$

In a first step, we will discuss a situation, where the non-zero statistical weights are all equal ($w_{c,n} = 1$ for $n \leq 3$). In addition, we will assume that the chosen weights do not change as function of the mixture-composition. In the mixture, however, the hydrogen-bond of TEA to each of the two anion-species varies in strength. This will, hence, also modify the hydrogen-bond acceptance probability for each of the anions. In all cases, the TEA cation points to one of the c surrounding neighbors with a site-specific probability p_i . Of course, those probabilities do add all up to unity:

$$1 = \sum_{i=1}^c p_i. \quad (5)$$

Since each of the sites i is assumed to be statistically occupied by one of the two anion-species according to their mixture composition $x = x_{\text{MS}}$, the average probability p_i of accepting a hydrogen-bond is hence a composition-weighted sum of the individual probabilities of the anions according to

$$p_i = x \cdot p_{\text{MS}} + (1-x) \cdot p_{\text{TF}} \quad (6)$$

From eqn (5) and (6), the universal anion-specific hydrogen-bond-acceptance probabilities follow as

$$\begin{aligned} p_{\text{MS}} &= \frac{1}{cx + c(1-x)f} \\ p_{\text{TF}} &= \frac{1}{cx f^{-1} + c(1-x)}, \end{aligned} \quad (7)$$

with $f = p_{\text{TF}}/p_{\text{MS}}$. From eqn (7) we can directly determine the fraction of times, a N-H bond of a TEA-cation points to either a methylsulfonate- or triflate-ion as

$$\begin{aligned} y_{\text{HB,MS}} &= cx \cdot p_{\text{MS}} \\ &= \frac{1}{1 + f(1-x)x^{-1}} \end{aligned} \quad (8)$$

and

$$\begin{aligned} y_{\text{HB,TF}} &= c(1-x) \cdot p_{\text{TF}} \\ &= \frac{1}{1 + f^{-1}(1-x)^{-1}x}. \end{aligned} \quad (9)$$

The ratio f can be determined from MD simulation data by taking the values for the fraction of hydrogen-bonds of one TEA-molecule to each of the two anion-species from the equimolar mixture. Using the data shown in Fig. 11, we determine $f = y_{\text{HB,TF}}/y_{\text{HB,MS}} \approx 0.13$. Assuming that f does not change significantly as a function of the composition x , we can now compute the hydrogen-bonded cluster sizes $P_{c,n}$ for both, the methylsulfonate and the triflate anions, as well as the average number of hydrogen bonds accepted by each anion according to

$$N_{\text{HB}} = \sum_{n=0}^c n \cdot P_{c,n} \quad (10)$$

Fig. 15 shows the prediction of the sizes of the hydrogen-bonded aggregates according the model using equal weights with $w_{6,n} = 1$ for $n \leq 3$ and $w_{6,n} = 0$ for $n > 3$. Essential features of the distributions obtained from the MD-simulation, such as the existence of a maximum of MS-TEA aggregates with two hydrogen bonds, are well recovered by just using an approximate coordination number, and taking into account that both anions can accept no more than three hydrogen bonds. Also, the percentage of hydrogen-bonds of TEA to either anion-species, as well as the total number of accepted hydrogen bonds (Fig. 16) are nicely captured. However, the distribution of aggregate-sizes in the pure TEAMS and TEATF liquids are not correctly represented. In particular, the model underestimates the single-bonded configurations and overestimates the configurations with no hydrogen-bond. To better represent the distribution within the pure liquids and to improve the model, we adjust the non-zero weight-factors $w_{c,n}$ for $n \leq 3$ to match the MD simulation results (as shown in Fig. 13) for the respective pure ionic liquids with $P_{6,0} = 0.24$, $P_{6,1} = 0.51$, $P_{6,2} = 0.22$, and $P_{6,3} = 0.03$. For simplicity, we use the same values for both, TEATF and TAMS. Those probabilities are recovered by using statistical weights of $w_{6,0} = 0.75$, $w_{6,1} = 1.3$, $w_{6,2} = 1.12$,

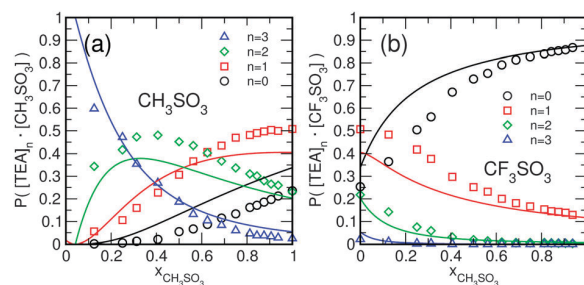


Fig. 15 Percentage of methylsulfonate- (a) and triflate-ions (b) hydrogen-bonded to zero, one, two, and three TEA-cations, as a function of the mixture-composition at 400 K. Symbols: MD-simulation. Solid lines: model using equal statistical weights with $w_{6,n} = 1$ for $n \leq 3$ and $w_{6,n} = 0$ for $n > 3$.



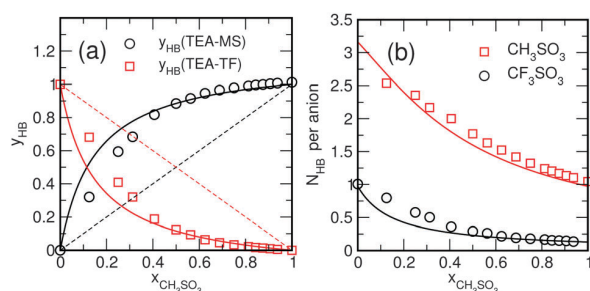


Fig. 16 (a) Percentage of TEA-cations connected *via* a hydrogen bond to either a triflate-ion or a methylsulfonate-ion as a function of the mixture-composition. (b) Average number of hydrogen bonds accepted by the triflate- and methylsulfonate-ions. Open symbols: MD-data obtained at 400 K. Solid lines: model using equal statistical weights with $w_{6,n} = 1$ for $n \leq 3$ and $w_{6,n} = 0$ for $n > 3$.

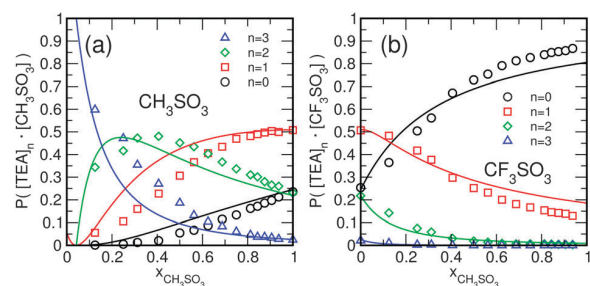


Fig. 17 Percentage of methylsulfonate- (a) and triflate-ions (b) hydrogen-bonded to zero, one, two, and three TEA-cations, as a function of the mixture-composition at 400 K. Symbols: MD-simulation. Solid lines: model using statistical weights adjusted to the distribution in the pure liquids with $w_{6,0} = 0.75$, $w_{6,1} = 1.3$, $w_{6,2} = 1.12$, $w_{6,3} = 0.5$, and $w_{6,n} = 0$ for $n > 3$.

and $w_{6,3} = 0.5$ for both anions. The weight-factors indicate that the anions in the pure IL feel most comfortable with just one hydrogen bond pointing towards them. Situations with three hydrogen bonds have a significantly lower statistical weight, most likely due to orientational restraints, introduced by a configuration involving three hydrogen bonds to adjacent ions. Particularly, the situation without any hydrogen-bonds exhibits a significantly reduced statistical weight compared to the random distribution of hydrogen-bonds. The distribution of clusters shown in Fig. 17 demonstrate a significant improvement, leading to a semi-quantitative description of the MD-data. Moreover, the good overall description of the simulation-data by our model is suggesting that the two anion-species are statistically distributed in the liquid. However, also certain weaknesses of the model are evident, particularly for the percentage of hydrogen-bonds of TEA to either anion-species in the range $x_{MS} < 0.3$. By introducing a composition-dependent factor $f(x_{MS})$ a better representation of the data shown in Fig. 16a and 18a could be achieved (not shown). Interestingly, this does, in fact, worsen the description of the distribution of cluster-sizes, indicating the need to also account for the changing coordination-numbers, and thus pointing at the limits of the model.

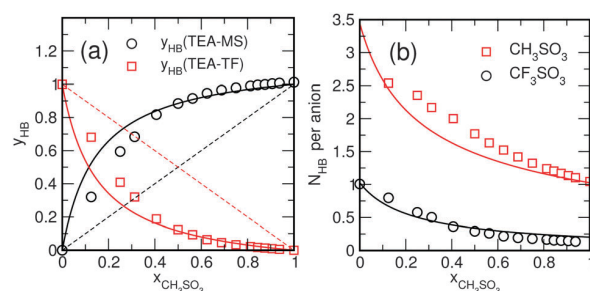


Fig. 18 (a) Percentage of TEA-cations connected *via* a hydrogen bond to either a triflate-ion or a methylsulfonate-ion as a function of the mixture-composition. (b) Average number of hydrogen bonds accepted by the triflate- and methylsulfonate-ions. Open symbols: MD-data obtained at 400 K. Solid lines: model using statistical weights adjusted to the distribution in the pure liquids with $w_{6,0} = 0.75$, $w_{6,1} = 1.3$, $w_{6,2} = 1.12$, $w_{6,3} = 0.5$, and $w_{6,n} = 0$ for $n > 3$.

4 Conclusions

We have reported results of molecular dynamics simulations characterising the hydrogen bonding in mixtures of two protic ionic liquids sharing the same cation: triethylammonium-methylsulfonate and triethylammonium-triflate. The triethylammonium-cation acts as a hydrogen-bond donor, being able to donate a single hydrogen bond. Both, the methylsulfonate- and the triflate-anions can act as hydrogen-bond acceptors, which can accept multiple hydrogen bonds *via* their SO_3^- groups. Replacing a methyl-group in the methylsulfonate by a trifluoromethyl-group in the triflate significantly weakens the strength of a hydrogen bond from an adjacent triethylammonium-cation to the oxygen-site in the SO_3^- -group of the respective anion. Our MD simulations show that these rather subtle differences in hydrogen bond strength significantly affect the formation of differently-sized hydrogen-bonded aggregates in the mixtures as a function of the mixture-composition. A defining structural feature of ionic liquids in general and of the studied protic ionic liquid in particular is the charge-alternating order of the ions, leading to counter-ion coordination numbers between six and eight. This fact is represented in a simple “cartoon-like” lattice model of the liquid, placing ions on a cubic lattice in an alternating fashion with an approximate counter-ion coordination number of six. By introducing statistical weights that mostly account for the fact that each anion can only accept up to three hydrogen bonds, and by adjusting the balance between the hydrogen bond of TEA to either of the two anions, the simple model is able to qualitatively predict the distribution of differently-sized hydrogen-bonded aggregates as well as the total number of hydrogen bonds accepted by the anions as a function of the mixture-composition. By adjusting the statistical weights for each cluster in such a way that the cluster sizes match the distribution observed in the pure liquids, an even semi-quantitative description of the data obtained from MD simulation emerges. Finally, we would like to comment of the issue of the “doublesaltiness” of the studied ionic liquid mixture as



pointed out by Rogers *et al.*⁶ Their line of reasoning is that in a mixture of ILs, the constituents (ions) do not seem to retain their individual nature. Hence, they proposed to consider them as double-salt ionic liquids. We think that our model-system is a particularly nice demonstration of the concept: although the pure ionic liquids and their mixtures exhibit great similarity with respect to the overall ion-alternating structure, each of the statistically distributed anions experiences a completely different local environment.

Acknowledgements

This work was supported by the Deutsche Forschungsgemeinschaft (DFG) Priority Programme SPP 1191 “Ionic Liquids” and the DFG Collaborative Research Center SFB 652 “Strong correlations and collective effects in radiation fields: Coulomb systems, clusters and particles”

References

- P. Wasserscheid and T. Welton, *Ionic Liquids in Synthesis*, Wiley-VCH, 2nd edn, 2008.
- F. Endres and S. Z. El Abedin, *Phys. Chem. Chem. Phys.*, 2006, **8**, 2101–2116.
- H. Weingärtner, *Angew. Chem., Int. Ed.*, 2008, **47**, 654–670.
- N. V. Plechkova and K. R. Seddon, *Chem. Soc. Rev.*, 2008, **37**, 123–150.
- H. Niedermeyer, J. P. Hallett, I. J. Villar-Garcia, P. A. Hunt and T. Welton, *Chem. Soc. Rev.*, 2012, **41**, 7780–7802.
- G. Chatel, J. F. B. Pereira, V. Debbeti, H. Wang and R. D. Rogers, *Green Chem.*, 2014, **16**, 2051–2083.
- K. Fumino, A. Wulf and R. Ludwig, *Angew. Chem., Int. Ed.*, 2008, **47**, 8731–8734.
- K. Fumino and R. Ludwig, *J. Mol. Liq.*, 2014, **192**, 94–102.
- M. Y. Lui, L. Crowhurst, J. P. Hallett, P. A. Hunt, H. Niedermeyer and T. Welton, *Chem. Sci.*, 2011, **2**, 1491–1496.
- P. Navia, J. Troncoso and L. Romani, *J. Chem. Eng. Data*, 2007, **52**, 1369–1374.
- A. Arce, M. J. Earle, S. P. Katdare, H. Rodriguez and K. R. Seddon, *Chem. Commun.*, 2006, 2548–2550.
- J. N. Canongia Lopes, T. C. Cordeiro, J. M. S. S. Esperanca, H. J. R. Guedes, S. Huq, L. P. N. Rebelo and K. R. Seddon, *J. Phys. Chem. B*, 2005, **109**, 3519–3525.
- D. Xiao, J. R. Rajian, L. G. Hines, S. Li, R. A. Bartsch and E. L. Quitevis, *J. Phys. Chem. B*, 2008, **112**, 13316–13325.
- K. Fumino, V. Fossog, K. Wittler, R. Hempelmann and R. Ludwig, *Angew. Chem., Int. Ed.*, 2013, **52**, 2368–2372.
- P. Stange, K. Fumino and R. Ludwig, *Angew. Chem., Int. Ed.*, 2013, **52**, 2990–2994.
- K. Fumino, A. M. Bonsa, B. Golub, D. Paschek and R. Ludwig, *ChemPhysChem*, 2015, **16**, 299–304.
- S. Nosé, *Mol. Phys.*, 1984, **52**, 255–268.
- W. G. Hoover, *Phys. Rev. A: At., Mol., Opt. Phys.*, 1985, **31**, 1695–1697.
- M. Parrinello and A. Rahman, *J. Appl. Phys.*, 1981, **52**, 7182–7190.
- S. Nosé and M. L. Klein, *Mol. Phys.*, 1983, **50**, 1055–1076.
- U. Essmann, L. Perera, M. L. Berkowitz, T. A. Darden, H. Lee and L. G. Pedersen, *J. Chem. Phys.*, 1995, **103**, 8577–8593.
- S. Miyamoto and P. A. Kollman, *J. Comput. Chem.*, 1992, **13**, 952–962.
- E. Lindahl, B. Hess and D. van der Spoel, *J. Mol. Model.*, 2001, **7**, 306–317.
- M. Abraham, E. Apol, R. Apostolov, H. J. Berendsen, A. van Buuren, P. Bjelkmar, R. van Drunen, A. Feenstra, S. Fritsch, G. Groenhof, C. Junghans, J. Hub, P. Kasson, C. Kutzner, B. Lambeth, P. Larsson, J. A. Lemkul, E. Marklund, P. Meulenhoff, T. Murtola, S. Pall, S. Pronk, R. Schulz, M. Shirts, A. Sijbers, P. Tieleman, M. Wolf, B. Hess, D. van der Spoel and E. Lindahl, *GROMACS - Groningen Machine for Chemical Simulations User Manual Version 4.6.1*, 2013.
- H. Flyvbjerg and H. G. Petersen, *J. Chem. Phys.*, 1989, **91**, 461–466.
- H. J. C. Berendsen, J. P. M. Postma, W. F. van Gunsteren, A. DiNola and J. R. Haak, *J. Chem. Phys.*, 1984, **81**, 3684–3690.
- W. L. Jorgensen and M. Ibrahim, *J. Am. Chem. Soc.*, 1981, **103**, 3976–3985.
- M. J. Frisch, G. W. Trucks, H. B. Schlegel, G. E. Scuseria, M. A. Robb, J. R. Cheeseman, G. Scalmani, V. Barone, B. Mennucci, G. A. Petersson, H. Nakatsuji, M. Caricato, X. Li, H. P. Hratchian, A. F. Izmaylov, J. Bloino, G. Zheng, J. L. Sonnenberg, M. Hada, M. Ehara, K. Toyota, R. Fukuda, J. Hasegawa, M. Ishida, T. Nakajima, Y. Honda, O. Kitao, H. Nakai, T. Vreven, J. A. Montgomery Jr, J. E. Peralta, F. Ogliaro, M. Bearpark, J. J. Heyd, E. Brothers, K. N. Kudin, V. N. Staroverov, R. Kobayashi, J. Normand, K. Raghavachari, A. Rendell, J. C. Burant, S. S. Iyengar, J. Tomasi, M. Cossi, N. Rega, J. M. Millam, M. Klene, J. E. Knox, J. B. Cross, V. Bakken, C. Adamo, J. Jaramillo, R. Gomperts, R. E. Stratmann, O. Yazyev, A. J. Austin, R. Cammi, C. Pomelli, J. W. Ochterski, R. L. Martin, K. Morokuma, V. G. Zakrzewski, G. A. Voth, P. Salvador, J. J. Dannenberg, S. Dapprich, A. D. Daniels, Ö. Farkas, J. B. Foresman, J. V. Ortiz, J. Cioslowski and D. J. Fox, *Gaussian 09, Revision D.01*, Gaussian Inc, Wallingford, CT, 2009.
- U. C. Singh and P. Kollman, *J. Comput. Chem.*, 1984, **5**, 129–145.
- C. I. Bayly, P. Cieplak, W. D. Cornell and P. A. Kollman, *J. Phys. Chem.*, 1993, **97**, 10269–10280.
- T. Köddermann, D. Paschek and R. Ludwig, *ChemPhysChem*, 2007, **8**, 2464–2470.
- H. Krienke, V. Vlachy, G. Ahn-Ercan and I. Bako, *J. Phys. Chem. B*, 2009, **113**, 4360–4371.
- M. G. Martin and J. I. Siepmann, *J. Phys. Chem. B*, 1998, **102**, 2569–2577.
- D. Roy, N. Patel, S. Conte and M. Maroncelli, *J. Phys. Chem. B*, 2010, **114**, 8410–8424.
- R. Kumar, J. R. Schmidt and J. L. Skinner, *J. Chem. Phys.*, 2007, **126**, 204107.
- A. Luzar and D. Chandler, *Nature*, 1996, **379**, 55–57.



4.4 Publication III

Hydrogen Bond Redistribution in Mixtures of Protic Ionic Liquids Sharing the Same Cation: Nonideal Mixing Behavior with large Mixing Enthalpies

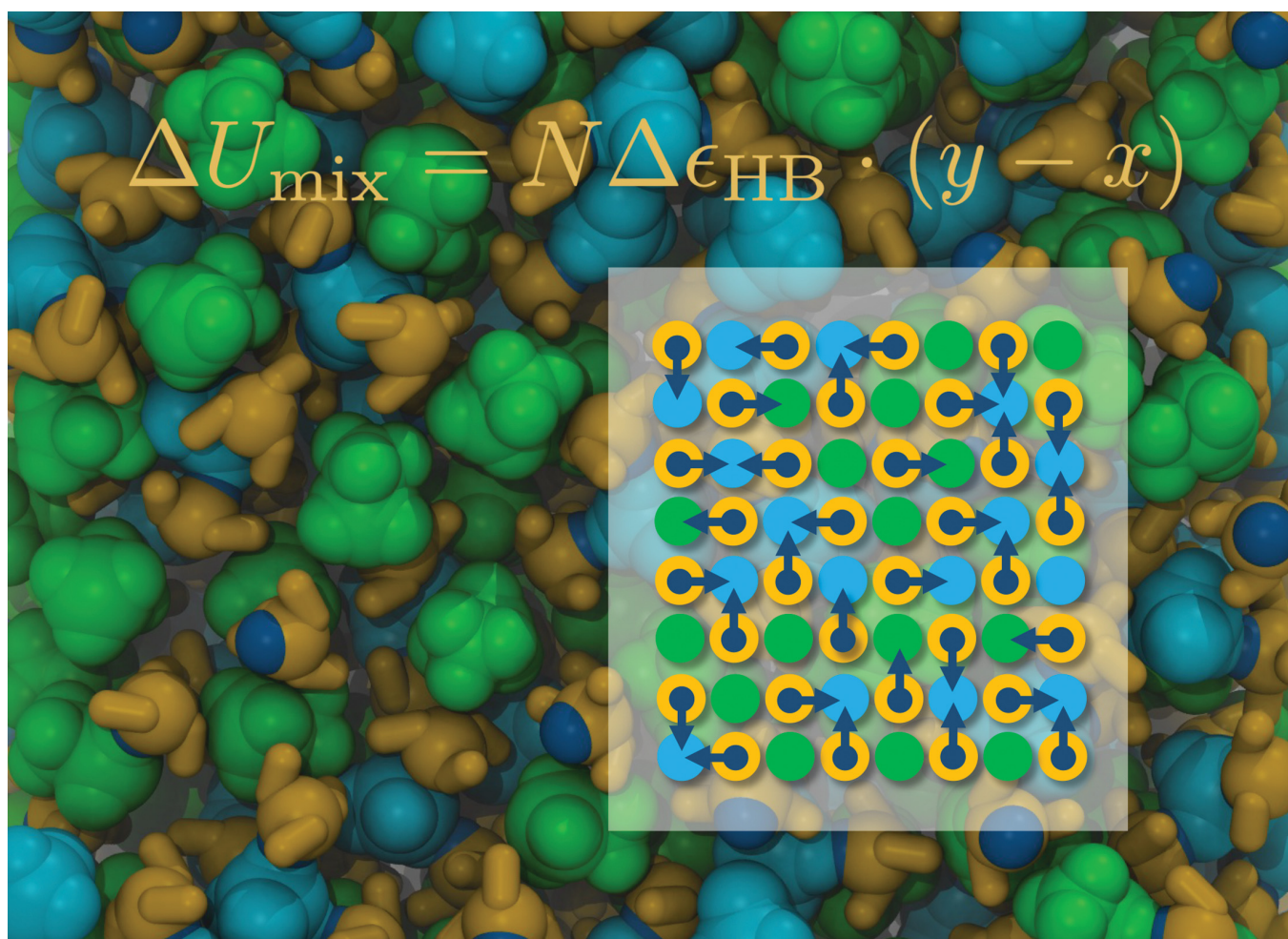
B. Golub, D. Ondo, V. Overbeck, R. Ludwig and D. Paschek

Phys. Chem. Chem. Phys., 2022, **24**, 14740-14750

CRedit roles: Data curation (MD simulations), Formal analysis (MD simulations), Investigation (MD simulations), Visualization, Writing - original draft

Approximated contribution to the publication in percent: 50 %

Reproduced from Ref.: B. Golub, D. Ondo, V. Overbeck, R. Ludwig, and D. Paschek, *Phys. Chem. Chem. Phys.*, 2022, **24**, 14740-14750, DOI: 10.1039/D2CP01209J with permission from the Royal Society of Chemistry.

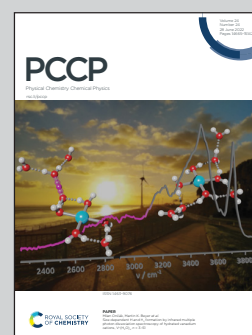


Showcasing research from the University of Rostock, and the University of Chemistry and Technology, Prague

Hydrogen bond redistribution effects in mixtures of protic ionic liquids sharing the same cation: non-ideal mixing with large negative mixing enthalpies

This work is a joint experimental and theoretical study investigating hydrogen bond redistribution in mixtures of protic ionic liquids which exhibit unusually large negative energies of mixing. Due to the ordered structure of the liquid, solely the redistribution of hydrogen bonds causes these enthalpic effects. By connecting the equilibrium of hydrogen bonds to the two anion species with the mixing energies *via* a lattice model, a simple quantitative relation emerges describing the mixing energies.

As featured in:



See Dietmar Paschek *et al.*,
Phys. Chem. Chem. Phys.,
2022, **24**, 14740.



Cite this: *Phys. Chem. Chem. Phys.*,
2022, 24, 14740

Hydrogen bond redistribution effects in mixtures of protic ionic liquids sharing the same cation: non-ideal mixing with large negative mixing enthalpies†

Benjamin Golub,^a Daniel Ondo,^b Viviane Overbeck,^a Ralf Ludwig^{a,c} and Dietmar Paschek^{ID}*^a

We report a joint experimental and theoretical study characterising the hydrogen bond (HB) redistribution in mixtures of two different protic ionic liquids (PILs) sharing the same cation: triethylammonium–methanesulfonate ([TEA][OMs]) and triethylammonium–trifluoromethanesulfonate ([TEA][OTf]). The mixing behaviour deviates strongly from ideality, exhibiting large negative energies of mixing. In the PIL, the [TEA] cation acts as a HB donor, being able to donate a single HB. Both, the [OMs] and the [OTf] anions can act as HB acceptors, which can accept multiple HBs via their respective SO₃-groups. We use a combination of molecular dynamics (MD) simulations, calorimetry, and ¹H-NMR chemical shift measurements to determine the difference in HB strength between the two species to be about 13 kJ mol^{−1}, favouring the [TEA]–[OMs] interaction. Based on our MD simulations we are able to formulate a lattice model, discriminating between HB and nonspecific intermolecular interactions. We demonstrate that, due to the ordered structure of the PILs, mostly the HB interactions contribute to the mixing energy. This allows us to connect the equilibrium of HBs to each of the two anion species with the mixing energies by a simple relation, which is obeyed by both, MD-simulation as well as experimental calorimetry and ¹H-NMR chemical shift data.

Received 13th March 2022,
Accepted 11th May 2022

DOI: 10.1039/d2cp01209j

rsc.li/pccp

1 Introduction

Protic ionic liquids (PILs)^{1–4} have attracted considerable interest since they exhibit qualities other solvents often lack: a gentle solvation behaviour,⁵ low toxicity,⁶ electrochemical stability,⁷ and biocompatibility.⁸ Mixtures of ionic liquids (ILs), also called “Double Salt ILs” (DSILs),⁹ have gained increasing attention in recent years.^{10–41} The concept of DSILs has been introduced since pure ILs already consist of two components with possibly antagonistic properties. Hence mixtures of two ILs experience a degree of variability, typically not accessible to mixtures of molecular liquids. Ions may even “switch their identity” in the mixture.⁹ IL mixtures are often characterised according to their deviation from Raoult's law, which is indicating *ideal* mixing.⁴² The interactions between the ions, of course, dictate whether *nonideal* behavior is observed.

Hydrogen bonding,^{43,44} but also strong dispersion interactions⁴⁵ can introduce a significant *nonideality*. By measuring the enthalpy of mixing,^{42–51} those changing interactions can be investigated directly. If the enthalpy of mixing is close to zero, the interactions scale exactly proportional to the mixture composition, which is the very definition of *ideal* mixing. Positive or negative enthalpies of mixing, however, imply the “making or breaking”⁹ of interactions and are therefore often related with changes of the liquid-structure.⁵²

Mixtures of ILs have been studied extensively. Navia *et al.* have investigated mixtures of imidazolium-based ILs with [BF₄][−], [PF₆][−], and [OMs][−] as counter ions.⁴⁶ For mixtures sharing the same anion but with different cations (with varying chain length) positive enthalpies of mixing were observed, whereas the opposite was found for mixture with the same cation but different anions.

Molecular dynamics (MD) simulations by Castejón and Lashock analysed volume-related effects on mixtures.⁴⁷ Their simulations revealed that mixtures of ions with comparable molar volumes exhibit a negative enthalpy of mixing and follow the cross-square rules of mixing. Mixtures with different molar volumes, however, exhibited a positive enthalpy of mixing.

Since 2013 Costa Gomes and coworkers have thoroughly investigated mixtures of imidazolium-based ILs. First they

^a Universität Rostock, Institut für Chemie, Physikalische und Theoretische Chemie, Albert-Einstein-Straße 27, 18059 Rostock, Germany. E-mail: dietmar.paschek@uni-rostock.de

^b University of Chemistry and Technology, Department of Physical Chemistry, Technická 5., 166 28 Prague 6, Czech Republic

^c Leibniz-Institut für Katalyse, Albert-Einstein-Straße 29a, D-18059 Rostock, Germany

† Electronic supplementary information (ESI) available. See DOI: <https://doi.org/10.1039/d2cp01209j>

focused on mixtures of ILs sharing the same anion with varying cations. Initially, they could confirm the findings by Navia *et al.*⁴⁵ A mixture with two different anions ([C₄mim][NTf₂] and [C₄mim][PF₆]), however, exhibited a strongly positive enthalpy of mixing, which is contradicting the findings of Navia *et al.* Strong negative enthalpies of mixing could be observed for mixtures of [C₄mim][OAc] and [C₄mim][C(CN)₃], which were attributed to changes in the hydrogen bonded network.⁴³ In a subsequent study⁴⁹ they concluded that mixtures with the same cation but different anions typically show a negative enthalpy of mixing. A recent study,⁵¹ however, is less conclusive: the mixture of [C₄mim][OAc] and [P₄₄₄₄][OAc] is showing a strong negative enthalpy of mixing, whereas mixtures of [C₂mim][N(CN)₂] and [N₄₄₄₁][N(CN)₂] showed a positive enthalpy of mixing with a maximum slightly moved to larger mole fractions of [C₂mim][N(CN)₂].

Hydrogen bonding has been shown to have a strong influence on the mixing behaviour. Herrera *et al.* investigated imidazolium-based IL mixtures with amino acid anions and found both, negative as well as positive enthalpies of mixing. These observations were attributed to different hydrogen bonded structures.⁴⁴ Docampo-Álarez *et al.* have mixed protic and aprotic ILs and could show that all of these mixtures exhibit negative enthalpies of mixing, depending on the alkyl chain length, size of polar regions and hydrogen bonding.⁵⁰

Extensive reviews of IL mixtures, including discussions of the enthalpies of mixing are given in publications from 2012,⁴² 2014,⁹ and 2016.⁴⁸

In this study we investigate a mixture of the two PILs: triethylammonium methanesulfonate ([TEA][OMs]) and triethylammonium trifluoromethanesulfonate ([TEA][OTf]). This particular mixture offers the possibility to separate contributions due to hydrogen bonding from other nonspecific intermolecular interactions to the energy of mixing. In the mixtures the N–H group of the [TEA] cation can act as a HB donor, whereas the SO₃-groups of both anions can accept up to three HBs. It has been shown by both, experiment and theory that HBs between [TEA] and [OMs] are stronger than those between [TEA] and [OTf].^{23,53,54} As a consequence, MD simulations were able to detect a significant redistribution of HBs between a cation and the two anions in the mixture.^{22,55,56} Since the solvation shell of each anion is almost entirely composed of [TEA] cations, the local environment of each anion in the mixture and in the pure PILs are very similar, such that HB redistribution is most likely a dominant contribution to the nonideal mixing behaviour. In a recent statistical mechanical analysis we were able to show that HB redistribution could even lead to an overall negative entropy of mixing, and create a situation that the entire mixing process is driven by enthalpy, and not entropy.⁵⁶

In this contribution, we will use MD simulations to demonstrate that HB redistribution is leading to large negative energies of mixing by formulating a lattice model relating the energy of mixing with the amount of HB redistribution and the difference in strength of HB interactions. Subsequently, this model is applied to experimental enthalpies of mixing and

experimental HB redistribution data obtained from ¹H-NMR chemical shift measurements, and will enable us to experimentally obtain the difference in HB interaction strength between a [TEA] cation and the two anion species.

2 Methods

2.1 Molecular dynamics simulations

To study pure PILs and their mixtures, we performed isobaric isothermal (*NPT*) MD simulations using GROMACS 5.0.6.⁵⁷ We investigated eleven compositions between $x_{\text{OMs}} = 0.0$ and $x_{\text{OMs}} = 1.0$ for six temperatures between $T = 300$ K and $T = 400$ K at a pressure of 1 bar. All studied systems were composed of 500 ion pairs. Simulation boxes were constructed using PACKMOL⁵⁸ and equilibrated for 3 ns using the Berendsen-thermostat with a coupling constant of $\tau_T = 0.5$ ps as well as the Berendsen-barostat with a coupling constant of $\tau_P = 0.5$ ps.⁵⁹ For all mixtures, production runs of 50 ns were carried out employing the Nosé–Hoover-thermostat^{60,61} ($\tau_T = 0.5$ ps) and the Rahman–Parrinello-barostat^{62,63} ($\tau_P = 2.0$ ps and $\chi_T = 33 \times 10^{-6}$ bar⁻¹) using a time-step of 2.0 fs. Bond lengths were kept fixed by employing the LINCS algorithm.⁶⁴ Long range electrostatic interactions were treated by using smooth particle mesh Ewald summation⁶⁵ (real space cutoff 0.9 nm, mesh spacing of 0.12 nm, 4th order interpolation and convergence factor 3.38 nm⁻¹). For analysing the simulations we used GROMACS⁵⁷ and MOSCITO⁶⁶ tools. In addition, the computation of the properties from MD data were determined using home-built software based on the MDAnalysis,^{67,68} NumPy,⁶⁹ and SciPy⁷⁰ frameworks. All force fields used are described in detail in ref. 22. An extensive summary of the performed simulations and of the computed properties can be found in Section S1.1 of the ESI†. Simulation-related files are permanently publicly available from the RosDok repository of the University of Rostock.⁷¹

2.2 Preparation of PILs and mixtures

The pure PILs were synthesised, properly dried, and characterised as described in earlier studies.⁵³ The water content of the pure PILs was below 100 ppm, as detected by using the Karl Fischer titration method. The PIL mixtures were prepared under an argon atmosphere and properly stirred until they reached homogeneity as described in ref. 23. We estimate that indicated mixture compositions are accurate within ≤ 0.5 Mol%.

2.3 ¹H-NMR chemical shift measurements

All NMR measurements were performed using a BRUKER Avance 500 spectrometer. Details about the spectrometer setup can be found in ref. 72. We measured the ¹H-NMR chemical shifts of the N–H proton located on the [TEA] cation in the pure PILs and in mixtures with compositions $x_{\text{OMs}} = 0.25$, $x_{\text{OMs}} = 0.5$, and $x_{\text{OMs}} = 0.75$. The measured spectra are provided in Section S3 of the ESI†. Using tetramethylsilane (TMS) as an external reference, we obtained downfield chemical shifts for the N–H proton of $\delta(^1\text{H}, [\text{TEA}][\text{OMs}]) = 7.22$ ppm for [TEA][OMs] and

$\delta(^1\text{H}, [\text{TEA}][\text{OTf}]) = 8.88$ ppm for $[\text{TEA}][\text{OTf}]$ at 298 K, respectively. This reflects the expected order for the increasing interaction strength of the anions in the sequence $[\text{OMs}] > [\text{OTf}]$, as obtained from FIR measurements^{23,53} and quantum chemical calculations.⁵⁴ The ^1H -NMR chemical shifts of the N-H proton in the mixtures were obtained as follows: $\delta(^1\text{H}, x_{\text{OMs}} = 0.25) = 7.87$ ppm, $\delta(^1\text{H}, x_{\text{OMs}} = 0.5) = 8.32$ ppm, and $\delta(^1\text{H}, x_{\text{OMs}} = 0.75) = 8.68$ ppm.

2.4 Calorimetric measurements

The partial molar excess enthalpies of the mixtures were measured at $T = 298.15$ K using the TAM titration calorimeter (Thermometric, Sweden). The systems were measured in a 4 mL stainless steel reaction cell. The cell was filled with pure PILs $[\text{TEA}][\text{OMs}]$, or $[\text{TEA}][\text{OTf}]$ or the mixture of PILs and titrated by pure $[\text{TEA}][\text{OMs}]$ or $[\text{TEA}][\text{OTf}]$ from 250 μL syringe using the Lund pump. 20 injections of 10 μL of pure PIL were injected into cell. The content of the cell was stirred at 85 and 100 rpm using the gold propeller stirrer. The reference cell contained 0.9456 g of $[\text{TEA}][\text{OMs}]$. More details on experimental settings and data analysis are given in Section S3 of the ESI.†

3 Results and discussion

3.1 Hydrogen bonds and hydrogen bond redistribution

Charge-induced order plays an important role in ionic liquids.^{73–76} This applies also to pure $[\text{TEA}][\text{OMs}]$, $[\text{TEA}][\text{OTf}]$, and their mixtures, as illustrated in Fig. 1a. In an IL each ion is typically surrounded by a solvation shell predominantly consisting of counter ions, leading to long-ranged structural correlations.^{74,75} Since the $[\text{OTf}]$ and $[\text{OMs}]$ anions are of similar size, the average coordination number was found to vary only marginally between 6.8 and 6.9 as a function of the mixture composition.²² Here the coordination number was defined by a center of mass distance of 0.8 nm between ions of opposite charge, representing the location of the first

minimum of anion-cation pair correlation functions. The narrow distribution of coordination numbers (see Fig. 6 of ref. 22) with a maximum at seven neighbours and a half width of about 2.5 neighbours, also suggests a rather well preserved structural uniformity. As illustration, a representative snapshot of a $[\text{TEA}]$ cation solvated by anions in a $[\text{TEA}][\text{OMs}]/[\text{TEA}][\text{OTf}]$ mixture is provided in Fig. 1b.

The studied $[\text{TEA}]^+ / [\text{OMs}]^- / [\text{OTf}]^-$ systems are defined by doubly ionic hydrogen bonding. A comprehensive characterisation of the HBs would perhaps need to consider their electronic structure.^{77–79} Since quantum mechanical calculations on this scale are not yet feasible, the use of geometrical criteria is the second best alternative. Here bonded states are identified as a basin of the free energy as a function of appropriate geometrical parameters, separated by barriers from non-bonded states.^{80,81} Previously, we have shown that no angular constraints are required for identifying HBs donated by the N-H group of the $[\text{TEA}]$ cations and accepted by the SO_3 groups of $[\text{OMs}]$ and $[\text{OTf}]$ anions²² (see Fig. 1c). Instead, the distance distribution between the ammonium-hydrogen and the sulfonate-oxygen alone does sufficiently discriminate between hydrogen bonded and non-hydrogen bonded states. Based on the analysis discussed in ref. 22, we use a distance criterion of $r_{\text{H}\cdots\text{O}} \leq 0.24$ nm to define a HB for both, the $[\text{OMs}]$ and the $[\text{OTf}]$ anions. The identified HBs are linear in nature and even more perfectly aligned than in liquid water.²² Fig. 2 depicts the fraction of HBs donated by the cation y_{OMs} and y_{OTf} to the $[\text{OMs}]$ and $[\text{OTf}]$ anions, respectively. From Fig. 2 it is also evident that the N-H group of the cation always stays involved in a HB to either of the two anions, significantly favouring the interaction with the $[\text{OMs}]$ anion. Increasing the temperature, shifts the equilibrium slightly towards a more uniform distribution. The favouring of the $[\text{TEA}]-[\text{OMs}]$ HBs is apparently the consequence of a stronger $[\text{TEA}]-[\text{OMs}]$ interaction. To illustrate this behaviour, we have calculated the potential energies of pairs of cations and anions found within a distance

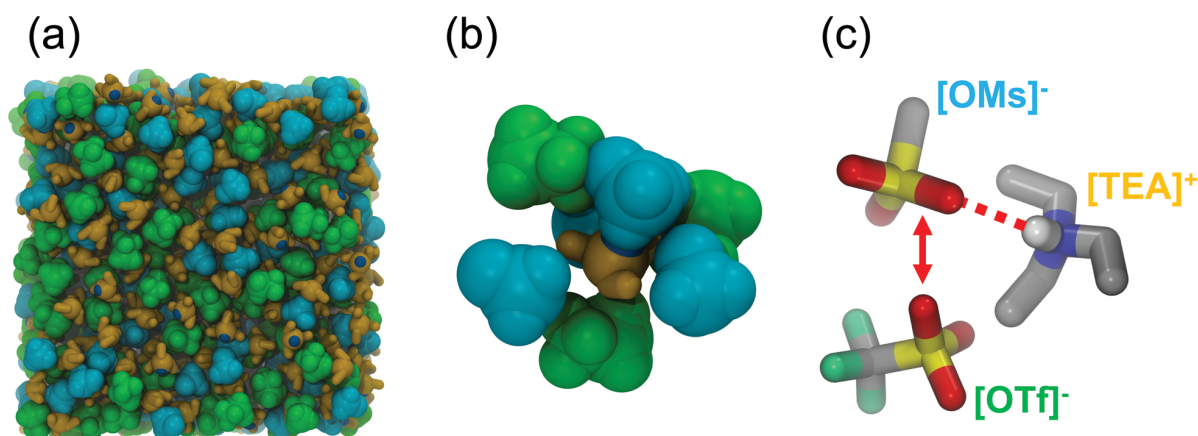


Fig. 1 (a) Snapshot of the MD simulation box of an equimolar $[\text{TEA}][\text{OMs}]/[\text{TEA}][\text{OTf}]$ mixture at 300 K. The $[\text{TEA}]$ cations are depicted in orange while the N-H hydrogen is depicted as a dark blue sphere. The $[\text{OMs}]$ and $[\text{OTf}]$ anions are shown in blue and green, respectively. (b) Snapshot of the solvation of a central $[\text{TEA}]$ cation, shown in orange, in a $[\text{TEA}][\text{OMs}]/[\text{TEA}][\text{OTf}]$ mixture engaged in a HB to an adjacent $[\text{OMs}]$ anion. The color coding is the same as in (a). (c) Illustrated equilibrium of the HBs donated by a $[\text{TEA}]$ cation and accepted by the SO_3 groups of the $[\text{OMs}]$ and $[\text{OTf}]$ anions.

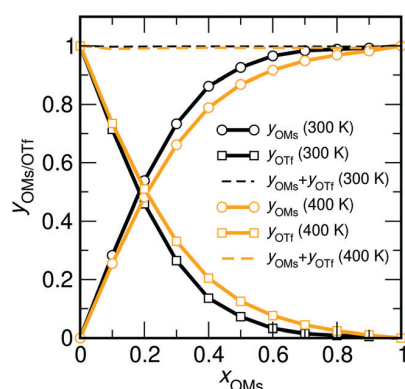


Fig. 2 Fraction of [TEA] cations involved in a HB y_x with $\alpha = \text{OTf}$, or $\alpha = \text{OMs}$ as function of the mole fraction x_{OMs} for $T = 300$ K (black symbols) and $T = 400$ K (orange symbols). The lines are guides for the eye. The dashed lines indicate the sum of the respective fractions.

of $r_{\text{cat.-an.}} \leq 0.8$ nm (with respect to their centers of mass) shown in Fig. 3 and 4. Fig. 3 correlates the computed pair energies with the smallest respective $r_{\text{H}\cdots\text{O}}$ distance. Note that for both anions, the hydrogen bonded states with $r_{\text{H}\cdots\text{O}} \leq 0.24$ nm are well separated from the non-hydrogen bonded states. In addition, comparing the behaviour of two anions shown in Fig. 3a and b is indicating that the “island” defining hydrogen bonded states is extending to significantly lower pair energies for the case of the [OMs] anion. This behaviour is also well pronounced in Fig. 4, where the maximum of the peak indicating hydrogen bonded states with a [OMs] anion is shifted by about 25–30 kJ mol^{-1} to lower values compared to the respective peak associated with the [OTf] anion. We would like to point out that this difference in pair energies between hydrogen bonded [TEA][OMs] and [TEA][OTf] neighbours compares well with the (mass corrected) shift in frequency of -14.8 cm^{-1} found in far infrared spectra for associated pairs of the two species by Fumino *et al.*⁵³ In their study, based on a comparison between five different PILs, they conclude that a shift of 1 cm^{-1} to larger wavenumbers is associated with a gain of 1.69 kJ mol^{-1} in interaction. For the comparison between [TEA][OMs] and [TEA][OTf] PILs this would amount to -25 kJ mol^{-1} . In addition, the composition-independent shift in the peaks associated with the cation–anion interaction found in the FIR spectra of [TEA][OTf], [TEA][OMs], and their mixtures (shown in Fig. 2 of ref. 23) suggest that interaction between cation and anion in the mixtures is very similar to the pure liquids.

Of course, this shift in pair energies is not solely qualified to determine the different HB acceptor strengths of the two anions. Hence the molar standard enthalpy associated with switching a HB between the two anion species is determined from fitting the logarithm of the equilibrium constant

$$K = \frac{y_{\text{OMs}}}{y_{\text{OTf}}} \quad (1)$$

as function of the inverse temperature, and is shown in Fig. 5 as van't Hoff plot. Depicted are data for compositions of $x_{\text{OMs}} \in \{0.5, 0.6\}$, indicating a value of about $\Delta H^\circ = -R \cdot \partial \ln(K) /$

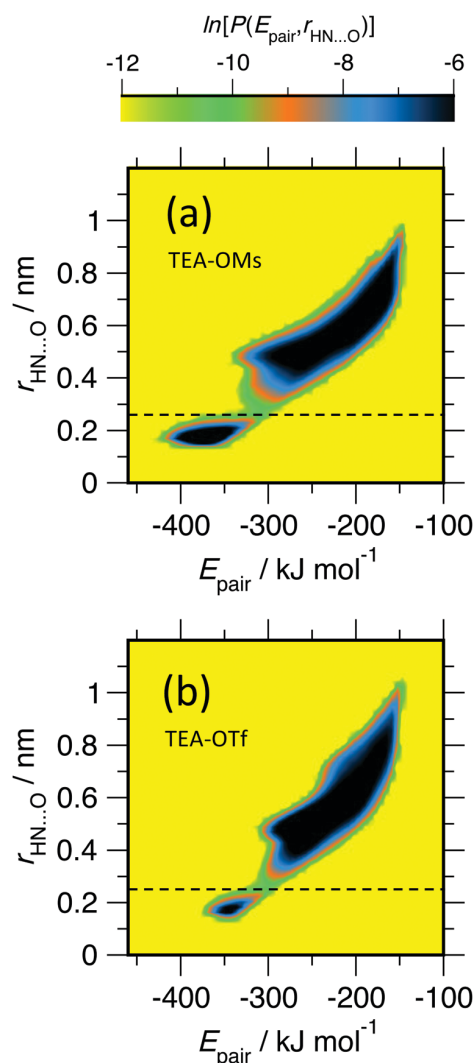


Fig. 3 Logarithmic representation of the probability density of finding a cation–anion pair interaction energy in combination with the smallest respective intermolecular $\text{H}\cdots\text{O}$ distance found between the two ions. Here only neighbouring pairs of ions are considered, lying within a center of mass cutoff radius of 0.8 nm. Note: distances $r_{\text{H}\cdots\text{O}} \leq 0.24$ nm indicate the presence of a HB, marked by the dashed line. The data shown was computed from MD-data of an equimolar mixture at 400 K.

$\partial(1/T) = -10.5 \text{ kJ mol}^{-1}$. Considering that the contribution due to differences in volume of the two corresponding HB states is negligible at pressure conditions of 1 bar, one can state that energy associated with breaking a [TEA]–[OTf] and forming a [TEA]–[OMs] HB is about $\Delta U_{\text{HB}} \approx -10.5 \text{ kJ mol}^{-1}$.

3.2 Energies of mixing: the effect of hydrogen bond redistribution

From the MD simulations we can directly determine the energies of mixing according to

$$\Delta U_{\text{mix}} = U(x_{\text{OMs}}) - x_{\text{OMs}} \cdot U_{[\text{TEA}][\text{OMs}]} - (1 - x_{\text{OMs}}) \cdot U_{[\text{TEA}][\text{OTf}]}, \quad (2)$$

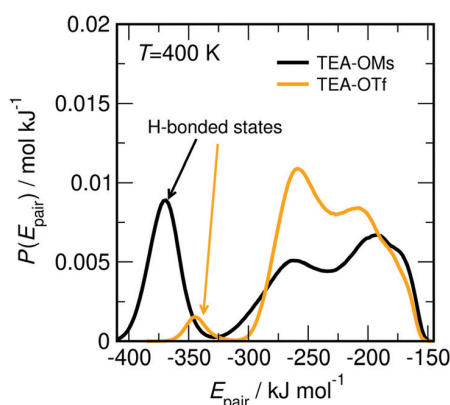


Fig. 4 Distribution of pair energies between [TEA] cations and neighbouring [OMs] and [OTf] anions defined by a nearest neighbour center of mass cutoff radius of 0.8 nm obtained for a equimolar mixture at a temperature of 400 K. Hydrogen bonded states appear as low-energy states in the energy-distribution.

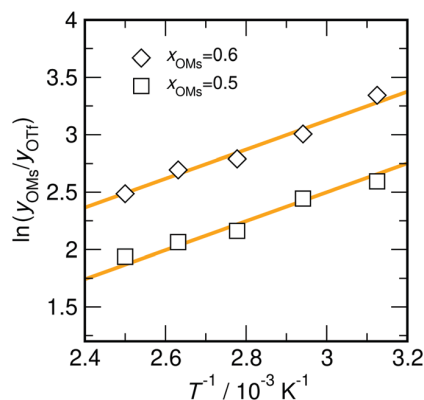


Fig. 5 Van 't Hoff plot of the logarithm of the equilibrium constant $K = y_{\text{OMs}}/y_{\text{OTf}}$ vs. the inverse temperature for compositions with $x_{\text{OMs}} = 0.5$, and $x_{\text{OMs}} = 0.6$. The slope of the orange solid lines correspond to $\Delta H^\circ = -R \cdot \partial \ln(K)/\partial(1/T) = -10.5 \text{ kJ mol}^{-1}$.

where $U(x_{\text{OMs}})$ represents the total energy of the mixture [TEA][OTf]/[TEA][OMs] of composition x_{OMs} , while $U_{[\text{TEA}][\text{OTf}]}$ and $U_{[\text{TEA}][\text{OMs}]}$ are the energies of the pure PILs. As shown in Fig. 6, a strong *nonideal* mixing behaviour is observed over the whole investigated temperature range. Negative mixing energies, varying between $(-4.50 \pm 0.21) \text{ kJ mol}^{-1}$ and $(-4.02 \pm 0.18) \text{ kJ mol}^{-1}$ are observed for equimolar mixtures. As shown in Table S12 in the ESI,[†] an increase in temperature leads to lower absolute mixing energies. The minima are located at about $x_{\text{OMs}} = 0.4$, which is mostly independent of temperature. We would like to emphasise again that for mixing under constant pressure conditions at atmospheric pressure, the enthalpy and energy of mixing are practically identical.

As discussed above, we could demonstrate that the intermolecular structure of the PILs and their mixture is characterised by a well defined order.²² For a mixture of two PILs

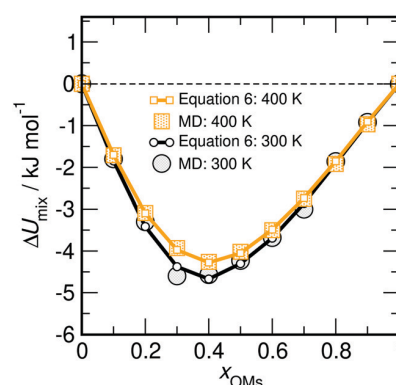


Fig. 6 Mixing energies as function of the mole fraction x_{OMs} for $T = 300 \text{ K}$ and $T = 400 \text{ K}$. Large open symbols: Data obtained directly from the MD simulations. Small open symbols: data according to the HB redistribution model employing y_{OMs} – data taken from the MD simulations at the respective temperatures. The lines are a guide to the eye.

sharing the same cation, it follows that the immediate solvation shell of each of the anions in the mixture is very similar that of their respective pure PIL counterparts. An idealised representation of such a structure is illustrated in Fig. 7a. Here the cations act as “buffer” between the different anion species. Such mixtures should be nearly ideal, since direct cross-interactions are prevented by the separating cations. However, as the MD simulations have shown, a [TEA] cation stays always involved in a HB to the SO_3 groups of either of the two anion species (see Fig. 2 and ref. 22) Hence we attribute the bulk of the nonideal mixing behaviour to the redistribution of HBs donated by the [TEA] cation as indicated by the little arrows in Fig. 7b.

The regular charge-induced structure of the PILs has motivated us to describe the mixture in terms of a simple lattice model based solely on local nearest neighbour interactions. In the model we distinguish between HBs and nonspecific interactions (*i.e.* van der Waals and non-localised polar interactions). Here each of the ions in the PILs is placed on a regular lattice with a coordination number c . As illustrated in Fig. 7 the anions and cations are arranged in an alternating fashion on the lattice. Hence there exist $N_{\text{TEA}} \cdot c$ nonspecific nearest neighbour interactions and N_{TEA} HBs. The interaction energy of the pure PILs follows as

$$U_{[\text{TEA}][\text{OMs}]} = N_{\text{TEA}} \cdot c \cdot \varepsilon_{\text{TEA-OMs}} + N_{\text{TEA}} \cdot \varepsilon_{\text{HB:TEA-OMs}} \quad (3)$$

and

$$U_{[\text{TEA}][\text{OTf}]} = N_{\text{TEA}} \cdot c \cdot \varepsilon_{\text{TEA-OTf}} + N_{\text{TEA}} \cdot \varepsilon_{\text{HB:TEA-OTf}} \quad (4)$$

where N_{TEA} is the number of [TEA] cations, c is the coordination number, and $\varepsilon_{\text{TEA-OMs}}$, $\varepsilon_{\text{TEA-OTf}}$, $\varepsilon_{\text{HB:TEA-OMs}}$, and $\varepsilon_{\text{HB:TEA-OTf}}$ are the parameters characterising the respective nonspecific and HB interactions of the cation with either of the anions. The energy of the mixture with a composition x_{OMs} is given by

$$U(x_{\text{OMs}}) = N_{\text{TEA}} \cdot c \cdot x_{\text{OMs}} \cdot \varepsilon_{\text{TEA-OMs}} + N_{\text{TEA}} \cdot y_{\text{OMs}} \cdot \varepsilon_{\text{HB:TEA-OMs}} + N_{\text{TEA}} \cdot c \cdot (1 - x_{\text{OMs}}) \cdot \varepsilon_{\text{TEA-OTf}} + N_{\text{TEA}} \cdot (1 - y_{\text{OMs}}) \cdot \varepsilon_{\text{HB:TEA-OTf}} \quad (5)$$

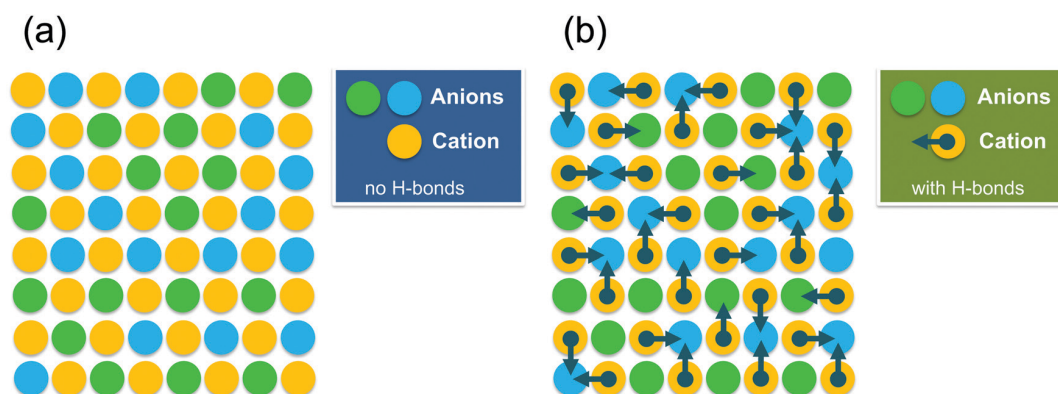


Fig. 7 Idealised 2D lattice representation (with coordination number $c = 4$) of an equimolar mixture of [TEA][OMs] and [TEA][OTf]. The color coding is: orange = [TEA]⁺, blue = [OMs][−], and green = [OTf][−]. (a) Lattice sites are occupied by cations and anions in an alternate fashion, leading to a number of nonspecific cation–anion contacts of $N_{\text{TEA}} \cdot c$. The anions are randomly distributed on the lattice-sites of the anion-sublattice according to their mixture composition. (b) The arrows indicate HBs between the cations and one of the adjacent anions, therefore representing one additional HB interaction per cation. Note that the majority of HBs is found between [TEA] cations and [OMs] anions.

where y_{OMs} represents the fraction of cations forming a HB to the neighbouring [OMs] anions. Here we are assuming that in a mixture the anion-sites are statistically occupied by either one of the two anion species in accordance with the mixture composition. Since the condition $y_{\text{OMs}} + y_{\text{OTf}} \approx 1$ with the deviation from one $\leq 1\%$ is well fulfilled, it follows from eqn (2)–(5) directly that

$$\Delta U_{\text{mix}} = N_{\text{TEA}} \cdot (y_{\text{OMs}} - x_{\text{OMs}}) \cdot \Delta \epsilon_{\text{HB}} \quad (6)$$

with

$$\Delta \epsilon_{\text{HB}} = \epsilon_{\text{HB:TEA-OMs}} - \epsilon_{\text{HB:TEA-OTf}} \quad (7)$$

Note that eqn (7) predicts negative mixing energies for $\Delta \epsilon_{\text{HB}} < 0$ if the condition $y_{\text{OMs}} > x_{\text{OMs}}$ is fulfilled. Moreover, eqn (6) suggests that the difference of the hydrogen bonding strengths of HBs to each of the two anion species can be calculated from the knowledge of ΔU_{mix} , y_{OMs} and x_{OMs} . This can be achieved by either employing MD simulation data, or experimental mixing enthalpies and corresponding ¹H-NMR chemical shift data obtained for the N–H proton.

Fig. 6 represent fits of eqn (6) to the MD simulation data, denoted by the small symbols connected by solid lines. Fitting the mixing energies is leading to values for $N_{\text{A}} \Delta \epsilon_{\text{HB}}$ between $(-10.1 \pm 0.5) \text{ kJ mol}^{-1}$ and $(-11.0 \pm 0.3) \text{ kJ mol}^{-1}$ for temperatures ranging from 300 K to 400 K, as indicated in Table 1. The average over all temperatures of $N_{\text{A}} \overline{\Delta \epsilon_{\text{HB}}} = (-10.6 \pm 0.5) \text{ kJ mol}^{-1}$, where N_{A} represents Avogadro's constant, is in good agreement with the data fitting to the van't Hoff equation as shown in Fig. 5. This consistency can be seen as strong evidence that the enthalpic effect caused by HB redistributions is the dominant contribution to the energy of mixing.

In Fig. 8a and b the same procedure is applied to the titration calorimetry and NMR experimental data. The enthalpy of mixing data shown in Fig. 8a was determined from partial molar enthalpies obtained using calorimetric titration data

Table 1 HB strength differences $\Delta \epsilon_{\text{HB}}$ for all temperatures calculated from MD simulations using eqn (6)

T/K	$N_{\text{A}} \Delta \epsilon_{\text{HB}} / \text{kJ mol}^{-1}$
300	-10.1 ± 0.5
320	-10.4 ± 0.5
340	-10.5 ± 0.4
360	-10.8 ± 0.4
380	-10.8 ± 0.3
400	-11.0 ± 0.3
	-10.6 ± 0.5

analysed *via* the Redlich–Kister approach discussed in Section S3.3 of the ESI.† The fraction of HBs to [OMs] anions is determined from the ¹H-NMR chemical shifts according to

$$y_{\text{OMs}} = \frac{\delta(^1\text{H}, x_{\text{OMs}}) - \delta(^1\text{H}, [\text{TEA}][\text{OTf}])}{\delta(^1\text{H}, [\text{TEA}][\text{OMs}]) - \delta(^1\text{H}, [\text{TEA}][\text{OTf}])} \quad (8)$$

assuming that the [TEA] cation stays always involved in a HB. Eqn (6) quantitatively relates the experimental mixing energy data with the obtained fraction of HBs to the [OMs] anion using $N_{\text{A}} \Delta \epsilon_{\text{HB}} = -13 \text{ kJ mol}^{-1}$, suggesting that the difference in HB binding energy in both, MD simulation and experiment are found in a similar range. Since the experimental mixing enthalpy of $-2.24 \text{ kJ mol}^{-1}$ for the equimolar mixture is only about half the value of what was observed from MD simulation, this smaller mixing enthalpy is apparently solely attributed to a less pronounced shift of the equilibrium of $K = y_{\text{OMs}}/y_{\text{OTf}}$ towards [OMs] anions.

3.3 An idealised model for relating HB redistribution effects with mixing energies

Previously we have introduced an idealised model for the HB redistribution in mixtures of PILs²² to predict the formation of hydrogen bonded clusters as a function of the mixture composition. A similar approach was recently shown to be successful in describing “water in salt” mixtures of protic ionic liquids.⁵⁵ Here we will demonstrate that such a model is also helpful for

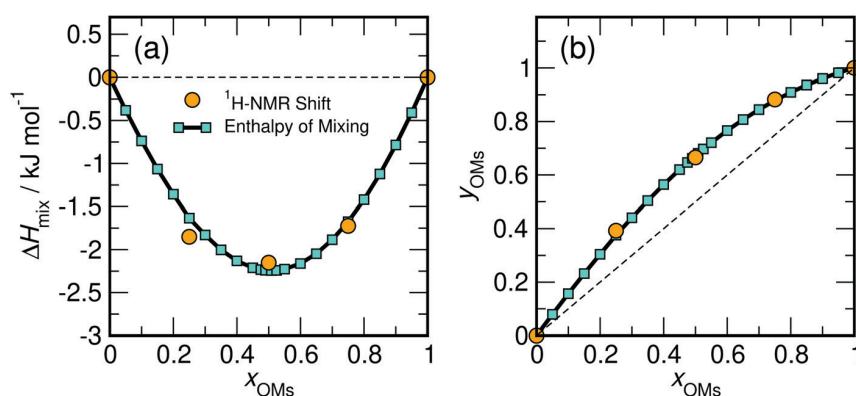


Fig. 8 Experimental mixing enthalpies and HB redistribution data as function of the mole fraction of [TEA][OMs] at $T = 298$ K. (a) Filled cyan squares indicate the experimental enthalpy of mixing data as function of the mole fraction x_{OMs} at $T = 298$ K according to the Redlich–Kister approach outlined in Section S4.3 of the ESI.† The filled orange circles correspond to mixing energies employing the y_{OMs} obtained from ^1H -NMR chemical shift measurements in combination with $N_{\text{A}}\Delta\epsilon_{\text{HB}} = -13$ kJ mol $^{-1}$. (b) The fraction y_{OMs} of [TEA] cations involved in a HB with [OMs] as function of x_{OMs} at $T = 298$ K according to experimental data. The filled orange circles indicate data for y_{OMs} obtained from ^1H -NMR chemical shift measurements. The filled cyan squares represent data for y_{OMs} according to from the enthalpy of mixing data employing the relation $y_{\text{OMs}} = \Delta H_{\text{mix}}/(N_{\text{A}}\Delta\epsilon_{\text{HB}}) + x_{\text{OMs}}$ using $N_{\text{A}}\Delta\epsilon_{\text{HB}} = -13$ kJ mol $^{-1}$.

describing the HB redistribution effects resulting in strong negative mixing energies.

Again, the PIL is represented by a lattice with a coordination number c , where the anions and cations occupy sites in an alternating fashion. We also assume that each [TEA]-cation stays always involved in a HB *via* its N–H-bond with one of its c surrounding anions. In a pure PIL, the cation–anion HB is, of course, supposed to connect the [TEA]-cation randomly with one of its c anion neighbours. Hence the probability of accepting a HB by one of the surrounding anions is $p_i = 1/c$. Since the [TEA] N–H group has to point to one of the surrounding anions, those site-specific probabilities have to add all up to unity:

$$1 = \sum_{i=1}^c p_i. \quad (9)$$

In the mixture, the [OMs] and [OTf] anions are supposed to have different HB accepting capabilities. If the sites i are assumed to be statistically occupied by one of the two anion species according to their mixture composition $x = x_{\text{OMs}}$, the average probability p_i of donating a HB to site i is a composition-weighted sum of the HB acceptance probabilities of the two anion species according to

$$p_i = x \cdot p_{\text{OMs}} + (1 - x) \cdot p_{\text{OTf}}. \quad (10)$$

From eqn (9) and (10) we can determine the HB acceptance probabilities p_{OTf} and p_{OMs} as follows:

$$p_{\text{OMs}} = \frac{1}{cx + c(1-x)f} \quad (11)$$

$$p_{\text{OTf}} = \frac{1}{cx f^{-1} + c(1-x)} \quad (12)$$

with $f = p_{\text{OTf}}/p_{\text{OMs}}$ describing the ratio of the individual HB acceptance capabilities of the two anion species. The fraction of HBs of to each of the two anions is then given by:

$$y_{\text{OMs}} = c \cdot x \cdot p_{\text{OMs}} \quad (13)$$

$$y_{\text{OTf}} = c \cdot (1 - x) \cdot p_{\text{OTf}}. \quad (14)$$

With the help of eqn (11) and (12), we can express these as:

$$y_{\text{OMs}} = \frac{1}{1 + f(1-x)x^{-1}} \quad (15)$$

$$y_{\text{OTf}} = \frac{1}{1 + x f^{-1}(1-x)^{-1}}. \quad (16)$$

By combining eqn (6) and (16), we can derive an expression for the mixing energy:

$$\Delta U_{\text{mix}} = N_{\text{A}} \cdot \frac{(1-x)(1-f)}{1 + f(1-x)x^{-1}} \cdot \Delta\epsilon_{\text{HB}}. \quad (17)$$

Ideally, the ratio of HB acceptance probabilities f should be independent of the composition of the mixture. However, we find a much better agreement with both, MD simulation, and experimental data, if we assume a mixture dependence, which is slightly favouring HBs towards [OMs] anions with increasing [OMs] content x . We account for this behaviour by introducing a linear x dependence *via*

$$f = a + b \cdot x. \quad (18)$$

Here a is an adjustable parameter, largely responsible for shifting the overall [OTf]/[OMs] equilibrium, whereas the parameter b expresses the shift in equilibrium due to the mixture composition. We find that all studied systems, including MD simulations at different temperatures as well as the experimental data, are very well reproduced by a common parameter $b = -0.24$. Fig. 9 explores the parameter space of a with a fixed value of $b = -0.24$, demonstrating that a lowering of the a -value leads to an increasing deviation from an *ideal* mixing behaviour. Of course, a fully ideal behaviour would have been associated with $f = 1 = \text{const}$. Note that a decreasing value of a leads to an increasingly negative mixing energy. Moreover, also the

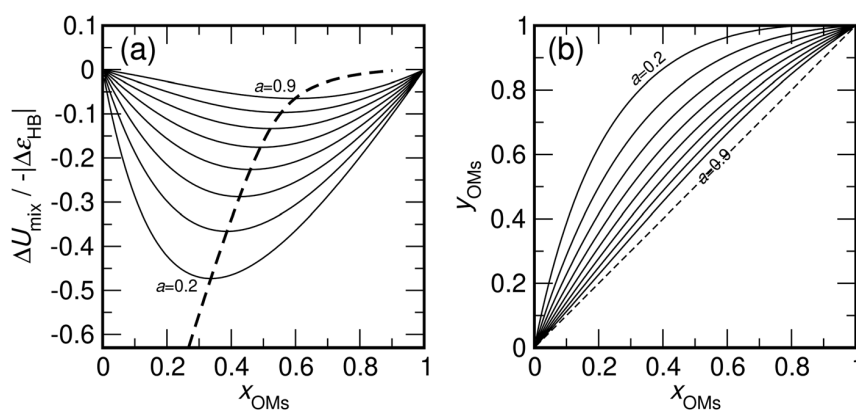


Fig. 9 Exploration of the parameter space of mixing energies according to eqn (17) and HB redistribution data according to (eqn (16)). (a) Reduced mixing energies in units of $|\Delta\epsilon_{\text{HB}}|$ as function of the mole fraction x_{OMs} . The shown data are based on eqn (17) for the parameter a varying from $a = 0.2$ to $a = 0.9$ in steps of 0.1 with $b = -0.24$. The heavy dashed line connects the loci of the minima observed for the mixing energies as a function of a . The shown line linearly connects data points obtained for an increment of $\Delta a = 0.001$. The minima have been determined numerically using the Newton–Raphson method. (b) Fraction of [TEA] cations involved in a HB y_{OMs} with an [OMs] anion according to the same model. The dashed line indicates $y_{\text{OMs}} = x_{\text{OMs}}$.

location of the minimum of the mixing energy shifts towards pure [TEA][OTf] with a decreasing value of a .

Fig. 10 shows the model described by eqn (17) and (18) fitted to the mixing energies obtained from MD simulations. The corresponding fitted parameters $\Delta\epsilon_{\text{HB}}$ and a are summarised in Table 2. The model is nearly quantitatively able to describe the effect of a changing $y_{\text{OMs}}/y_{\text{OTf}}$ equilibrium on the mixing energy as a function of temperature. However, exactly the same model is also able to describe the experimental data sets shown in Fig. 11, albeit with a significantly increased parameter $a = 0.6$, suggesting a shift towards a more uniform distribution of HBs between the two anion species. Note that the different position of the minimum mixing energy observed in our MD simulation and experimental data sets is well accounted for by the idealised model. A slight deviation of the fitted line for $x < 0.3$ from the simulated data shown in Fig. 10 has to be attributed to the assumed linear dependence of f .

Table 2 HB strength differences $\Delta\epsilon_{\text{HB}}$ and parameter a obtained from fitting eqn (17) and (18) to the mixing energies and eqn (16) to the fraction of HBs to [OMs] anions obtained from our MD simulations using a common parameter $b = -0.24$

T/K	$N_{\text{A}}\Delta\epsilon_{\text{HB}}/\text{kJ mol}^{-1}$	a
300	−10.4	0.236
320	−10.8	0.240
340	−10.9	0.253
360	−11.1	0.266
380	−11.1	0.281
400	−11.2	0.298

Finally, we would also like to point out that the model described by eqn (17) and (18) can be used to directly analyse the measured partial molar enthalpies of ILs in the mixture. The corresponding equations for the composition dependent partial molar excess enthalpies and their counterparts for

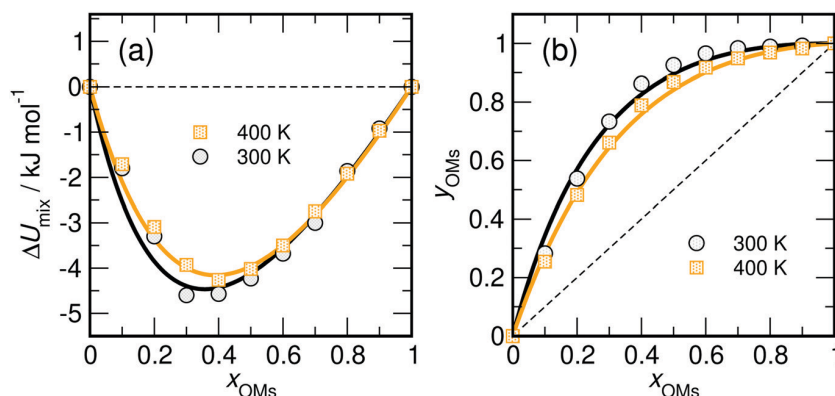


Fig. 10 Mixing energies and HB redistribution as function of the mole fraction of [TEA][OMs] at $T = 300\text{ K}$ and $T = 400\text{ K}$. (a) Open symbols: MD simulation data. Heavy lines are model data according to eqn (17) with the parameters a and $\Delta\epsilon_{\text{HB}}$ given in Table 2. (b) Fraction of [TEA] cations involved in a HB y_{OMs} with an adjacent [OMs] anion. Open Symbols indicate data obtained from MD simulations, while the heavy solid lines represents data from the model using the same parameters as used in panel (a). In both panels the dotted lines indicate *ideal* behaviour.

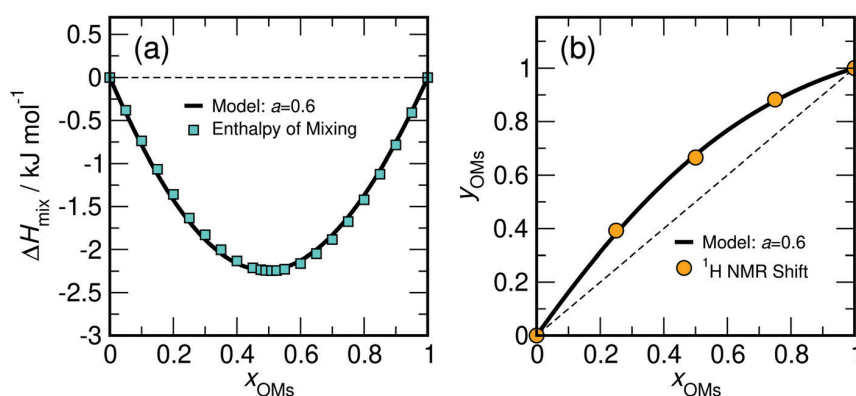


Fig. 11 Experimental mixing enthalpies and HB redistribution data as function of the mole fraction of [TEA][OMs] at $T = 298$ K. (a) Cyan filled squares indicate the experimental enthalpies of mixing calculated by the Redlich–Kister approach (see Section S3.3 in ESI†) from measured partial molar enthalpies. The heavy solid line represents a fit to ΔH_{mix} by eqn (17) and (18) with $N_A \Delta \varepsilon_{\text{HB}} = -12.7$ kJ mol $^{-1}$, $a = 0.6$ and $b = -0.24$. (b) Shown are the fraction y_{OMs} of [TEA] cations involved in a HB with [OMs]. Filled orange circles represent experimental data obtained from ^1H -NMR chemical shift measurements. The heavy solid line represents data according to parameter $a = 0.6$ with $b = -0.24$. In both panels the dashed lines indicate the behaviour for an ideal system.

infinite dilution are derived in Section S3.4 of the ESI.† The fits reported in Section S3.4 of the ESI,† provide a representation of comparable quality as the Redlich–Kister approach with parameters $a = 0.655$ and $b = -0.242$ and $N_A \Delta \varepsilon_{\text{HB}} = -14.9$ kJ mol $^{-1}$, however, slightly larger than the values obtained using the Redlich–Kister approach.

4 Conclusions

We have studied a mixture of two PILs sharing the same cation. This allows us to largely disentangle the contribution from hydrogen bonding and other nonspecific forms of intermolecular interactions. We could demonstrate that a mixture of those PILs experiences a redistribution of HBs between the cation and the anions in the mixture due to the different HB accepting capabilities of the two anion species. This HB redistribution is identified as the dominant enthalpic effect in the PILs mixtures, leading to large negative mixing energies. The existence of negative mixing enthalpies could be confirmed by calorimetric measurements, albeit the effect was found to be less strongly pronounced than in the MD simulations. A lattice model has been introduced to quantitatively relate the amount of HBs redistributed between the two anion species with the changing mixing energies. The difference in interactions energies associated with switching a HB donated by a [TEA] cation from a [OTf] anion to a [OMs] anion of about -10.5 kJ mol $^{-1}$, as determined from the lattice model, is found to be in good agreement with a van't Hoff analysis of the temperature dependent HB equilibrium. From ^1H -NMR chemical shift measurements of the N–H proton in the mixtures, the fraction of HB species to either of the two species could be determined experimentally, assuming that the N–H group stays always involved in a HB. The NMR-data also indicate favourable [TEA]–[OMs] HB interactions, in agreement with the MD simulations. By combining experimental mixing enthalpies with the HB redistribution data obtained from the ^1H -NMR chemical

shift measurements, the energy difference of HBs between the two anion species could be determined as -13 kJ mol $^{-1}$.

Data availability statement

The data that support the findings of this study are available from the corresponding author upon reasonable request. Simulation-related files are permanently publicly available from the RosDok repository of the University of Rostock.⁷¹

Conflicts of interest

There are no conflicts to declare.

Acknowledgements

We thank the Leibniz Association, the State of Mecklenburg-Vorpommern, and the University of Rostock for financial support within the ComBioCat programme. This work has been supported by the Deutsche Forschungsgemeinschaft (Research Grant No. 401427621). D. O. acknowledges the support from the grant No. A1_FCHI_2021_002 of specific university research by the Ministry of Education, Youth and Sports (Czech Republic).

Notes and references

- 1 T. L. Greaves and C. J. Drummond, *Chem. Rev.*, 2008, **108**, 206–237.
- 2 J. Belieres and C. A. Angell, *J. Phys. Chem. B*, 2007, **111**, 4926–4937.
- 3 X. Lu, G. Burrell, F. Separovic and C. Zhao, *J. Phys. Chem. B*, 2012, **116**, 9160–9170.
- 4 L. E. Shmukler, I. V. Fedorova, Y. A. Fadeeva and L. Safonova, *J. Mol. Liq.*, 2021, **321**, 114350.

- 5 A. Benedetto and P. Ballone, *ACS Sustainable Chem. Eng.*, 2016, **4**, 392–421.
- 6 B. Peric, S. Sierra, E. Martí, R. Cruanas, M. A. Garau, J. Arning, U. Bottin-Weber and S. Stolte, *J. Hazard. Mater.*, 2013, **261**, 99–105.
- 7 L. E. Shmukler, M. S. Gruzdev, N. O. Kudryakova, Y. A. Fadeeva, A. M. Kolker and L. P. Safonova, *J. Mol. Liq.*, 2018, **266**, 139–146.
- 8 R. Caparica, A. Júlio, E. U.-A. M. Araújo, A. R. Baby, P. Fonte, J. G. Costa and T. Santos de Almeida, *Biomolecules*, 2020, **10**, 233.
- 9 G. Chatel, F. F.-B. Pereira, V. Debbeti, H. Wang and R. D. Rogers, *Green Chem.*, 2014, **16**, 2051–2083.
- 10 H. Every, A. G. Bishop, M. Forsyth and D. R. MacFarlane, *Electrochim. Acta*, 2000, **45**, 1279–1284.
- 11 K. A. Fletcher, S. N. Baker, G. A. Baker and S. Pandey, *New J. Chem.*, 2003, **27**, 1706–1712.
- 12 R. W. Berg, M. Deetlefs, K. R. Seddon, I. Shim and J. M. Thompson, *J. Phys. Chem. B*, 2005, **109**, 19018–19025.
- 13 J. N. Canongia Lopes, T. C. Cordeiro, J. M.-S. S. Esperanca, H. J.-R. Guedes, S. Huq, L. P.-N. Rebelo and K. R. Seddon, *J. Phys. Chem. B*, 2005, **109**, 3519–3525.
- 14 P. Navia, J. Troncoso and L. Romani, *J. Solution Chem.*, 2008, **37**, 677–688.
- 15 D. Xiao, J. R. Rajian, L. G. Hines, S. Li, R. A. Bratsch and E. L. Quitevis, *J. Phys. Chem. B*, 2008, **112**, 13316–13325.
- 16 F. Llovel, E. Valente, O. Vilaseca and L. F. Vega, *J. Phys. Chem. B*, 2011, **115**, 4387–4398.
- 17 G. Annat, M. Forsyth and D. R. MacFarlane, *J. Phys. Chem. B*, 2012, **116**, 8251–8258.
- 18 M. B. Oliveira, M. Domínguez-Pérez, O. Cabeza, J. A.-L. da Silva, M. G. Freire and J. A.-P. Coutinho, *J. Chem. Thermodynamics*, 2013, **64**, 22–27.
- 19 R. S. Payal and S. Balasubramanian, *Phys. Chem. Chem. Phys.*, 2013, **15**, 21077–21083.
- 20 M. S. Miran, T. Yasuda, M. A.-B. H. Susan, K. Dokko and M. Watanabe, *J. Phys. Chem. C*, 2014, **118**, 27631–27639.
- 21 P. Navarro, M. Larriba, J. García and F. Rodríguez, *J. Chem. Thermodynamics*, 2014, **76**, 152–160.
- 22 D. Paschek, B. Golub and R. Ludwig, *Phys. Chem. Chem. Phys.*, 2015, **17**, 8431–8440.
- 23 K. Fumino, A.-M. Bónsa, B. Golub, D. Paschek and R. Ludwig, *ChemPhysChem*, 2015, **16**, 299–304.
- 24 H. F.-D. Almeida, J. N. Canongia Lopes, L. P.-N. Rebelo, J. A.-P. Coutinho, M. G. Freire and I. M. Marrucho, *J. Chem. Eng. Data*, 2016, **61**, 2828–2843.
- 25 R. P. Matthews, I. J. Villar-García, C. C. Weber, J. Griffith, F. Cameron, J. P. Hallett, P. A. Hunt and T. Welton, *Phys. Chem. Chem. Phys.*, 2016, **18**, 8608–8624.
- 26 N. J. Brooks, F. Castiglione, C. M. Doherty, A. Dolan, A. J. Hill, P. A. Hunt, R. P. Matthews, M. Mauri, A. Mele, R. Simonutti, C. C.-W. I.-J. Villar-García and T. Welton, *Chem. Sci.*, 2017, **8**, 6359–6374.
- 27 D. W. Bruce, C. P. Cabry, J. N. Canongia Lopes, M. L. Costen, L. D'Andrea, I. Grillo, B. C. Marshall, K. G. McKendrick, T. K. Minton, S. M. Purcell, S. Rogers, J. M. Slattery, K. Shimizu, E. Smoll and M. A. Tesa-Serrate, *J. Phys. Chem. B*, 2017, **121**, 6002–6020.
- 28 E. P. Yambou, B. Gorska and F. Béguin, *J. Chem. Eng. Data*, 2017, **62**, 1884–1901.
- 29 M. S. Páez, Y. A. Vega and C. M. Romero, *J. Mol. Liq.*, 2017, **243**, 78–84.
- 30 O. Russina, F. L. Celso, N. V. Plechkova and A. Triolo, *J. Phys. Chem. Lett.*, 2017, **8**, 1197–1204.
- 31 T. Vogl, S. Passerini and A. Balducci, *Electrochem. Commun.*, 2017, **78**, 47–50.
- 32 C. P. Cabry, L. D'Andrea, K. Shimizu, I. Grillo, P. Li, S. Rogers, D. W. Bruce, J. N. Canongia Lopes and J. M. Slattery, *Faraday Discuss.*, 2018, **206**, 265–289.
- 33 S. Cha and D. Kim, *J. Chem. Phys.*, 2018, **148**, 193827.
- 34 M. Chakraborty, T. Ahmed, R. S. Dhale, D. Majhi and M. Sarkar, *J. Phys. Chem. B*, 2018, **122**, 12114–12130.
- 35 S. Gehrke, M. von Domaros, R. Clark, O. Hollóczki, M. Brehm, T. Welton, A. Luzar and B. Kirchner, *Faraday Discuss.*, 2018, **206**, 219–245.
- 36 T. Cosby, U. Kapoor, J. K. Shah and J. Sangoro, *J. Phys. Chem. Lett.*, 2019, **10**, 6274–6280.
- 37 U. Kapoor and J. K. Shah, *J. Phys. Chem. B*, 2020, **124**, 7849–7856.
- 38 M. E.-D. Pietro, F. Castiglione and A. Mele, *J. Phys. Chem. B*, 2020, **124**, 2879–2891.
- 39 S. Thawarkar, N. D. Khupse and A. Kumar, *J. Sol. Chem.*, 2020, **49**, 210–221.
- 40 E. P. Yambou, B. Gorska and F. Béguin, *J. Mol. Liq.*, 2020, **298**, 111959.
- 41 M. Chakraborty, S. Barik, A. Mahapatra and M. Sarkar, *J. Chem. Phys.*, 2021, **154**, 224507.
- 42 H. Niedermeyer, J. P. Hallett, I. J. Villar-García, P. A. Hunt and T. Welton, *Chem. Soc. Rev.*, 2012, **41**, 7780–7802.
- 43 L. F. Lepre, J. Szala-Bilnik, A. A.-H. Pádua, M. Traikia, R. A. Ando and M. F.-C. Gomes, *Phys. Chem. Chem. Phys.*, 2016, **18**, 23285–23295.
- 44 C. Herrera, M. Atilhan and S. Aparicio, *Phys. Chem. Chem. Phys.*, 2018, **20**, 10213–10223.
- 45 A. Podgorsek, A. S. Pensado, C. C. Santini, M. F.-C. Gomes and A. A.-H. Pádua, *J. Phys. Chem. C*, 2013, **117**, 3537–3547.
- 46 P. Navia, J. Troncoso and L. Romani, *J. Chem. Eng. Data*, 2007, **52**, 1369–1374.
- 47 H. J. Castejón and R. J. Lashock, *J. Mol. Liq.*, 2012, **167**, 1–4.
- 48 A. Podgorsek, J. Jacquemin, A. A.-H. Pádua and M. F.-C. Gomes, *Chem. Rev.*, 2016, **116**, 6075–6106.
- 49 I. Otero, L. F. Lepre, A. Dequidt, P. Husson and M. F.-C. Gomes, *J. Phys. Chem. B*, 2017, **121**, 9725–9736.
- 50 B. Docampo-Álvarez, V. Gómez-González, T. Méndez-Morales, J. R. Rodríguez, O. Cabeza, M. Turmine, L. J. Gallego and L. M. Varela, *Phys. Chem. Chem. Phys.*, 2018, **20**, 9938–9949.
- 51 L. F. Lepre, M. C. Gomes, A. A.-H. Pádua, R. A. Ando and M. C.-C. Ribeiro, *J. Phys. Chem. B*, 2019, **123**, 6579–6587.
- 52 *The Structure of Ionic Liquids*, ed. R. Caminiti and L. Gontrani, Springer, 2014.
- 53 K. Fumino, V. Fossog, K. Wittler, R. Hempelmann and R. Ludwig, *Angew. Chem., Int. Ed.*, 2013, **52**, 2368–2372.
- 54 E. Bodo, M. Bonomo and A. Mariani, *J. Phys. Chem. B*, 2021, **125**, 2781–2792.

- 55 B. Golub, K. Fumino, P. Stange, V. Fossog, R. Hempelmann, D. Ondo, D. Paschek and R. Ludwig, *J. Phys. Chem. B*, 2021, **125**, 4476–4488.
- 56 B. Golub, D. Ondo, R. Ludwig and D. Paschek, *J. Phys. Chem. Lett.*, 2022, **13**, 3556–3561.
- 57 M. J. Abraham, D. van der Spoel, E. Lindahl, B. Hess and the GROMACS development team, *GROMACS User Manual version 5.0.6*, 2015.
- 58 L. Martinez, R. Andrade, E. G. Birgin and J. M. Martinez, *J. Comput. Chem.*, 2009, **30**, 2157–2164.
- 59 H. J.-C. Berendsen, J. P.-M. Postma, W. F. van Gunsteren, A. DiNola and J. R. Haak, *J. Chem. Phys.*, 1984, **81**, 3684–3690.
- 60 S. Nosé, *Mol. Phys.*, 1984, **52**, 255–268.
- 61 W. G. Hoover, *Phys. Rev. A: At., Mol., Opt. Phys.*, 1985, **31**, 1695–1697.
- 62 M. Parrinello and A. Rahman, *J. Appl. Phys.*, 1981, **52**, 7182–7190.
- 63 S. Nosé and M. L. Klein, *Mol. Phys.*, 1983, **50**, 1055–1076.
- 64 B. Hess, H. Bekker, H. J.-C. Berendsen and J. G.-E. M. Fraaije, *J. Comput. Chem.*, 1997, **18**, 1463–1472.
- 65 U. Essmann, L. Perera, M. L. Berkowitz, T. A. Darden, H. Lee and L. G. Pedersen, *J. Chem. Phys.*, 1995, **103**, 8577–8593.
- 66 D. Paschek and A. Geiger, *MOSCITO (Version 4.180)*, 2012, <https://www.moscitumd.org>.
- 67 N. Michaud-Agraval, E. J. Denning, T. B. Woolf and O. Beckstein, *J. Comput. Chem.*, 2011, **32**, 2319–2327.
- 68 R. J. Gowers, M. Linke, J. Barnoud, T. J. E. Reddy, M. N. Melo, S. L. Seyler, J. Domański, D. L. Dotson, S. Buchoux, I. M. Kenney and O. Beckstein, Proceedings of the 15th Python in Science Conference, Austin, TX, 2016, pp. 98–105.
- 69 T. Oliphant, *NumPy: A guide to NumPy*, Trelgol Publishing, USA, 2006, <https://www.numpy.org/>.
- 70 P. Virtanen, R. Gommers, T. E. Oliphant, M. Haberland, T. Reddy, D. Cournapeau, E. Burovski, P. Peterson, W. Weckesser, J. Bright, S. J. van der Walt, M. Brett, J. Wilson, K. J. Millman, N. Mayorov, A. R.-J. Nelson, E. Jones, R. Kern, E. Larson, C. J. Carey, I. Polat, Y. Feng, E. W. Moore, J. VanderPlas, D. Laxalde, J. Perktold, R. Cimrman, I. Henriksen, E. A. Quintero, C. R. Harris, A. M. Archibald, A. H. Ribeiro, F. Pedregosa, P. van Mulbregt and SciPy 1.0 Contributors, *Nat. Methods*, 2020, **17**, 261–272.
- 71 D. Paschek, B. Golub and R. Ludwig, *MD Simulation Data Supporting the Publication “Hydrogen Bond Redistribution Effects in Mixtures of Protic Ionic Liquids Sharing the Same Cation: Nonideal Mixing with Large Negative Mixing Enthalpies”*, RosDok repository of the University of Rostock, 2022, DOI: [10.18453/rosdok_id00003537](https://doi.org/10.18453/rosdok_id00003537).
- 72 M. Strauch, A.-M. Bónsa, B. Golub, V. Overbeck, D. Michalik, D. Paschek and R. Ludwig, *Phys. Chem. Chem. Phys.*, 2016, **18**, 17788–17794.
- 73 J. N.-A. Canongia Lopes and A. A.-H. Pádua, *J. Phys. Chem. B*, 2006, **110**, 3330–3335.
- 74 D. Roy, N. Patel, S. Conte and M. Maroncelli, *J. Phys. Chem. B*, 2010, **114**, 8410–8424.
- 75 E. A. Shelepova, D. Paschek, R. Ludwig and N. N. Medvedev, *J. Mol. Liq.*, 2020, **299**, 112121.
- 76 E. A. Shelepova, R. Ludwig, D. Paschek and N. N. Medvedev, *J. Mol. Liq.*, 2021, **329**, 115589.
- 77 P. A. Hunt, C. R. Ashworth and R. P. Matthews, *Chem. Soc. Rev.*, 2015, **44**, 1257–1288.
- 78 S. J. Grabowski, *Chem. Rev.*, 2011, **111**, 2597–2625.
- 79 F. Weinhold and C. R. Landis, *Valency and Bonding: A Natural Bond Orbital Donor-Acceptor Perspective*, Cambridge University Press, 2005.
- 80 R. Kumar, J. R. Schmidt and J. L. Skinner, *J. Chem. Phys.*, 2007, **126**, 204107.
- 81 S. Gehrke and B. Kirchner, *J. Chem. Eng. Data*, 2020, **65**, 1146–1158.

Supporting Information:

Hydrogen Bond Redistribution Effects in Mixtures of Protic Ionic Liquids Sharing the Same Cation: Nonideal Mixing with Large Negative Mixing Enthalpies

Benjamin Golub[†], Daniel Ondo[‡], Viviane Overbeck[†], Ralf Ludwig^{†,§}, and Dietmar Paschek^{†,*}

[†] *Physikalische und Theoretische Chemie, Institut für Chemie, Universität Rostock, Albert-Einstein-Straße 27,
D-18059 Rostock, Germany*

[‡] *Department of Physical Chemistry, University of Chemistry and Technology, Technická 5., 166 28 Prague 6,
Czech Republic*

[§] *Leibniz-Institut für Katalyse an der Universität Rostock, Albert-Einstein-Straße 29a, D-18059 Rostock,
Germany*

*E-mail: dietmar.paschek@uni-rostock.de

Contents

S1 MD Simulations	S2
S1.1 Outline/Results of the MD Simulations	S2
S1.2 Energies of Mixing Obtained from MD Simulation	S5
S2 ¹H-NMR-Spectra	S6
S3 Experimental Determination of the Excess Enthalpies	S7
S3.1 Apparatus	S7
S3.2 Data analysis	S7
S3.3 Fitting by Redlich-Kister Equation	S7
S3.4 Fitting by Lattice Model	S11
References	S12

S1 MD Simulations

S1.1 Outline/Results of the MD Simulations

To study the pure PILs and mixtures we performed isobaric isothermal (NPT) MD simulations using GROMACS 5.0.6. We investigated eleven compositions between $x_{\text{OMs}} = 0.0$ and $x_{\text{OMs}} = 1.0$ for six temperatures between $T = 300$ K and $T = 400$ K at a pressure of 1 bar. Tables S1 to S11 contain a summary of selected properties for each performed MD simulation: the average mass density ρ , the average potential energy E_p , the fraction of hydrogen bonds of the [TEA] cations to [OMs] anions y_{OMs} , and the fraction of hydrogen bonds of the [TEA] cations to [OTf] anions y_{OTf} .

Table S1: $x_{\text{OMs}} = 0.0$

T / K	$\rho / \text{kg m}^{-3}$	$E_p / \text{kJ mol}^{-1}$	y_{OMs}	y_{OTf}
300	1245.2	-996	-	0.997
320	1229.1	1186	-	0.995
340	1213.4	3287	-	0.993
360	1198.0	5394	-	0.991
380	1183.3	7461	-	0.988
400	1168.2	9525	-	0.984

Table S2: $x_{\text{OMs}} = 0.1$

T / K	$\rho / \text{kg m}^{-3}$	$E_p / \text{kJ mol}^{-1}$	y_{OMs}	y_{OTf}
300	1232.5	-21008	0.283	0.718
320	1216.8	-18844	0.272	0.725
340	1201.2	-16772	0.274	0.721
360	1186.1	-14677	0.269	0.724
380	1171.6	-12603	0.261	0.729
400	1156.9	-10544	0.255	0.732

Table S3: $x_{\text{OMs}} = 0.2$

T / K	$\rho / \text{kg m}^{-3}$	$E_p / \text{kJ mol}^{-1}$	y_{OMs}	y_{OTf}
300	1220.1	-40840	0.538	0.460
320	1204.2	-38845	0.540	0.457
340	1189.4	-36729	0.525	0.471
360	1175.0	-34631	0.510	0.484
380	1160.3	-32537	0.497	0.496
400	1145.6	-30450	0.482	0.508

Table S4: $x_{\text{OMs}} = 0.3$

T / K	$\rho / \text{kg m}^{-3}$	$E_p / \text{kJ mol}^{-1}$	y_{OMs}	y_{OTf}
300	1208.1	-40840	0.734	0.265
320	1192.5	-38845	0.730	0.268
340	1177.3	-36729	0.717	0.280
360	1163.1	-34631	0.707	0.289
380	1148.5	-32537	0.683	0.312
400	1134.1	-30450	0.661	0.331

Table S5: $x_{\text{OMs}} = 0.4$

T / K	$\rho / \text{kg m}^{-3}$	$E_p / \text{kJ mol}^{-1}$	y_{OMs}	y_{OTf}
300	1194.3	-79688	0.863	0.136
320	1179.7	-77765	0.869	0.130
340	1165.1	-75594	0.839	0.158
360	1150.6	-73518	0.825	0.172
380	1136.9	-71487	0.806	0.188
400	1122.9	-69461	0.789	0.204

Table S6: $x_{\text{OMs}} = 0.5$

T / K	$\rho / \text{kg m}^{-3}$	$E_p / \text{kJ mol}^{-1}$	y_{OMs}	y_{OTf}
300	1181.6	-98623	0.927	0.072
320	1166.7	-96721	0.929	0.069
340	1153.2	-94669	0.918	0.080
360	1139.4	-92582	0.894	0.103
380	1124.9	-90565	0.884	0.112
400	1111.1	-88554	0.869	0.125

Table S7: $x_{\text{OMs}} = 0.6$

T / K	$\rho / \text{kg m}^{-3}$	$E_p / \text{kJ mol}^{-1}$	y_{OMs}	y_{OTf}
300	1167.9	-117448	0.966	0.032
320	1154.3	-115502	0.964	0.034
340	1139.7	-113423	0.950	0.047
360	1126.2	-111437	0.939	0.058
380	1112.8	-109500	0.933	0.063
400	1099.3	-107510	0.918	0.076

Table S8: $x_{\text{OMs}} = 0.7$

T / K	$\rho / \text{kg m}^{-3}$	$E_{\text{p}} / \text{kJ mol}^{-1}$	y_{OMs}	y_{OTf}
300	1154.2	-136208	0.984	0.015
320	1140.4	-134120	0.972	0.026
340	1126.2	-132153	0.970	0.028
360	1112.8	-130204	0.966	0.031
380	1099.8	-128272	0.956	0.039
400	1086.7	-126348	0.950	0.044

Table S9: $x_{\text{OMs}} = 0.8$

T / K	$\rho / \text{kg m}^{-3}$	$E_{\text{p}} / \text{kJ mol}^{-1}$	y_{OMs}	y_{OTf}
300	1139.0	-154745	0.990	0.009
320	1126.2	-152787	0.986	0.012
340	1112.5	-160857	0.983	0.014
360	1099.5	-148934	0.978	0.018
380	1086.6	-147031	0.975	0.020
400	1074.0	-145144	0.970	0.024

Table S10: $x_{\text{OMs}} = 0.9$

T / K	$\rho / \text{kg m}^{-3}$	$E_{\text{p}} / \text{kJ mol}^{-1}$	y_{OMs}	y_{OTf}
300	1124.9	-173373	0.993	0.005
320	1111.6	-171490	0.994	0.004
340	1098.2	-169514	0.992	0.005
360	1085.3	-167605	0.988	0.008
380	1073.0	-165740	0.987	0.008
400	1060.4	-163886	0.984	0.010

Table S11: $x_{\text{OMs}} = 1.0$

T / K	$\rho / \text{kg m}^{-3}$	$E_{\text{p}} / \text{kJ mol}^{-1}$	y_{OMs}	y_{OTf}
300	1109.5	-191997	0.998	-
320	1096.0	-190126	0.998	-
340	1083.4	-188176	0.997	-
360	1070.7	-186284	0.996	-
380	1058.7	-184451	0.995	-
400	1046.5	-182612	0.993	-

S1.2 Energies of Mixing Obtained from MD Simulation

From the MD simulations we can directly determine the energies of mixing according to

$$\begin{aligned}
 \Delta U_{\text{mix}} &= U(x_{\text{OMs}}) - x_{\text{OMs}} \cdot U_{[\text{TEA}][\text{OMs}]} \\
 &\quad - (1 - x_{\text{OMs}}) \cdot U_{[\text{TEA}][\text{OTf}]} \\
 &= E_p(x_{\text{OMs}}) - x_{\text{OMs}} \cdot E_{p,[\text{TEA}][\text{OMs}]} \\
 &\quad - (1 - x_{\text{OMs}}) \cdot E_{p,[\text{TEA}][\text{OTf}]} ,
 \end{aligned} \tag{1}$$

where $U(x_{\text{OMs}})$ represents the total energy of the mixture $[\text{TEA}][\text{OTf}]/[\text{TEA}][\text{OMs}]$ with a given composition x_{OMs} , while $U_{[\text{TEA}][\text{OTf}]}$ and $U_{[\text{TEA}][\text{OMs}]}$ are the energies of the pure PILs. The E_p -values represent the corresponding potential energies. All computed excess energies of mixing are summarised in Table S12.

Table S12: Excess energies of mixing calculated from molecular dynamics simulation data given in Tables S1 to S11.

x_{OMs}	$\Delta U_{\text{mix}} / \text{kJ mol}^{-1}$					
	300 K	320 K	340 K	360 K	380 K	400 K
0.0	0.0	0.0	0.0	0.0	0.0	0.0
0.1	-1.8±0.3	-1.80±0.23	-1.83±0.18	-1.81±0.17	-1.75±0.17	-1.71±0.16
0.2	-3.3±0.3	-3.54±0.24	-3.45±0.24	-3.38±0.24	-3.23±0.15	-3.09±0.16
0.3	-4.6±0.4	-4.46±0.23	-4.37±0.25	-4.45±0.19	-4.14±0.20	-3.93±0.20
0.4	-4.57±0.23	-4.85±0.23	-4.59±0.24	-4.48±0.23	-4.37±0.19	-4.26±0.19
0.5	-4.23±0.28	-4.50±0.21	-4.45±0.16	-4.27±0.20	-4.14±0.16	-4.02±0.18
0.6	-3.68±0.21	-3.80±0.24	-3.66±0.18	-3.65±0.18	-3.63±0.20	-3.50±0.14
0.7	-3.00±0.19	-2.78±0.22	-2.83±0.22	-2.85±0.18	-2.79±0.18	-2.75±0.14
0.8	-1.86±0.24	-1.9±0.3	-1.95±0.23	-1.97±0.18	-1.92±0.16	-1.92±0.12
0.9	-0.92±0.22	-0.99±0.25	-0.97±0.22	-0.98±0.21	-0.96±0.15	-0.97±0.13
1.0	0.0	0.0	0.0	0.0	0.0	0.0

S2 ^1H -NMR-Spectra

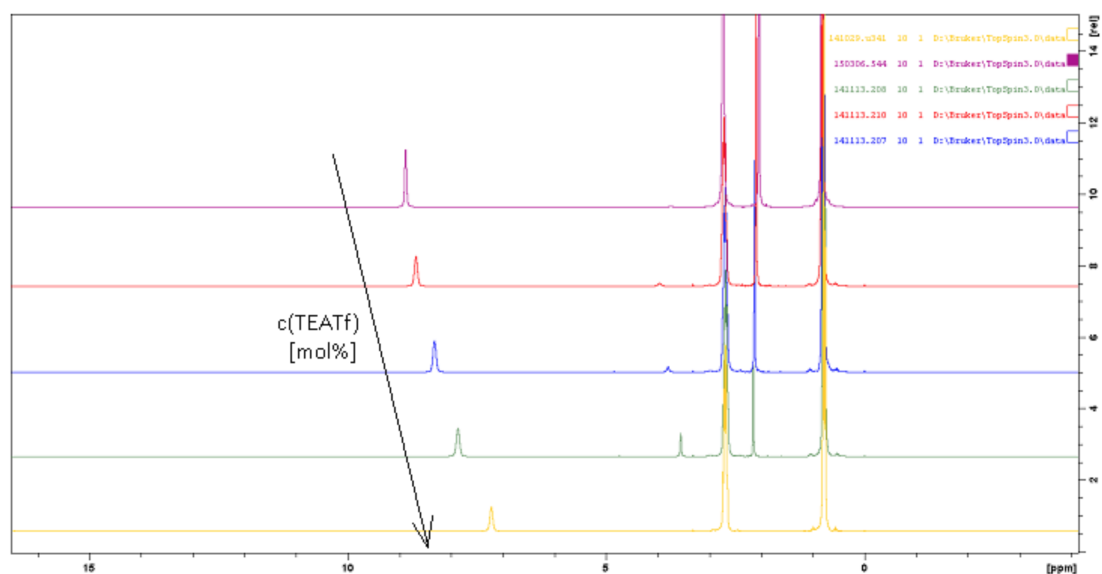


Figure S1: Experimental ^1H -NMR spectra obtained at 298 K for [TEA][OMS]/[TEA][OTf] mixtures with mol fractions $x_{\text{OMS}} = 1.0$, $x_{\text{OMS}} = 0.25$, $x_{\text{OMS}} = 0.5$, $x_{\text{OMS}} = 0.75$, and $x_{\text{OMS}} = 0.0$ (from top to bottom). The arrow indicates the shift of the N-H proton peak as a function of mixture composition.

S3 Experimental Determination of the Excess Enthalpies

S3.1 Apparatus

The partial molar excess enthalpies \overline{H}_{ILj}^E in IL(1) + [TEA][OTf](2) mixtures were measured at $T = 298.15$ K using the TAM isothermal titration calorimeter (Thermometric, Sweden). The \overline{H}_{ILj}^E in [TEA][OMs](1) + [TEA][OTf](2) system were measured in 4 mL stainless steel reaction cell. Four experiments were conducted: the cell filled with pure [TEA][OMs](1) was titrated with pure [TEA][OTf](2) and vice versa; the cell filled with mixture of [TEA][OMs](1) + [TEA][OTf](2) ($x_{\text{OMs}} = 0.4602$) was titrated with [TEA][OMs](1) or [TEA][OTf](2). 20 injections of 10 μL of pure IL were injected into cell from 250 μL syringe using the Lund pump. The content of the cell was stirred at 85 and 100 rpm using the gold propeller stirrer. The reference cell contained 0.9456 g of [TEA][OMs](1). All four experiments were conducted at 3000 μW range of the calorimeter. The reaction cell and propeller were washed with acetone and dried in oven after experiment termination. Dynamic calibration was performed before start of own titration procedure.

Table S13: Experimental settings of TAM-ITC for measurement of \overline{H}^E in mixture of [TEA][OMs](1) + [TEA][OTf](2) at $T = 298.15$ K.

$m_0^{\text{cell}} / \text{g}$	0.9446	1.4399	1.2815	1.2522
$x_{0,IL1}^{\text{cell}}$	1	0	0.4602	0.4602
IL syringe	2	1	1	2
Main section /min	90	90	60	60
Baseline section /min	15	15	15	15

S3.2 Data analysis

The partial molar excess enthalpy of injected IL at i -th injection is directly related to the measured heat

$$\overline{H}_{ILj,i}^E = \frac{\Delta q_i}{\Delta n_{j,i}}, \quad (2)$$

where Δq_i is the measured peak area after injection of Δn_i molar amount of the j -th IL into cell. The measured $\overline{H}_{IL,i}^E$ at i -th injection is tangent to H^E at $(x_{IL,i} + x_{IL,i-1})/2$ between two injections. Here $x_{IL,i}$ and $x_{IL,i-1}$ denote the composition of the mixture in cell after i -th and $(i - 1)$ th injection.

The molar amount of injected component was calculated from pure IL densities [2] and injected volume. The numerical values of $\overline{H}_{ILj,i}^E$ measured by TAM-ITC and used further for fitting are listed in Tables S14 and S15.

S3.3 Fitting by Redlich-Kister Equation

The composition dependence of H^E by Redlich-Kister equation is given as

$$H^E = x_1 x_2 [A_1 + A_2(x_1 - x_2) + A_3(x_1 - x_2)^2]. \quad (3)$$

Table S14: Measured \overline{H}^E of [TEA][OMs](1) ionic liquid in mixture of [TEA][OMs](1) + [TEA][OTf](2) at $T = 298.15$ K as function of mixture composition.

x_{OMs}	$\overline{H}_{IL1}^E / (\text{J}\cdot\text{mol}^{-1})$	x_{OMs}	$\overline{H}_{IL1}^E / (\text{J}\cdot\text{mol}^{-1})$
0.0049	-7935	0.4682	-2675
0.0146	-7764	0.4734	-2632
0.0241	-7679	0.4785	-2580
0.0334	-7582	0.4835	-2538
0.0426	-7572	0.4884	-2494
0.0516	-7399	0.4932	-2469
0.0604	-7305	0.4979	-2394
0.0690	-7174	0.5025	-2360
0.0775	-7134	0.5071	-2307
0.0859	-7071	0.5115	-2264
0.0941	-6949	0.5159	-2205
0.1021	-6827	0.5202	-2187
0.1100	-6783	0.5245	-2138
0.1178	-6639	0.5286	-2111
0.1254	-6588	0.5327	-2076
0.1329	-6492	0.5367	-2015
0.1403	-6384	0.5407	-1987
0.1475	-6330	0.5446	-1930
0.1546	-6261	0.5484	-1938
0.1617	-6210	0.5521	-1884
0.1685	-6116		

Table S15: Measured \overline{H}^E of [TEA][OTf](2) ionic liquid in mixture of [TEA][OMs](1) + [TEA][OTf](2) at $T = 298.15$ K as function of mixture composition.

x_{OMs}	$\overline{H}_{IL2}^E / (\text{J}\cdot\text{mol}^{-1})$	x_{OMs}	$\overline{H}_{IL2}^E / (\text{J}\cdot\text{mol}^{-1})$
0.9845	-8381	0.4581	-1795
0.9745	-8119	0.4540	-1753
0.9646	-8038	0.4500	-1718
0.9549	-7891	0.4460	-1692
0.9455	-7840	0.4421	-1661
0.9362	-7690	0.4383	-1632
0.9271	-7533	0.4345	-1594
0.9181	-7448	0.4308	-1563
0.9094	-7346	0.4272	-1532
0.9008	-7223	0.4236	-1511
0.8923	-7110	0.4201	-1484
0.8841	-7003	0.4167	-1452
0.8759	-6868	0.4133	-1424
0.8679	-6774	0.4099	-1390
0.8601	-6716	0.4066	-1377
0.8524	-6556	0.4034	-1354
0.8449	-6442	0.4002	-1314
0.8374	-6350	0.3971	-1301
0.8301	-6283	0.394	-1277
0.8230	-6206	0.3909	-1255
0.8159	-6070		

The partial molar enthalpies \overline{H}^E in binary system are calculated from H^E by

$$\overline{H}_1^E = H^E - (1 - x_1) \frac{\partial H^E}{\partial x_1} \quad (4)$$

$$\overline{H}_2^E = H^E - x_1 \frac{\partial H^E}{\partial x_1} \quad (5)$$

Applying Eqs. 4 and 5 on Eq. 3 for the measured partial molar excess enthalpies $\overline{H}_{IL1,i}^E$ and $\overline{H}_{IL2,i}^E$ follows

$$\overline{H}_{IL1}^E = x_2^2[A_1 + A_2(4x_1 - 1) + A_3(x_1 - x_2)(6x_1 - 1)], \quad (6)$$

$$\overline{H}_{IL2}^E = x_1^2[A_1 + A_2(1 - 4x_2) + A_3(x_1 - x_2)(1 - 6x_2)]. \quad (7)$$

The partial molar excess enthalpies at infinite dilution then follows

$$\overline{H}_1^{E,\infty} = A_1 - A_2 + A_3 \quad (8)$$

and

$$\overline{H}_2^{E,\infty} = A_1 + A_2 + A_3 \quad (9)$$

To evaluate the parameters A_n of Redlich-Kister equation given above, the experiments were treated by simultaneous linear non-weighted fit using 76 discrete $\overline{H}_{IL,i}^E$ points. Table S16 lists the values for one to three parameter fit of experimental \overline{H}_{IL1}^E and \overline{H}_{IL2}^E by Eqs (6) and (7), respectively, together with the calculated values of partial molar excess enthalpies at infinite dilution $\overline{H}_{IL1}^{E,\infty}$ and $\overline{H}_{IL2}^{E,\infty}$. The \overline{H}^E composition dependence of the excess enthalpies is best represented by three parameter Redlich-Kister equation. Figure S2 illustrates the dependence of the H^E , \overline{H}_{IL1}^E and \overline{H}_{IL2}^E as function of mixture composition. The minimum in H^E is at $x_1 = 0.5083$ with the value $H^E = -2.24 \text{ kJ} \cdot \text{mol}^{-1}$.

Table S16: Values of adjustable parameters A_n of Redlich-Kister equations (6) and (7), standard deviation of fit s and calculated partial molar excess enthalpies at infinite dilution $\overline{H}_1^{E,\infty}$ and $\overline{H}_2^{E,\infty}$ by Eqs. (8) and (9) for [TEA][OMs](1) + [TEA][OTf](2) mixture at $T = 298.15 \text{ K}$.

A_1	A_2	A_3	$s/(\text{J} \cdot \text{mol}^{-1})$	$\overline{H}_1^{E,\infty}/(\text{kJ} \cdot \text{mol}^{-1})$	$\overline{H}_2^{E,\infty}/(\text{kJ} \cdot \text{mol}^{-1})$
-8662.17			210	-8.66	-8.66
-8673.45	-385.90		136	-8.29	-9.06
-8974.27	-324.99	804.735	40	-7.85	-8.50

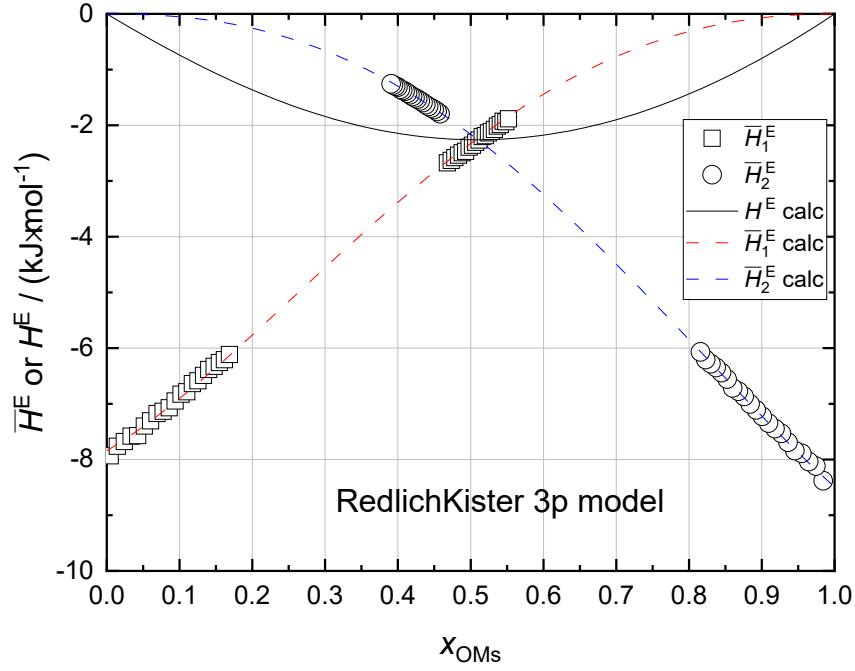


Figure S2: Excess molar enthalpies \overline{H}^E and H^E in the [TEA][OMs](1) + [TEA][OTf](2) mixture at $T = 298.15$ K. Points are experimental \overline{H}^E : (square) \overline{H}_1^E of [TEA][OMs](1); (circle) \overline{H}_2^E of [TEA][OTf](2). Dashed lines are fits to experimental \overline{H}_1^E and \overline{H}_2^E data by Redlich-Kister Eqs. (6) and (7), with parameters A_n listed in Table S16. Solid line is the calculated H^E by Eq. (3).

S3.4 Fitting by Lattice Model

From the lattice model for ΔU_{mix} at constant pressure for H^E follows

$$\Delta U_{\text{mix}} = H^E = \Delta\epsilon_{\text{HB}}x_1 \frac{(1-x_1)(1-f)}{x_1 + f(1-x_1)} \quad (10)$$

where x_1 is the mole fraction of [TEA][OMs](1) and $f = a + bx_1$

$$\overline{H}_1^E = \Delta\epsilon_{\text{HB}}(1-x_1) \frac{a(ax_1^3 - 3ax_1^2 + 3ax_1 - a - x_1 + 1)}{(ax_1^2 - 2ax_1 + a + x_1)^2} \quad (11)$$

$$\overline{H}_2^E = \Delta\epsilon_{\text{HB}}x_1^2 \frac{2ax_1 - 2a + 1}{(ax_1^2 - 2ax_1 + a + x_1)^2} \quad (12)$$

For the partial molar excess enthalpies at infinite dilution then follows

$$\overline{H}_1^{E,\infty} = \Delta\epsilon_{\text{HB}}(1-a)/a \quad (13)$$

and

$$\overline{H}_2^{E,\infty} = \Delta\epsilon_{\text{HB}}(1-a-b) \quad (14)$$

The following parameters of Eqs. (10) were fitted $\Delta\epsilon_{\text{HB}} = -14.9 \text{ kJ} \cdot \text{mol}^{-1}$, $a = 0.6559$, $b = -0.2416$ to experimental \overline{H}_1^E and \overline{H}_2^E data. Figure S3 illustrates the composition dependence of experimental and calculated \overline{H}^E and H^E . The calculated $\overline{H}_1^{E,\infty}$ and $\overline{H}_2^{E,\infty}$ by Eqs. (13) and (14) are $\overline{H}_1^{E,\infty} = -7.83 \text{ kJ} \cdot \text{mol}^{-1}$ and $\overline{H}_2^{E,\infty} = -8.74 \text{ kJ} \cdot \text{mol}^{-1}$, respectively. The minimum in H^E is at $x_1 = 0.5082$ with the value $H^E = -2.26 \text{ kJ} \cdot \text{mol}^{-1}$.

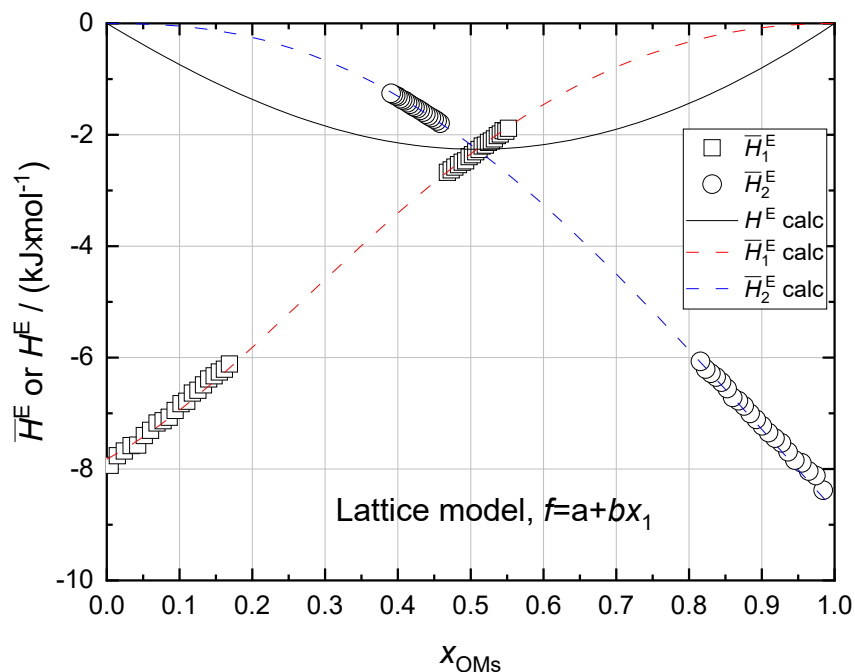


Figure S3: Excess molar enthalpies \overline{H}^E and H^E in the [TEA][OMs](1) + [TEA][OTf](2) mixture at $T = 298.15 \text{ K}$. Points are experimental \overline{H}^E : (square) \overline{H}_1^E of [TEA][OMs](1); (circle) \overline{H}_2^E of [TEA][OTf](2). Dashed lines are fits to experimental \overline{H}_1^E and \overline{H}_2^E data by Lattice model, with parameters $\Delta\epsilon_{\text{HB}} = -14.9 \text{ kJ} \cdot \text{mol}^{-1}$, $a = 0.6558$, $b = -0.2416$. Solid line is the calculated H^E by Eq. (10).

References

- [1] K. Fumino, V. Fossog, K. Wittler, R. Hempelmann, R. Ludwig, *Angew. Chem. Int. Ed.* **2013**, 52, 2368–2372.
- [2] K. Fumino, A.-M. Bónsa, B. Golub, D. Paschek, R. Ludwig, *ChemPhysChem* **2015**, 16, 299–304.

4.5 Publication IV

Why Do Liquids Mix? The Mixing of Protic Ionic Liquids Sharing the Same Cation is Apparently Driven by Enthalpy, not Entropy

B. Golub, D. Ondo, R. Ludwig and D. Paschek

J. Phys. Chem. Lett., 2022, **13**, 3556-3561

CRedit roles: Formal analysis (MD simulations), Investigation (MD simulations), Visualization, Writing - review & editing

Approximated contribution to the publication in present: 40 %

Reprinted with permission from B.Golub D. Ondo, R. Ludwig and D. Paschek, *J. Phys. Chem. Lett.*, 2022 **13**, 3556-3561. Copyright 2023 American Chemical Society

Why Do Liquids Mix? The Mixing of Protic Ionic Liquids Sharing the Same Cation Is Apparently Driven by Enthalpy, Not Entropy

Benjamin Golub, Daniel Ondo, Ralf Ludwig, and Dietmar Paschek*



Cite This: *J. Phys. Chem. Lett.* 2022, 13, 3556–3561



Read Online

ACCESS |



Metrics & More

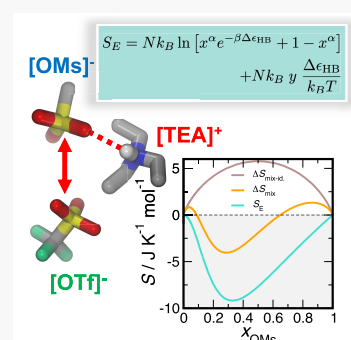


Article Recommendations



Supporting Information

ABSTRACT: We study hydrogen bond (HB) redistribution in mixtures of two protic ionic liquids (PILs) sharing the same cation: triethylammonium methanesulfonate ([TEA][OMs]) and triethylammonium trifluoromethanesulfonate ([TEA][OTf]). The mixtures exhibit large negative energies of mixing. Based on results obtained from atomic detail molecular dynamics (MD) simulations, we derive a lattice model, discriminating between HB and nonspecific intermolecular interactions. We demonstrate that due to the ordered structure of the PILs, mostly the HB interactions contribute to the mixing energy. This allows us to connect the equilibrium of HBs to each of the two anion species with the corresponding excess energies and entropies. The entropy associated with HB redistribution is shown to be negative, and even overcompensating the positive entropy associated with a statistical distribution of the ions in the mixture. This is strongly suggesting that the mixing process is driven by enthalpy, not entropy.



Protic ionic liquids (PILs)¹ have attracted considerable interest since they possess qualities such as biocompatibility² and low toxicity.³ Mixtures of ionic liquids (ILs) have gained increasing attention in recent years.^{4–19} Mixtures of ILs are often characterized by their general mixing behavior, analyzing to what degree they are deviating from Raoult's law (i.e., ideal mixing behavior).²⁰ As a rule of thumb, ILs often mix well.²⁰ However, whether we find a *nonideal* mixing behavior is, of course, depending on the interaction forces between the ions. Combinations of strong dispersion forces,²¹ but also hydrogen bonding,^{22,23} can lead to a significant *nonideal* mixing. A direct way to investigate the formation or change of interactions due to mixing is to determine the enthalpy or energy of mixing.^{20–29} If the enthalpy of mixing is close to zero, the mixing is, of course, nearly ideal. Positive or negative enthalpies of mixing, however, imply the “making or breaking”³⁰ of interactions and are therefore often related to changes of the structure of the liquid.³¹ Extensive reviews of mixtures of ionic liquids are available in refs 20, 26, and 30. In this study, we would like to focus on a specific mixture of PILs, which has the potential to disentangle the contribution from hydrogen bonding and other *nonspecific* forms of intermolecular interactions: the mixture of two rather common protic ionic liquids sharing the same cation. The two PILs are triethylammonium methanesulfonate ([TEA][OMs]) and triethylammonium trifluoromethanesulfonate ([TEA][OTf]). In the PIL, a [TEA] cation acts as a hydrogen bond (HB) donor, being able to donate a single HB. Both, the [OMs] and the [OTf] anions can act as HB acceptors, which can accept multiple HBs via their respective SO₃-groups. In previous publications,^{11,12,32} we could demonstrate that a mixture of those PILs experiences a redistribution of HBs between the

cation and the anions in the mixture apparently due to stronger HBs between [TEA] and [OMs] ions.^{12,33,34} This is leading to *nonideal* mixing behavior, almost completely stripping the [OTf] anion of HB partners in the [OMs]-rich region.¹¹ Note that the local environment of each of the anions is formed by a solvation shell composed predominantly of cations. Hence the environment of each anion is very similar in the mixture compared to the respective pure PILs, such that the *nonideal* mixing behavior is most likely only due to HB redistribution effects.

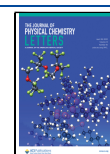
To study the pure PILs and mixtures, we performed isobaric isothermal (NPT) molecular dynamics (MD) simulations investigating 11 compositions with mole fractions $x_{\text{OMs}} = N_{\text{OMs}} / (N_{\text{OMs}} + N_{\text{OTf}})$ between $x_{\text{OMs}} = 0.0$ and $x_{\text{OMs}} = 1.0$ for five temperatures between $T = 320$ K and $T = 400$ K at a pressure of 1 bar. All studied systems were composed of 500 ion pairs. More details about the performed MD simulations and the employed force field are provided in sections S1–S3 of the Supporting Information.

In a previous contribution we have shown that MD simulations of pure [TEA][OMs] and [TEA][OTf] as well as their mixtures exhibit a well-defined charge-induced intermolecular order.¹¹ Here each ion was found to be surrounded by a solvation shell predominantly consisting of

Received: March 2, 2022

Accepted: April 12, 2022

Published: April 14, 2022



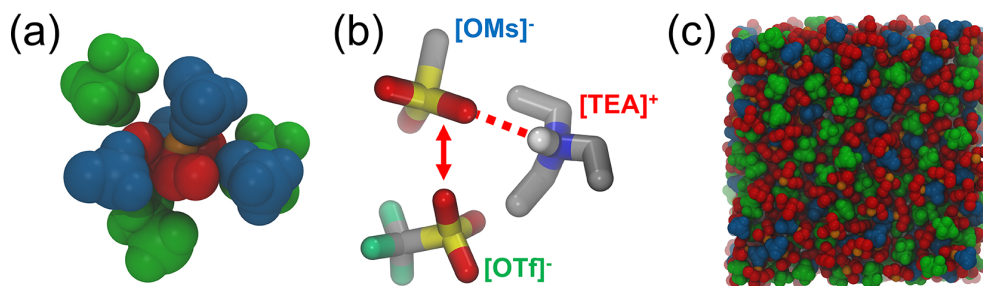


Figure 1. (a) Snapshot of the solvation of a central [TEA] cation, shown in red, in a [TEA][OMs]/[TEA][OTf] mixture engaged in a HB to an adjacent [OMs] anion. The [OMs] anions are shown in blue and the [OTf] anions are depicted in green. (b) Illustrated equilibrium of the HBs donated by a [TEA] cation and accepted by the SO_3 groups of the [OMs] and [OTf] anions. (c) Snapshot of an entire MD simulation box of an equimolar mixture containing 500 ion pairs using the same color coding as in part a.

counterions. The average coordination number c , defined by a center of mass distance of 0.8 nm between ions of opposite charge (corresponding to the location of the first minimum of anion–cation pair correlation functions) was found to vary only slightly between 6.8 and 6.9 as a function of the mixture composition. The corresponding distribution functions are shown in section S6 of the Supporting Information and are characterized by a maximum at seven neighbors with a half-width of about 2.5 neighbors. A representative snapshot of the solvation of a [TEA] cation in [TEA][OMs]/[TEA][OTf] mixture is shown in Figure 1a.

HBs are characterized here by means of geometric criteria. Based on the analysis discussed in ref 11, we use a distance criterion of $r_{\text{H}\cdots\text{O}} \leq 0.24$ nm to define a HB for both, the [OMs] and the [OTf] ions. We obtain the standard enthalpy associated with switching a HB between the two anion species $\Delta H'^\circ$ from a van 't Hoff plot of the logarithm of the equilibrium constant

$$K' = \frac{y_{\text{OMs}}}{y_{\text{OTf}}} \quad (1)$$

versus the inverse temperature shown in Figure 2. The motivation for this definition of K' and its relation to the “chemical” equilibrium constant K_{eq} is outlined in section S5.3.1 of the Supporting Information. Here y_{OMs} and y_{OTf}

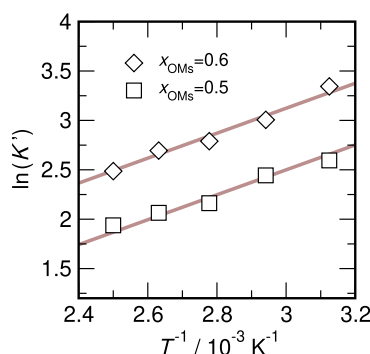


Figure 2. Van't Hoff plot of the logarithm of the equilibrium constant K' according to eq 1 vs the inverse temperature for compositions with $x_{\text{OMs}} = 0.5$, and $x_{\text{OMs}} = 0.6$. The slope of the solid lines correspond to a standard molar enthalpy difference of $\Delta H'^\circ$ of -10.5 kJ mol $^{-1}$. From the axis intercept we obtain the corresponding standard molar entropy differences with $\Delta S'^\circ = -10.7$ J K $^{-1}$ mol $^{-1}$ for $x_{\text{OMs}} = 0.5$, and $\Delta S'^\circ = -5.5$ J K $^{-1}$ mol $^{-1}$ for $x_{\text{OMs}} = 0.6$.

represent the fraction of HBs donated by the [TEA] cation to either of the two anion species. Depicted are data for compositions of $x_{\text{OMs}} = \{0.5, 0.6\}$, indicating a value of about $\Delta H'^\circ = -10.5$ kJ mol $^{-1}$ for the enthalpy associated with breaking a [TEA][OTf] HB and forming a new [TEA][OMs] HB.

From the energies recorded during the MD simulations we can directly determine the energies of mixing according to

$$\Delta U_{\text{mix}} = U(x_{\text{OMs}}) - x_{\text{OMs}} \cdot U_{[\text{TEA}][\text{OMs}]} - (1 - x_{\text{OMs}}) \cdot U_{[\text{TEA}][\text{OTf}]} \quad (2)$$

where $U(x_{\text{OMs}})$ represents the average total energy of the mixture [TEA][OTf]/[TEA][OMs] with a given composition x_{OMs} , while $U_{[\text{TEA}][\text{OTf}]}$ and $U_{[\text{TEA}][\text{OMs}]}$ are the average total energies of the pure PILs. The MD simulations indicate a strong *nonideal* mixing behavior. The computed negative mixing energies of the equimolar mixture are found to be (-4.02 ± 0.18) kJ mol $^{-1}$ at 400 K and (-4.50 ± 0.21) kJ mol $^{-1}$ at 320 K as shown in Table S16 in the Supporting Information. In addition, we observe that the energy minima are shifted to a x_{OMs} value of about $x_{\text{OMs}} = 0.4$, which is almost temperature independent.

The regular local structure of the PILs is characterized by a well-defined anion–cation order as discussed in ref 11. This has inspired us to describe the mixture in terms of a lattice model based solely on local nearest neighbor interactions. In the model, we discriminate between HBs and *nonspecific* interactions (i.e., van der Waals and nonlocalized polar interactions). Here each of the ions in the PILs is placed on a regular lattice with a coordination number c . As illustrated in Figure 4 the anions and cations are arranged in an alternating fashion on the lattice. Hence there exist $(N_{\text{TEA}} \cdot c)$ *nonspecific* nearest neighbor interactions and (N_{TEA}) HBs. The total energy of the pure PILs follows as

$$U_{[\text{TEA}][\text{OMs}]} = N_{\text{TEA}} \cdot c \cdot \epsilon_{\text{TEA-OMs}} + N_{\text{TEA}} \cdot \epsilon_{\text{HB:TEA-OMs}} \quad (3)$$

and

$$U_{[\text{TEA}][\text{OTf}]} = N_{\text{TEA}} \cdot c \cdot \epsilon_{\text{TEA-OTf}} + N_{\text{TEA}} \cdot \epsilon_{\text{HB:TEA-OTf}} \quad (4)$$

where N_{TEA} is the number of [TEA] cations, c is the coordination number, and $\epsilon_{\text{TEA-OMs}}$, $\epsilon_{\text{TEA-OTf}}$, $\epsilon_{\text{HB:TEA-OMs}}$ and $\epsilon_{\text{HB:TEA-OTf}}$ are the parameters characterizing the respective *nonspecific* and HB interactions of the cation with either of the two anions. Assuming that in a mixture the sites of the anion sublattice are statistically occupied by one of the two anion

species in accordance with the mixture composition, the energy of the mixture with a composition x_{OMs} is given by

$$U(x_{\text{OMs}}) = N_{\text{TEA}} \cdot c \cdot x_{\text{OMs}} \cdot \epsilon_{\text{TEA-OMs}} + N_{\text{TEA}} \cdot y_{\text{OMs}} \cdot \epsilon_{\text{HB:TEA-OMs}} + N_{\text{TEA}} \cdot c \cdot (1 - x_{\text{OMs}}) \cdot \epsilon_{\text{TEA-OTf}} + N_{\text{TEA}} \cdot (1 - y_{\text{OMs}}) \cdot \epsilon_{\text{HB:TEA-OTf}} \quad (5)$$

where y_{OMs} represents the fraction of cations forming a HB to the neighboring [OMs] anions. Note that in the present case the condition $y_{\text{OMs}} + y_{\text{OTf}} \approx 1$ is well fulfilled with $y_{\text{OMs}} + y_{\text{OTf}}$ deviating from one $\leq 1\%$ for all compositions. From eqs 2, 3, 4, and 5 follows directly that

$$\Delta U_{\text{mix}} = N_{\text{TEA}} \cdot (y_{\text{OMs}} - x_{\text{OMs}}) \cdot \Delta \epsilon_{\text{HB}} \quad (6)$$

with

$$\Delta \epsilon_{\text{HB}} = \epsilon_{\text{HB:TEA-OMs}} - \epsilon_{\text{HB:TEA-OTf}} \quad (7)$$

Note that $\Delta \epsilon_{\text{HB}} < 0$ for the case of $\epsilon_{\text{HB:TEA-OMs}} < \epsilon_{\text{HB:TEA-OTf}}$ is leading to negative mixing energies if the condition $y_{\text{OMs}} > x_{\text{OMs}}$ is fulfilled. It is evident from eq 6 that the difference of the hydrogen bonding strengths of HBs donated by the [TEA] cation to each of the two anion species can thus be obtained from the knowledge of ΔU_{mix} , y_{OMs} , and x_{OMs} . The data shown in Figure 3 demonstrate that eq 6 almost perfectly predicts the

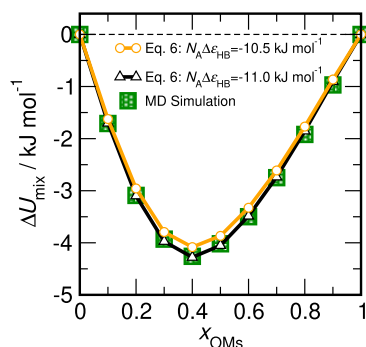


Figure 3. Mixing energies as a function of the mole fraction x_{OMs} for $T = 400$ K. Large filled squares: Mixing energies obtained directly from MD simulations according to Table S16 of the Supporting Information. Small open circles: Data computed from eq 6 using y_{OMs} data (see Tables S5–S15 of the Supporting Information) computed directly from the MD simulations with $N_A \Delta \epsilon_{\text{HB}} = -10.5$ kJ mol $^{-1}$. Small open triangles: eq 6 with $N_A \Delta \epsilon_{\text{HB}} = -11.0$ kJ mol $^{-1}$. The heavy lines linearly connect the data points and are just guides to the eye.

energies of mixing when using values for y_{OMs} obtained directly from MD simulations in combination with $N_A \Delta \epsilon_{\text{HB}} = -10.5$ kJ mol $^{-1}$, where N_A is Avogadro's number. This is strongly suggesting that HB redistribution is indeed the dominant contribution to the energy of mixing. To quantify the amount, we fit $\Delta \epsilon_{\text{HB}}$ to the mixing energies via eq 6, which is resulting in a perfect fit, and is providing us with a value of $N_A \Delta \epsilon_{\text{HB}} = -11.0$ kJ mol $^{-1}$. Hence we conclude that HB redistribution is responsible for about 95% of the total energy of mixing.

Considering the dominance of HB redistribution to the energy of mixing, the lattice model outlined in Figure 4 also allows us to derive the entropic contributions. First, let us assume that the anions in the mixture occupy the anion positions on the anion sublattice randomly according to their mixture composition. Since none of the nonbonded

interactions change during the mixing process, the corresponding energy of mixing is $\Delta U_{\text{mix-id}} = 0$, and

$$\Delta S_{\text{mix-id}} = -Nk_B [x \ln(x) + (1 - x) \ln(1 - x)] \quad (8)$$

is the associated ideal mixing entropy contribution due to the statistical distribution of the anions on the anion sublattice, with $x = x_{\text{OMs}}$ and k_B being the Boltzmann constant and N representing the total number of anions in the mixture. Hence

$$\Delta A_{\text{mix-id}} = Nk_B T [x \ln(x) + (1 - x) \ln(1 - x)] \quad (9)$$

is the related ideal Helmholtz free energy of mixing.

Assuming that the *nonideal* behavior is solely based on HB redistribution, we derive the associated thermodynamic excess properties of mixing from a partition function of the HB states for the cations, which are grouped into two distinct energy states with $\epsilon_{\text{HB,OMs}} = \Delta \epsilon_{\text{HB}}$ and $\epsilon_{\text{HB,OTf}} = 0$, populating the c surrounding HB acceptance-sites according to the mixture composition with

$$q_{\text{HB}}^N = [cx^\alpha e^{-\beta \Delta \epsilon_{\text{HB}}} + c(1 - x^\alpha)]^N, \quad (10)$$

where $\beta = (k_B T)^{-1}$, $N = N_{\text{TEA}}$, and $x = x_{\text{OMs}}$. Here $cx^\alpha e^{-\beta \Delta \epsilon_{\text{HB}}}$ describes the HBs to the [OMs] anions and $c(1 - x^\alpha)$ the corresponding HBs to the [OTf] anions. The parameter α is introduced to account for the different phase-space volumes associated with the two hydrogen-bonded states, therefore taking their different entropy contributions effectively into account. We would like to point the reader to section S5 of the Supporting Information for a thorough derivation of the employed model and its associated thermodynamic quantities. In addition to the model used here ("Model B"), we also introduce a "Model A" with fixed phase-space contributions. This model shows qualitatively the same behavior as "Model B", but is exhibiting slightly worse agreement with the MD simulation data. Moreover, in section S5.3.1 of the Supporting Information we demonstrate that the following relation between the standard molar enthalpy $\Delta H'^\circ$ obtained from the van 't Hoff analysis shown in Figure 2 and $\Delta \epsilon_{\text{HB}}$ is fulfilled: $\Delta H'^\circ / R = \Delta \epsilon_{\text{HB}} / k_B$.

From the definition of the partition functions follows that the fraction of HB to the [OMs] anions is given by

$$y = \frac{x^\alpha e^{-\beta \Delta \epsilon_{\text{HB}}}}{x^\alpha e^{-\beta \Delta \epsilon_{\text{HB}}} + 1 - x^\alpha} \quad (11)$$

with $y = y_{\text{OMs}}$ and $(1 - y) = y_{\text{OTf}}$. A statistical mechanical treatment of the partition function given by eq 10 using basic textbook definitions³⁵ (details are given in section S5 of the Supporting Information) is leading directly to

$$U_E = N \Delta \epsilon_{\text{HB}} \cdot \frac{x^\alpha e^{-\beta \Delta \epsilon_{\text{HB}}}}{x^\alpha e^{-\beta \Delta \epsilon_{\text{HB}}} + 1 - x^\alpha} - N x \Delta \epsilon_{\text{HB}} \quad (12)$$

$$U_E = N \Delta \epsilon_{\text{HB}} \cdot (y - x). \quad (13)$$

Note that eq 13 is identical with eq 6. The excess Helmholtz energy is accordingly

$$A_E = -x N \Delta \epsilon_{\text{HB}} - Nk_B T \ln [x^\alpha e^{-\beta \Delta \epsilon_{\text{HB}}} + 1 - x^\alpha]. \quad (14)$$

Since the term $P \Delta V_{\text{mix}}$ is about 5 orders of magnitude smaller than A_E , the excess Helmholtz energy A_E and excess Gibbs energy G_E are practically identical. Values for ΔV_{mix} for all temperatures and compositions are given in Table S17 in the Supporting Information. In addition, the composition

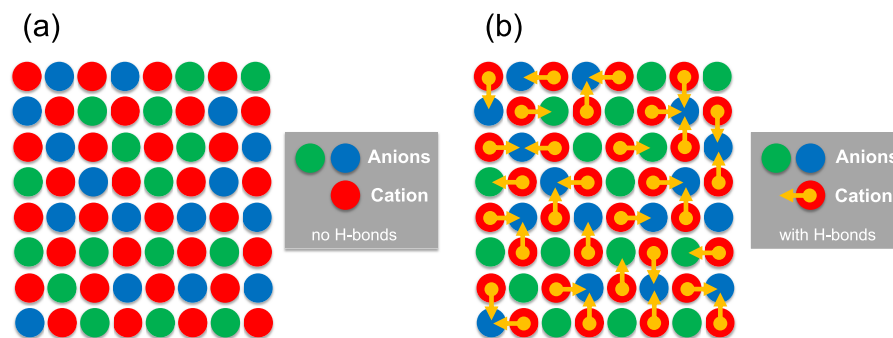


Figure 4. 2D lattice representation (with coordination number $c = 4$) of an equimolar mixture of [TEA][OMs] and [TEA][OTf]. The color coding is red = [TEA]⁺, blue = [OMs][−], and green = [OTf][−], similar to parts a and c of Figure 1. (a) Lattice sites are occupied by cations and anions in an alternate fashion, leading to a number of nonspecific cation–anion contacts of $N_{\text{TEA}} \cdot c$. The anions are randomly distributed on the lattice-sites of the anion-sublattice according to their mixture composition. (b) Arrows indicate HBs between the cations and one of the adjacent anions, therefore representing one additional HB interaction per cation. Note that the majority of HBs are found between [TEA] and [OMs] ions.

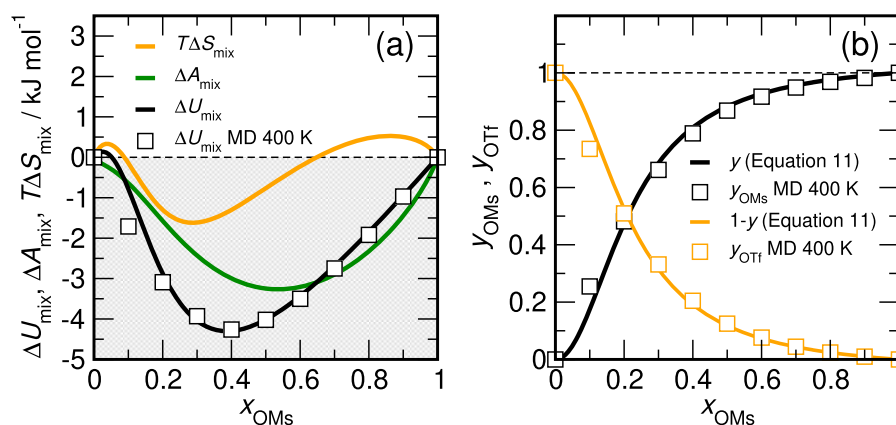


Figure 5. Theoretical predictions of the thermodynamic mixing properties for mixtures at $T = 400$ K using $N_A \Delta \epsilon_{\text{HB}} = -10.5$ kJ mol^{−1} and $\alpha = 2.05$. (a) Open squares indicate the energies of mixing as a function of x_{OMs} obtained from MD simulations. The heavy solid lines represent the ΔA_{mix} , ΔU_{mix} and $T\Delta S_{\text{mix}}$ according to eqs 14, 13, and 15, respectively. (b) Shown are the fraction y_{OMs} and y_{OTf} of [TEA] cations involved in a HB with [OMs] and [OTf] anions. Open circles represent data obtained from MD simulations. The heavy solid line represents data according to eq 11.

dependence of $P\Delta V_{\text{mix}}$ for $T = 400$ K is shown in Figure S5 of the Supporting Information. From eq 14 and eq 13 follows the excess entropy as

$$S_E = Nk_B \ln[x^\alpha e^{-\beta \Delta \epsilon_{\text{HB}}} + 1 - x^\alpha] + Nk_B \frac{\Delta \epsilon_{\text{HB}}}{k_B T}. \quad (15)$$

Figure 5 shows a comparison of the thermodynamic mixing properties obtained from MD simulations at $T = 400$ K with theoretical predictions employing $N_A \Delta \epsilon_{\text{HB}} = -10.5$ kJ mol^{−1} and $\alpha = 2.05$. We would like to point out that the behavior obtained at the highest temperature of 400 K is representative for the entire investigated temperature range, but is offering the best statistics. Obviously, the model is describing the simulation data very well using the energy difference $\Delta \epsilon_{\text{HB}}$ obtained independently from the van 't Hoff analysis discussed in Figure 2. In addition, as shown in Figure 5b, the corresponding fractions of HBs to both anion species are described similarly well. This is underlining again that HB redistribution is indeed the dominating contribution to the energy of mixing.

Earlier we have argued, that the parameter α accounts for the entropy differences of the two hydrogen-bonded states. In section S5.3.2 in the Supporting Information, we have derived

the relation between the standard molar entropy difference $\Delta S'^\circ$ obtained from the van 't Hoff analysis in Figure 2, the composition x , and the parameter α as follows:

$$\Delta S'^\circ = R \ln \frac{x^\alpha}{1 - x^\alpha}. \quad (16)$$

For $\alpha = 2.05$, we obtain $\Delta S'^\circ = -9.5$ J K^{−1} mol^{−1} for $x = 0.5$ and $\Delta S'^\circ = -5.1$ J K^{−1} mol^{−1} for $x = 0.6$, which is reasonably close to the values of $\Delta S'^\circ = -10.7$ J K^{−1} mol^{−1} and $\Delta S'^\circ = -5.5$ J K^{−1} mol^{−1}, according to the van 't Hoff analysis. We conclude that our model is also reasonably well taking into account the entropy difference of the two hydrogen-bonded states.

Finally, we would also make use of the fact that our statistical mechanical model of hydrogen bond redistribution is also capable of predicting the entropic contribution to the free energy of mixing. In particular, we would like to point out the curious negative mixing entropies $T\Delta S_{\text{mix}}$ observed in the range $0.1 \leq x_{\text{OMs}} \leq 0.65$ in Figure 5a. As illustrated in Figure 6, this feature is observed because the excess entropy caused by HB redistribution effects according to eq 15 is throughout negative and overcompensating the positive ideal contribution $\Delta S_{\text{mix-id}}$ to the entropy of mixing. The fact that $S_E < 0$ can be understood as follows: the interaction $\Delta \epsilon_{\text{HB}}$ is steering the HBs

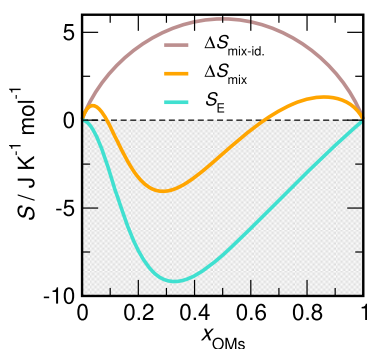


Figure 6. Different contributions to the entropy of mixing ΔS_{mix} of the PIL mixture at $T = 400$ K. The excess entropy S_E due to HB redistribution according to eq 15 is negative, even overcompensating for the positive ideal contribution $\Delta S_{\text{mix-id.}}$ due to the statistical distribution of the anions in the mixture in the range $0.1 \leq x_{\text{OMs}} \leq 0.65$.

donated by the [TEA] cations toward [TEA]–[OMs] accepting sites and is therefore effectively reducing the orientational configuration space accessible to the cations in the mixture. This is contrasted by the situation in the pure liquid, where the HB-interactions with surrounding HB-acceptors all have the same energy. Here the cation can freely explore the HB-accepting sites of all the surrounding anions. By construction, the negative excess energy due to HB redistribution is connected with an excess entropy of the same sign, also called enthalpy–entropy compensation effect.³⁶ Such a behavior is often observed in phenomena, where hydrogen bonding is involved in equilibria affecting molecular (re-)organization, such as hydrophobic hydration,³⁷ or the thermodynamics of protein folding.³⁸ A prominent example involving hydrogen bonding, where negative excess enthalpies and excess entropies correlate with one another, are of course, aqueous alcohol mixtures.³⁹ In those systems, however, the excess entropies do not dominate the ideal mixing entropy. A solvent with the capability to donate and accept HBs and which is possessing the discussed thermodynamic features, however, could be of interest for a variety of applications in the emerging field of “solvation science”.⁴⁰ Finally, we would like to stress that the resulting Helmholtz energies of mixing of the PIL-systems are negative, and are leading to the formation of thermodynamically stable mixtures. In addition to the purely theoretical considerations outlined above, we will demonstrate in a forthcoming paper that both experimental and simulated mixtures behave qualitatively similar with respect to the enthalpic and structural effects associated with HB redistribution.⁴¹ In conclusion, this particular mixture of PILs seems to be one prominent example with a negative mixing entropy, where the mixing process is driven by enthalpy, not entropy.

■ ASSOCIATED CONTENT

SI Supporting Information

The Supporting Information is available free of charge at <https://pubs.acs.org/doi/10.1021/acs.jpclett.2c00634>.

Outline of the MD simulations and the employed force field, the mixing energies and volumes, and a detailed description of a statistical mechanical model for hydrogen bond redistribution (PDF)

■ AUTHOR INFORMATION

Corresponding Author

Dietmar Paschek – *Physikalische und Theoretische Chemie, Institut für Chemie, Universität Rostock, D-18059 Rostock, Germany*; orcid.org/0000-0002-0342-324X; Email: dietmar.paschek@uni-rostock.de

Authors

Benjamin Golub – *Physikalische und Theoretische Chemie, Institut für Chemie, Universität Rostock, D-18059 Rostock, Germany*

Daniel Ondo – *Department of Physical Chemistry, University of Chemistry and Technology, 166 28 Prague 6, Czech Republic*

Ralf Ludwig – *Physikalische und Theoretische Chemie, Institut für Chemie, Universität Rostock, D-18059 Rostock, Germany; Leibniz-Institut für Katalyse, D-18059 Rostock, Germany*; orcid.org/0000-0002-8549-071X

Complete contact information is available at:

<https://pubs.acs.org/doi/10.1021/acs.jpclett.2c00634>

Notes

The authors declare no competing financial interest.

■ ACKNOWLEDGMENTS

We thank the Leibniz Association, the State of Mecklenburg-Vorpommern, and the University of Rostock for financial support within the ComBioCat programme. This work has been supported by a DFG Research Grant (No. 401427621). D.O. acknowledges the support from Grant No. A1_FCHI_2021_002 of Specific University Research by the Ministry of Education, Youth, and Sports (Czech Republic). The proof in section S5.4 of the Supporting Information has been contributed by A. Appenhagen.

■ REFERENCES

- (1) Belieres, J.; Angell, C. A. Protic Ionic Liquids: Preparation, Characterization, and Proton Free Energy Level Representation. *J. Phys. Chem. B* **2007**, *111*, 4926–4937.
- (2) Caparica, R.; Júlio, A.; Baby, A. R.; Araújo, E. U. A. M.; Fernandes, A. S.; Costa, J. G.; Santos de Almeida, T. Choline-Amino Acid Ionic Liquids as Green Functional Excipients to Enhance Drug Solubility. *Pharmaceutics* **2018**, *10*, 288.
- (3) Peric, B.; Sierra, S.; Martí, E.; Cruanas, R.; Garau, M. A.; Arning, J.; Bottin-Weber, U.; Stolte, S. (Eco)toxicity and biodegradability of selected protic and aprotic ionic liquids. *J. Hazard Mater.* **2013**, *261*, 99–105.
- (4) Every, H.; Bishop, A. G.; Forsyth, M.; MacFarlane, D. R. Ion Diffusion in Molten Salt Mixtures. *Electrochim. Acta* **2000**, *45*, 1279–1284.
- (5) Fletcher, K. A.; Baker, S. N.; Baker, G. A.; Pandey, S. Probing Solute and Solvent Interactions within Binary Ionic Liquid Mixtures. *New J. Chem.* **2003**, *27*, 1706–1712.
- (6) Canongia Lopes, J. N.; Cordeiro, T. C.; Esperanca, J. M. S. S.; Guedes, H. J. R.; Huq, S.; Rebelo, L. P. N.; Seddon, K. R. Deviations from Ideality in Mixtures of Two Ionic Liquids Containing a Common Ion. *J. Phys. Chem. B* **2005**, *109*, 3519–3525.
- (7) Navia, P.; Troncoso, J.; Romaní, L. Viscosities for Ionic Liquid Binary Mixtures with a Common Ion. *J. Solution Chem.* **2008**, *37*, 677–688.
- (8) Annat, G.; Forsyth, M.; MacFarlane, D. R. Ionic Liquid Mixtures - Variations in Physical Properties and Their Origins in Molecular Structure. *J. Phys. Chem. B* **2012**, *116*, 8251–8258.
- (9) Oliveira, M. B.; Domínguez-Pérez, M.; Cabeza, O.; Lopes da Silva, J. A.; Freire, M. G.; Coutinho, J. A. P. Surface Tensions of

Binary Mixtures of Ionic Liquids with Bis(trifluoromethylsulfonyl)-imide as the Common Anion. *J. Chem. Thermodynamics* **2013**, *64*, 22–27.

(10) Payal, R. S.; Balasubramanian, S. Homogenous Mixing of Ionic Liquids: Molecular Dynamics Simulations. *Phys. Chem. Chem. Phys.* **2013**, *15*, 21077–21083.

(11) Paschek, D.; Golub, B.; Ludwig, R. Hydrogen Bonding in a Mixture of Protic Ionic Liquids: A Molecular Dynamics Simulation Study. *Phys. Chem. Chem. Phys.* **2015**, *17*, 8431–8440.

(12) Fumino, K.; Bonsa, A.-M.; Golub, B.; Paschek, D.; Ludwig, R. Non-Ideal Mixing Behaviour of Hydrogen Bonding in Mixtures of Protic Ionic Liquids. *ChemPhysChem* **2015**, *16*, 299–304.

(13) Matthews, R. P.; Villar-Garcia, I. J.; Weber, C. C.; Griffith, J.; Cameron, F.; Hallett, J. P.; Hunt, P. A.; Welton, T. A Structural Investigation of Ionic Liquid Mixtures. *Phys. Chem. Chem. Phys.* **2016**, *18*, 8608–8624.

(14) Bruce, D. W.; Cabry, C. P.; Canongia Lopes, J. N.; Costen, M. L.; D'Andrea, L.; Grillo, I.; Marshall, B. C.; McKendrick, K. G.; Minton, T. K.; Purcell, S. M.; et al. Nanosegregation and Structuring in the Bulk and at the Surface of Ionic-Liquid Mixtures. *J. Phys. Chem. B* **2017**, *121*, 6002–6020.

(15) Vogl, T.; Passerini, S.; Balducci, A. The Impact of Mixtures of Protic Ionic Liquids on the Operative Temperature Range of Use of Battery Systems. *Electrochem. Commun.* **2017**, *78*, 47–50.

(16) Cabry, C. P.; D'Andrea, L.; Shimizu, K.; Grillo, I.; Li, P.; Rogers, S.; Bruce, D. W.; Canongia Lopes, J. N.; Slattery, J. M. Exploring the Bulk-Phase Structure of Ionic Liquid Mixtures using Small-Angle Neutron Scattering. *Faraday Discuss.* **2018**, *206*, 265–289.

(17) Thawarkar, S.; Khupse, N. D.; Kumar, A. Binary Mixtures of Aprotic and Protic Ionic Liquids Demonstrate Synergistic Polarity Effect: An Unusual Observation. *J. Sol. Chem.* **2020**, *49*, 210–221.

(18) Yambou, E. P.; Gorska, B.; Béguin, F. Binary Mixtures of Ionic Liquids Based on EMIm Cation and Fluorinated Anions: Physico-Chemical Characterization in View of Their Application as Low-Temperature Electrolytes. *J. Mol. Liq.* **2020**, *298*, 111959.

(19) Chakraborty, M.; Barik, S.; Mahapatra, A.; Sarkar, M. Binary mixtures of ionic liquids: Ideal, non-ideal, or quasi-ideal? *J. Chem. Phys.* **2021**, *154*, 224507.

(20) Niedermeyer, H.; Hallett, J. P.; Villar-Garcia, I. J.; Hunt, P. A.; Welton, T. Mixtures of Ionic Liquids. *Chem. Soc. Rev.* **2012**, *41*, 7780–7802.

(21) Podgorsek, A.; Pensado, A. S.; Santini, C. C.; Costa Gomes, M. F.; Pádua, A. A. H. Interaction Energies of Ionic Liquids with Metallic Nanoparticles: Solvation and Stabilization Effects. *J. Phys. Chem. C* **2013**, *117*, 3537–3547.

(22) Lepre, L. F.; Szala-Bilnik, J.; Padua, A. A. H.; Traikia, M.; Ando, R. A.; Costa Gomes, M. F. Tailoring the Properties of Acetate-Based Ionic Liquids Using The Tricyanomethanide Anion. *Phys. Chem. Chem. Phys.* **2016**, *18*, 23285–23295.

(23) Herrera, C.; Atilhan, M.; Aparicio, S. A Theoretical Study on Mixtures of Amino Acid-Based Ionic Liquids. *Phys. Chem. Chem. Phys.* **2018**, *20*, 10213–10223.

(24) Navia, P.; Troncoso, J.; Romani, L. Excess Magnitudes for Ionic Liquid Binary Mixtures with a Common Ion. *J. Chem. Eng. Data* **2007**, *52*, 1369–1374.

(25) Castejón, H. J.; Lashock, R. J. Mixtures of Ionic Liquids with Similar Molar Volumes Form Regular Solutions and Obey the Cross-Square Rules for Electrolyte Mixtures. *J. Mol. Liq.* **2012**, *167*, 1–4.

(26) Podgorsek, A.; Jacquemin, J.; Pádua, A. A. H.; Costa Gomes, M. F. Mixing Enthalpy for Binary Mixtures Containing Ionic Liquids. *Chem. Rev.* **2016**, *116*, 6075–6106.

(27) Otero, I.; Lepre, L. F.; Dequidt, A.; Husson, P.; Costa Gomes, M. F. How Does the Addition of a Third Ion Affect the Molecular Interactions and the Thermodynamic Properties to Acetate-Based Ionic Liquids? *J. Phys. Chem. B* **2017**, *121*, 9725–9736.

(28) Docampo-Álvarez, B.; Gómez-González, V.; Méndez-Morales, T.; Rodríguez, J. R.; Cabeza, O.; Turmine, M.; Gallego, L. J.; Varela, L. M. The Effect of Alkyl Chain Length on the Structure and

Thermodynamics of Protic-Aprotic Ionic Liquid Mixtures: A Molecular Dynamics Study. *Phys. Chem. Chem. Phys.* **2018**, *20*, 9938–9949.

(29) Lepre, L. F.; Costa Gomes, M. F.; Pádua, A. A. H.; Ando, R. A.; Ribeiro, M. C. C. On the Regular Behavior of a Binary Mixture of Ionic Liquids. *J. Phys. Chem. B* **2019**, *123*, 6579–6587.

(30) Chatel, G.; Pereira, F. F. B.; Debbeti, V.; Wang, H.; Rogers, R. D. Mixing Ionic Liquids - Simple Mixture or Double Salts? *Green Chem.* **2014**, *16*, 2051–2083.

(31) Caminiti, R.; Gontrani, L., Eds. *The Structure of Ionic Liquids*; Springer: 2014.

(32) Golub, B.; Fumino, K.; Stange, P.; Fossog, V.; Hempelmann, R.; Ondo, D.; Paschek, D.; Ludwig, R. Balance Between Contact and Solvent Separated Ion Pairs in Mixtures of the Protic Ionic Liquid [Et₃NH][MeSO₃] with Water Controlled by Water Content and Temperature. *J. Phys. Chem. B* **2021**, *125*, 4476–4488.

(33) Fumino, K.; Fossog, V.; Wittler, K.; Hempelmann, R.; Ludwig, R. Dissecting Anion-Cation Interaction Energies in Protic Ionic Liquids. *Angew. Chem., Int. Ed.* **2013**, *52*, 2368–2372.

(34) Bodo, E.; Bonomo, M.; Mariani, A. Assessing the Structure of Protic Ionic Liquids Based on Triethylammonium and Organic Acid Anions. *J. Phys. Chem. B* **2021**, *125*, 2781–2792.

(35) Hill, T. L. *An Introduction to Statistical Thermodynamics*; Dover: 1960.

(36) Qian, H.; Hopfield, J. J. Entropy-enthalpy compensation: Perturbation and relaxation in thermodynamic systems. *J. Chem. Phys.* **1996**, *105*, 9292–9298.

(37) Koga, K.; Bhimalapuram, B.; Widom, B. The hydrophobic effect. *Phys. Chem. Chem. Phys.* **2003**, *5*, 3085–3093.

(38) Dill, K. A.; MacCallum, J. A. The Protein-Folding Problem, 50 Years On. *Science* **2012**, *338*, 1042–1046.

(39) Lama, R. F.; Lu, B. Excess Thermodynamics Properties of Aqueous Alcohol Solutions. *J. Chem. Eng. Data* **1965**, *10*, 216–219.

(40) Havenith, M. Solvation Science: A New Interdisciplinary Field. *Angew. Chem., Int. Ed.* **2016**, *55*, 1218–1219.

(41) Golub, B.; Ondo, D.; Overbeck, V.; Ludwig, R.; Paschek, D. Hydrogen Bond Redistribution Effects in Mixtures of Protic Ionic Liquids Sharing the Same Cation: Nonideal Mixing with Large Negative Mixing Enthalpies. *ChemRxiv*; DOI: 10.26434/chemrxiv-2022-w2x2w.

Supporting Information:

Why Do Liquids Mix? The Mixing of Protic Ionic Liquids Sharing the Same Cation is Apparently Driven by Enthalpy, not Entropy

Benjamin Golub[†], Daniel Ondo[‡], Ralf Ludwig^{†,§}, Dietmar Paschek^{†,*}

[†] *Physikalische und Theoretische Chemie, Institut für Chemie, Universität Rostock, Albert-Einstein-Straße 27, D-18059 Rostock, Germany*

[‡] *Department of Physical Chemistry, University of Chemistry and Technology, Technická 5., 166 28 Prague 6, Czech Republic*

[§] *Leibniz-Institut für Katalyse, Albert-Einstein-Straße 29a, D-18059 Rostock, Germany*

*E-mail: dietmar.paschek@uni-rostock.de

Contents

S1 Outline of the MD Simulations	S2
S2 Forcefield	S2
S3 Results of the MD Simulations	S5
S4 Computed Energies and Volumes of Mixing	S10
S5 Detailed Description of a Statistical Mechanical Model for Hydrogen Bond Re-distribution	S13
S5.1 Model A	S14
S5.2 Model B	S17
S5.3 Van 't Hoff Analysis	S20
S5.3.1 The Relationship Between $\Delta\epsilon_{\text{HB}}/k_{\text{B}}$, $\Delta H'^{\circ}/R$, and $\Delta H^{\circ}/R$	S20
S5.3.2 The Relationship Between n_0/n_1 and $\Delta S'^{\circ}$	S21
S5.4 Limiting Behavior of the Function $a(x)$	S22
S6 Coordination Numbers, Pair Correlations and Hydrogen Bond Fractions of the Ions in the PIL Mixtures	S23
References	S25

S1 Outline of the MD Simulations

To study the pure PILs and mixtures, we performed isobaric isothermal (NPT) MD simulations using GROMACS 5.0.6.[1] We investigated eleven compositions between $x_{\text{OMs}} = 0.0$ and $x_{\text{OMs}} = 1.0$ for five temperatures between $T = 320$ K and $T = 400$ K at a pressure of 1 bar. All studied systems were composed of 500 ion pairs. Simulation boxes were constructed using PACKMOL [2] and equilibrated for 3 ns using the Berendsen-thermostat with a coupling constant of $\tau_T = 0.5$ ps as well as the Berendsen-barostat with a coupling constant of $\tau_p = 0.5$ ps.[3] For all mixtures production runs of 50 ns were carried out employing the Nosé-Hoover-thermostat [4, 5] ($\tau_T = 0.5$ ps) and the Rahman-Parrinello-barostat [6, 7] ($\tau_p = 2.0$ ps and $\chi_T = 33.0 \cdot 10^{-6} \text{ bar}^{-1}$) using a time-step of 2.0 fs. Bond lengths were kept fixed by employing the LINCS algorithm.[8] by using smooth particle mesh Ewald summation [9] (real space cutoff 0.9 nm, mesh spacing of 0.12 nm, 4th order interpolation and convergence factor 3.38 nm^{-1}). For analysing the simulations we used GROMACS [1] and MOSCITO [10] tools.

S2 Forcefield

The forcefield discussed here is taken from Ref. [11]. For the description of the potential model, a classical forcefield approach has been used, similar to the OPLS-model of Jorgensen et al.[12]. All employed partial charges are atom-centered and were determined from ab-initio calculations of the individual ions by applying many body perturbation theory (MP2) and using the 6-311++G** basis set. All reported ab initio calculations were performed with the Gaussian 09 program [13]. The charges were fitted to the electrostatic potential surrounded by the atoms using the ESP [14] and RESP [15] methods. Due to the rather small size of the ions no significant changes were found between the ESP and RESP charges. CH_3 - and CH_2 -groups treated as united atoms and represented by a single interaction site. Nonbonded Lennard-Jones Parameters for the Triflate-ions were taken from the [NTF₂] forcefield-model of Köddermann et al. [16], while the starting point for the nonbonded parameters for the Triethylammonium were parameters reported by Krienke et al. [17] for the ammonium group, in addition to the TraPPE-parameters of Martin and Siepmann [18] for the united-atom CH_3 - and CH_2 -groups. The σ -parameter for the nitrogen atom needed to be resized to 3.25 Å in order to match the H...O distance of the hydrogen bonded ion pair in the gas-phase with the distance obtained for the energy minimized structure using ab initio calculations. Constant pressure simulations of the model describes the density of Triethylammonium-Triflate quite satisfactorily. For the Methylsulfonate-ion, the Lennard-Jones parameters of Köddermann were also used for the SO_3 -group. The starting point for the Lennard-Jones parameters for the methyl-group was again the forcefield of Martin and Siepmann [18]. In this case, the Lennard-Jones σ of the methyl-group needed to be resized to match the density of the liquid phase of neat Triethylammonium-Methylsulfonate. Due to a significantly stronger bond-polarization of the S-O bond within the Methylsulfonate-ion, compared to the Triflate-ion, larger partial charges on the oxygens were obtained for the Methylsulfonate, leading to stronger hydrogen-bonding with the Triethylammonium ion. In order to represent molecular configurations of the ions properly, the equilibrium bond distances and angles were adjusted in such a way that they lead to minimum energy configurations close to the structures obtained from the ab initio calculations. All nonbonded Lennard-Jones parameters and partial charges are summarized in Table S1. The Bond-length and bond-bending parameters can be found in Tables S2 and S3. Dihedral potentials for intramolecular torsions around the N-C2-bond in the Triethylammonium ion and the S-C-bond in the Triflate ions were fitted to ab initio calculation to represent the molecular configurations accurately. The values are summarized in Table S4. The full torsion potential also include nonbonded 1-4-interactions. Here both, the nonbonded

Lennard-Jones and Coulomb 1-4-interactions are scaled by a factor of 0.5.

Table S1: Non-bonding Lennard-Jones interaction parameters with $V_{ij} = 4\epsilon_{ij} \left[(\sigma_{ij}/r_{ij})^{12} - (\sigma_{ij}/r_{ij})^6 \right]$ and partial charges used in the MD Simulations of the PIL-mixtures. Lorentz-Berthelot mixing-rules with $\sigma_{ij} = (\sigma_{ii} + \sigma_{jj})/2$ and $\epsilon_{ij} = (\epsilon_{ii} \cdot \epsilon_{jj})^{1/2}$ were applied for determining the cross-parameters.

Atom i	$\sigma_{ii}/\text{\AA}$	$\epsilon_{ii} \cdot k_B^{-1}/\text{K}$	$q_i/ e $
Triflate:			
S	4.08	37.3	-0.73
O	3.46	31.7	1.40
C	3.15	10.0	0.48
F	2.66	8.0	-0.23
Methylsulfonate:			
S	4.08	37.3	-0.825
O	3.46	31.7	1.620
C3	2.90	98.0	-0.145
Triethylammonium:			
H	0.0	0.0	0.37
N	3.25	75.0	-0.39
C2	3.95	46.0	0.28
C3	3.75	98.0	0.06

Table S2: Harmonic bond-stretching parameters employed in the forcefield model using $V_{ij}^b = (k_{ij}^b/2) \cdot (r_{ij} - r_{ij}^0)^2$.

Bond $i - j$	$r_{ij}^0 / \text{\AA}$	$k_{ij}^b / \text{kJ mol}^{-1} \text{\AA}^{-2}$
Triflate:		
C-F	1.347	3700.0
C-S	1.860	1850.0
O-S	1.469	5850.0
Methylsulfonate:		
C3-S	1.8040	1850.0
O-S	1.4816	5850.0
Triethylammonium:		
H-N	1.020	2500.0
C2-N	1.500	2500.0
C2-C3	1.540	2500.0

Table S3: Harmonic bond-bending parameters employed in the forcefield model using $V_{ijk}^a = (k_{ijk}^a/2) \cdot (\theta_{ijk} - \theta_{ijk}^0)^2$.

Angle $i - j - k$	θ_{ijk}^0 / degrees	k_{ijk}^a / kJ mol ⁻¹ rad ⁻²
Triflate:		
F-C-F	108.4	650.0
F-C-S	110.5	420.0
C-S-O	102.6	620.0
O-S-O	119.5	850.0
Methylsulfonate:		
C3-S-O	104.26	620.0
O-S-O	114.14	850.0
Triethylammonium:		
H-N-C2	108.4	460.0
C2-N-C2	108.4	460.0
C3-C2-N	108.4	460.0

Table S4: Dihedral-Potential for the rotation around the N-C2 bond in the Triethylammonium-ion and for the C-S bond in the Triflate-ion according to $V_{ijkl} = \sum_m k_m^d [1 + \cos(n_m \cdot \phi)]$.

$m(i - j - k - l)$	n_m	k_m^d / kJ mol ⁻¹
Triflate F-C-S-O:		
1	3.0	0.8619
Triethylammonium H-N-C2-C3:		
1	1.0	8.734
2	2.0	3.224
3	3.0	5.514
4	4.0	-0.465
5	5.0	-0.481
6	6.0	0.756

S3 Results of the MD Simulations

Report of the performed MD simulations of systems composed of 500 ion pairs at the indicated temperatures with composition x_{OMs} . E_p indicates the average potential energy of the systems computed from the MD trajectories over 50 ns. V_{box} , y_{OMs} , and y_{OTf} denote the average volume of the MD box, and fractions of hydrogen bonds of the [TEA] cations to the [OMs] and [OTf] anions, respectively.

Table S5: $x_{\text{OMs}} = 0.0$

T / K	$\rho / \text{kg m}^{-3}$	$V_{\text{box}} / \text{nm}^3$	$E_p / \text{kJ mol}^{-1}$	y_{OMs}	y_{OTf}
320	1229.1	169.7	1186	-	0.995
340	1213.4	171.9	3287	-	0.993
360	1198.0	174.1	5394	-	0.991
380	1183.3	176.3	7461	-	0.988
400	1168.2	178.6	9525	-	0.984

Table S6: $x_{\text{OMs}} = 0.1$

T / K	$\rho / \text{kg m}^{-3}$	$V_{\text{box}} / \text{nm}^3$	$E_p / \text{kJ mol}^{-1}$	y_{OMs}	y_{OTf}
320	1216.8	167.8	-18844	0.272	0.725
340	1201.2	169.9	-16772	0.274	0.721
360	1186.1	172.1	-14677	0.269	0.724
380	1171.6	174.2	-12603	0.261	0.729
400	1156.9	176.5	-10544	0.255	0.732

Table S7: $x_{\text{OMs}} = 0.2$

T / K	$\rho / \text{kg m}^{-3}$	$V_{\text{box}} / \text{nm}^3$	$E_p / \text{kJ mol}^{-1}$	y_{OMs}	y_{OTf}
320	1204.2	165.8	-38845	0.540	0.457
340	1189.4	167.9	-36729	0.525	0.471
360	1175.0	169.9	-34631	0.510	0.484
380	1160.3	172.1	-32537	0.497	0.496
400	1145.6	174.3	-30450	0.482	0.508

Table S8: $x_{\text{OMs}} = 0.3$

T / K	$\rho / \text{kg m}^{-3}$	$V_{\text{box}} / \text{nm}^3$	$E_{\text{p}} / \text{kJ mol}^{-1}$	y_{OMs}	y_{OTf}
320	1192.5	163.7	-38845	0.730	0.268
340	1177.3	165.8	-36729	0.717	0.280
360	1163.1	167.8	-34631	0.707	0.289
380	1148.5	169.9	-32537	0.683	0.312
400	1134.1	172.1	-30450	0.661	0.331

Table S9: $x_{\text{OMs}} = 0.4$

T / K	$\rho / \text{kg m}^{-3}$	$V_{\text{box}} / \text{nm}^3$	$E_{\text{p}} / \text{kJ mol}^{-1}$	y_{OMs}	y_{OTf}
320	1179.7	161.6	-77765	0.869	0.130
340	1165.1	163.7	-75594	0.839	0.158
360	1150.6	165.7	-73518	0.825	0.172
380	1136.9	167.7	-71487	0.806	0.188
400	1122.9	169.8	-69461	0.789	0.204

Table S10: $x_{\text{OMs}} = 0.5$

T / K	$\rho / \text{kg m}^{-3}$	$V_{\text{box}} / \text{nm}^3$	$E_{\text{p}} / \text{kJ mol}^{-1}$	y_{OMs}	y_{OTf}
320	1166.7	159.6	-96721	0.929	0.069
340	1153.2	161.5	-94669	0.918	0.080
360	1139.4	163.4	-92582	0.894	0.103
380	1124.9	165.5	-90565	0.884	0.112
400	1111.1	167.6	-88554	0.869	0.125

Table S11: $x_{\text{OMs}} = 0.6$

T / K	$\rho / \text{kg m}^{-3}$	$V_{\text{box}} / \text{nm}^3$	$E_{\text{p}} / \text{kJ mol}^{-1}$	y_{OMs}	y_{OTf}
320	1154.3	157.4	-115502	0.964	0.034
340	1139.7	159.5	-113423	0.950	0.047
360	1126.2	161.4	-111437	0.939	0.058
380	1112.8	163.3	-109500	0.933	0.063
400	1099.3	165.3	-107510	0.918	0.076

Table S12: $x_{\text{OMs}} = 0.7$

T / K	$\rho / \text{kg m}^{-3}$	$V_{\text{box}} / \text{nm}^3$	$E_{\text{p}} / \text{kJ mol}^{-1}$	y_{OMs}	y_{OTf}
320	1140.4	155.4	-134120	0.972	0.026
340	1126.2	157.4	-132153	0.970	0.028
360	1112.8	159.3	-130204	0.966	0.031
380	1099.8	161.2	-128272	0.956	0.039
400	1086.7	163.1	-126348	0.950	0.044

Table S13: $x_{\text{OMs}} = 0.8$

T / K	$\rho / \text{kg m}^{-3}$	$V_{\text{box}} / \text{nm}^3$	$E_{\text{p}} / \text{kJ mol}^{-1}$	y_{OMs}	y_{OTf}
320	1126.2	153.4	-152787	0.986	0.012
340	1112.5	155.3	-160857	0.983	0.014
360	1099.5	157.1	-148934	0.978	0.018
380	1086.6	159.0	-147031	0.975	0.020
400	1074.0	160.9	-145144	0.970	0.024

Table S14: $x_{\text{OMs}} = 0.9$

T / K	$\rho / \text{kg m}^{-3}$	$V_{\text{box}} / \text{nm}^3$	$E_{\text{p}} / \text{kJ mol}^{-1}$	y_{OMs}	y_{OTf}
320	1111.6	151.4	-171490	0.994	0.004
340	1098.2	153.2	-169514	0.992	0.005
360	1085.3	155.1	-167605	0.988	0.008
380	1073.0	156.8	-165740	0.987	0.008
400	1060.4	158.7	-163886	0.984	0.010

Table S15: $x_{\text{OMs}} = 1.0$

T / K	$\rho / \text{kg m}^{-3}$	$V_{\text{box}} / \text{nm}^3$	$E_{\text{p}} / \text{kJ mol}^{-1}$	y_{OMs}	y_{OTf}
320	1096.0	149.5	-190126	0.998	-
340	1083.4	151.2	-188176	0.997	-
360	1070.7	153.0	-186284	0.996	-
380	1058.7	154.7	-184451	0.995	-
400	1046.5	156.5	-182612	0.993	-

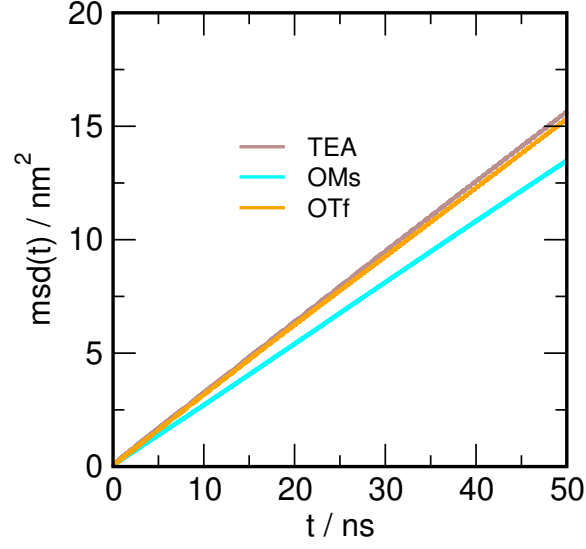


Figure S1: Mean square displacement of the center of mass of the ions in an equimolar mixture of [TEA][OMs] and [TEA][OTf] at $T = 400$ K.

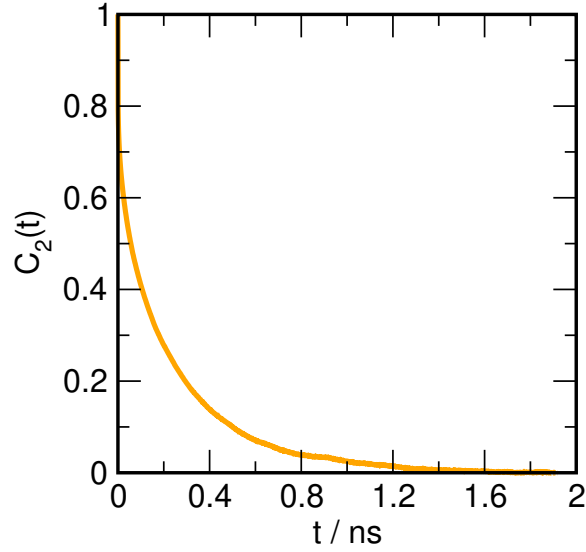


Figure S2: Computed reorientational correlation function $C_2(t) = \langle P_2[\vec{u}_{\text{NH}}(0) \cdot \vec{u}_{\text{NH}}(t)] \rangle$ of the N-H vector of the [TEA] cations in an equimolar mixture of [TEA][OMs] and [TEA][OTf] at $T = 400$ K. Here $P_2(\dots)$ denotes the 2nd Legendre polynome and $\vec{u}_{\text{NH}}(t)$ the time evolution of a unit vector describing the orientation of the N-H bond. The integrated correlation time $\tau_2 = \int_0^\infty C_2(t) dt$ is determined to be $\tau_2 = 171$ ps.

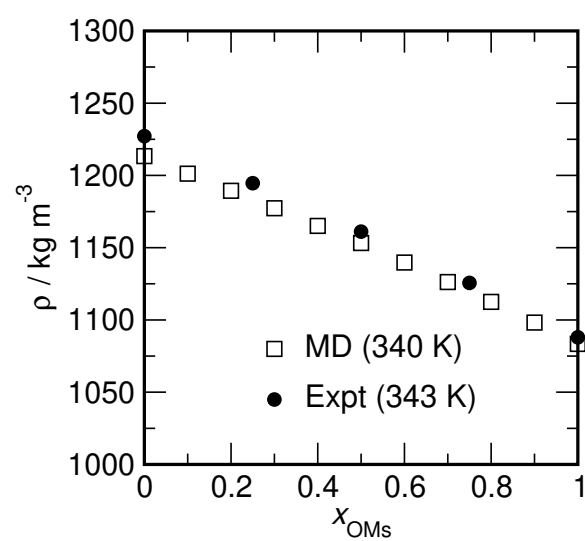


Figure S3: Densities of selected [TEA][OMs]/[TEA][OTf] mixtures as a function of their composition as obtained from the molecular dynamics simulations at 340 K. The filled circles refer to experimental densities obtained at 343 K [19].

S4 Computed Energies and Volumes of Mixing

From the MD simulations we can directly determine the energies of mixing ΔU_{mix} according to

$$\begin{aligned}\Delta U_{\text{mix}} &= U(x_{\text{OMs}}) - x_{\text{OMs}} \cdot U_{[\text{TEA}][\text{OMs}]} \\ &\quad - (1 - x_{\text{OMs}}) \cdot U_{[\text{TEA}][\text{OTf}]} \\ &= E_p(x_{\text{OMs}}) - x_{\text{OMs}} \cdot E_{p,[\text{TEA}][\text{OMs}]} \\ &\quad - (1 - x_{\text{OMs}}) \cdot E_{p,[\text{TEA}][\text{OTf}]} ,\end{aligned}\tag{1}$$

and

$$\begin{aligned}\Delta V_{\text{mix}} &= V(x_{\text{OMs}}) - x_{\text{OMs}} \cdot V_{[\text{TEA}][\text{OMs}]} \\ &\quad - (1 - x_{\text{OMs}}) \cdot V_{[\text{TEA}][\text{OTf}]} \end{aligned}\tag{2}$$

where $U(x_{\text{OMs}})$ and $V(x_{\text{OMs}})$ represents the total energy and volume of the mixture [TEA][OTf]/[TEA][OMs] with a given composition x_{OMs} , while $U_{[\text{TEA}][\text{OTf}]}$ and $U_{[\text{TEA}][\text{OMs}]}$ are the energies and $V_{[\text{TEA}][\text{OTf}]}$ and $V_{[\text{TEA}][\text{OMs}]}$ are the volumes of the pure PILs. The E_p -values represent the corresponding potential energies. All computed energies of mixing are summarised in Table S16. The volumes of mixing are given in Table S17.

Table S16: Energies of mixing ΔU_{mix} calculated from molecular dynamics simulation data given in Tables S5 to S15.

x_{OMs}	$\Delta U_{\text{mix}} / \text{kJ mol}^{-1}$				
	320 K	340 K	360 K	380 K	400 K
0.0	0.0	0.0	0.0	0.0	0.0
0.1	-1.80±0.23	-1.83±0.18	-1.81±0.17	-1.75±0.17	-1.71±0.16
0.2	-3.54±0.24	-3.45±0.24	-3.38±0.24	-3.23±0.15	-3.09±0.16
0.3	-4.46±0.23	-4.37±0.25	-4.45±0.19	-4.14±0.20	-3.93±0.20
0.4	-4.85±0.23	-4.59±0.24	-4.48±0.23	-4.37±0.19	-4.26±0.19
0.5	-4.50±0.21	-4.45±0.16	-4.27±0.20	-4.14±0.16	-4.02±0.18
0.6	-3.80±0.24	-3.66±0.18	-3.65±0.18	-3.63±0.20	-3.50±0.14
0.7	-2.78±0.22	-2.83±0.22	-2.85±0.18	-2.79±0.18	-2.75±0.14
0.8	-1.9±0.3	-1.95±0.23	-1.97±0.18	-1.92±0.16	-1.92±0.12
0.9	-0.99±0.25	-0.97±0.22	-0.98±0.21	-0.96±0.15	-0.97±0.13
1.0	0.0	0.0	0.0	0.0	0.0

Table S17: Volumes of mixing ΔV_{mix} calculated from molecular dynamics simulation data given in Tables S5 to S15.

x_{OMs}	$\Delta V_{\text{mix}} / \text{cm}^3 \text{mol}^{-1}$				
	320 K	340 K	360 K	380 K	400 K
0.0	0.000	0.000	0.000	0.000	0.000
0.1	0.063	0.103	0.105	0.101	0.086
0.2	0.145	0.097	0.023	0.099	0.127
0.3	0.021	0.096	0.016	0.124	0.144
0.4	0.029	0.039	0.065	0.077	0.064
0.5	0.002	-0.100	-0.155	0.026	0.039
0.6	-0.166	-0.040	-0.095	-0.053	-0.048
0.7	-0.140	-0.031	-0.074	-0.049	-0.044
0.8	-0.127	-0.061	-0.101	-0.053	-0.083
0.9	-0.111	-0.046	-0.066	-0.046	-0.040
1.0	0.000	0.000	0.000	0.000	0.000

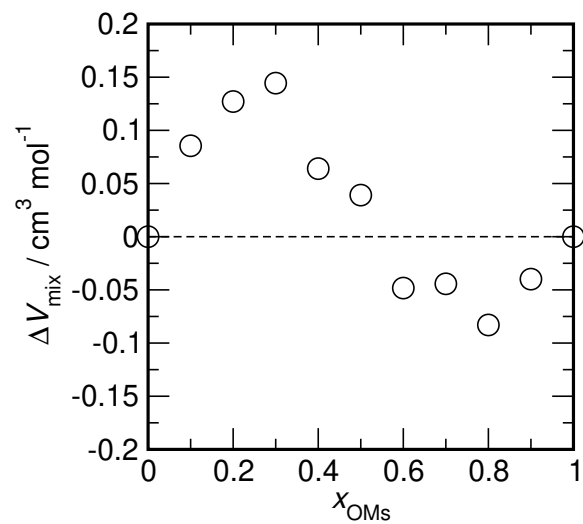


Figure S4: Volumes of mixing ΔV_{mix} for all mixtures as a function of their composition as obtained from the molecular dynamics simulations at 400 K.

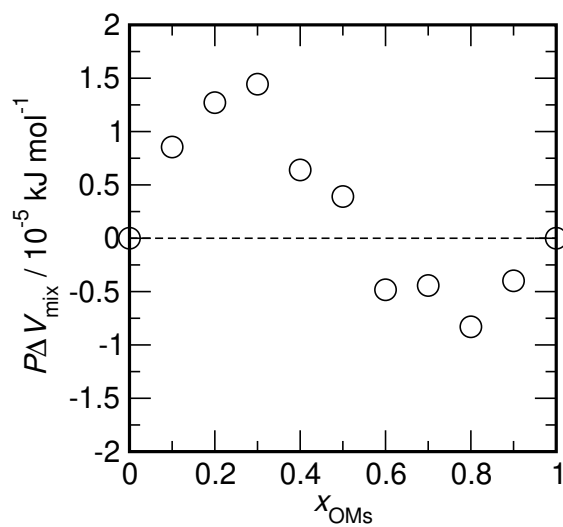


Figure S5: $P\Delta V_{\text{mix}}$ for all mixtures as a function of their composition as obtained from the molecular dynamics simulations at 400 K.

S5 Detailed Description of a Statistical Mechanical Model for Hydrogen Bond Redistribution

The statistical mechanical model for describing hydrogen bond redistribution is in its essence a two state model, which is introduced and discussed in detail in the remainder of this section.

We start with the definition of a statistical mechanical two-state model. Consider a canonical ensemble of N indistinguishable particles, where each particle can adopt two different energy states ϵ_0 and ϵ_1 . In addition, each of two energy states is n_γ -fold degenerated (with $\gamma \in \{0, 1\}$). The canonical partition function of such a system can be expressed as

$$Z = \frac{1}{N!} q^N \quad (3)$$

where q is the two-state “molecular” partition function according to

$$q = n_0 \cdot e^{-\beta\epsilon_0} + n_1 \cdot e^{-\beta\epsilon_1} \quad (4)$$

with $\beta = 1/(k_B T)$, where T is the temperature and k_B denotes the Boltzmann-constant. By introducing $\Delta\epsilon = \epsilon_0 - \epsilon_1$ and defining $\epsilon_1 = 0$, Equation 4 can be expressed as

$$q = n_0 \cdot e^{-\beta\Delta\epsilon} + n_1 . \quad (5)$$

From the molecular partition function outlined in Equation 5 follows immediately that the population y_γ of each state is given by

$$y_0 = n_0 \cdot e^{-\beta\Delta\epsilon} / q \quad (6)$$

and

$$y_1 = n_1 / q . \quad (7)$$

In the following paragraph we will derive the thermodynamic properties discussed in this paper starting from the partition function using standard textbook definitions, as e.g. found in the classic textbook of Hill [20]. Having defined the partition function, the free Helmholtz free energy A follows as

$$A = -k_B T \ln Z \quad (8)$$

$$= -N k_B T \ln q + N k_B T [\ln(N) - 1] \quad (9)$$

employing Stirling’s approximation with $\ln(N!) \approx N \ln(N) - N$. The internal energy U is defined as

$$U = - \left(\frac{\partial \ln Z}{\partial \beta} \right) = -N \left(\frac{\partial \ln q}{\partial \beta} \right) \quad (10)$$

$$= N \Delta\epsilon \cdot n_0 \cdot e^{-\beta\Delta\epsilon} / q \quad (11)$$

$$= N \Delta\epsilon \cdot y_0 . \quad (12)$$

Finally, the entropy is given as

$$S = U/T - A/T \quad (13)$$

$$= N k_B \left(\frac{\Delta\epsilon}{k_B T} \right) \cdot y_0 + N k_B \ln q - N k_B [\ln(N) - 1] . \quad (14)$$

S5.1 Model A

First, we have to realize that the quantities n_0 and n_1 essentially define the amount of phase-space allocated to each of the states. Consequently, n_0 and n_1 do not necessarily have to be integer numbers. Let us assume that the states ‘0’ and ‘1’ are composed out of m_0 and m_1 ‘substates’. We are now acknowledging that the amount of phase-space allocated to each of the substates m_0 and m_1 can differ, such that

$$n_0 = m_0 \quad (15)$$

and

$$n_1 = a \cdot m_1 . \quad (16)$$

Here $a > 1$ increases the phase-space of each substate of ‘1’ with respect to ‘0’, whereas $a < 1$ decreases its phase-space. By changing a we have now control over the entropy contribution of each of the states.

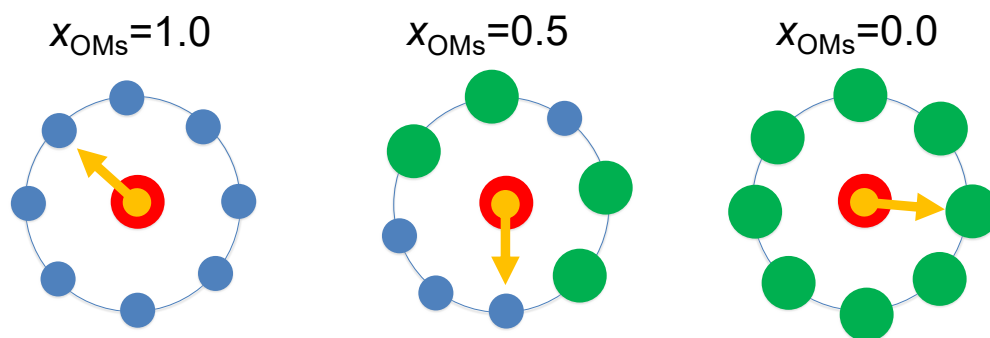


Figure S6: Illustration of the statistical mechanical ‘Model A’: The orange arrow is representing a HB donor located on a [TEA] cation, shown in red, which is able to connect with c surrounding HB acceptor sites, representing [OMs] (blue) and [OTf] (green) anions, respectively. The different area of the circles indicate the different size of the phase-space associated with each HB interaction. Hence the area is also indicative of the entropy of the two different HB interactions. In fact, the ratio of the area of the green and blue circles defines the parameter a , introduced in Equation 16. The sites in the solvation shell of the central [TEA] cation are statistically occupied by the two anion species according to their mixture composition x_{OMs} .

Let us assume that the total number (sub)states is a constant $c = m_0 + m_1$ and that we can control the number of each of the states m_0 and m_1 by some continuous parameter $x \in [0, 1]$ such that

$$n_0 = c \cdot x \quad (17)$$

and

$$n_1 = a \cdot c \cdot (1 - x) . \quad (18)$$

Imagine now that our model describes a hydrogen bond (HB) donor as outlined in Figure S6. Here the HB donor can access c HB acceptor sites in its local environment. Keep in mind that we have two different HB interaction strengths (i.e interaction energies). It is obvious that the parameter x in our model can be identified with describing the mixture composition of the two hydrogen bond acceptor sites. If we identify state ‘0’ with HBs to OMs ions and state ‘1’ with HBs to OTf ions, the parameter x

is essentially the mixture composition (mole fraction) with $x = x_{\text{OMs}}$ assuming a statistical occupation of the neighboring HB acceptor sites by the different anion species. According to Equation 6, the fraction of HBs to OM_s ions can be expressed by

$$y_0(x) = \frac{x \cdot e^{-\beta\Delta\epsilon}}{x \cdot e^{-\beta\Delta\epsilon} + a(1-x)} . \quad (19)$$

Let us now compute the excess thermodynamic properties of the model starting with the Helmholtz free energy

$$A_E = A(x) - x \cdot A_{x=1} - (1-x) \cdot A_{x=0} \quad (20)$$

$$= -Nk_B T \ln q(x) + x \cdot Nk_B T \ln q_{x=1} + (1-x) \cdot Nk_B T \ln q_{x=0} . \quad (21)$$

Note that the contributions due to the $\ln(N!)$ terms cancel out each other exactly. Since

$$q(x) = c \cdot x \cdot e^{-\beta\Delta\epsilon} + a \cdot c \cdot (1-x) \quad (22)$$

with

$$q_{x=0} = a \cdot c \quad (23)$$

and

$$q_{x=1} = c \cdot e^{-\beta\Delta\epsilon} \quad (24)$$

the excess Helmholtz free energy is given by:

$$A_E = -Nk_B T \ln \left[x e^{-\beta\Delta\epsilon} + a(1-x) \right] - x N \Delta\epsilon + (1-x) N k_B T \ln a . \quad (25)$$

Note that the contributions from the $\ln c$ terms cancel out each other as well. Next, let us derive the excess energy:

$$U_E = U(x) - x \cdot U_{x=1} - (1-x) \cdot U_{x=0} \quad (26)$$

$$= N \Delta\epsilon \frac{x \cdot e^{-\beta\Delta\epsilon}}{x \cdot e^{-\beta\Delta\epsilon} + a(1-x)} - x \cdot N \Delta\epsilon \quad (27)$$

$$= N \Delta\epsilon y_0(x) - x \cdot N \Delta\epsilon \quad (28)$$

$$= N \Delta\epsilon \cdot [y_0(x) - x] , \quad (29)$$

taking into account that $y_{0,x=1} = 1$ and $y_{0,x=0} = 0$. Finally, the excess entropy is available via

$$S_E = S(x) - x \cdot S_{x=1} - (1-x) \cdot S_{x=0} \quad (30)$$

$$= U_E/T - A_E/T \quad (31)$$

$$= Nk_B \cdot y_0(x) \cdot \frac{\Delta\epsilon}{k_B T} + Nk_B \ln \left[x e^{-\beta\Delta\epsilon} + a(1-x) \right] - (1-x) N k_B \ln a . \quad (32)$$

The thermodynamic mixing properties are defined as

$$\Delta U_{\text{mix}} = U_E , \quad (33)$$

$$\Delta A_{\text{mix}} = A_E + \Delta A_{\text{mix,id}} , \quad (34)$$

and

$$\Delta S_{\text{mix}} = S_E + \Delta S_{\text{mix,id}} , \quad (35)$$

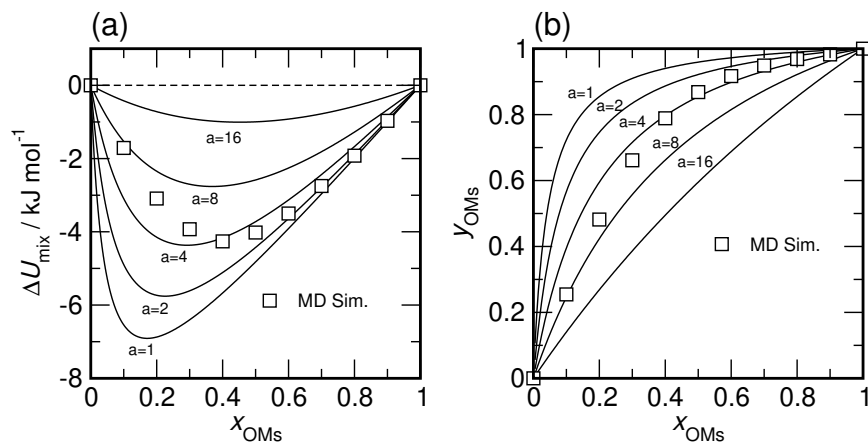


Figure S7: Theoretical predictions of the thermodynamic mixing properties for mixtures at $T = 400$ K using $\Delta\epsilon_{\text{HB}} = -10.5 \text{ kJ mol}^{-1}$ for varying a . a) Open squares indicate the energies of mixing as function of x_{OMs} obtained from MD simulations. The solid lines represent the data for ΔU_{mix} according to Equation 29 for the indicated values of a . b) Shown is the fraction y_{OMs} of [TEA] cations involved in a HB with [OMs] anions. Open circles represent data obtained from MD simulations. The solid line represents data according to Equation 19 for the indicated values of a .

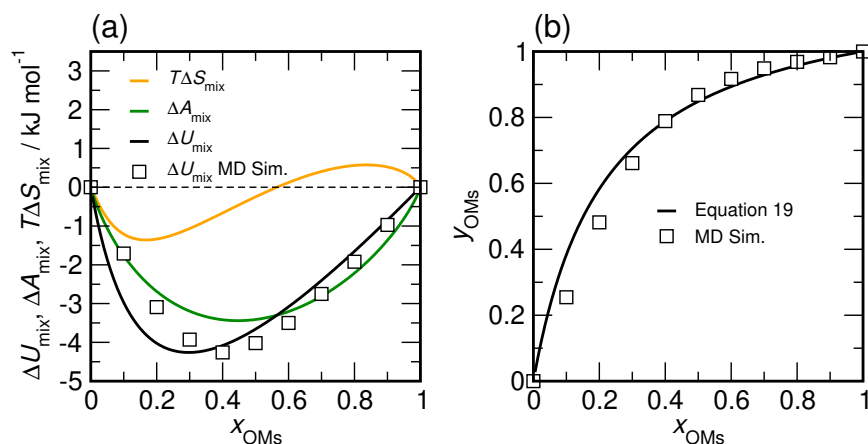


Figure S8: Theoretical predictions of the thermodynamic mixing properties for mixtures at $T = 400$ K using $\Delta\epsilon_{\text{HB}} = -10.5 \text{ kJ mol}^{-1}$ and $a = 4.2$. a) Open squares indicate the energies of mixing as function of x_{OMs} obtained from MD simulations. The heavy solid lines represent the ΔA_{mix} , ΔU_{mix} and $T\Delta S_{\text{mix}}$, respectively. b) Shown is the fraction y_{OMs} of [TEA] cations involved in a HB with [OMs] anions. Open circles represent data obtained from MD simulations. The heavy solid line represents data according to Equation 19.

with

$$\Delta A_{\text{mix,id.}} = Nk_{\text{B}}T [x \ln(x) + (1 - x) \ln(1 - x)] \quad (36)$$

and

$$\Delta S_{\text{mix,id.}} = -Nk_{\text{B}} [x \ln(x) + (1 - x) \ln(1 - x)] . \quad (37)$$

Here the ideal mixing contribution arise from the statistical distribution of both anion species in the mixture.

Figure S7 shows the behavior of the mixing energy ΔU_{mix} and fraction y_{OMs} of [TEA] cations involved in a HB with [OMs] anions as a function of the parameter a and the mixture composition x_{OMs} in comparison with data obtained from MD simulation. Note that for $a \approx 4$ both datasets are described semiquantitatively by the model. Figure S8 shows the computed composition dependence of ΔA_{mix} , ΔU_{mix} , $T\Delta S_{\text{mix}}$, and y_{OMs} for a value of $a = 4.2$. Most prominently, “Model A” predicts a negative mixing entropy for $x \leq 0.56$.

S5.2 Model B

In the paper we have used the following definition of the partition function, which we will call “Model B”. Here we use definitions for n_0 and n_1 according to

$$n_0 = c \cdot x^\alpha \quad (38)$$

and

$$n_1 = c \cdot (1 - x^\alpha) . \quad (39)$$

In essence, this approach also results in different phase-space contributions associated with the two-states, not unlike in “Model A”. However, unlike in “Model A”, the sizes of the phase-space volumes of the two species are not fixed, but vary as a function of the mixture composition. To illustrate the relationship between the parameter a used in “Model A” and the parameter α of “Model B”, we consider the ratio n_1/n_0 . For Model A, we have

$$\frac{n_1}{n_0} = a \frac{(1 - x)}{x} . \quad (40)$$

For Model B the ratio is given by

$$\frac{n_1}{n_0} = \frac{(1 - x^\alpha)}{x^\alpha} . \quad (41)$$

By equating Equations 40 and 41, we can compute the size of a hypothetical parameter a for Model B as a function of the mixture composition x according to

$$a(x) = \frac{(1 - x^\alpha)}{x^\alpha} \cdot \frac{x}{(1 - x)} . \quad (42)$$

The x -dependence of $a(x)$ for $\alpha = 2$ is shown in Figure S9. For $\lim_{x \rightarrow 1} a(x) = \alpha$, the function approaches a constant value of α and for $\lim_{x \rightarrow 0} a(x) = x^{1-\alpha}$ (for further information see section S5.4).

An argument can actually be made why the particular shape of the function $a(x)$, shown in Figure S9, suits our MD simulation data so well. Let us consider a mixture of [TEA][OMs] and [TEA][OTf] with a low [OMs] content. Let us now zoom in on a solvation shell, where a [TEA] cation is engaged in a HB with one of the relatively few available [OMs] anions. Ideally, neighboring [TEA] cations in one

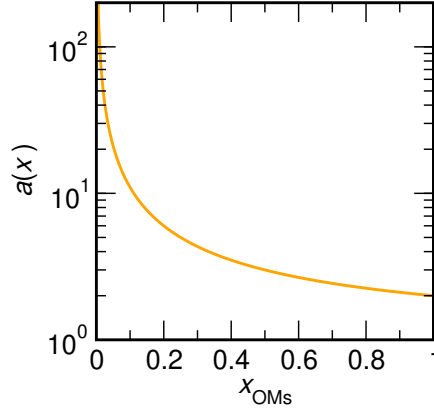


Figure S9: Illustration of the composition dependence of $a(x)$ of “Model B” according to Equation 42 for $\alpha = 2$.

or two of the adjacent solvation shells should be able to connect to that particular [OMs] anion equally well. However, since the HB acceptor sites are located in the SO_3 group of the [OMs] anion, they are concentrated one side of the ion. Therefore the [TEA] cations in the immediate neighborhood of the central cation will find it a little harder to engage in a HB. In essence, the HB of the central [TEA] to a [OMs] anion yields in a scarcity of available HB accepting sites in its immediate surrounding, and, is therefore steering the equilibrium of those adjacent [TEA] ions towards the [OTf] anions. On average, this leads to an overall reduced availability of [OMs] acceptor sites, which corresponds to an increasing parameter $a(x)$ for $x \rightarrow 0$.

According to Equation 6, the fraction of HBs to OMs ions can be expressed by

$$y_0(x) = \frac{x^\alpha \cdot e^{-\beta\Delta\epsilon}}{x^\alpha \cdot e^{-\beta\Delta\epsilon} + (1 - x^\alpha)} . \quad (43)$$

Let us now compute the excess thermodynamic properties of the model starting with the Helmholtz free energy

$$A_E = A(x) - x \cdot A_{x=1} - (1 - x) \cdot A_{x=0} \quad (44)$$

$$= -Nk_B T \ln q(x) + x \cdot Nk_B T \ln q_{x=1} + (1 - x) \cdot Nk_B T \ln q_{x=0} . \quad (45)$$

Note that the contributions due to the $\ln(N!)$ terms cancel out each other exactly. Since

$$q(x) = c \cdot x^\alpha \cdot e^{-\beta\Delta\epsilon} + c \cdot (1 - x^\alpha) \quad (46)$$

with

$$q_{x=0} = c \quad (47)$$

and

$$q_{x=1} = c \cdot e^{-\beta\Delta\epsilon} \quad (48)$$

the excess Helmholtz free energy is given by:

$$A_E = -Nk_B T \ln \left[x^\alpha e^{-\beta\Delta\epsilon} + (1 - x^\alpha) \right] - xN\Delta\epsilon . \quad (49)$$

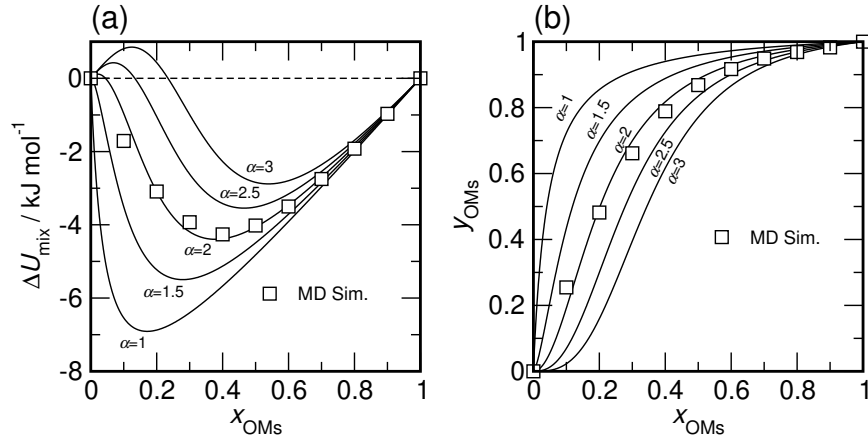


Figure S10: Theoretical predictions of the thermodynamic mixing properties for mixtures at $T = 400$ K using $\Delta\epsilon_{\text{HB}} = -10.5 \text{ kJ mol}^{-1}$ for varying α . a) Open squares indicate the energies of mixing as function of x_{OMs} obtained from MD simulations. The solid lines represent the data for ΔU_{mix} according to Equation 53 for the indicated values of α . b) Shown is the fraction y_{OMs} of [TEA] cations involved in a HB with [OMs] anions. Open circles represent data obtained from MD simulations. The solid line represents data according to Equation 43 for the indicated values of α .

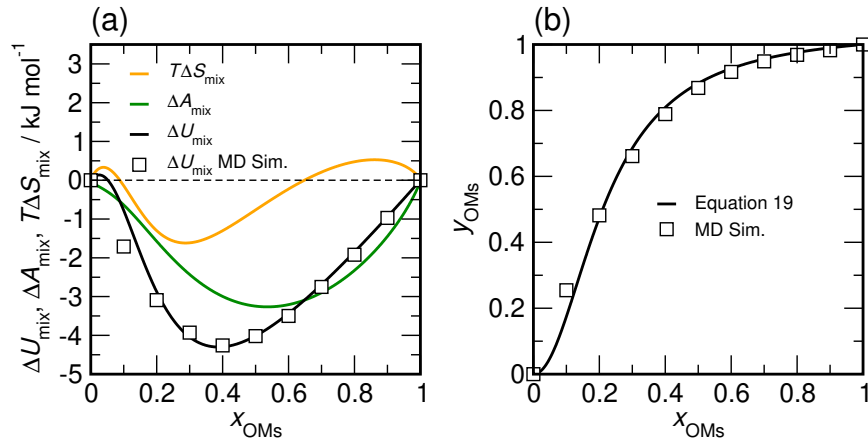


Figure S11: Theoretical predictions of the thermodynamic mixing properties for mixtures at $T = 400$ K using $\Delta\epsilon_{\text{HB}} = -10.5 \text{ kJ mol}^{-1}$ and $\alpha = 2.05$. a) Open squares indicate the energies of mixing as function of x_{OMs} obtained from MD simulations. The heavy solid lines represent the ΔA_{mix} , ΔU_{mix} and $T\Delta S_{\text{mix}}$, respectively. b) Shown is the fraction y_{OMs} of [TEA] cations involved in a HB with [OMs] anions. Open circles represent data obtained from MD simulations. The heavy solid line represents data according to Equation 43.

Note that the contributions from the $\ln c$ terms cancel out each other again. Next, let us derive the excess energy:

$$U_E = U(x) - x \cdot U_{x=1} - (1-x) \cdot U_{x=0} \quad (50)$$

$$= N\Delta\epsilon \frac{x^\alpha \cdot e^{-\beta\Delta\epsilon}}{x^\alpha \cdot e^{-\beta\Delta\epsilon} + (1-x^\alpha)} - x \cdot N\Delta\epsilon \quad (51)$$

$$= N\Delta\epsilon y_0(x) - x \cdot N\Delta\epsilon \quad (52)$$

$$= N\Delta\epsilon \cdot [y_0(x) - x] , \quad (53)$$

taking into account that $y_{0,x=1} = 1$ and $y_{0,x=0} = 0$. Finally, the excess entropy is available via

$$S_E = S(x) - x \cdot S_{x=1} - (1-x) \cdot S_{x=0} \quad (54)$$

$$= U_E/T - A_E/T \quad (55)$$

$$= Nk_B \cdot y_0(x) \cdot \frac{\Delta\epsilon}{k_B T} + Nk_B \ln [x^\alpha e^{-\beta\Delta\epsilon} + (1-x^\alpha)] . \quad (56)$$

Figure S10 shows the behavior of the mixing energy ΔU_{mix} and fraction y_{OMs} of [TEA] cations involved in a HB with [OMs] anions as a function of the parameter α and the mixture composition x in comparison with data obtained from MD simulation. Note that for $\alpha \approx 2$ both datasets are described almost quantitatively. Figure S11 shows the computed composition dependence of ΔA_{mix} , ΔU_{mix} , $T\Delta S_{\text{mix}}$, and y_{OMs} for a value of $\alpha = 2.05$. In addition to “Model A”, also “Model B” predicts a negative mixing entropy, albeit for $0.1 \leq x \leq 0.65$.

We would like to point out the qualitative similarity of the behavior of “Model A” shown in Figure S8 and “Model B” shown in Figure S11 with respect to the composition dependence of the entropy and the free energy of mixing.

S5.3 Van ’t Hoff Analysis

S5.3.1 The Relationship Between $\Delta\epsilon_{\text{HB}}/k_B$, $\Delta H'^{\circ}/R$, and $\Delta H^{\circ}/R$

We start with the van ’t Hoff equation, relating the temperature dependence of the equilibrium constant with the standard molar enthalpy difference.

$$-\frac{\Delta H^{\circ}}{R} = \frac{\partial \ln(K_{\text{eq}})}{\partial (1/T)} . \quad (57)$$

The equilibrium constant K_{eq} for a “chemical” HB exchange reaction describing the breaking of a [TEA]-[OTf] HB and formation of a [TEA]-[OMs] HB according to



is given as

$$K_{\text{eq}} = \frac{y_{\text{OMs}} \cdot (3x_{\text{OTf}} - y_{\text{OTf}})}{y_{\text{OTf}} \cdot (3x_{\text{OMs}} - y_{\text{OMs}})} . \quad (59)$$

Note that each anion has 3 HB accepting sites. Here we identify $x = x_{\text{OMs}}$, $(1-x) = x_{\text{OTf}}$, $y = y_{\text{OMs}}$, and $(1-y) = y_{\text{OTf}}$, since the condition $y_{\text{OTf}} + y_{\text{OMs}} \approx 1$ is well fulfilled. Hence we can express the equilibrium constant as

$$K_{\text{eq}} = \frac{y \cdot [3(1-x) - (1-y)]}{(1-y) \cdot (3x - y)} . \quad (60)$$

Accordingly, we can write

$$\ln K_{\text{eq}} = \ln \frac{y}{1-y} + \ln \frac{3(1-x) - (1-y)}{3x-y} . \quad (61)$$

Now, we associate the argument of the first logarithmic term in Equation 61 with another equilibrium constant

$$K' = \frac{y}{1-y} = \frac{y_{\text{OMs}}}{y_{\text{OTf}}} , \quad (62)$$

which is associated with a slightly different standard molar enthalpy difference according to

$$-\frac{\Delta H'^{\circ}}{R} = \frac{\partial \ln(K')}{\partial (1/T)} . \quad (63)$$

Substituting the inverse temperature by $\beta = (k_{\text{B}}T)^{-1}$ leads to

$$\frac{\partial}{\partial (1/T)} = k_{\text{B}}^{-1} \frac{\partial}{\partial \beta} . \quad (64)$$

Using the definitions of y and $(1-y)$ from Equations 6 and 7, we obtain

$$k_{\text{B}}^{-1} \frac{\partial}{\partial \beta} \ln \frac{y}{1-y} = k_{\text{B}}^{-1} \frac{\partial}{\partial \beta} \ln \frac{n_0 \cdot e^{-\beta \Delta \epsilon}}{n_1} \quad (65)$$

$$= k_{\text{B}}^{-1} (-\Delta \epsilon) . \quad (66)$$

Hence, we can conclude that if we use the equilibrium constant K' defined by Equation 62, the corresponding van 't Hoff equation essentially delivers us the difference in HB interactions used in our statistical mechanical models:

$$\frac{\Delta H'^{\circ}}{R} = \frac{\Delta \epsilon}{k_{\text{B}}} = \frac{\Delta \epsilon_{\text{HB}}}{k_{\text{B}}} . \quad (67)$$

S5.3.2 The Relationship Between n_0/n_1 and $\Delta S'^{\circ}$

Associated with the equilibrium constant K' defined in Equation 62 is the following standard molar Gibbs free energy difference with

$$\Delta G'^{\circ} = -RT \ln K' = -RT \ln \frac{y}{(1-y)} . \quad (68)$$

Using the definitions of y and $(1-y)$ from Equations 6 and 7, we obtain

$$\Delta G'^{\circ} = -RT \ln \frac{n_0 \cdot e^{-\beta \Delta \epsilon}}{n_1} \quad (69)$$

$$= -RT \ln \left(\frac{n_0}{n_1} \right) + N_{\text{A}} \Delta \epsilon \quad (70)$$

with N_{A} denoting the Avogadro constant. Recognizing from Equation 67 that $\Delta H'^{\circ} = N_{\text{A}} \Delta \epsilon$, it follows from Equation 70 and the thermodynamic definition of the Gibbs free energy with

$$\Delta G'^{\circ} = \Delta H'^{\circ} - T \Delta S'^{\circ} \quad (71)$$

that the related standard molar entropy difference is given by

$$\Delta S'^{\circ} = R \ln \left(\frac{n_0}{n_1} \right) . \quad (72)$$

From Equation 72 follows for “Model A”:

$$\Delta S'^{\circ} = R \ln \left(\frac{1}{a} \cdot \frac{x}{1-x} \right) , \quad (73)$$

and for “Model B”

$$\Delta S'^{\circ} = R \ln \left(\frac{x^{\alpha}}{1-x^{\alpha}} \right) . \quad (74)$$

S5.4 Limiting Behavior of the Function $a(x)$

The function $a(x)$ introduced in Equation 42 can be expressed as

$$a(x) = \frac{x^{\alpha} - 1}{x - 1} \cdot \frac{x}{x^{\alpha}} = \frac{x^{\alpha} - 1}{x - 1} \cdot \frac{1}{x^{\alpha-1}} . \quad (75)$$

From Equation 75 follows directly that

$$\lim_{x \rightarrow 0} a(x) = 1 \cdot \frac{1}{x^{\alpha-1}} = x^{1-\alpha} . \quad (76)$$

To show that $\lim_{x \rightarrow 1} a(x) = \alpha$ as discussed in section S5.2, we introduce the variable $z = x - 1$ such that

$$a(z) = \frac{(1+z)^{\alpha} - 1}{z} \cdot \frac{1}{(1+z)^{\alpha-1}} . \quad (77)$$

We perform a Taylor-expansion of the function $(1+z)^{\alpha}$ around $z = 0$ via

$$(1+z)^{\alpha} = \sum_{i=0}^{\infty} \frac{1}{i!} \left(\frac{d^i}{dz^i} (1+z)^{\alpha} \right)_{z=0} \times z^i \quad (78)$$

$$= 1 + \alpha z + \frac{1}{2} \alpha(\alpha-1)z^2 + \frac{1}{6} \alpha(\alpha-1)(\alpha-2)z^3 + \dots \quad (79)$$

For $z \ll 1$, we arrive at $(1+z)^{\alpha} \approx 1 + \alpha z$. Hence

$$\lim_{x \rightarrow 1} a(x) = \lim_{z \rightarrow 0} a(z) \quad (80)$$

$$= \lim_{z \rightarrow 0} \frac{(1+z)^{\alpha} - 1}{z} \cdot \frac{1}{(1+z)^{\alpha-1}} \quad (81)$$

$$= \lim_{z \rightarrow 0} \frac{(1+z)^{\alpha} - 1}{z} \cdot 1 \quad (82)$$

$$\approx \lim_{z \rightarrow 0} \frac{1 + \alpha z - 1}{z} \quad (83)$$

$$= \alpha \quad (84)$$

S6 Coordination Numbers, Pair Correlations and Hydrogen Bond Fractions of the Ions in the PIL Mixtures

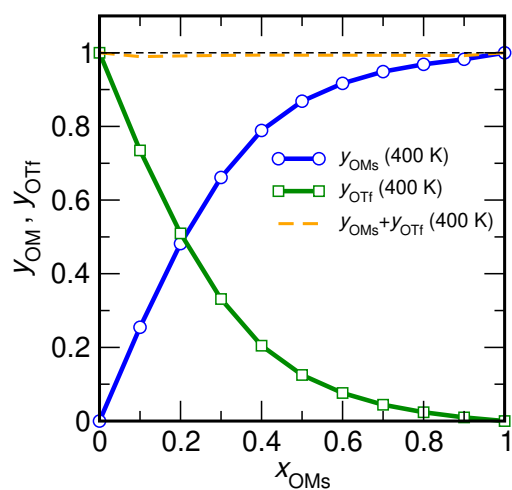


Figure S12: Fraction of [TEA] cations involved in a HB y_{α} with $\alpha = \text{OTf}$, or $\alpha = \text{OMs}$ as function of the mole fraction x_{OMs} for $T = 400 \text{ K}$. The lines are guides for the eye. The orange heavy dashed line indicates the sum of the respective fractions, while the black dashed line indicates 1.

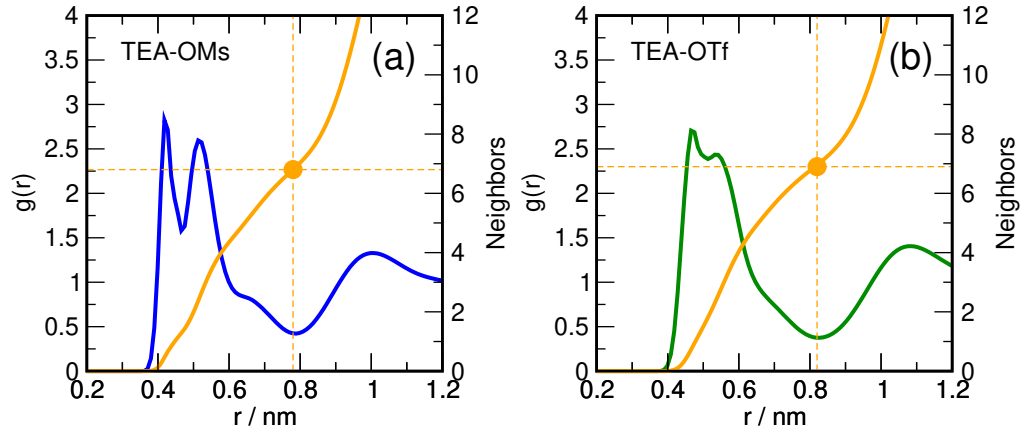


Figure S13: Anion-cation center of mass pair distribution functions $g(r)$ obtained for a) pure [TEA][OMs] and b) pure [TEA][OTf] at $T = 300$ K. The position of minimum is used as a cut-off radius for the nearest neighbor computation (TEA-OMs: 0.78 nm, TEA-OTf: 0.81 nm). The data are taken from Ref. [11].

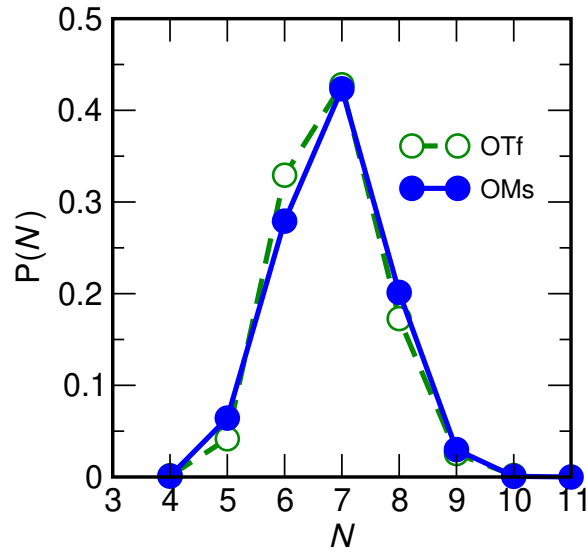


Figure S14: Distribution of the number N of TEA-cations in the first solvation shell of the OTf- and OMs-anions at $T = 300$ K determined from pure ionic liquids. The data is taken from Ref. [11].

References

- (1) Abraham, M. J.; van der Spoel, D.; Lindahl, E.; Hess, B.; the GROMACS development team GROMACS User Manual version 5.0.6, 2015.
- (2) Martinez, L.; Andrade, R.; Birgin, E. G.; Martinez, J. M. *J. Comput. Chem.* **2009**, *30*, 2157–2164.
- (3) Berendsen, H. J. C.; Postma, J. P. M.; van Gunsteren, W. F.; DiNola, A.; Haak, J. R. *J. Chem. Phys.* **1984**, *81*, 3684–3690.
- (4) Nosé, S. *Mol. Phys.* **1984**, *52*, 255–268.
- (5) Hoover, W. G. *Phys. Rev. A* **1985**, *31*, 1695–1697.
- (6) Parrinello, M.; Rahman, A. *J. Appl. Phys.* **1981**, *52*, 7182–7190.
- (7) Nosé, S.; Klein, M. L. *Mol. Phys.* **1983**, *50*, 1055–1076.
- (8) Hess, B.; Bekker, H.; Berendsen, H. J. C.; Fraaije, J. G. E. M. *J. Comp. Chem.* **1997**, *18*, 1463–1472.
- (9) Essmann, U.; Perera, L.; Berkowitz, M. L.; Darden, T. A.; Lee, H.; Pedersen, L. G. *J. Chem. Phys.* **1995**, *103*, 8577–8593.
- (10) Paschek, D.; Geiger, A. MOSCITO (Version 4.180), <http://www.moscitomd.org>, 2012.
- (11) Paschek, D.; Golub, B.; Ludwig, R. *Phys. Chem. Chem. Phys.* **2015**, *17*, 8431–8440.
- (12) Jorgensen, W. L.; Ibrahim, M. *J. Am. Chem. Soc.* **1981**, *103*, 3976–3985.
- (13) Frisch, M. J. et al. Gaussian 09 Revision D.01, Gaussian Inc. Wallingford CT 2009.
- (14) U.C.Singh; Kollman, P. *J. Comput. Chem.* **1984**, *5*, 129–145.
- (15) Bayly, C. I.; Cieplak, P.; Cornell, W. D.; Kollman, P. A. *J. Phys. Chem.* **1993**, *97*, 10269–10280.
- (16) Ködderman, T.; Paschek, D.; Ludwig, R. *ChemPhysChem* **2007**, *8*, 2464–2470.
- (17) Krienke, H.; Vlachy, V.; Ahn-Ercan, G.; Bako, I. *J. Phys. Chem. B* **2009**, *113*, 4360–4371.
- (18) Martin, M. G.; Siepmann, J. I. *J. Phys. Chem. B* **1998**, *102*, 2569–2577.
- (19) Fumino, K.; Bansa, A.-M.; Golub, B.; Paschek, D.; Ludwig, R. *ChemPhysChem* **2015**, *16*, 299–304.
- (20) Hill, T. L., *An Introduction to Statistical Thermodynamics*; Dover: 1960.

4.6 Publication V

Balance Between Contact and Solvent-Separated Ion Pairs in Mixtures of the Protic Ionic Liquid [Et₃NH][MeSO₃] with Water Controlled by Water Content and Temperature

B. Golub, K. Fumino, P. Stange, V. Fossog, R. Hempelmann, D. Ondo, D. Paschek, R. Ludwig

J. Phys. Chem. B, 2021, **125**, 4476-4488

CRedit roles: Formal analysis (MD simulations), Investigation (MD simulations), Visualization (MD simulations), Writing - review & editing

Approximated contribution to the publication in percent: 30 %

Reprinted with permission from B.Golub K. Fumino, P. Stange, V. Fossog, R. Hempelmann, D. Ondo, D. Pachek and R. Ludwig, *J. Phys. Chem. B.*, 2021 **125**, 4476-4488.
Copyright 2023 American Chemical Society

Balance Between Contact and Solvent-Separated Ion Pairs in Mixtures of the Protic Ionic Liquid $[\text{Et}_3\text{NH}][\text{MeSO}_3]$ with Water Controlled by Water Content and Temperature

Benjamin Golub, Koichi Fumino, Peter Stange, Verlaïne Fossog, Rolf Hempelmann, Daniel Ondo, Dietmar Paschek,* and Ralf Ludwig*



Cite This: *J. Phys. Chem. B* 2021, 125, 4476–4488



Read Online

ACCESS |



Metrics & More

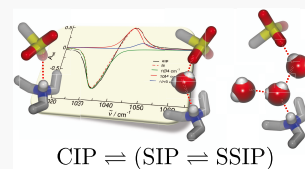


Article Recommendations



Supporting Information

ABSTRACT: The formation of aggregates of ionic species is a crucial process in liquids and solutions. Ion speciation is particularly interesting for the case of ionic liquids (ILs) since these Coulombic fluids consist solely of ions. Most of their unique properties, such as enthalpies of vaporization and conductivities, are strongly related to ion pair formation. Here, we show that the balance of hydrogen-bonded contact ion pairs (CIP) and solvent-separated (SIP) ion pairs in protic ionic liquids (PILs) and in their mixtures with water can be well understood by a combination of far-infrared (FIR) and mid-infrared (MIR) spectroscopy, density functional theory (DFT) calculations of PIL/water aggregates, and molecular dynamics (MD) simulations of PIL/water mixtures. This combined approach is applied to mixtures of triethylammonium methanesulfonate $[\text{Et}_3\text{NH}][\text{MeSO}_3]$ with water. It is shown that ion speciation in this mixture depends on three parameters: the relative hydrogen bond acceptor strength of the counter ion and the molecular solvent, the solvent concentration, and the temperature. For selected PIL/water mixtures, the equilibrium constants for CIPs and SIPs were determined as a function of the solvent content and temperature. Finally, for the studied PIL/water mixtures, the transition from CIPs to SIPs could be understood on enthalpic and entropic grounds. A detailed picture of this interconversion process could be described at the molecular level by means of MD simulations. In addition, the concentration dependence of ion pair formation can be well understood with help of a simplified “cartoon-like” statistical model describing hydrogen bond redistribution.



INTRODUCTION

Ion pairing plays a crucial role for reaction mechanisms in organic chemistry, macromolecular catalysis, biochemical hydrolysis, and protein stability.¹ Phase-transfer catalysis and gel stability are strongly controlled by ion pair formation.² Ion pair chromatography is even based on the formation of aggregates between an analyte and a pairing ion that is retained at the stationary phase.^{3,4} Different ionic species may react with their own characteristic rate constants and result in specific dynamic equilibria.^{5–12} It has been shown for aqueous salt solutions that these properties depend on the structure of the reacting ion, the type of the counter ion, the solvent polarity, and the temperature. These phenomena are of particular importance for ionic liquids (ILs), which are formed solely by ions. ILs and their mixtures are receiving an increasing amount of interest based on the prospect of their potential applications.^{13–17} The function of electrolyte devices, photochemical cells, separation, and catalysis strongly depend on the subtle balance of different kinds of interaction forces between cations and anions in these Coulombic systems.^{9,10} It has been shown that a balanced mix of Coulombic interactions, hydrogen bonds, and dispersion forces is responsible for the unique properties of ionic liquids (ILs).^{18–21} Ion pair formation, in particular, strongly affects the behavior of ILs: ion pair formation in the gas phase results in surprisingly low enthalpies of vaporization.^{22–24} In the liquid phase, the

formation of ion pairs or neutral aggregates thereof can lead to a strongly reduced electrical conductivity.^{25,26} The role of ion pairing and ion dissociation in ILs and IL solutions has been recently extensively reviewed by Nordness and Brennecke.²⁷

Often, the methods for determining ion pairing are indirect in the sense that they depend on observing physical properties of a solution that are affected by ion association. Here, spectroscopic methods are the exception, as they allow for a direct observation of ion pair formation. However, it has been argued that they are prone to insufficient resolution and that they are poor at detecting solvent-separated ion pairing.¹ In this contribution we would like to show that infrared spectroscopy in the far-infrared (FIR) and in the mid-infrared (MIR) regions represent suitable methods to both detect and quantify ion speciation. A general scheme for solvolysis reactions has been proposed and is widely accepted.¹ In this paper, we want to focus on the interconversion between

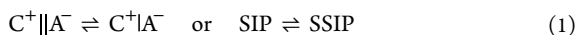
Received: March 1, 2021

Revised: April 14, 2021

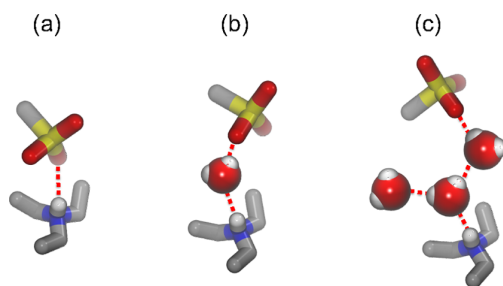
Published: April 24, 2021



contact ion pairs (CIP) and solvent-separated ion pairs (SIP), making no further distinction between SIPs and solvent-shared ion pairs (SSIP) (see Scheme 1)



Scheme 1. Schematic Representation of Ion Pair Types: (a) Contact Ion Pair (CIP), (b) Solvent-Shared Ion Pair (SSIP), and (c) Solvent-Separated Ion Pair (SIP)



Here, the total potential energy of the solutions consists of the sum of solvent–solvent, solvent–ion, and ion–ion interactions. It can be stated that if the anion–cation interaction is sufficiently strong, CIPs are the dominant structures in solution. However, if the ion–solvent interaction is able to compete with the ion–ion interaction, solvent-shared ion pairs (SIPs) may be formed. This subtle equilibrium is affected by the ion–ion interaction strength, the polarity of the solvent, and the temperature.

In this work, we aim to extend our previous study of the formation of CIP and SIP configurations for the protic ionic liquid (PILs) triethylammonium methanesulfonate $[\text{Et}_3\text{NH}][\text{MeSO}_3]$ (TEAMS). In PILs, the proton transfer from the Brønsted acid to the Brønsted base is possible, leading to the formation of proton acceptor and proton donor sites while introducing significant hydrogen bonding.^{28–37} Strong hydrogen bonding between the ions may even allow for the existence of CIPs in the neat PIL.³⁸ For aprotic and protic ionic liquids, we could demonstrate that the cation–anion interaction can indeed be studied by far-infrared (FIR) and terahertz (THz) spectroscopy. Supported by density functional theory (DFT) calculations of IL aggregates, we were able to relate the low vibrational frequencies to cation–anion interaction energies depending on the anion interaction strength or inductive effects due to the variation of the alkyl chain length of the cations.^{39–44} In particular, we used this combination of experimental and theoretical methods to study the transition from CIPs to SIPs of TEAMS dissolved in water. We could show that four water molecules were needed to initiate the transition from CIPs to SIPs. This was indicated by characteristic changes in the FIR difference spectra for PIL/water mixtures above 80 mol % water content, and supported by DFT calculations, showing favorable enthalpies for the SIP configurations due to the strong water affinity and cooperative effects. Moreover, recently Kumari et al. reported from molecular dynamics (MD) simulations that in the case of TEAMS, the different numbers and distributions of ion–ion, ion–water, and water–water hydrogen bonds drive the formation of salt-in-water and water-in-salt nanodomains.⁴⁵ We would also like to stress the fact that even in a PIL/water mixture with 90 mol % water content, there are only between four and five water molecules available for solvating each ion.

In this concentration range, any spectroscopically detectable change associated with hydration phenomena is basically linked to the formation of an SSIP or SIP configuration.

In this contribution, we now would like to provide more quantitative information expressed by equilibrium constants and free energy differences for the ion pair species. First, we briefly recall our recent results for the FIR measurements of the TEAMS/water mixtures. We then significantly extended the study by investigating the equilibrium of CIPs and SIPs for the variation of water content and temperature. In addition, we will show that the spectra of TEAMS/water mixtures in the mid-infrared region, in particular the SO vibrational modes, provide useful quantitative information about ion speciation. Moreover, we will demonstrate that for PIL/water mixtures, the free energy difference between CIP and SIP configurations is sufficiently small, such that changing the temperature affects the interconversion, and can be measured, resulting in estimates for the CIP/SIP equilibrium constants. To complement the IR spectroscopy experiments and DFT studies, we have performed MD simulations of TEAMS/water and related triethylammonium trifluoromethanesulfonate/water (TEATF/water) mixtures. To be able to describe the CIP/SIP equilibrium observed in both, experiment and MD simulation analytically, we propose a simplified lattice model. This allows us to provide a comprehensive description of these solvation phenomena at the molecular level via hydrogen bond redistribution of the cation.

■ EXPERIMENT AND THEORY

IR Experiments. The pure ionic liquid was dried in vacuum ($p = 8 \times 10^{-3}$ mbar) for approx. 36 h. The water content was then determined by Karl-Fischer titration and found to be below 200 ppm. Further purification was not carried out.

The far-infrared (FIR) measurements were performed with a Bruker Vertex 70 FTIR spectrometer equipped with an extension for measurements in the FIR region that consists of a multilayer Mylar beam splitter and a room temperature DLaTGS detector with a preamplifier. Polyethylene (PE) windows with an internal optical path of 0.1 mm were used. Further improvement could be achieved using a high-pressure mercury lamp and a silica beam splitter. The accessible spectral region for this configuration now lies between 10 and 680 cm^{-1} (0.3 and 20.3 THz).

Mid-infrared (MIR) measurements were performed with a Bruker Vector 22 FTIR spectrometer. A L.O.T.-Oriol variable-temperature cell equipped with CaF_2 windows having a path length of 0.05 mm was used for the variable-temperature experiments. Temperatures were maintained with an external Haake C25P cryostat and were monitored with a thermocouple attached directly to the cell. For each spectrum, 128 scans were recorded at a spectral resolution of 1 cm^{-1} . Solvent (ILs) subtraction was carried out using reference spectra obtained at exactly the same temperatures as the sample spectra. The sample chamber was purged with dry air during data collection. The infrared spectra were deconvoluted simultaneously as well as separately into a number of Voigt profiles (convolution of Lorentzian and Gaussian functions) following the Levenberg–Marquardt procedure. The Voigt profile has four parameters: the absorption, the frequency, the half-width of the Lorentzian, and the half-width of the Gaussian. The deconvolution procedure is described in detail elsewhere.^{20,21}

DFT Calculations. The geometries and frequencies of ion pair aggregates TEAMS of various sizes and of one single ion pair TEAMS “dissolved” in the environment of n water molecules ($n = 1-9$) have been calculated at the DFT level B3LYP//6-31+G*. Different conformers were calculated for all structures but only the conformations with the lowest energy have been considered. The structures and geometries of all CIP and SIP clusters are given in the [Supporting Information](#).

Also, the frequencies of the minimum energy configurations have been calculated at the DFT level B3LYP//6-31+G* using the Gaussian 09 program.⁴⁶ The computed binding energies have been corrected for the basis set superposition error (BSSE).⁴⁷ Again, various different conformers were calculated for all structures but only the best in energy have been considered.

MD Simulations. The simulated mixtures of the protic ionic liquids with water are represented by systems composed of 216 ion pairs plus n_W additional water molecules (with $n_W = 0, 24, 54, 93, 144, 216, 324, 504, 648, 864$, and 1296) to arrive at the following 11 different compositions with water content $x_W = 0.0, 0.10, 0.20, 0.30, 0.40, 0.50, 0.60, 0.70, 0.75, 0.80$, and 0.86. To study the effect of varying the hydrogen bond acceptor strength, we perform simulations using two different anions: in addition to the methanesulfonate (MS) anion, we also study the trifluoromethanesulfonate (TF) anion, which has been shown to exhibit a slightly weaker cation–anion hydrogen bond to the triethylammonium (TEA) cation^{38,48} The employed forcefield for both ionic liquids has been described in ref 38. Water molecules are represented by the rigid 4-site TIP4P/2005 water model.⁴⁹ The simulations are carried out using a cubic simulation box employing periodic boundary conditions. A snapshot from an MD simulation of a TEAMS/water mixture with 75 mol % water content at 300 K is shown in [Figure 1](#). All MD simulations (production runs) are performed in the isobaric isothermal (NPT) ensemble, employing Nosé–Hoover thermostats^{50,51} and Rahman–Parrinello barostats,^{52,53} using coupling times of $\tau_T = 1$ ps and $\tau_p = 2$ ps, respectively. The electrostatic interactions are

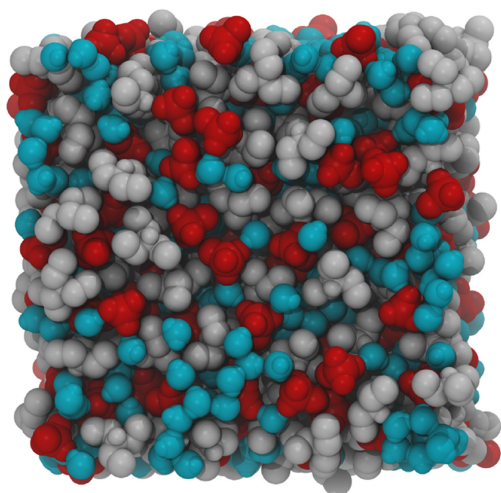


Figure 1. Snapshot of the entire MD box from an MD simulation of a TEAMS/water mixture with 75 mol % water content at 300 K. TEA cations are shown in white, whereas the MS anions are depicted in red. Water molecules are shown in cyan. The image was created using VMD.⁵⁵

treated in the “full potential” approach by the smooth particle-mesh Ewald summation⁵⁴ with a real space cutoff of 0.9 nm and a mesh spacing of approximately 0.12 nm and 4th order interpolation. The Ewald convergence factor α was set to 3.38 nm⁻¹ (corresponding to a relative accuracy of the Ewald sum of 10⁻⁵).

A 2.0 fs time step was used for all simulations and the constraints were solved using the LINCS procedure⁵⁶ for both, anions and cations, while the SETTLE algorithm⁵⁷ was employed for the rigid TIP4P/2005 water molecules. During the simulations, just the bond lengths of the ions were kept fixed, thus allowing for bond-bending and conformational changes. All simulations reported here were carried out using the GROMACS program.^{58,59} For all reported compositions and temperatures, initial equilibration runs of 2 ns length were performed using the Berendsen weak coupling scheme for pressure and temperature control $\tau_T = \tau_p = 0.5$ ps.⁶⁰ Production runs of up to 50 ns simulation length for 300, 320, 340, 360, 380, 400, and 420 K were finally recorded and analyzed for each composition. All simulations were carried out at a pressure of 1 bar.

Simplified Solvation Model. Recently, we have proposed a “cartoon-like” model capable of properly describing the effect of hydrogen bond redistribution in mixtures of protic ionic liquids.⁴⁸ To analytically describe the water content dependence, we extend this model to water mixtures.

For simplicity, the liquid is thought to be represented by a lattice, where the anions and cations occupy sites in an alternating fashion. Each ion is coordinated and surrounded by c_A counterions. In addition, depending on the water content, further c_W sites need to be introduced to be able to accommodate the additional water molecules, as can be seen from the snapshot of a solvation shell of a TEA cation shown in [Figure 2](#). Since each TEA N–H bond is involved in a

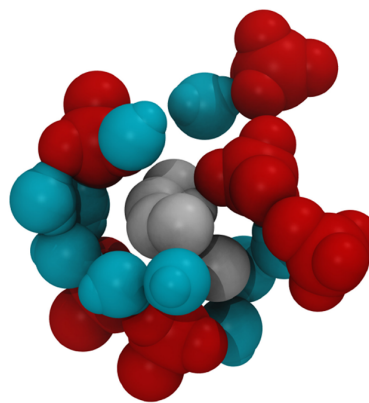
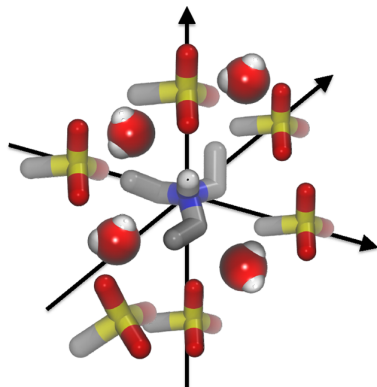


Figure 2. Solvation of a TEA cation engaged in a CIP configuration obtained as a snapshot from MD simulation of a TEAMS/water mixture with 75 mol % water content at 300 K. The color coding is the same as in [Figure 1](#). The image was created using VMD.⁵⁵

hydrogen bond to one of their $c = c_A + c_W$ surrounding neighbors, it can either form a hydrogen bond to a neighboring anion and form contact ion pair (CIP), or it can form a hydrogen bond to a water molecule, which we assign to the solvent-separated state (SIP), as outlined in [Scheme 2](#). Moreover, we assume that each N–H group stays always involved in a hydrogen bond, pointing to one of the hydrogen bond acceptor sites, either located on a water molecule or on

Scheme 2. “Cartoon-Like Representation” of the Ionic Liquid/Water Mixture: The Liquid is Represented as a Lattice, Where the Anions and Cations Occupy Sites in an Alternating Fashion with a Coordination Number c_A^a



^aAdditional c_W sites are occupied by water molecules, with c_W changing according to the water content. Each TEA N–H bond is involved in a hydrogen bond to an anion or a water molecule, both being randomly distributed on the $c = c_A + c_W$ surrounding neighbor sites.

an anion. Thus, the sum of hydrogen bond acceptance probabilities p_i to each of the surrounding c sites has to add up to unity with

$$1 = \sum_{i=1}^c p_i \quad (2)$$

Assuming a random occupation of the sites surrounding each cation by anions and water molecules according to the molecular composition, the hydrogen bond acceptance probability for each site can be expressed as a composition-weighted sum of the individual acceptance probabilities for water (p_W) and anions (p_A) with

$$p_i = x_W p_W + (1 - x_W) p_A \quad (3)$$

Assuming equality between the sites, the hydrogen bond acceptance probabilities are thus determined by

$$p_W = \frac{1}{c x_W + c(1 - x_W)f}, \text{ and} \quad (4)$$

$$p_A = \frac{1}{c x_W f^{-1} + c(1 - x_W)} \quad (5)$$

with $f = p_A/p_W$. We can directly determine the fraction of times, a N–H bond of a TEA-cation points to either a methanesulfonate anion or a water molecule

$$y_W = c \cdot x_W p_W = \frac{x_W}{x_W + f(1 - x_W)} \quad (6)$$

and

$$y_A = c \cdot (1 - x_W) p_A = \frac{1 - x_W}{x_W f^{-1} + (1 - x_W)} \quad (7)$$

Now, the equilibrium between contact ion pairs and solvent-separated ion pairs can be simply computed as the ratio of fractions of hydrogen bond to either an anion or a water molecule

$$K = \frac{[\text{CIP}]}{[\text{SIP}]} = \frac{y_A}{y_W} = \frac{1 - x_W}{x_W} \cdot f \quad (8)$$

with the corresponding standard Gibbs free energy difference being

$$\begin{aligned} \Delta G^\circ(x_W) &= -RT \ln K(x_W) \\ &= RT \left[\ln \frac{x_W}{1 - x_W} - \ln f \right] \end{aligned} \quad (9)$$

Thus, a change in the water content independent ratio of individual hydrogen bond acceptance probabilities just leads to a different vertical offset of the $\Delta G^\circ(x_W)$ function. Note, that for the case of the equimolar mixtures, the standard Gibbs free energy difference is solely related to the ratio of hydrogen bond acceptance probabilities

$$\Delta G^\circ(x_W = 0.5) = -RT \ln f \quad (10)$$

Considering the fact that each SO_3 group provides three possible hydrogen bond accepting oxygen atoms, instead of one for water, one would expect $f \approx 3$ for the case of equally strong N–H hydrogen bonds to either of both species.

RESULTS AND DISCUSSION

FIR Experiments. First, we briefly highlight and complement our recent investigations of TEAMS in mixtures with water.^{36,37} Initially, we measured the far-infrared spectra for the pure PIL and for pure water, as shown in Figure 3a. Here, we

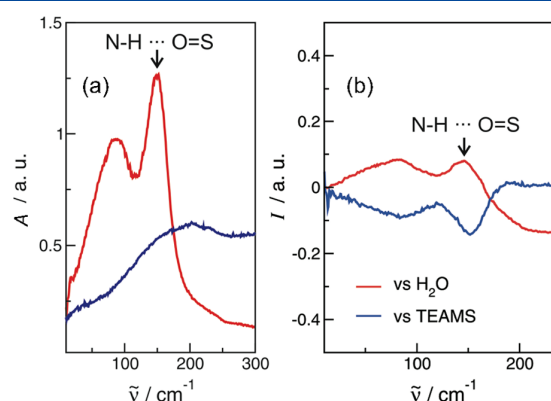


Figure 3. (a) Far-infrared (FIR) spectra for triethylammonium methanesulfonate (red line) and water (blue line). (b) Far-infrared (FIR) difference spectra for a 50 mol % mixture of TEAMS and water. The spectra were obtained by subtracting the pure PIL (blue line) or pure water (red line) contributions as backgrounds. The vibrational band at about 150 cm^{-1} in the difference spectra could be assigned to remaining contributions from the anion–cation interaction along the bond $^+\text{N}-\text{H}\cdots\text{MeSO}_3^-$ indicating the CIP configurations.

covered the low-frequency range between 10 and 300 cm^{-1} . It was well known from earlier studies that the vibrational band at 150 cm^{-1} in the FIR spectrum of the TEAMS can be assigned to the cation–anion interaction along the $^+\text{N}-\text{H}\cdots\text{O}^-$ bond.^{61–63} The main feature in the water spectrum is the broad vibrational band around 200 cm^{-1} , which is usually referred to the intermolecular interaction within the extended hydrogen bonding network of water.^{64–68} The pure TEAMS and water spectra are now used as background spectra for measuring the difference spectra for PIL/water mixtures.

In Figure 3b, the difference spectra of the 50 mol % TEAMS/water mixture measured versus the pure water and the pure TEAMS contributions are shown. If the water spectra are subtracted from the mixture spectra, positive contributions can stem only from vibrational modes of the remaining internal cation–anion interaction in TEAMS or new TEAMS/water interactions. Additionally, we know from other studies that the TEAMS/water interaction mainly occurs via the methanesulfonate anion. Negative absorptions in the difference spectra can be attributed to missing pure water contributions. More generally speaking, we are able to subtract the solvent–solvent interactions from the sum of solvent–solvent, solvent–ion, and ion–ion interactions. If we subtract the pure TEAMS spectrum, we obtain negative contributions for the TEAMS spectral features in particular for the mode at 150 cm^{-1} , indicating the presence or the absence of contact ion pairs. For the 50 mol % mixture, we observe nearly the same positive and negative band absorptions, supporting the hypothesis that CIPs are the absolutely dominant ion pair species.

In Figure 4, we now show the obtained difference spectra of the 50, 70, 80, and 90 mol % TEAMS/water mixtures

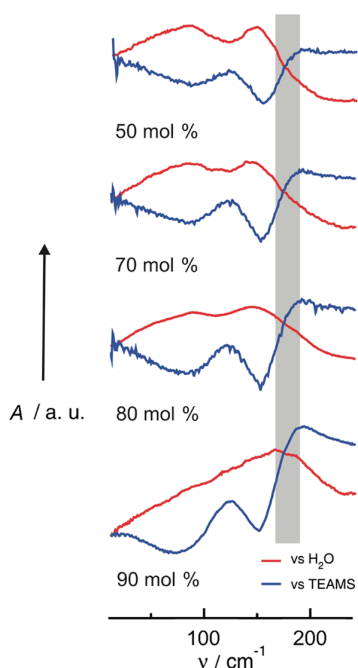


Figure 4. Far-infrared (FIR) difference spectra of the mixtures of triethylammonium methanesulfonate $[\text{Et}_3\text{NH}][\text{MeSO}_3]$ (TEAMS) with water (taken with kind permission from ref 62). The spectra were obtained by subtracting the pure water (red line) and the pure TEAMS (blue line) contributions as background. The vibrational band at about 150 cm^{-1} in both difference spectra could be assigned to remaining or missing contributions from $^+\text{N}-\text{H}\cdots\text{MeSO}_3^-$ intermolecular interaction. With increasing water content, this vibrational mode disappears and a new maximum occurs at about 180 cm^{-1} above 80 mol % water (indicated by the gray bar).

measured versus both, pure water and pure TEAMS, respectively. It is clearly observed from the 80 mol % mixtures that the vibrational mode at 150 cm^{-1} , indicating the CIPs, is successively replaced by new contributions at about 190 cm^{-1} . The calculated low vibrational frequencies of TEAMS/water aggregates can be related to intermolecular interactions

between the PIL cation and the water molecule. Obviously, from 80 mol % water content on, the CIPs are increasingly converted into SIPs.

DFT Calculations. The conversion between CIP and SIP states can be understood on the basis of calculated energies and free energies of TEAMS/water aggregates including one TEAMS ion pair (CIP and SIP) and $n = 1-9$ water molecules. Computed aggregates are shown in Figure 5 for CIPs and SIPs

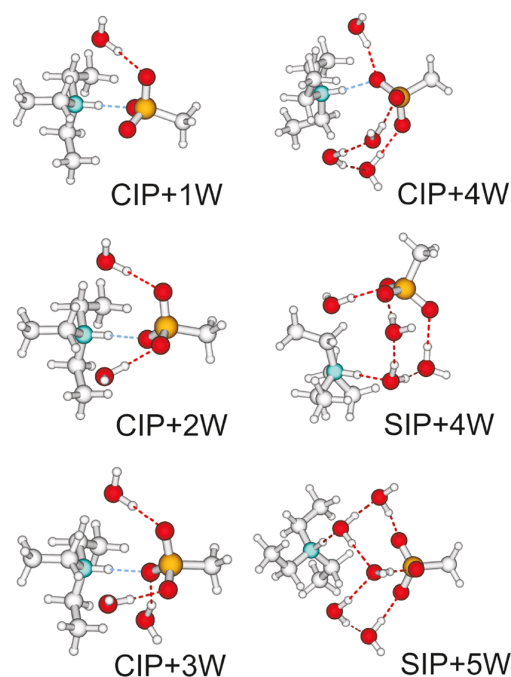


Figure 5. Density functional calculated clusters of triethylammonium methanesulfonate $[\text{Et}_3\text{NH}][\text{MeSO}_3]$ (TEAMS) ion pairs and different numbers of water molecules representing 50, 66, 75, 80, and 83 mol % water content (taken with kind permission from ref 62). Starting with the configurations including four water molecules (4W), the solvent-separated ion pairs (SIP) are enthalpically favored over the contact ion pairs (CIP). The intermolecular interaction between a cation and an anion ($^+\text{N}-\text{H}\cdots\text{anion}$, the blue dotted line) is replaced by the intermolecular interaction between the cation and water ($^+\text{N}-\text{H}\cdots\text{water}$, the red dotted line). In these SIP configurations (e.g., SIP + 5W), one additional H bond can be formed due to the coordination ability of the water molecules.

with one to five water molecules. The first three water molecules were successively attached to the oxygen atoms of the methanesulfonate anion without disrupting the CIP configuration. Prearranged SIP configurations with fewer or equal than three water molecules would not stay in that configuration during the DFT geometry optimization procedure. However, from the fourth water molecule, “stable” minimum energy configurations for both, CIPs and SIPs were observed.

As shown in Figure 6, the SIP configurations represent always both, a lower energy and free energy state, compared to the CIPs. However, the difference in binding energy between 20 and 30 kJ mol^{-1} does not further increase with an increasing number of added solvent molecules. Similar behavior is observed for the calculated free energies. However, the SIP configurations are still found to be favored over the CIPs, but the free energy differences are smaller, decreasing down to

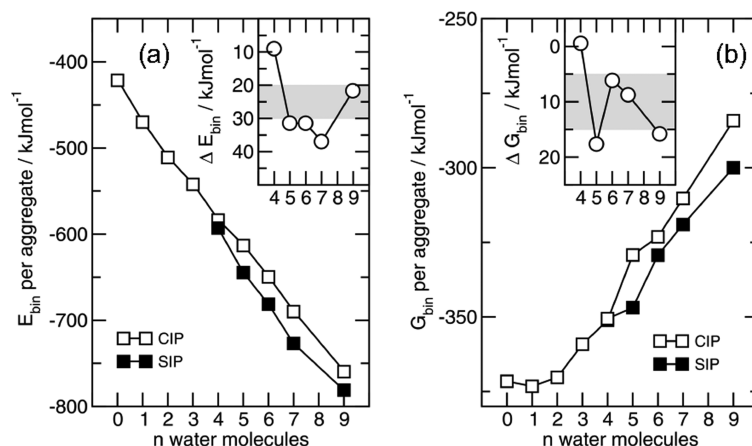


Figure 6. (a) Binding energies and (b) binding free energies, obtained from DFT calculations for aggregates of triethylammonium methanesulfonate ion pairs with added water molecules, roughly representing a water content between 50 and 90 mol %. It is shown that the solvent-separated ion pairs (SIP) are energetically favored over the contact ion pair (CIP) configurations with four or more water molecules. The binding energies SIPs are lower by about 20–30 kJ mol^{−1} due to the formation of one additional H bond in the SIPs (see inset). The binding free energies also indicate the preference of SIPs over CIPs but to a smaller extent. Apparently, the SIPs are subject to an entropic penalty.

between 10 and 15 kJ mol^{−1}. From these calculations, we conclude that SIPs are strongly enthalpically favored from the fourth water molecule. At the same time, there is an entropic penalty associated with the SIP configurations, solely related to the local atomic motions within the respective cluster configurations. If water molecules are being trapped between a cation and an anion, the motional degrees of freedom are significantly altered, possibly becoming more harmonic. In summary, this finding suggests an increasing conversion from SIPs to CIPs with increasing temperature.

MIR Experiments. To obtain quantitative information about the SIP and CIP equilibrium, we switched from FIR to MIR spectroscopy, focusing on the SO stretch frequency region of the PIL anion, which ranges from 1020 to 1250 cm^{−1}. The difference spectra of the PIL/water mixtures were recorded versus the pure PIL as background. The asymmetric and symmetric SO stretch vibrational modes are shown separately in Figures 7 and 8, respectively. It has been shown earlier that ion association occurs at the SO₃ end of the anion,⁶⁹ thus the symmetric and asymmetric SO₃ stretching modes are highly sensitive to changes in the coordination state of the anion.⁷⁰ Frech and co-workers could show in several studies that the stretching modes in this frequency range can

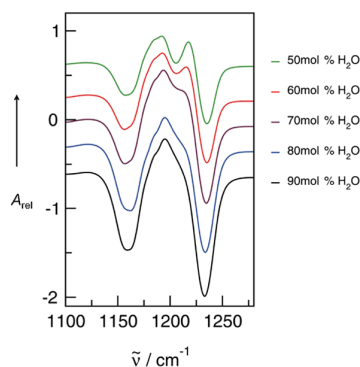


Figure 7. Asymmetric SO₃ stretching band for triethylammonium methanesulfonate in water as a function of water content.

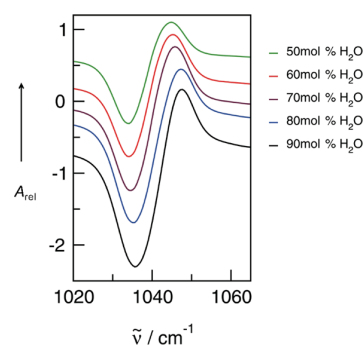


Figure 8. Symmetric SO₃ stretching band for triethylammonium methanesulfonate in water as a function of water content.

be exclusively characterized as $\nu_{as}(\text{SO}_3)$ and $\nu_s(\text{SO}_3)$ since they consist almost completely of S–O stretching motions. The measurement of the doubly degenerate SO₃ asymmetric stretching mode $\nu_{as}(\text{SO}_3)$ provides important information about the strength of the cation–anion interaction. The degeneracy is strongly reduced when an ion pair is formed, resulting in two bands. The width of the splitting can be viewed as a measure of the perturbation of the local C_{3v} symmetry of the SO₃ groups. Thus, when the methanesulfonate anion is coordinated by a single triethylammonium cation, the band is split into two peaks, one at higher and one at lower wavenumber than the “free” ion band.⁷⁰ This is demonstrated in the difference spectra of the TEAMS/water mixture, which were measured against the pure PIL, consisting solely of contact ion pairs. By subtracting the spectra of pure TEAMS, we observe two negative peaks at 1160 and 1234 cm^{−1}, respectively. As expected, the degeneracy is maximally reduced if only one S=O strongly interacts with the triethylammonium cation. At the same time, positive peaks can be observed, which change characteristically with increasing water content. In Figure 9, the calculated and experimental frequency shifts due to changing degeneracy with increasing water content are demonstrated. The degeneracy and thus the splitting of the pairs of peaks is largest for CIPs. In the 50 mol % mixtures, the second S = O bond of the anion interacts with the water

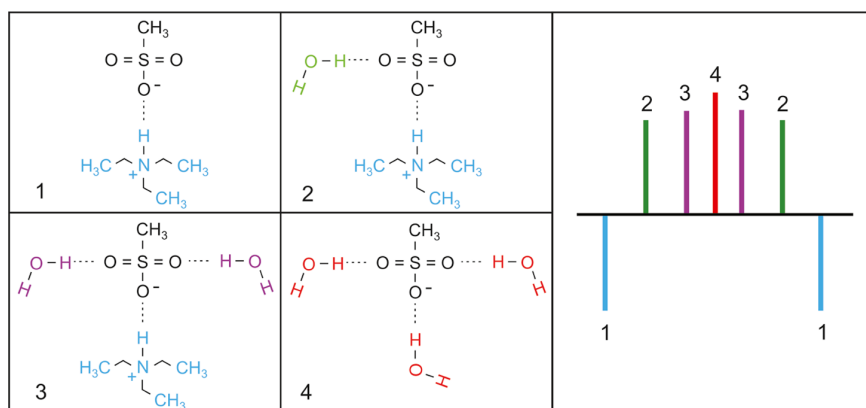


Figure 9. Asymmetric SO_3 stretching modes for triethylammonium methanesulfonate in water as a function of water content: for the contact ion pairs, we obtain a maximally reduced degeneracy, as indicated by the wide spacing between the negative bands (1) if the pure PIL is subtracted as background. With increasing water content, the anion within the CIPs is additionally coordinated by water molecules (2 and 3), leading to a reduction in spacing between both bands, increasingly restoring the degeneracy of the $\nu_{\text{as}}(\text{SO}_3)$ vibrational modes. If the anion is fully hydrated (4), the situation approaches that in the gas phase and C_{3v} symmetry is nearly restored.

molecules as shown before. This leads to the first step toward degeneracy again, indicated by smaller frequency differences between both modes. This trend is further enhanced if a second water molecule interacts with the third $\text{S}=\text{O}$ bond. The FIR spectra of the TEAMS/water mixtures indicated significant changes in the spectral features from the 80 mol % water content. If a fourth water molecule was added, the CIPs were replaced by SIP configurations. This behavior can also be observed for the asymmetric SO stretch frequencies in the MIR region. If the SO_3 group is fully hydrated, as is the case in a SIP configuration, all $\text{S}=\text{O}$ bonds interact with water molecules, leading to a near full reconstruction of the degeneracy, similar to that in the gas phase. A characteristic change can be observed from the fourth water molecule and can be related to the transfer from CIPs to SIPs. However, although we tried to decompose the complicated difference spectra in the asymmetric SO stretch region shown in Figure 7, we were not able to properly assign the resulting contributions to CIP and SIP configurations.

Fortunately, the situation is more comfortable for the symmetric SO stretch vibrational modes as $\nu_{\text{s}}(\text{SO}_3)$. The symmetric SO_3 stretching mode is found to consist of two or more peaks. The different anion environments may be attributed to ion association, considering the nondegenerate A_1 symmetry of this mode. The symmetry of the anion is lowered by coordination to the cation. Deconvolution of the SO_3 region reveals the peak components, which arise from various ion aggregates. In Figure 8, the difference spectra of the TEAMS/water mixtures are shown. The negative absorptions at 1035 cm^{-1} stem from the vibrational modes of the anions in the pure CIP configurations of the neat PIL, whereas the positive absorption can be assigned to ion pairs interacting with water molecules either in CIP or in SIP configurations. The DFT calculations depicted in Figure 9 clearly show a characteristic shift to higher wavenumbers for mixtures including one ion pair and minimum four water molecules, indicating the formation of SIPs. This is in agreement with the observed MIR spectra showing a significant shift to higher wavenumbers from 80 mol % water content on (see Figures 8, 10, and 11). Thus, the positive band can be deconvoluted into two contributions representing CIPs and SIPs at the lower and higher frequencies, respectively, as shown in Figure 10.

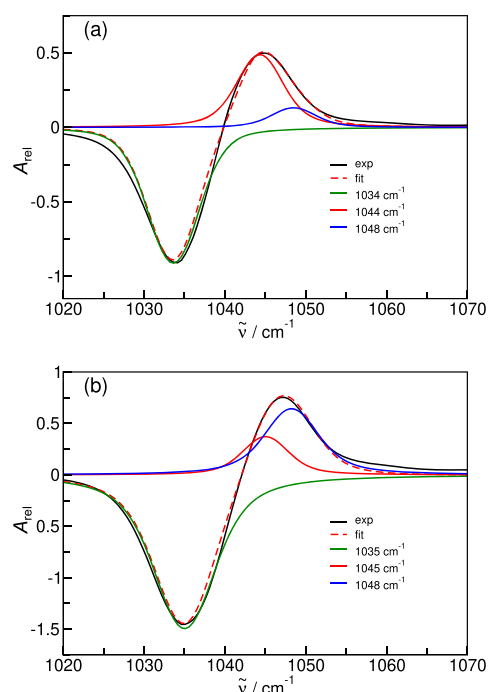


Figure 10. Deconvoluted difference MIR spectra of the symmetric SO_3 vibrational band for TEAMS/water mixtures with (a) 50 mol % and (b) 80 mol % water content measured versus pure TEAMS at 298 K.

Assuming that the absorptions of the symmetric SO stretch vibrational modes for the CIP and SIP configurations are roughly equal, we are able to refer to distinct contributions to CIP or SIP species.

Based on the assumptions discussed above, we are now able to derive the equilibrium between CIP and SIP configurations from the absorptions of the CIP and SIP vibrational bands, as given in Table 1. The calculated equilibrium constants

$$K = A_{\text{CIP}}/A_{\text{SIP}} \quad (11)$$

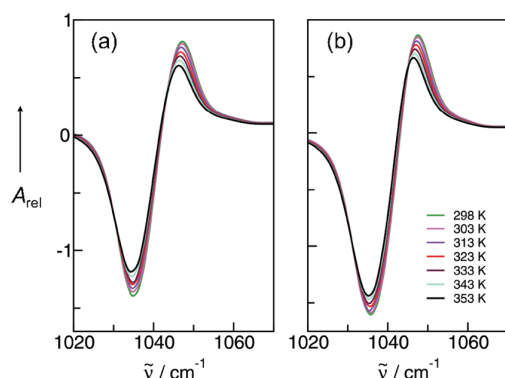


Figure 11. Difference MIR spectra for TEAMS/water mixtures with (a) 80 mol % and (b) 90 mol % water content measured versus the pure TEAMS as a function of temperature.

Table 1. Absorptions A_{CIP} and A_{SIP} from Deconvoluted MIR Spectra of the TEAMS/Water Mixtures as a Function of Water Content for 298 K^a

$x_{\text{W}}/\text{mol } \%$	A_{CIP}	A_{SIP}	K	$\Delta G^\circ/\text{kJ mol}^{-1}$
50	1.360	0.342	3.97	-3.42
60	1.847	0.678	2.73	-2.48
70	1.825	1.250	1.46	-0.94
80	1.025	2.217	0.46	1.91
90	0.650	2.974	0.22	3.77

^aFrom the equilibrium constants, we derived the standard free energy differences ΔG° for the different ion pair species present in the TEAMS/water mixtures.

are also given in Table 1. In Figure 12, the standard Gibbs free energies ($\Delta G^\circ = -RT \ln K$) calculated from K defined above

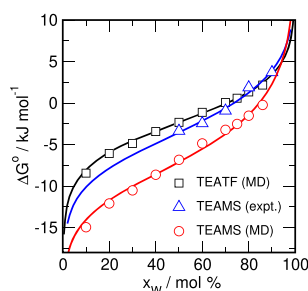


Figure 12. Standard Gibbs free energy differences ΔG° for the interconversion of CIP and SIP configurations as a function of the water content obtained from MD simulations for TEAMS/water and TEATF/water mixtures at 300 K and experiments for TEAMS/water mixtures at 298 K. Solid lines are predictions by eq 9 with y_{W} data from Figure 15a.

are shown as a function of temperature and water content. According to our MIR data, in the 50 mol % mixture, both ion pair species seem to exist in same amount. For the water content ranging from 20 to 90 mol %, the free energies change by about 6 kJ mol⁻¹. For mixtures of TEATF/dimethyl sulfoxide (DMSO), only half of this value (3 kJ mol⁻¹) has been reported,⁶³ possibly reflecting the weaker interaction between the TEA cation and the TF anion compared to that between the TEA cation and the MS methanesulfonate anion in the PIL investigated in this study.⁶³ However, there is only a

subtle difference in the free energies of CIPs and SIPs and it requires the polarity of water to dissociate the CIPs and to initiate the transfer to SIPs.

For the TEAMS/water mixtures with small water content (not shown), we could not observe characteristic temperature dependences of the spectra. For the temperature range between 303 and 383 K, the band absorptions decrease but their frequencies do not shift. Obviously, there is no measurable shift between the two ion pair species with increasing temperature for the mixtures with low water content. Therefore, we focus on the mixtures exhibiting significant amounts of SIP species already at room temperature. This could be shown for the TEAMS/water mixtures containing 80 and 90 mol % water, as shown in Figure 11.

Interestingly, the maxima of the vibrational bands shift to lower wavenumbers indicates the transfer from SIPs to CIPs with increasing temperature. Assuming that the absorption ratio of 1:1 for the CIP and SIP vibrational bands is temperature independent, we could evaluate the equilibrium constants as a function of temperature for both mixtures. The data are listed in Tables 2 and 3 for the 80 and 90 mol %

Table 2. Absorptions A_{CIP} and A_{SIP} from Deconvoluted MIR Spectra of the TEAMS/Water Mixture with 80 and 90 mol % Water for the Temperature Range between 298 and 353 K^a

T/K	A_{CIP}	A_{SIP}	K	$\Delta G^\circ/\text{kJ mol}^{-1}$
$x_{\text{W}} = 80 \text{ mol } \%$				
298	1.025	2.217	0.462	1.91
303	1.143	2.189	0.522	1.64
313	1.154	1.826	0.632	1.19
323	1.265	1.649	0.768	0.71
333	1.368	1.501	0.911	0.25
343	1.366	1.478	0.924	0.22
353	1.388	1.327	1.046	-0.13
$x_{\text{W}} = 90 \text{ mol } \%$				
298	0.650	2.974	0.219	3.77
303	0.768	2.818	0.273	3.27
313	0.778	2.637	0.295	3.18
323	0.890	2.360	0.377	2.62
333	0.993	2.130	0.466	2.11
343	0.991	1.952	0.508	1.93
353	1.013	1.757	0.577	1.62

^aFinally, the equilibrium constants and free energies could be derived for the ionic species present in the TEAMS/water mixtures.

Table 3. Computed Standard Enthalpy and Entropy Differences for the Equilibrium between CIPs and SIPs in the 80 and 90 mol % Mixtures of TEAMS/Water

$x_{\text{W}}/\text{mol } \%$	$\Delta H^\circ/\text{kJ mol}^{-1}$	$\Delta S^\circ/\text{J mol}^{-1} \text{ K}^{-1}$
80	13.0	37.6
90	14.4	36.5

mixtures, respectively. We can now plot the equilibrium constant versus the inverse temperature as van't Hoff plot expressed by

$$\ln(K) = -\Delta H^\circ/(RT) + \Delta S^\circ/R \quad (12)$$

As shown in Figure 13, the temperature-dependent conversion from SIPs to CIPs can be well described by a constant enthalpy difference. The enthalpies taken from the slopes of the curves

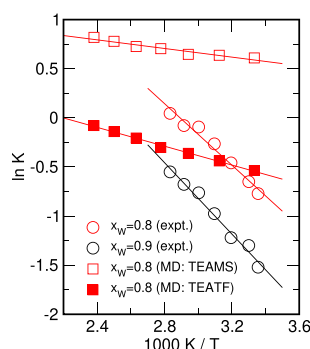


Figure 13. Van't Hoff plots. Shown are the experimental equilibrium constants K of the CIP/SIP ratios in TEAMS/water mixtures with 80 and 90 mol % water content. In addition, equilibrium constants K determined from MD for a water content of 80 mol % are given for two different ILs: TEAMS and TEATF.

are 13.0 and 14.4 kJ mol^{−1} for the 80 and 90 mol % mixtures, respectively. A qualitatively similar temperature dependence has been reported previously from MD simulations of aqueous salt solutions.^{71,72} The shift toward a smaller CIP/SIP ratio with increasing water content is also in accordance with observations from MD simulations from aqueous NaCl solutions.⁷³ It is plausible that the enthalpy difference for the 90 mol % mixture is slightly larger than that for 80 mol % mixture since with increasing water content, more energy is required for the conversion of SIP to CIP configurations. In addition, we also have access to the standard molar entropy changes ΔS° , as given likewise in Table 3. The entropies ΔS° are 37.6 J mol^{−1} K^{−1} for the 80 mol % mixture and 36.5 J mol^{−1} K^{−1} for the 90 mol % mixture, respectively. The positive values of ΔS° shown in Table 3 suggest that solvent molecules are possibly released to the bulk solvent from the SIPs during the formation of CIPs. It is fair to assume that in the related SIP configurations, the water molecules are more tightly bound between the cation and the anion due to strong cooperative effects.⁶² The significantly reduced orientational degrees of freedom are likely to result in an entropic penalty, as indicated by the calculated Gibbs free energies for both ion pair configurations.

MD Simulations/Simplified Solvation Model. To complement our spectroscopic investigations, we have performed MD simulations of two different PIL/water (TEAMS and TEATF) mixtures with varying water concentrations up to a water content of 86 mol % over a broad temperature range. Considering mixtures with ILs composed of anions with different hydrogen bond acceptor strengths⁴⁸ is allowing us to explore the influence of the acceptor strength. This is of relevance in the case the IL models and the water models do not match perfectly. Figure 14 shows the H...O radial pair distribution functions between the N–H group of the TEA cation as a hydrogen bond donor and the oxygen atoms located on the MS anion (OA) and water (OW), respectively for a 75 mol % mixture of TEAMS and water at 300 K. Here, hydrogen-bonded configurations are well separated from nonhydrogen-bonded configurations by a distance threshold of $r_{OH} = 0.24$ nm. Moreover, the computed number of nearest neighbors add up perfectly to one, indicating that the N–H group of the TEA cation stays always involved in a hydrogen bond. This observation holds true for all studied mixtures for both studied ILs. Note that for the 75

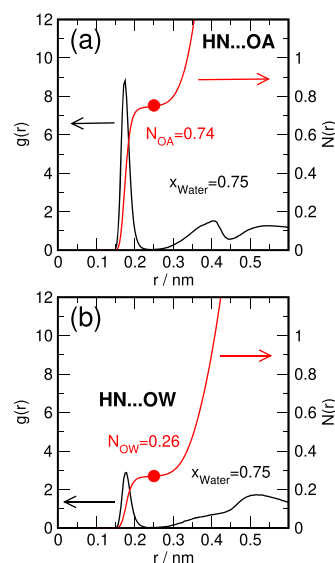


Figure 14. Hydrogen–oxygen radial pair distribution functions describing the hydrogen bonds involving the TEA N–H group for a 75 mol % TEAMS/water mixture at 300 K: (a) TEA–MS. (b) TEA–water. The sum of OA and OW neighbors adds up to one, indicating that the N–H group stays always involved in a hydrogen bond.

mol % mixture, a perfectly OA/OW balanced hydrogen bond acceptor strength would lead to an equal number of nearest neighbors with $N_{OA} = N_{OW} = 0.5$, since each MS anion possess three possible hydrogen bond acceptors. The fact that we observe $N_{OA} = 0.76$ is indicating a significantly stronger N–H...OA hydrogen bond compared to water. The fraction of N–H hydrogen bonds pointing toward either the anion or the water with $y_W = N_{OW}$ and $y_A = N_{OA}$ determines the CIP/SIP equilibrium constant according to

$$K = [\text{CIP}]/[\text{SIP}] = y_A/y_W = N_{OA}/N_{OW} \quad (13)$$

which is depicted as a van't Hoff plot in Figure 13 and as a function of water content in Figure 12 (in both cases, in addition to the experimental data). Similar to the experimental data, the MD simulations indicate a shift of the equilibrium toward CIP species with increasing temperature, however, with a significantly reduced slope, corresponding to a transition enthalpy between about 4 and 5 kJ mol^{−1}. Whether this reflects a deficiency of the forcefield model or is related to issues of the deconvolution procedures struggling with resolving the delicate shifts in configurational populations introduced by temperature changes is not clear. When comparing the simulations of TEAMS and TEATF with our experimental data, the CIP/SIP equilibrium found in the TEATF/water mixtures seems to better agree with the data obtained from the analysis of our MIR data. Apparently, the oxygen-acceptor strength of the TF anion seems to better match the strength of the oxygen-acceptor site within the TIP4P/2005 water model. This is also apparently clear from the water content variation shown in Figure 12, where the experimental data follows rather closely the TEATF MD data, whereas the TEAMS data is significantly shifted to lower ΔG° values, and is also indicating an increasing slope around x_W of 50 mol %.

The solid lines in Figure 12 represent the composition-dependent prediction according to the cartoon-like solvation model outlined earlier and are based on the equilibrium

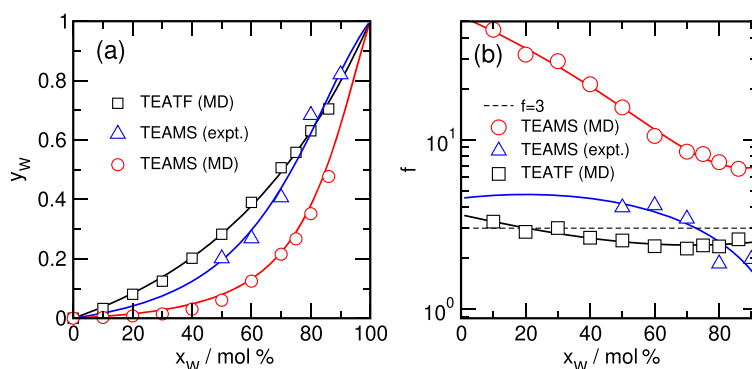


Figure 15. (a) Fraction of N–H hydrogen bonds involved in TEA–water interactions y_W obtained from MD simulations for TEAMS/water and TEATF/water mixtures at 300 K and experiments for TEAMS/water mixtures at 298 K. Solid lines represent predictions according to eq 6. (b) Directly computed f -parameters, indicating the ratio of individual hydrogen bond acceptance probabilities with $f = p_A/p_W$ (see eqs 4 and 5) as a function of water content. The lines represent second-order polynomial fits to the data.

according to eq 9 with y_W vs x_W being depicted in Figure 15a. The preference of the hydrogen bond toward the anion is reflected by the parameter $f = p_A/p_W$, shown in Figure 15b, where p_W and p_A are representing the individual hydrogen bond acceptance probabilities of water and anion, respectively. The bulge of the curves shown in Figure 15a is according to a preference of hydrogen bonding to the anion with $f > 1$. In fact, a value of $f = 1$ would lead to $y_W = x_W$. The solid lines represent second-order polynomial fits to the computed values for f as a function of x_W , as shown in Figure 15b. Note that the experimental data and TEATF data for f show only a little variation with respect to x_W and are relatively close to $f \approx 3$, indicating roughly equal hydrogen bond acceptor strengths for the TF anion and water. This contrasted by the significantly larger and x_W -dependent values for the simulated TEAMS/water mixtures.

Finally, we would like to address the apparent differences that were used to describe the CIP/SIP equilibrium in both experiment and MD simulation. The definition used for the analysis of our MD data is unambiguous: a hydrogen bond between an anion and a cation is per definition the requirement for a hydrogen-bonded ion pair. On the other hand, a hydrogen bond to a solvent obviously leads to solvent-shared and solvent-separated ion pairs. The analysis of the MIR spectra, however, has been focusing on the solvation state of the anion, which comprises a multitude of possible configurations, some of which are outlined in Figure 9. To illustrate, that the solvation state of the SO_3 group changes in accordance with what has been used as the basis for the interpretation of the MIR spectra is shown in Figure 16: here, we depict the population of selected important solvation configurations of the SO_3 group in TEAMS/water mixtures. In the neat PIL, the hydrogen-bonded solvation by a single cation is the dominant species. With increasing water content, more and more hydrogen bonds are donated by adjacent water molecules, finally fully replacing the TEA-cation, and leading to a dominance of fully hydrated anion species. Given the size of the anion, it is fair to assume the change between a direct hydrogen bond from a TEA cation toward the SO_3 group ($\text{TEA} = 1$) to a fully hydrated state ($\text{TEA} = 0$) is the single most significant change of the solvation state, possibly also leading to the most severe change in perturbation of the vibrational state of the SO_3 group. We would like to point out that the change from ($\text{TEA} = 1$) to ($\text{TEA} = 0$) is also exactly in

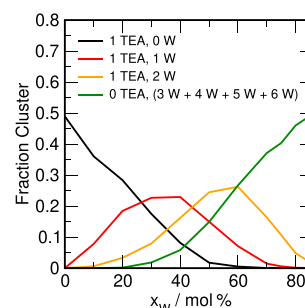


Figure 16. Hydrogen-bonded solvation state of the SO_3 group of the methanesulfonate anion in TEAMS/water mixtures of varying composition at 300 K obtained from MD simulations: Population of species of the indicated composition. The green line indicates solely hydrated SO_3 groups with three to six water molecules attached.

accordance with a definition with the change from a CIP to a SIP configuration. To further support this analogy, we also have plotted the fraction of ($\text{TEA} = 0$) configurations versus the fraction of SIP species (y_W) in Figure 17 for both, TEAMS/water and TEATF/water mixtures, respectively. In both cases, the populations are very well linearly related, thus allowing for quantitative analysis. This leads us to the conclusion that the changing solvation state of the SO_3 group, as probed by the MIR experiments, is indeed very likely quantitatively indicative of the CIP/SIP equilibrium.

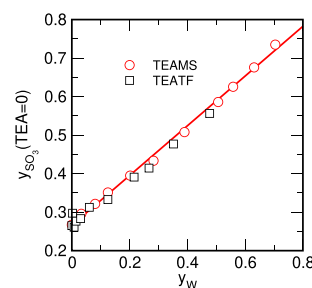


Figure 17. Fraction of MS or TF anions, where no hydrogen bond is formed between a TEA cation and the SO_3 group $y_{\text{SO}_3}(\text{TEA} = 0)$ vs the fraction of N–H hydrogen bonds involved in TEA–water interactions y_W , both obtained from MD simulations at 300 K.

CONCLUSIONS

Ion speciation is crucial for important chemical reactions. In this work, we have studied the balance between contact and solvent-separated ion pairs in the aqueous solutions of the protic ionic liquid triethylammonium methanesulfonate by means of infrared spectroscopy, DFT calculations, and MD simulations in combination with a simple cartoon-like solvation model. We could show that infrared spectroscopy is sufficiently sensitive to detect ion pair species beyond CIPs. Whereas in the far-infrared, the results are more qualitative in nature due to the broad vibrational bands of the water, quantitative information about ion speciation could be obtained from the mid-infrared spectra. The symmetric stretching mode in the SO_3 group within the methanesulfonate anion is sensitive to both types of ion pairs indicated by formation or loss of maximum degeneracy. Supported by DFT-calculated frequencies and absorptions and supported by an analysis of the hydrogen-bonded solvation state of the SO_3 groups, we could calculate equilibrium constants for the CIP and SIP populations and thus quantitatively describe the CIP/SIP equilibrium. The equilibrium between the two ion pair species could be studied as a function of water content and temperature. It requires a minimum of 50 mol % water to observe SIPs in the MIR experiments. However, 80 mol % water and thus four water molecules are needed to favor SIPs over CIPs in agreement with our earlier FIR studies. The reformation of CIPs with increasing temperature could be referred to entropic effects, qualitatively similar to what is observed in our MD simulation. Solvent molecules are squeezed out in favor of the reformation of CIPs via the $^+\text{N}-\text{H}\cdots\text{O}=\text{S}^-$ bond. Our measurements provide important thermodynamic information. Gibbs free energy, enthalpy, and entropy changes nicely characterize the dissociation and back-formation of CIPs in the aqueous solution of the protic ionic liquid. We would like to point out that a reasonable quantitative analysis is only possible if a minimum of 10% of any ion pair species is present in the mixture. The interconversion reaction from CIPs to SIPs involves a concerted sequence of local solvent molecule reorganization coupled to the interionic separation coordinate, which is studied in detail by MD simulations and is quantitatively captured by our cartoon-like solvation lattice model.

ASSOCIATED CONTENT

Supporting Information

The Supporting Information is available free of charge at <https://pubs.acs.org/doi/10.1021/acs.jpcb.1c01850>.

Far-infrared (FIR) spectra of pure TEAMS and pure water and optimized geometries of DFT-calculated TEAMS/water aggregates (PDF)

AUTHOR INFORMATION

Corresponding Authors

Dietmar Paschek – Institut für Chemie, Abteilung Physikalische und Theoretische Chemie, Universität Rostock, D-18059 Rostock, Germany; orcid.org/0000-0002-0342-324X; Email: dietmar.paschek@uni-rostock.de

Ralf Ludwig – Institut für Chemie, Abteilung Physikalische und Theoretische Chemie, Universität Rostock, D-18059 Rostock, Germany; Leibniz Institut für Katalyse an der Universität Rostock, D-18059 Rostock, Germany;

orcid.org/0000-0002-8549-071X; Email: ralf.ludwig@uni-rostock.de

Authors

Benjamin Golub – Institut für Chemie, Abteilung Physikalische und Theoretische Chemie, Universität Rostock, D-18059 Rostock, Germany

Koichi Fumino – Institut für Chemie, Abteilung Physikalische und Theoretische Chemie, Universität Rostock, D-18059 Rostock, Germany

Peter Stange – Institut für Chemie, Abteilung Physikalische und Theoretische Chemie, Universität Rostock, D-18059 Rostock, Germany

Verlaine Fossog – Transfercenter Sustainable Electrochemistry, Saarland University and KIST Europe, D-66123 Saarbrücken, Germany

Rolf Hempelmann – Transfercenter Sustainable Electrochemistry, Saarland University and KIST Europe, D-66123 Saarbrücken, Germany; orcid.org/0000-0002-0607-3302

Daniel Ondo – Department of Physical Chemistry, University of Chemistry and Technology, CZ-166 28 Prague 6, Czech Republic

Complete contact information is available at:

<https://pubs.acs.org/doi/10.1021/acs.jpcb.1c01850>

Notes

The authors declare no competing financial interest.

ACKNOWLEDGMENTS

This work was supported by the Deutsche Forschungsgemeinschaft (DFG SFB 652, “Strong correlations and collective effects in radiation fields: Coulomb systems, clusters and particles”, Project No. 5486320). R.L. gratefully acknowledges the support of the Leibniz-Institute for Catalysis.

REFERENCES

- (1) Marcus, Y.; Hefter, G. Ion Pairing. *Chem. Rev.* **2006**, *106*, 4585–4621.
- (2) Fritz, J. S.; Gjerde, D. T. *Ion Chromatography*, 4th ed.; Wiley-VCH: Weinheim, 2009.
- (3) Zugmann, S.; Fleischmann, M.; Amereller, M.; Gschwind, R. M.; Winter, M.; Gores, H. J. Salt Diffusion Coefficients, Concentration Dependence of Cell Potentials, and Transference Numbers of Lithium Difluoromono(oxalato)borate-Based Solutions. *J. Chem. Eng. Data* **2011**, *56*, 4786–4789.
- (4) Kapoor, I.; Schön, E.-M.; Bachl, J.; Kühbeck, D.; Cativiela, C.; Saha, S.; Banerjee, R.; Roelens, S.; Marrero-Tellado, J. J.; Díaz, D. D. Competition between gelation and crystallisation of a peculiar multicomponent liquid system based on ammonium salts. *Soft Matter* **2012**, *8*, 3446–3456.
- (5) Smid, J. Structure of ion-pair solvation complexes. *Angew. Chem., Int. Ed.* **1972**, *11*, 112–127.
- (6) *Ions and Ion Pairs in Organic Reactions*; Szwarc, M., Ed.; John Wiley & Sons Inc., 1972; Vol. 1.
- (7) *Ions and Ion Pairs in Organic Reactions*; Szwarc, M., Ed.; John Wiley & Sons Inc., 1974; Vol. 2.
- (8) Reichardt, C.; Welton, T. *Solvents and Solvent Effects in Organic Chemistry*, 4th ed.; Wiley-VCH: Weinheim, 2010.
- (9) Dupont, J. On the solid, liquid and solution structural organization of imidazolium ionic liquids. *J. Braz. Chem. Soc.* **2004**, *15*, 341–350.
- (10) Huang, M.-M.; Schneiders, K.; Schulz, P. S.; Wasserscheid, P.; Weingärtner, H. Ion speciation driving chirality transfer in

imidazolium-based camphorsulfonate ionic liquid solutions. *Phys. Chem. Chem. Phys.* **2011**, *13*, 4126–4131.

(11) Hunger, J.; Stoppa, A.; Buchner, R.; Hefter, G. From Ionic Liquid to Electrolyte Solution: Dynamics of 1-N-Butyl-3-N-methylimidazolium Tetrafluoroborate/Dichloromethane Mixtures. *J. Phys. Chem. B* **2008**, *112*, 12913–12919.

(12) Jiang, Y.; Nadolny, H.; Käshammer, S.; Weibels, S.; Schröer, W.; Weingärtner, H. The ion speciation of ionic liquids in molecular solvents of low and medium polarity. *Faraday Discuss.* **2012**, *154*, 391–407.

(13) Plechkova, N. V.; Seddon, K. R. Applications of ionic liquids in the chemical industry. *Chem. Soc. Rev.* **2008**, *37*, 123–150.

(14) Marcus, Y. *Ionic Liquid Properties*; Springer, 2016.

(15) *The Structure of Ionic Liquids*; Caminiti, R.; Gontrani, L., Eds.; Springer, 2014.

(16) *Ionic Liquids: Current State and Future Directions*; Shiflett, M. B.; Scurto, A. M., Eds.; ACS Symposium Series; American Chemical Society, 2017; Vol. 1250.

(17) Podgoršek, A.; Jaquemin, J.; Pádua, A. A. H.; Costa Gomes, M. F. Mixing Enthalpy for Binary Mixtures Containing Ionic Liquids. *Chem. Rev.* **2016**, *116*, 6075–6106.

(18) Fumino, K.; Peppel, T.; Geppert-Rybczynska, M.; Zaitsau, D. H.; Lehmann, J. K.; Verevkin, S. P.; Köckerling, M.; Ludwig, R. The influence of hydrogen bonding on the physical properties of ionic liquids. *Phys. Chem. Chem. Phys.* **2011**, *13*, 14064–14075.

(19) Peppel, T.; Roth, C.; Fumino, K.; Paschek, D.; Köckerling, M.; Ludwig, R. The Influence of Hydrogen-Bond Defects on the Properties of Ionic Liquids. *Angew. Chem., Int. Ed.* **2011**, *50*, 6661–6665.

(20) Fumino, K.; Ludwig, R. Analyzing the interaction energies between cation and anion in ionic liquids: The subtle balance between Coulomb forces and hydrogen bonding. *J. Mol. Liq.* **2014**, *192*, 94–102.

(21) Fumino, K.; Reimann, S.; Ludwig, R. Probing molecular interaction in ionic liquids by low frequency spectroscopy: Coulomb energy, hydrogen bonding and dispersion forces. *Phys. Chem. Chem. Phys.* **2014**, *40*, 21903–21929.

(22) Zaitsau, D. H.; Neumann, J.; Niemann, T.; Strate, A.; Paschek, D.; Verevkin, S. P.; Ludwig, R. Isolating the Role of Hydrogen Bonding in Hydroxyl-Functionalized Ionic Liquids by Means of Vaporization Enthalpies, Infrared Spectroscopy and Molecular Dynamics Simulations. *Phys. Chem. Chem. Phys.* **2019**, *21*, 20308–20314.

(23) Zaitsau, D. H.; Emel'yanenko, V. N.; Stange, P.; Verevkin, S. P.; Ludwig, R. Dissecting the Vaporization Enthalpies of Ionic Liquids by Exclusively Experimental Methods: Coulomb Interaction, Hydrogen Bonding, and Dispersion Forces. *Angew. Chem., Int. Ed.* **2019**, *58*, 8589–8592.

(24) Zaitsau, D. H.; Emel'yanenko, V. N.; Stange, P.; Schick, C.; Verevkin, S. P.; Ludwig, R. Dispersion and Hydrogen Bonding Rule: Why the Vaporization Enthalpies of Aprotic Ionic Liquids are Significantly Larger than those of Protic Ionic liquids. *Angew. Chem., Int. Ed.* **2016**, *55*, 11682–11686.

(25) Stassen, H. K.; Ludwig, R.; Wulf, A.; Dupont, J. Imidazolium Salts Ion Pairs in Solution. *Chem. - Eur. J.* **2015**, *21*, 8324–8335.

(26) Köddermann, T.; Klemmt, S.; Klasen, D.; Paschek, D.; Kragl, U.; Ludwig, R. The Effect of Neutral Ion Aggregate Formation on the Electrical Conductivity of an Ionic Liquid and its Mixtures with Chloroform. *ChemPhysChem* **2012**, *13*, 1748–1752.

(27) Nordness, O.; Brennecke, J. F. Ion Dissociation in Ionic Liquids and Ionic Liquid Solutions. *Chem. Rev.* **2020**, *120*, 12873–12902.

(28) Greaves, T. L.; Drummond, C. J. Protic ionic liquids: Properties and applications. *Chem. Rev.* **2008**, *108*, 206–237.

(29) Angell, C. A.; Byrne, N.; Belieres, J.-P. Parallel developments in aprotic and protic ionic liquids: Physical chemistry and applications. *Acc. Chem. Res.* **2007**, *40*, 1228–1236.

(30) Xu, W.; Angell, C. A. Solvent-free electrolytes with aqueous solution – Like conductivities. *Science* **2003**, *302*, 422–425.

(31) Yoshizawa, M.; Xu, W.; Angell, C. A. Ionic liquids by proton transfer: Vapor pressure, conductivity, and the relevance of ΔpK_a from aqueous solutions. *J. Am. Chem. Soc.* **2003**, *125*, 15411–15419.

(32) Stoimenovski, J.; Izgorodina, E. I.; MacFarlane, D. R. Ionivity and proton transfer in protic ionic liquids. *Phys. Chem. Chem. Phys.* **2010**, *12*, 10341–10347.

(33) Fumino, K.; Wulf, A.; Ludwig, R. Hydrogen Bonding in Protic Ionic Liquids: Reminiscent of Water. *Angew. Chem., Int. Ed.* **2009**, *48*, 3184–3186.

(34) Fumino, K.; Reichert, E.; Wittler, K.; Hempelmann, R.; Ludwig, R. Low-Frequency Vibrational Modes of Protic Molten Salts and Ionic Liquids: Detecting and Quantifying Hydrogen Bonds. *Angew. Chem., Int. Ed.* **2012**, *51*, 6236–6240.

(35) Hayes, R.; Imberti, S.; Warr, G. G.; Atkin, R. How Water Dissolves in Protic Ionic Liquids. *Angew. Chem., Int. Ed.* **2012**, *51*, 7468–7471.

(36) Fumino, K.; Fossog, V.; Stange, P.; Wittler, K.; Polet, W.; Hempelmann, R.; Ludwig, R. Ion Pairing in Protic Ionic Liquids Probed by Far-Infrared Spectroscopy: Effects of Solvent Polarity and Temperature. *ChemPhysChem* **2014**, *15*, 2604–2609.

(37) Fumino, K.; Stange, P.; Fossog, V.; Hempelmann, R.; Ludwig, R. Equilibrium of Contact and Solvent-Separated Ion-Pairs in Mixtures of Protic Ionic Liquids and Molecular Solvents Controlled by Polarity. *Angew. Chem., Int. Ed.* **2013**, *52*, 12439–12442.

(38) Fumino, K.; Bonsa, A.-M.; Golub, B.; Paschek, D.; Ludwig, R. Non-Ideal Mixing Behaviour of Hydrogen Bonding in Mixtures of Protic Ionic Liquids. *ChemPhysChem* **2015**, *16*, 299–304.

(39) Fumino, K.; Wulf, A.; Ludwig, R. The cation–anion interaction in ionic liquids probed by far-infrared spectroscopy. *Angew. Chem., Int. Ed.* **2008**, *47*, 3830–3834.

(40) Fumino, K.; Wulf, A.; Ludwig, R. Strong, Localized, and Directional Hydrogen Bonds Fluidize Ionic Liquids. *Angew. Chem., Int. Ed.* **2008**, *47*, 8731–8734.

(41) Roth, C.; Peppel, T.; Fumino, K.; Köckerling, M.; Ludwig, R. The Importance of Hydrogen Bonds for the Structure of Ionic Liquids: Single-Crystal X-ray Diffraction and Transmission and Attenuated Total Reflection Spectroscopy in the Terahertz Region. *Angew. Chem., Int. Ed.* **2010**, *49*, 10221–10224.

(42) Wulf, A.; Fumino, K.; Ludwig, R.; Taday, P. F. Combined THz, FIR and Raman Spectroscopy Studies of Imidazolium-Based Ionic Liquids Covering the Frequency Range 2–300 cm^{-1} . *ChemPhysChem* **2010**, *11*, 349–353.

(43) Wulf, A.; Fumino, K.; Ludwig, R. Spectroscopic Evidence for an Enhanced Anion-Cation Interaction from Hydrogen Bonding in Pure Imidazolium Ionic Liquids. *Angew. Chem., Int. Ed.* **2010**, *49*, 449–453.

(44) Fumino, K.; Wulf, A.; Verevkin, S. P.; Heintz, A.; Ludwig, R. Estimating Enthalpies of Vaporization of Imidazolium-Based Ionic Liquids from Far-Infrared Measurements. *ChemPhysChem* **2010**, *11*, 1623–1626.

(45) Kumari, P.; Pillai, V. V. S.; Gobbo, D.; Ballone, P.; Benedetto, A. The transition from salt-in-water to water-in-salt nanostructures in water solutions of organic ionic liquids relevant for biological applications. *Phys. Chem. Chem. Phys.* **2021**, *23*, 944–959.

(46) Frisch, M. J.; Trucks, G. W.; Schlegel, H. B.; Scuseria, G. E.; Robb, M. A.; Cheeseman, J. R.; Scalmani, G.; Barone, V.; Mennucci, B.; Petersson, G. A.; et al. *Gaussian 09*, revision E.01; Gaussian Inc.: Wallingford, CT, 2009.

(47) Boys, S. F.; Bernardi, F. Calculation of small molecular interactions by differences of separate total energies—some procedures with reduced errors. *Mol. Phys.* **1970**, *19*, 553–566.

(48) Paschek, D.; Golub, B.; Ludwig, R. Hydrogen bonding in a mixture of protic ionic liquids: a molecular dynamics simulation study. *Phys. Chem. Chem. Phys.* **2015**, *17*, 8431–8440.

(49) Abascal, J. L. F.; Vega, C. A general purpose model for the condensed phases of water: TIP4P/2005. *J. Chem. Phys.* **2005**, *123*, No. 234505.

(50) Nosé, S. A molecular dynamics method for simulating in the canonical ensemble. *Mol. Phys.* **1984**, *52*, 255–268.

- (51) Hoover, W. G. Canonical Dynamics: Equilibrium Phase space distributions. *Phys. Rev. A* **1985**, *31*, No. 1695.
- (52) Parrinello, M.; Rahman, A. Polymorphic transitions in single crystals: A new molecular dynamics method. *J. Appl. Phys.* **1981**, *52*, 7182–7180.
- (53) Nosé, S.; Klein, M. L. Constant pressure molecular dynamics for molecular systems. *Mol. Phys.* **1983**, *50*, 1055–1076.
- (54) Essmann, U.; Perera, L.; Berkowitz, M. L.; Darden, T. A.; Lee, H.; Pedersen, L. G. A smooth particle mesh Ewald method. *J. Chem. Phys.* **1995**, *103*, 8577–8593.
- (55) Humphrey, W.; Dalke, A.; Schulten, K. VMD-Visual Molecular Dynamics. *J. Mol. Graphics* **1996**, *14*, 33–38.
- (56) Hess, B.; Bekker, H.; Berendsen, H. J. C.; Fraaije, J. G. E. M. LINCS: A linear constraint solver for molecular simulations. *J. Comput. Chem.* **1997**, *18*, 1463–1472.
- (57) Miyamoto, S.; Kollman, P. A. Settle: An analytical version of the SHAKE and RATTLE algorithm for rigid water models. *J. Comput. Chem.* **1992**, *13*, 952–962.
- (58) Lindahl, E.; Hess, B.; van der Spoel, D. Gromacs 3.0: A package for molecular simulation and trajectory analysis. *J. Mol. Model.* **2001**, *7*, 306–317.
- (59) Abraham, M.; Apol, E.; Apostolov, R.; Berendsen, H. J.; van Buuren, A.; Bjelkmar, P.; van Drunen, R.; Feenstra, A.; Fritsch, S.; Groenhof, G.; et al. *GROMACS—Groningen Machine for Chemical Simulations User Manual*, version 4.6.1, 2013.
- (60) Berendsen, H. J. C.; Postma, J. P. M.; van Gunsteren, W. F.; DiNola, A.; Haak, J. R. Molecular dynamics with coupling to an external bath. *J. Chem. Phys.* **1984**, *81*, 3684–3690.
- (61) Fumino, K.; Fossog, V.; Wittler, K.; Hempelmann, R.; Ludwig, R. Dissecting Anion-Cation Interaction Energies in Protic Ionic Liquids. *Angew. Chem., Int. Ed.* **2013**, *52*, 2368–2372.
- (62) Stange, P.; Fumino, K.; Ludwig, R. Ion Speciation of Protic Ionic Liquids in Water: Transition from Contact to Solvent-Separated Ion Pairs. *Angew. Chem., Int. Ed.* **2013**, *52*, 2990–2994.
- (63) Fumino, K.; Stange, P.; Fossog, V.; Hempelmann, R.; Ludwig, R. Equilibrium of Contact and Solvent-Separated Ion Pairs in Mixtures of Protic Ionic Liquids and Molecular Solvents Controlled by Polarity. *Angew. Chem., Int. Ed.* **2013**, *52*, 12439–12442.
- (64) Gaiduk, V. I.; Vij, J. K. The concept of two stochastic processes in liquid water and analytical theory of the complex permittivity in the wavenumber range 0–1000 cm^{−1}. *Phys. Chem. Chem. Phys.* **2001**, *3*, 5173–5181.
- (65) Gaiduk, V. I.; Crothers, C. S. F. Nonharmonic transverse vibration of the H-bonded molecules and the THz spectra in ice and water. *J. Mol. Liq.* **2006**, *128*, 145–160.
- (66) Brubach, J. B.; Mermet, A.; Filabozzi, A.; Gerschel, A.; Roy, P. Signatures of the hydrogen bonding in the infrared bands of water. *J. Chem. Phys.* **2005**, *122*, No. 184509.
- (67) Dominguez-Vidal, A.; Kaun, N.; Ayora-Canada, M. J.; Lendl, B. Probing intermolecular interactions in water/ionic liquid mixtures by far-infrared spectroscopy. *J. Phys. Chem. B* **2007**, *111*, 4446–4452.
- (68) Cammarata, L.; Kazarian, S. G.; Salter, P. A.; Welton, T. Molecular states of water in room temperature ionic liquids. *Phys. Chem. Chem. Phys.* **2001**, *3*, 5192–5200.
- (69) Burba, C. M.; Rocher, N. M.; Frech, R.; Powell, D. R. Cation–Anion Interactions in 1-Ethyl-3-Methylimidazolium Trifluoromethanesulfonate-Based Ionic Liquid Electrolytes. *J. Phys. Chem. B* **2008**, *112*, 2991–2995.
- (70) Burba, C. M.; Frech, R. Existence of Optical Phonons in the Room Temperature Ionic Liquid 1-Ethyl-3-Methylimidazolium Trifluoromethanesulfonate. *J. Chem. Phys.* **2011**, *134*, No. 134503.
- (71) Dang, L. X. Temperature dependence of interactions of an ion pair in water: A molecular dynamics study. *J. Chem. Phys.* **1992**, *97*, 1919–1921.
- (72) Smith, D. E.; Dang, L. X. Computer simulations of NaCl association in polarizable water. *J. Chem. Phys.* **1994**, *100*, 3757–3766.
- (73) Lyubartsev, A. P.; Laaksonen, A. Concentration Effects in Aqueous NaCl Solutions. A Molecular Dynamics Simulation. *J. Phys. Chem. A* **1996**, *100*, 16410–16418.

Supporting Information:

The Balance Between Contact and Solvent-Separated Ion-Pairs in Mixtures of the Protic Ionic Liquid [Et₃NH][Me₃SO₃] (TEAMS) with Water Controlled by Water-Content and Temperature

Benjamin Golub[•], Koichi Fumino[†], Peter Stange[†], Verlaïne Fossog[§], Rolf Hempelmann[§], Daniel Ondo[‡], Dietmar Paschek^{•,*}, Ralf Ludwig^{†,‡,§,*}

[•] *Institut für Chemie, Abteilung Physikalische und Theoretische Chemie, Universität Rostock, Albert-Einstein-Straße 21, D-18059 Rostock, Germany*

[†] *Institut für Chemie, Abteilung Physikalische und Theoretische Chemie, Universität Rostock, Dr.-Lorenz-Weg 2, D-18059 Rostock, Germany*

[§] *Physikalische Chemie, Universität des Saarlandes, D-66123 Saarbrücken, Germany*

[‡] *Dept. Phys. Chem., Tech. 5, University of Chemistry & Technology, Prague 16628 6, Czech Republic*

[‡] *Department Life, Light & Matter, Universität Rostock, Albert-Einstein-Straße 25, D-18059 Rostock, Germany*

[§] *Leibniz Institut für Katalyse an der Universität Rostock, Albert-Einstein-Straße 29a, D-18059 Rostock, Germany*

^{*}**E-mail:** dietmar.paschek@uni-rostock.de, ralf.ludwig@uni-rostock.de

Contents

S1 Far infrared (FIR) Spectra of Pure [Et₃NH][Me₃SO₃] (TEAMS) and Pure Water	S2
S2 Optimized Geometries of DFT Calculated TEAMS/Water Aggregates	S3
S2.1 Cluster: “CIP”	S3
S2.2 Cluster: “CIP+1W”	S4
S2.3 Cluster: “CIP+2W”	S5
S2.4 Cluster: “CIP+3W”	S6
S2.5 Cluster: “CIP+4W”	S7
S2.6 Cluster: “SIP+4W”	S8
S2.7 Cluster: “CIP+5W”	S9
S2.8 Cluster: “SIP+5W”	S10
S2.9 Cluster: “CIP+6W”	S11
S2.10 Cluster: “SIP+6W”	S12
S2.11 Cluster: “CIP+7W”	S13
S2.12 Cluster: “SIP+7W”	S14
S2.13 Cluster: “CIP+9W”	S15
S2.14 Cluster: “SIP+9W”	S16

S1 Far infrared (FIR) Spectra of Pure $[\text{Et}_3\text{NH}][\text{Me}_3\text{SO}_3]$ (TEAMS) and Pure Water

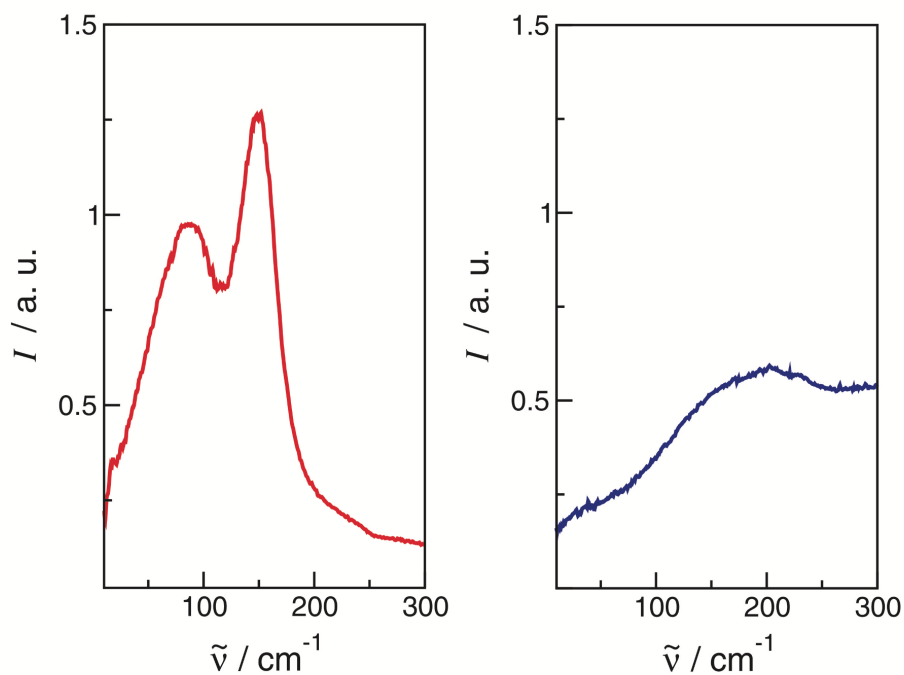


Figure S1: Far infrared (FIR) spectra of pure triethylammonium methanesulfonate $[\text{Et}_3\text{NH}][\text{Me}_3\text{SO}_3]$ (left) and pure water H_2O (right) in the frequency range between 10 and 300 cm^{-1} .

S2 Optimized Geometries of DFT Calculated TEAMS/Water Aggregates

S2.1 Cluster: "CIP"

*** TEAM_CH3SO3_1_b3lyp_6-31+Gp.g03, E(RB+HF-LYP) = -956.781493074, 05.02.2010

```
0 1
  6      0      2.935207   -0.934249   -1.716046
  6      0      1.598752   -0.979719   -0.983155
  7      0      1.375312    0.131582    0.016553
  8      0     -1.015230   -0.522023    0.980817
16     0     -2.078158   -0.093893   -0.032658
  6      0     -3.371192   -1.345644    0.116023
  6      0      1.264919    1.477115   -0.665897
  6      0      2.338454    0.139308    1.169832
  1      0      0.403878   -0.088150    0.429329
  1      0      1.486135   -1.914923   -0.430738
  1      0      0.749195   -0.912532   -1.667045
  1      0      2.978085   -1.785936   -2.403620
  1      0      3.053360   -0.026878   -2.316649
  1      0      3.793104   -1.018080   -1.039514
  1      0      2.013500    0.948872    1.825264
  6      0      2.356602   -1.171930    1.951573
  1      0      3.329938    0.396645    0.782686
  6      0      0.704984    2.581678    0.227580
  1      0      2.258832    1.735898   -1.044500
  1      0      0.590030    1.312812   -1.508923
  1      0      0.553603    3.470759   -0.394441
  1      0     -0.268832    2.306451    0.643834
  1      0      1.384413    2.864063    1.038420
  1      0      2.946842   -1.027262    2.862889
  1      0      1.343876   -1.466431    2.245895
  1      0      2.814527   -1.992383    1.390368
  8      0     -2.693542    1.207834    0.310004
  8      0     -1.530422   -0.196015   -1.420010
  1      0     -4.159937   -1.094753   -0.596593
  1      0     -2.942972   -2.323532   -0.113166
  1      0     -3.757041   -1.321151    1.137224
```

S2.2 Cluster: "CIP+1W"

*** TEAM_CH3S03_1_w_1_b3lyp_6-31+Gp.g09, E(RB3LYP) = -1033.22504754, 04.10.2012

0 1

6	0	2.882598	0.077686	-1.932709
6	0	1.495386	0.091360	-1.300331
7	0	1.483559	-0.119742	0.200808
6	0	2.080266	-1.427519	0.648230
6	0	1.475475	-2.641194	-0.052892
6	0	2.053907	1.070231	0.939469
6	0	1.740487	1.057878	2.434162
8	0	-1.079298	-0.269518	1.039591
16	0	-2.097762	-0.210584	-0.088259
8	0	-1.737628	-1.134184	-1.195012
6	0	-3.635459	-0.808885	0.639941
8	0	-2.368165	1.199554	-0.508950
1	0	0.455467	-0.164543	0.476319
1	0	0.846707	-0.678676	-1.722019
1	0	1.001560	1.053388	-1.458756
1	0	2.766632	0.258971	-3.006761
1	0	3.531501	0.867411	-1.539666
1	0	3.395800	-0.883551	-1.819131
1	0	1.890106	-1.490220	1.721218
1	0	3.163534	-1.367068	0.499822
1	0	3.132715	1.087171	0.755479
1	0	1.595303	1.945697	0.472778
1	0	2.038131	2.025053	2.853706
1	0	0.666885	0.931288	2.605193
1	0	2.284754	0.282018	2.982615
1	0	1.821139	-3.546258	0.458671
1	0	0.382204	-2.617175	-0.014130
1	0	1.780852	-2.715454	-1.100876
1	0	-4.405337	-0.776498	-0.133869
1	0	-3.478752	-1.833431	0.983389
1	0	-3.900591	-0.156114	1.473882
1	0	-1.001331	2.339124	-0.628952
8	0	-0.175636	2.879556	-0.712982
1	0	-0.458127	3.725809	-1.088814

S2.3 Cluster: "CIP+2W"

*** TEAM_CH3S03_2_w_2_b3lyp_6-31+Gp.g09, E(RB3LYP) = -2066.46349893, 21.07.2012

```
O 1
C      2.575818      0.033391     -1.931117
C      1.211945     -0.054224     -1.255381
N      1.149320      0.571185      0.124135
C      1.247267      2.078989      0.061810
C      0.836749      2.763413      1.363935
C      2.096487     -0.036207      1.124373
C      1.970655     -1.553566      1.234536
O     -1.288109      0.096694      1.186222
S     -2.178719     -0.772833      0.312422
O     -2.852870      0.031395     -0.754032
O     -1.454679     -1.974924     -0.175816
C     -3.495923     -1.339144      1.406505
O     -1.306221      1.932886     -2.043770
H      0.171482      0.360580      0.490694
H      0.880196     -1.087474     -1.137481
H      0.449843      0.465902     -1.841153
H      2.493486     -0.429128     -2.920662
H      2.903736      1.067051     -2.083562
H      3.359514     -0.503824     -1.385706
H      1.851936      0.423565      2.083645
H      3.111291      0.271337      0.850986
H      2.274642      2.331981     -0.218298
H      0.570649      2.378517     -0.742573
H      0.774116      3.841237      1.178434
H     -0.149511      2.418739      1.690107
H      1.555775      2.612510      2.175856
H      2.546609     -1.887943      2.104474
H      0.928020     -1.855752      1.372078
H      2.365899     -2.072052      0.355904
H     -4.171504     -1.964288      0.818860
H     -3.046636     -1.915857      2.217523
H     -4.021762     -0.465445      1.796385
H     -1.918843      1.293330     -1.600418
H     -1.814462      2.312573     -2.775020
H     -0.629639     -3.448929     -0.797603
O     -0.222232     -4.235280     -1.141364
H     -0.835271     -4.726579     -1.675506
```

S2.4 Cluster: "CIP+3W"

*** TEAM_CH3S03_1_w_3_b3lyp_6-31+Gp.g09, E(RB3LYP) = -1186.10192382, 2.10.2012

0 1

6	0	3.294388	1.778537	-0.068499
6	0	1.838790	1.331180	0.010869
7	0	1.651111	-0.166772	0.182788
6	0	2.236274	-1.003111	-0.933607
6	0	1.810826	-0.550752	-2.325915
6	0	2.104869	-0.632486	1.551210
6	0	1.642245	-2.044020	1.901184
8	0	-1.072939	-0.810436	0.143986
16	0	-2.234670	0.166844	0.064354
6	0	-3.711077	-0.828575	0.346199
8	0	-2.182651	1.165962	1.169451
8	0	-2.380719	0.750731	-1.297932
8	0	0.032919	1.612338	2.793317
8	0	-0.273754	2.227368	-2.429640
1	0	0.615449	-0.321421	0.154725
1	0	1.284220	1.617215	-0.886414
1	0	1.337820	1.781929	0.871248
1	0	3.303936	2.866522	-0.195491
1	0	3.859507	1.553406	0.842274
1	0	3.824442	1.347884	-0.924775
1	0	1.882231	-2.020974	-0.764822
1	0	3.323950	-0.979168	-0.812509
1	0	3.195820	-0.554697	1.569557
1	0	1.681609	0.086055	2.257220
1	0	1.908860	-2.237288	2.946319
1	0	0.556618	-2.137943	1.807316
1	0	2.112958	-2.818398	1.289103
1	0	2.165505	-1.296955	-3.045403
1	0	0.722576	-0.492943	-2.413517
1	0	2.224397	0.420024	-2.610365
1	0	-4.572159	-0.157662	0.319130
1	0	-3.784627	-1.576155	-0.446164
1	0	-3.623921	-1.305180	1.324523
1	0	-0.785645	1.457431	2.264645
1	0	-0.230275	2.208370	3.509365
1	0	-1.056014	1.746909	-2.074073
1	0	-0.593068	3.119245	-2.628904
1	0	-0.720028	-2.422769	-0.683690
8	0	-0.247592	-3.217948	-1.013336
1	0	-0.737233	-3.514302	-1.793891

S2.5 Cluster: "CIP+4W"

*** TEAM_CH3S03_1_w_4_b3lyp_6-31+Gp.g09, -1262.54391857, 02.10.2012

0 1

6	0	-3.275783	1.796586	1.124287
6	0	-1.961103	1.028297	1.073040
7	0	-1.827088	0.092169	-0.110834
6	0	-2.845967	-1.025992	-0.143266
6	0	-2.910300	-1.835731	1.147647
6	0	-1.775644	0.855564	-1.423077
6	0	-1.136442	0.058781	-2.555663
8	0	0.475681	-1.421861	0.364054
16	0	1.904224	-0.928879	0.516924
8	0	2.505857	-0.562531	-0.797315
8	0	2.018666	0.114239	1.573682
6	0	2.826838	-2.353822	1.122256
8	0	-0.778394	-3.306862	-1.289750
8	0	0.966073	2.662337	1.909410
1	0	-0.898224	-0.373636	0.016779
1	0	-1.821963	0.417228	1.966936
1	0	-1.113971	1.712575	1.012756
1	0	-3.256075	2.442306	2.008524
1	0	-3.409408	2.444263	0.252509
1	0	-4.148112	1.139998	1.214326
1	0	-2.544460	-1.679286	-0.963382
1	0	-3.811180	-0.571906	-0.386289
1	0	-2.805111	1.138590	-1.662047
1	0	-1.184685	1.757801	-1.230185
1	0	-1.105636	0.703799	-3.440876
1	0	-0.106674	-0.217455	-2.308805
1	0	-1.687744	-0.849056	-2.817492
1	0	-3.539909	-2.713506	0.968586
1	0	-1.918459	-2.194721	1.438736
1	0	-3.346993	-1.275324	1.980484
1	0	3.864707	-2.043608	1.259501
1	0	2.389330	-2.667539	2.071928
1	0	2.760521	-3.152587	0.380830
1	0	1.381261	1.773882	1.808457
1	0	-0.171235	-2.740791	-0.764579
1	0	-0.245471	-3.665936	-2.013763
1	0	2.725519	1.120371	-1.463175
8	0	2.752738	2.027794	-1.843758
1	0	1.169177	2.880000	-1.293583
8	0	0.352148	3.159984	-0.827808
1	0	0.603850	3.162165	0.119112
1	0	3.035618	1.923602	-2.763360
1	0	1.635610	3.218756	2.333669

S2.6 Cluster: "SIP+4W"

*** TEAM_CH3S03_1_w_4_b3lyp_6-31+Gp_neu.g09, E(RB3LYP) = -1262.54848324, 02.10.2012

0 1

6	0	-2.100123	-2.074907	-1.697144
6	0	-1.559477	-0.745224	-1.189862
7	0	-2.255237	-0.213035	0.049331
6	0	-2.091483	-1.136157	1.242480
6	0	-2.091819	-0.386794	2.572201
6	0	-3.702642	0.150129	-0.162159
6	0	-3.923683	1.231103	-1.215927
8	0	2.785793	1.078022	0.732508
16	0	2.749707	-0.124288	-0.161742
8	0	1.768774	0.028547	-1.293035
6	0	4.383077	-0.199834	-0.924850
8	0	2.580477	-1.414260	0.569930
8	0	0.401093	-3.118609	0.556442
8	0	0.780181	1.896652	2.381275
8	0	0.309758	2.237413	-1.918537
1	0	-1.759659	0.701823	0.268930
1	0	-1.637941	0.038417	-1.946569
1	0	-0.501972	-0.828322	-0.930169
1	0	-1.528143	-2.349909	-2.589540
1	0	-1.955847	-2.875807	-0.966946
1	0	-3.156457	-2.024797	-1.985511
1	0	-4.066466	0.497681	0.807743
1	0	-4.238154	-0.770849	-0.409875
1	0	-2.907819	-1.864076	1.192331
1	0	-1.155743	-1.684153	1.107406
1	0	-2.011958	-1.123230	3.379505
1	0	-1.234515	0.288356	2.654401
1	0	-3.010332	0.187125	2.740453
1	0	-4.980161	1.521282	-1.198535
1	0	-3.322541	2.119622	-1.001298
1	0	-3.694745	0.884528	-2.227995
1	0	4.399514	-1.050082	-1.609759
1	0	4.558114	0.733532	-1.463882
1	0	5.121845	-0.329416	-0.131376
1	0	1.186690	-2.520969	0.516562
1	0	0.724094	-3.923696	0.986238
1	0	0.920023	1.478086	-1.723558
1	0	0.879790	2.981607	-2.160634
1	0	1.536206	1.542480	1.842179
1	0	1.151462	2.614711	2.914260
1	0	-0.593209	2.387614	-0.395713
8	0	-1.120164	2.239172	0.428756
1	0	-0.461123	2.242919	1.166764

S2.7 Cluster: "CIP+5W"

*** TEAM_CH3S03_1_w_5_b3lyp_6-31+Gp.g09, E(RB3LYP) = -1338.97994346, 02.10.2012

0 1

6	0	-3.671782	-1.369992	-1.323640
6	0	-2.430219	-0.570155	-0.946560
7	0	-1.490292	-1.274351	0.017523
6	0	-2.118231	-1.618899	1.345722
6	0	-2.736210	-0.424014	2.064536
6	0	-0.808934	-2.459997	-0.633808
6	0	0.314692	-3.059377	0.206964
8	0	0.445692	0.616813	0.691722
16	0	0.432315	1.895471	-0.148997
8	0	0.040733	1.594176	-1.553317
8	0	-0.372784	2.965580	0.501505
6	0	2.141856	2.459939	-0.180232
8	0	1.085285	-0.853030	-2.662223
8	0	2.130326	-0.396657	2.557818
8	0	4.279638	-1.295942	1.109351
8	0	3.684977	-0.474859	-1.463600
8	0	-3.157671	2.490782	0.347570
1	0	-0.736836	-0.570428	0.221027
1	0	-2.701990	0.383335	-0.487119
1	0	-1.821472	-0.341928	-1.823186
1	0	-4.255480	-0.766696	-2.027205
1	0	-3.437392	-2.315631	-1.823223
1	0	-4.318271	-1.576873	-0.464064
1	0	-1.317050	-2.040628	1.955054
1	0	-2.851927	-2.409654	1.160539
1	0	-1.584106	-3.201198	-0.847470
1	0	-0.385949	-2.079527	-1.568453
1	0	0.855535	-3.775900	-0.420653
1	0	1.029468	-2.291649	0.519008
1	0	-0.040368	-3.596772	1.092138
1	0	-3.068312	-0.756214	3.054734
1	0	-2.004364	0.377149	2.202322
1	0	-3.597662	-0.002261	1.541895
1	0	2.173972	3.363854	-0.792612
1	0	2.455330	2.684322	0.841688
1	0	2.754629	1.668014	-0.619145
1	0	-2.209253	2.742153	0.428906
1	0	-3.546880	3.167260	-0.225282
1	0	1.525758	0.066750	1.922845
1	0	2.246157	0.200398	3.311387
1	0	3.548076	-0.964131	1.688749
1	0	4.363543	-2.241298	1.301198
1	0	3.937844	-0.816969	-0.571291
1	0	4.504011	-0.421395	-1.977049
1	0	0.756892	0.040387	-2.435247
1	0	2.004492	-0.851488	-2.326694

S2.8 Cluster: "SIP+5W"

*** TEAM_CH3S03_1_w_5_b3lyp_6-31+Gp_neu_1.g09, E(RB3LYP) = -1338.99439613, 02.10.2012

0 1

6	0	-1.463604	0.656135	2.661895
6	0	-1.106990	0.259230	1.235270
7	0	-2.282540	-0.175126	0.377995
6	0	-3.196359	0.988932	0.054641
6	0	-4.211966	0.673392	-1.041183
6	0	-3.031020	-1.367499	0.914385
6	0	-2.143363	-2.566579	1.237272
8	0	-1.237616	-0.958592	-2.050373
8	0	0.386669	-3.025157	-1.235862
8	0	1.806554	-1.500823	0.513967
16	0	2.688326	-0.308011	0.276554
6	0	4.364379	-0.841720	0.675803
1	0	4.630534	-1.668067	0.013577
8	0	2.384609	0.817743	1.210900
8	0	2.735518	0.101295	-1.166821
1	0	5.036856	0.004783	0.522912
1	0	4.378914	-1.162412	1.719324
8	0	0.680434	0.980716	-2.691182
8	0	1.204234	3.302665	0.932466
8	0	-0.765302	2.846477	-1.031096
1	0	-1.856359	-0.471761	-0.544788
1	0	-0.382609	-0.556429	1.216263
1	0	-0.665441	1.100756	0.699998
1	0	-0.536576	0.960003	3.158436
1	0	-2.148851	1.508931	2.702677
1	0	-1.893452	-0.169721	3.239780
1	0	-3.755214	-1.640722	0.144472
1	0	-3.586917	-1.030112	1.794999
1	0	-3.693493	1.280737	0.984494
1	0	-2.531533	1.797012	-0.266323
1	0	-4.703277	1.609173	-1.328888
1	0	-3.721764	0.265322	-1.931302
1	0	-4.994002	-0.021808	-0.718263
1	0	-2.791664	-3.412170	1.493797
1	0	-1.525988	-2.865021	0.384207
1	0	-1.484630	-2.384081	2.090942
1	0	1.669855	2.435434	1.005980
1	0	1.899395	3.968410	0.831033
1	0	0.993450	-2.511878	-0.641693
1	0	0.954996	-3.521665	-1.842248
1	0	1.451901	0.685513	-2.133610
1	0	1.034401	1.158020	-3.575210
1	0	-0.674236	-1.755807	-1.895430
1	0	-0.617453	-0.275015	-2.394292
1	0	-0.091455	3.155070	-0.386166
1	0	-0.258084	2.345634	-1.699995

S2.9 Cluster: "CIP+6W"

*** TEAM_CH3S03_1_w_6_b3lyp_6-31+Gp.g09, E(RB3LYP) = -1415.41927822, 02.10.2012

0 1

6	0	-3.906432	-1.686264	-0.803781
6	0	-2.638423	-0.842194	-0.748356
7	0	-1.663696	-1.243721	0.346675
6	0	-1.041514	-2.597876	0.072428
6	0	0.220577	-2.859012	0.888832
6	0	-2.225794	-1.144886	1.743991
6	0	-2.762278	0.237036	2.101495
8	0	0.332086	0.715742	0.428155
16	0	0.287703	1.880945	-0.561851
8	0	-0.604249	2.971312	-0.074187
6	0	1.960733	2.548748	-0.578580
8	0	-0.013703	1.398102	-1.934911
8	0	0.233869	-1.389252	-2.562263
8	0	1.509163	0.496761	2.849314
8	0	-3.368763	2.460055	-0.359728
1	0	-0.889572	-0.538365	0.290311
1	0	-2.876634	0.213204	-0.593642
1	0	-2.066441	-0.925718	-1.674413
1	0	-4.514404	-1.321698	-1.638685
1	0	-3.704395	-2.746800	-0.987427
1	0	-4.515106	-1.594062	0.102089
1	0	-1.406533	-1.407984	2.415818
1	0	-2.996407	-1.916618	1.833893
1	0	-1.810353	-3.351344	0.267090
1	0	-0.789774	-2.583531	-0.990284
1	0	0.672124	-3.788956	0.527310
1	0	0.954514	-2.061300	0.740326
1	0	0.030540	-2.975411	1.960652
1	0	-3.056260	0.225169	3.157301
1	0	-1.994592	1.004846	1.970790
1	0	-3.632607	0.531067	1.510088
1	0	1.988982	3.333576	-1.337713
1	0	2.176548	2.968198	0.406605
1	0	2.657754	1.741775	-0.817291
1	0	0.225106	-0.414902	-2.467907
1	0	1.162016	-1.655105	-2.389822
1	0	-2.425849	2.724559	-0.260447
1	0	-3.677370	2.930030	-1.147930
1	0	1.056822	0.677506	1.983753
1	0	1.415086	1.301690	3.379886
1	0	3.123850	-0.037070	2.460479
8	0	4.006451	-0.373418	2.156705
1	0	4.087802	-1.267854	2.519184
1	0	4.164423	-0.248520	0.419816
8	0	4.243337	-0.147782	-0.564351
8	0	2.916613	-2.178267	-1.956714
1	0	3.416219	-1.464824	-1.493133
1	0	5.171270	0.072263	-0.732842
1	0	3.416226	-2.372228	-2.763283

S2.10 Cluster: "SIP+6W"

*** TEAM_CH3S03_1_w_6_b3lyp_6-31+Gp_neu_1.g09, E(RB3LYP) = -1415.43363836, 02.10.2012

0 1

6	0	2.194702	0.936071	-2.445399
6	0	1.530273	0.321509	-1.221057
7	0	2.494845	-0.191806	-0.166697
6	0	3.236263	0.948497	0.504793
6	0	3.875912	0.549282	1.832111
6	0	3.429301	-1.271749	-0.649164
6	0	2.731991	-2.434660	-1.349426
8	0	1.027768	-1.497133	1.779221
8	0	-0.352471	-3.245724	0.146929
8	0	-1.683277	-1.216974	-1.149102
16	0	-2.712811	-0.423692	-0.403072
6	0	-4.275771	-0.681882	-1.262623
1	0	-4.510217	-1.747884	-1.234196
8	0	-2.460206	1.056959	-0.451590
8	0	-2.931298	-0.924459	0.993272
1	0	-5.046070	-0.103618	-0.748588
1	0	-4.158602	-0.341097	-2.293299
8	0	-1.193823	-0.237613	2.967466
8	0	-1.451798	2.442869	1.916961
8	0	-0.778938	2.720555	-1.940468
8	0	0.833442	3.179037	0.435386
1	0	1.889188	-0.632686	0.577846
1	0	0.877306	-0.510752	-1.488790
1	0	0.922205	1.065612	-0.707167
1	0	1.398293	1.318355	-3.090957
1	0	2.833081	1.786566	-2.186070
1	0	2.783556	0.212697	-3.020725
1	0	3.954700	-1.631279	0.238058
1	0	4.163168	-0.792911	-1.304927
1	0	3.989005	1.304771	-0.204850
1	0	2.498242	1.744854	0.646669
1	0	4.258324	1.456609	2.312083
1	0	3.145617	0.092692	2.507684
1	0	4.719027	-0.139911	1.714988
1	0	3.475499	-3.218026	-1.534994
1	0	1.932520	-2.867799	-0.740940
1	0	2.309677	-2.144991	-2.316062
1	0	-1.395968	2.084025	-1.510122
1	0	-1.338009	3.436574	-2.276298
1	0	-0.898401	-2.577017	-0.339761
1	0	-0.986717	-3.855816	0.551453
1	0	-1.881084	-0.520049	2.305917
1	0	-1.528337	-0.494517	3.839703
1	0	0.531525	-2.208770	1.305472
1	0	0.338830	-1.007857	2.284200
1	0	-1.281881	1.661948	2.479469
1	0	0.104919	3.021465	1.079565
1	0	-1.936708	2.069191	1.153411
1	0	0.367165	3.238791	-0.422752

S2.11 Cluster: "CIP+7W"

*** TEAM_CH3S03_1_w_7_b3lyp_6-31+Gp.g09, E(RB3LYP) = -1491.86023044, 02.10.2012

0 1

6	0	-4.203704	-1.033273	0.442248
6	0	-2.845830	-0.536262	-0.037010
7	0	-1.778131	-0.510815	1.046004
6	0	-2.096571	0.399899	2.209466
6	0	-2.360511	1.848140	1.812945
6	0	-1.414963	-1.907159	1.520326
6	0	0.001865	-1.998059	2.079499
8	0	0.525236	0.760999	0.049451
16	0	0.539741	1.436819	-1.321123
8	0	0.158441	0.479236	-2.391951
8	0	-0.247631	2.703178	-1.308732
6	0	2.258918	1.900178	-1.596079
8	0	1.644112	1.639029	2.353841
8	0	4.165704	0.576656	2.276076
8	0	4.398783	-0.543110	-0.208471
8	0	2.716437	-2.737757	-0.426333
8	0	-3.058259	2.535067	-1.423055
8	0	0.627093	-2.323551	-2.289820
1	0	-0.927520	-0.105883	0.589221
1	0	-2.914504	0.475567	-0.443780
1	0	-2.463449	-1.198784	-0.811566
1	0	-4.878179	-1.043398	-0.420473
1	0	-4.160926	-2.055238	0.833014
1	0	-4.654512	-0.379982	1.197285
1	0	-1.233134	0.344896	2.876361
1	0	-2.953431	-0.038867	2.728608
1	0	-2.160683	-2.187249	2.270854
1	0	-1.526974	-2.569145	0.658494
1	0	0.172423	-3.029060	2.408394
1	0	0.748980	-1.772022	1.313669
1	0	0.166056	-1.342105	2.940981
1	0	-2.486273	2.434657	2.730348
1	0	-1.520867	2.268053	1.252190
1	0	-3.261157	1.970008	1.206332
1	0	2.332009	2.293265	-2.612438
1	0	2.529766	2.671546	-0.871735
1	0	2.886110	1.015344	-1.465470
1	0	0.496307	-1.355435	-2.382331
1	0	1.360275	-2.436925	-1.645282
1	0	-2.082383	2.659277	-1.439684
1	0	-3.331077	2.571466	-2.351292
1	0	1.233879	1.392185	1.483095
1	0	1.575457	2.603234	2.419580
1	0	3.269142	0.996073	2.344591
1	0	4.220481	-0.048765	3.013671
1	0	4.348411	-0.141966	0.698401
1	0	3.360802	-1.991381	-0.378325
1	0	5.327437	-0.493959	-0.477856
1	0	3.230659	-3.520231	-0.673683
1	0	-0.832554	-3.044332	-1.755880
8	0	-1.692304	-3.382594	-1.381204
1	0	-2.005635	-4.052267	-2.006143

S2.12 Cluster: "SIP+7W"

*** TEAM_CH3S03_1_w_7_b3lyp_6-31+Gp_neu.g09, E(RB3LYP) = -1491.87816720, 02.10.2012

0 1

6	0	3.774738	-0.537125	1.718618
6	0	2.442810	0.023052	1.234257
7	0	2.489411	0.695212	-0.125912
6	0	3.412555	1.881886	-0.200010
6	0	3.141320	2.937973	0.867602
6	0	2.740667	-0.307689	-1.233640
6	0	2.501040	0.248159	-2.635251
8	0	-1.022817	0.625184	1.905523
8	0	-3.668680	0.999989	1.312016
8	0	-0.093357	-2.046206	1.394455
16	0	-0.586720	-2.754971	0.170109
8	0	-2.076737	-2.737596	0.029234
8	0	0.124718	-2.297077	-1.075017
6	0	-0.150593	-4.491133	0.386560
1	0	1.504105	1.068826	-0.267824
1	0	2.052043	0.768211	1.930229
1	0	1.685849	-0.761961	1.156152
1	0	3.608396	-0.993610	2.700042
1	0	4.165353	-1.319971	1.060694
1	0	4.544991	0.232410	1.841767
1	0	3.267146	2.315961	-1.190828
1	0	4.439185	1.506626	-0.145170
1	0	3.768979	-0.663282	-1.119482
1	0	2.051186	-1.135510	-1.046028
1	0	2.578327	-0.584615	-3.342348
1	0	1.494423	0.665158	-2.739981
1	0	3.237051	1.001148	-2.935147
1	0	3.747155	3.822648	0.643938
1	0	2.089429	3.240961	0.866489
1	0	3.406536	2.601167	1.873887
1	0	-0.489649	-5.040399	-0.493947
1	0	0.933342	-4.566460	0.494811
1	0	-0.653218	-4.854320	1.285199
8	0	-0.069463	1.644607	-0.347489
8	0	-1.079832	-0.016899	-2.220834
1	0	-0.847393	-0.339819	1.866967
1	0	-0.462986	1.280685	0.511565
1	0	-0.493170	1.094802	-1.070587
1	0	-0.672927	-0.872999	-1.950384
1	0	-0.790666	3.266388	-0.488311
8	0	-1.252753	4.142405	-0.528270
1	0	-0.826523	4.699439	0.139956
1	0	-2.937470	3.866446	-0.014449
8	0	-3.823669	3.653757	0.368410
1	0	-2.008890	0.737273	1.831498
1	0	-3.797026	1.931064	1.021648
1	0	-3.760694	0.453956	0.503959
1	0	-4.476770	3.898275	-0.303027
8	0	-3.550956	-0.711086	-0.997821
1	0	-3.070995	-1.482841	-0.593539
1	0	-4.356331	-1.074839	-1.395133
1	0	-2.034005	-0.135157	-2.023435

S2.13 Cluster: "CIP+9W"

*** TEAM_CH3S03_1_w_9_b3lyp_6-31+Gp_neu.g09, E(RB3LYP) = -1644.74385369, 02.10.2012

0 1

6	0	-0.028111	4.315339	-1.250951
6	0	0.124015	3.025305	-0.453432
7	0	0.348593	1.785129	-1.297915
6	0	-0.776329	1.460657	-2.255661
6	0	-2.158984	1.448467	-1.614334
6	0	1.695026	1.822963	-1.992260
6	0	2.133238	0.470673	-2.543980
8	0	0.079563	-0.344280	0.492122
16	0	0.054922	-0.226955	2.003929
8	0	0.961864	0.837782	2.500304
8	0	-1.352095	-0.081650	2.515956
6	0	0.653326	-1.806510	2.622638
8	0	-0.306823	-2.042702	-1.663451
8	0	1.915948	-3.582819	-1.552379
8	0	3.373777	-2.797013	0.634393
8	0	4.807481	-0.408648	0.516236
8	0	-2.742123	2.250611	1.905589
8	0	3.082056	1.849945	0.849930
1	0	0.376615	1.002063	-0.603762
1	0	-0.761236	2.831047	0.155994
1	0	0.987000	3.072421	0.213929
1	0	-0.199580	5.132769	-0.542482
1	0	0.871233	4.564192	-1.822971
1	0	-0.883658	4.290956	-1.934388
1	0	-0.548865	0.468922	-2.650478
1	0	-0.715780	2.184854	-3.074244
1	0	1.622782	2.574498	-2.783797
1	0	2.399690	2.152180	-1.225097
1	0	3.150030	0.581842	-2.936900
1	0	2.163589	-0.286894	-1.756070
1	0	1.501544	0.101337	-3.356645
1	0	-2.876097	1.083053	-2.357449
1	0	-2.197210	0.772038	-0.756852
1	0	-2.489436	2.438274	-1.287257
1	0	0.703632	-1.735270	3.711265
1	0	-0.054794	-2.581700	2.321542
1	0	1.638456	-1.997334	2.189534
1	0	2.453973	1.522352	1.524577
1	0	3.749034	1.136422	0.763610
1	0	-2.126457	1.574063	2.273565
1	0	-2.975592	2.826656	2.648571
1	0	-0.297425	-1.569292	-0.803836
1	0	-1.186016	-2.487923	-1.736118
1	0	1.076866	-3.047530	-1.636457
1	0	1.643353	-4.509471	-1.621182
1	0	2.854174	-3.105120	-0.154491
1	0	4.297996	-1.253252	0.521487
1	0	3.915639	-3.549596	0.913265
1	0	5.442776	-0.481632	-0.210042
8	0	-2.788148	-3.257659	-1.926688
1	0	-3.508121	-2.744199	-1.475017
1	0	-3.062434	-3.328512	-2.852848
8	0	-4.759745	-1.789697	-0.728384
1	0	-5.492183	-2.302840	-0.356317
1	0	-4.441744	-1.211203	0.016250
8	0	-3.926350	-0.323437	1.389477
1	0	-3.922156	0.654181	1.407681
1	0	-3.044804	-0.541805	1.759015

S2.14 Cluster: "SIP+9W"

*** TEAM_CH3S03_1_w_9_b3lyp_6-31+Gp.g09, E(RB3LYP) = -1644.74338180, 02.10.2012

0 1

6	0	-5.254307	1.631979	-1.447081
6	0	-4.029044	0.728046	-1.545379
7	0	-3.061129	0.814581	-0.388320
6	0	-3.650648	0.192123	0.861668
6	0	-2.743543	0.261069	2.081031
6	0	-2.486622	2.192659	-0.151328
6	0	-1.926278	2.850246	-1.409770
8	0	-1.098897	-0.431712	-1.790318
8	0	1.331185	-0.431188	-0.500459
16	0	2.326919	-1.559088	-0.674665
8	0	1.740796	-2.700391	-1.442654
8	0	3.632832	-1.087802	-1.215339
6	0	2.661031	-2.184552	0.981801
8	0	0.564444	1.439240	1.403474
8	0	0.308844	-0.088100	3.631969
8	0	-0.363443	-2.612197	2.725652
8	0	2.468559	3.415685	1.779622
8	0	4.413008	3.408407	-0.125854
8	0	4.416028	1.423907	-1.970075
8	0	-2.356992	-2.712729	0.638066
8	0	-0.887504	-3.226880	-1.805592
1	0	-2.251038	0.215111	-0.716173
1	0	-3.448312	0.945580	-2.443310
1	0	-4.324467	-0.323747	-1.598295
1	0	-5.864258	1.479036	-2.344070
1	0	-5.883566	1.400062	-0.582645
1	0	-4.989365	2.693389	-1.408984
1	0	-1.678367	2.056239	0.570742
1	0	-3.272473	2.799708	0.309779
1	0	-4.602128	0.697246	1.050749
1	0	-3.827580	-0.855588	0.607521
1	0	-3.185580	-0.363742	2.863818
1	0	-1.754581	-0.143276	1.863441
1	0	-2.631362	1.272094	2.482104
1	0	-1.389731	3.756054	-1.108246
1	0	-1.214825	2.192879	-1.917883
1	0	-2.702314	3.147481	-2.122756
1	0	3.365410	-3.013382	0.881866
1	0	3.105724	-1.377684	1.568720
1	0	1.722237	-2.520250	1.428798
1	0	0.090312	-3.115213	-1.654465
1	0	-1.893076	-3.057661	-0.149398
1	0	0.939686	0.821581	0.734438
1	0	1.229874	2.161961	1.512940
1	0	0.417357	0.517356	2.845281
1	0	1.123411	0.004451	4.147425
1	0	-0.126936	-1.724093	3.095289
1	0	-1.680567	-2.701522	1.347814
1	0	-0.619079	-3.158938	3.482894
1	0	3.190258	3.389280	1.096934
1	0	2.156697	4.332303	1.789612
1	0	5.329119	3.403803	0.188244
1	0	4.365020	2.686042	-0.808399
1	0	3.989107	1.572931	-2.826009
1	0	4.118303	0.525536	-1.678400
1	0	-0.192231	-0.378041	-1.396895
1	0	-1.208280	-1.394337	-1.956024
1	0	-0.979624	-3.898666	-2.497176

4.7 Publication VI

Revisiting Imidazolium Based Ionic Liquids: Effect of the Conformation Bias of the [NTf₂] Anion Studied by Molecular Dynamics Simulations

J. Neumann, B. Golub, L.-M. Odebrecht, R. Ludwig and D. Paschek

J. Chem. Phys., 2018, **148**, 193828/1-9

CRedit roles: Formal analysis, Investigation, Visualization, Methodology, Writing - original draft (equal)

Approximated contribution to the publication in present: 30 %

Reprinted from J. Neumann, B. Golub, L.-M. Odebrecht, R. Ludwig and D. Paschek, *J. Chem. Phys.*, 2018, **148**, 193828/1-9, with the permission of AIP Publishing.

Revisiting imidazolium based ionic liquids: Effect of the conformation bias of the [NTf₂] anion studied by molecular dynamics simulations

Cite as: J. Chem. Phys. **148**, 193828 (2018); <https://doi.org/10.1063/1.5013096>

Submitted: 10 November 2017 • Accepted: 31 January 2018 • Published Online: 20 February 2018

Jan Neumann, Benjamin Golub, Lisa-Marie Odebrecht, et al.

COLLECTIONS

Paper published as part of the special topic on [Chemical Physics of Ionic Liquids](#)



View Online



Export Citation



CrossMark

ARTICLES YOU MAY BE INTERESTED IN

[TRAVIS—A free analyzer for trajectories from molecular simulation](#)

The Journal of Chemical Physics **152**, 164105 (2020); <https://doi.org/10.1063/5.0005078>

[Rotational and translational dynamics and their relation to hydrogen bond lifetimes in an ionic liquid by means of NMR relaxation time experiments and molecular dynamics simulation](#)

The Journal of Chemical Physics **148**, 193843 (2018); <https://doi.org/10.1063/1.5011804>

[A molecular dynamics investigation of the structural and dynamic properties of the ionic liquid 1-n-butyl-3-methylimidazolium bis\(trifluoromethanesulfonyl\)imide](#)

The Journal of Chemical Physics **135**, 124507 (2011); <https://doi.org/10.1063/1.3643124>

The Journal of Chemical Physics Special Topics Open for Submissions

Learn More



Revisiting imidazolium based ionic liquids: Effect of the conformation bias of the [NTf₂] anion studied by molecular dynamics simulations

Jan Neumann,^{1,a)} Benjamin Golub,^{1,b)} Lisa-Marie Odebrecht,^{1,c)} Ralf Ludwig,^{2,3,d)} and Dietmar Paschek^{1,e)}

¹*Institut für Chemie, Abteilung Physikalische und Theoretische Chemie, Universität Rostock, Albert-Einstein-Straße 21, D-18059 Rostock, Germany*

²*Institut für Chemie, Abteilung Physikalische und Theoretische Chemie, Universität Rostock, Dr.-Lorenz-Weg 2, D-18059 Rostock, Germany*

³*Leibniz Institut für Katalyse an der Universität Rostock, Albert-Einstein-Straße 29a, D-18059 Rostock, Germany*

(Received 10 November 2017; accepted 31 January 2018; published online 20 February 2018)

We study ionic liquids composed of 1-alkyl-3-methylimidazolium cations and bis(trifluoromethylsulfonyl)imide anions ([C_nMIm][NTf₂]) with varying chain-length $n = 2, 4, 6, 8$ by using molecular dynamics simulations. We show that a reparametrization of the dihedral potentials as well as charges of the [NTf₂] anion leads to an improvement of the force field model introduced by Köddermann, Paschek, and Ludwig [ChemPhysChem **8**, 2464 (2007)] (KPL-force field). A crucial advantage of the new parameter set is that the minimum energy conformations of the anion (*trans* and *gauche*), as deduced from *ab initio* calculations and Raman experiments, are now both well represented by our model. In addition, the results for [C_nMIm][NTf₂] show that this modification leads to an even better agreement between experiment and molecular dynamics simulation as demonstrated for densities, diffusion coefficients, vaporization enthalpies, reorientational correlation times, and viscosities. Even though we focused on a better representation of the anion conformation, also the alkyl chain-length dependence of the cation behaves closer to the experiment. We strongly encourage to use the new NGOLP (Neumann, Golub, Odebrecht, Ludwig, Paschek) force field for the [NTf₂] anion instead of the earlier KPL parameter set for computer simulations aiming to describe the thermodynamics, dynamics, and also structure of imidazolium-based ionic liquids. *Published by AIP Publishing.* <https://doi.org/10.1063/1.5013096>

INTRODUCTION

Having a reliable force field available is one of the most important prerequisites for setting up a molecular dynamics (MD) simulation. Hence, a lot of effort has been put into the development of new as well as the improvement of existing force field models. There are essentially two different approaches on how to improve or optimize force fields:

One approach is trying to develop a “universal” force field parameter set which can be applied to a broad range of different molecules or ions, such as the force field parameters for ionic liquids introduced by Pádúa *et al.*^{1–10} These force fields are very popular in the ionic liquid molecular simulation community and yield in general good results in comparison with experimental data.

An alternative, less universal approach is to focus on a specific subset of molecules and ions and to enhance the quality of the model by fitting the parameters of a system to a set of selected thermodynamical, dynamical, and structural properties, which then can be accurately emulated by the force field. The most well-known example for the application of such

a strategy is perhaps the water molecule. In 2002, Bertrand Guillot gave a comprehensive overview over (at the time) more than 40 different water models,¹¹ and the number has been increasing since then.^{12–15} Obviously, water is of great scientific interest. As a consequence, there exist a variety of force field models consisting mostly of three (SPC, TIP3P) to five (TIP5P, ST2) interaction sites, including (POL5) or without (SPC/E) polarizability and even force fields optimized to best represent the solid phases of water (TIP4P/ICE) and their phase transitions.

The second strategy was employed by Köddermann *et al.* in 2007 to arrive at the KPL (Köddermann, Paschek, Ludwig) force field for a selected class of imidazolium-based ionic liquids composed of 1-alkyl-3-methylimidazolium cations and bis(trifluoromethylsulfonyl)imide anions ([C_nMIm][NTf₂]).¹⁶ The aim of this work was to further optimize the force field of Pádúa *et al.* to better represent dynamical properties like self-diffusion coefficients, reorientational correlation times, and viscosities. As shown in their original work from 2007 as well as in further studies published by different groups, the KPL force field has been proven to yield reliable results for dynamical properties, but also for thermodynamical properties, such as the free energies of solvation for light gases in ionic liquids,^{17,18} and is still used frequently to date.^{19–21}

Here we want to present our take on further improving the KPL force field by revisiting the conformation-space explored by the [NTf₂] anion. Extensive studies of the conformation of

^{a)}jan.neumann@uni-rostock.de

^{b)}benjamin.golub@uni-rostock.de

^{c)}lisa-marie.odebrecht@uni-rostock.de

^{d)}ralf.ludwig@uni-rostock.de

^{e)}dietmar.paschek@uni-rostock.de

the [NTf₂] anion using the KPL force field in comparison to experimental as well as quantum chemical calculations have revealed a significant mismatch of the energetically favored conformations. Therefore we feel the need for presenting a modified version of the force field, removing this conformation bias. We will discuss the implications of this modification for a wealth of thermodynamical, dynamical, and structural quantities.

CONFORMATION-SPACE OF THE ANION

During MD simulations of ionic liquids of the type [C_nMIm][NTf₂] with the force field of Köddermann *et al.*, it became apparent that the favored [NTf₂] anion conformations observed in the simulation differ from what has been shown earlier from quantum chemical (QC) calculations⁶ as well as from Raman experiments²² (see Figs. 1 and 2).

For locating the minimum energy conformations, we performed extensive quantum chemical calculations with the GAUSSIAN 09 program²³ following the approach of Lopes and Pádua.² We started by calculating the potential energy surface as a function of the two dihedral angles S1–N–S2–C2 (ϕ_1) and S2–N–S1–C1 (ϕ_2) on the Hartree-Fock (HF) level with a small basis set (6-31G*). Subsequent to these optimizations, we performed single point calculations on the 2nd order Møller-Plesset Many Body Perturbation Theory (MP2) level using the cc-pvtz basis set for all HF optimized conformations. In agreement with earlier calculations by Pádua *et al.*⁶ and Raman measurements of Fujii *et al.*,²² we observe essentially two structurally distinct minimum energy conformations that can be identified as energy minima on the energy landscape depicted in Fig. 3. The *trans* conformations of the [NTf₂] anion are energetically preferred, followed by the *gauche*-conformations, which are elevated by about 3 kJ mol⁻¹ (see Fig. 2). Due to the symmetry of the [NTf₂] anion, the in essence two structurally distinct conformations appear in the form of the six minima of the energy landscape shown in Fig. 3. The two global minima describe *trans* conformations located at $\phi_1 = 90^\circ$, $\phi_2 = 90^\circ$ and $\phi_1 = 270^\circ$, $\phi_2 = 270^\circ$, respectively. The four additional local minima are all representing structurally identical *gauche* conformations, based on the symmetry of the ion. This is in agreement with Pádua *et al.* and discussed in more detail in their publication from 2008.⁶

To compare these *ab initio* calculations with the KPL force field model, we employed the molecular dynamics package Moscerro 4.180 and computed the same potential energy

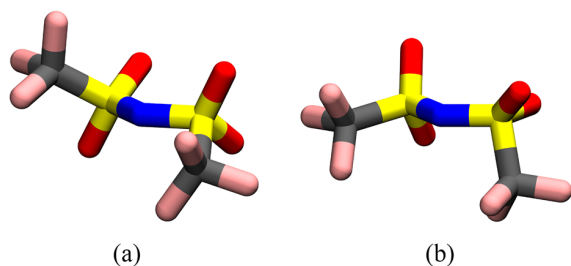


FIG. 1. Minimum energy conformations of the [NTf₂] anion taken from a MD simulation employing the KPL force field.

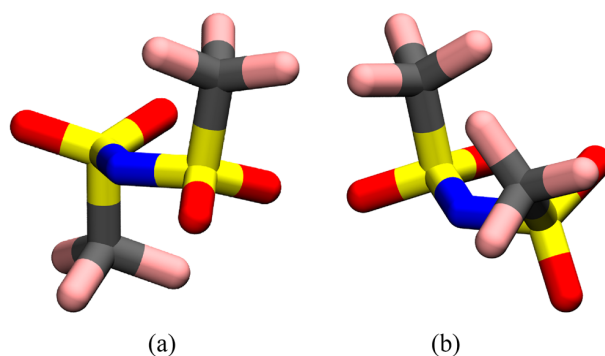


FIG. 2. Minimum energy conformations of the [NTf₂] anion obtained from *ab initio* calculations. The *trans* conformation (left) represents the global energy minimum, while the energy of the *gauche* conformation (right) is elevated by about 3 kJ mol⁻¹.

surface as a function of the two dihedral angles ϕ_1 and ϕ_2 (see Fig. 4, top panel) by fixing the two dihedral angles and optimizing all other degrees of freedom. We would like to add that in the force field-optimizations all bond lengths were kept fixed. It is quite obvious that the KPL force field does not adequately reproduce the potential energy surface obtained from the quantum chemical calculations (compare the top panel in Fig. 4 with Fig. 3). The minimum energy conformations of the KPL model reveal essentially two structurally distinct conformations illustrated in Fig. 1. However, both are somewhat similar, being positioned between the *trans* and *gauche* conformations favoured in the *ab initio* calculations. The fact that the energy landscape does not reflect all the symmetry-features of the molecule, however, might be a lesser problem since energy barriers are rather large and the anion could explore similar conformations simply by rotation.

However, for arriving at a better representation of the *ab initio* energy surface, we reparameterized the charges as well as the two distinct independent dihedral potentials (S–N–S–C and F–C–S–N), while keeping the other parameters unchanged. From our quantum chemical calculations, we yield the global minimum conformations at $\phi_1 = \phi_2 = 90^\circ$ and $\phi_1 = \phi_2 = 270^\circ$. Due to the symmetry of the [NTf₂] anion, these two minima are conformationally identical. To calculate the parameters for the S–N–S–C dihedral angle, we fixed ϕ_1 at 90° and calculated the energy as a function of the dihedral

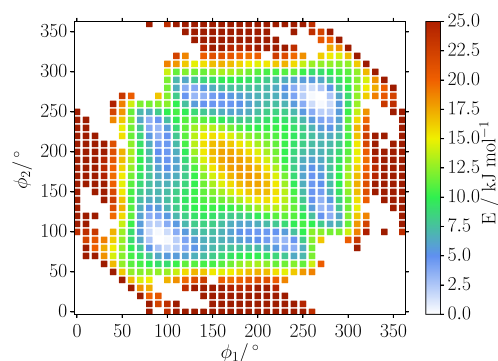


FIG. 3. *Ab initio* computation of the energy surface of the [NTf₂] anion as a function of the S1–N–S2–C2 and S2–N–S1–C1 dihedral angles ϕ_1 and ϕ_2 .

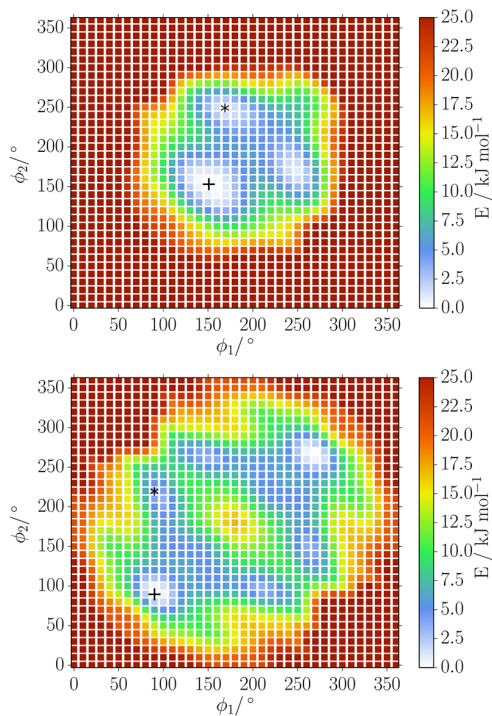


FIG. 4. Potential energy surface of the $[\text{NTf}_2]$ anion computed for the two force field models. The new force field (bottom panel) provides a much better representation of the *ab initio* calculations shown in Fig. 3 than the original KPL force field (top panel). The plus-sign and asterisk indicate the location of the global and local minima of the energy landscape as depicted in Figs. 1 and 2, respectively.

angle ϕ_2 on the MP2 level using a cc-pvtz basis set (as shown in Fig. 5). The same procedure was applied using the KPL

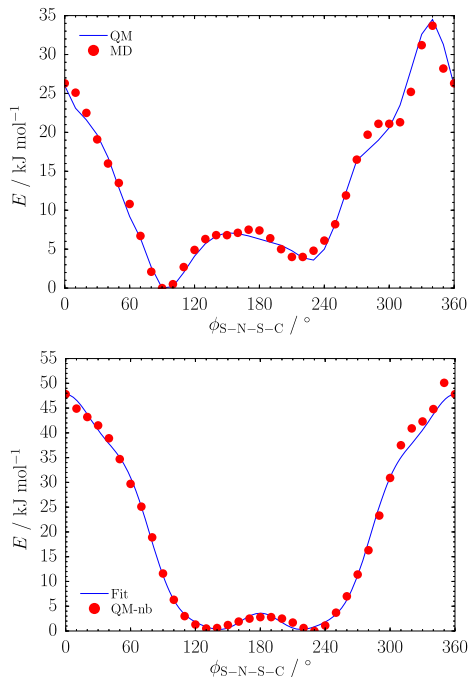


FIG. 5. (Top panel) Potential energy of the entire $[\text{NTf}_2]$ anion as a function of the S2-N-S1-C1 dihedral angle ϕ_2 with ϕ_1 being fixed at $\phi_1 = 90^\circ$. (Bottom panel) Torsion potential fitted to the difference between the QC and force field model (with switched off torsion potential).

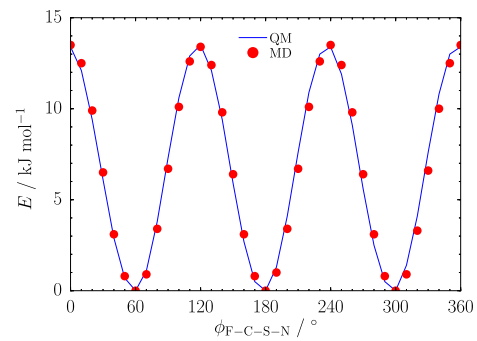


FIG. 6. Potential energy of the $[\text{NTf}_2]$ anion as a function of the F-C-S-N dihedral angle.

force field while switching of the dihedral potential, such that only the nonbonding (nb) interactions matter. We then subtracted the latter energy function from the energies obtained via the QC calculations and arrived at the dihedral potential for the dihedral angle S-N-S-C, which should be reproduced by the torsion potential in our force field (see Fig. 5, bottom panel). The value of ϕ_1 at 90° was chosen deliberately since it represents a path very close to the minimum energy transition path between adjacent *trans* and *gauche* conformations, thus providing an optimized representation of the states with the lowest energies and their interconversion.

In contrast to the work of Köddermann *et al.*, we chose to fit a dihedral potential function obeying the conformational symmetry-features of the anion using

$$V_{\kappa\lambda\omega\tau}^{\text{dp}} = \sum_n k_m^{\text{dp}} [1 + \cos(m_n\psi_m - \psi_m^0)] \quad (1)$$

(with $n = 6$ and $\psi_m^0 = 0$) to the computed *ab initio* potential, leading to the proper minimum energy conformations of the $[\text{NTf}_2]$ anion.² Similarly obtained were parameters for the F-C-S-N dihedral potential of the terminal CF_3 -groups (see Fig. 6). The complete set of new parameters for the NGOLP (Neumann, Golub, Odebrecht, Ludwig, Paschek) force field is given in Table III. Similar to the procedure used in the OPLS (Optimized Potential for Liquid Simulations) force field, Coulomb and Lennard-Jones non-bonded 1-4 interactions are scaled by a factor of 0.5. We would like to point out that the representation of the *ab initio* conformational energy landscape by our model requires an intricate interplay of electrostatic and Lennard-Jones nonbonding interactions and dihedral potentials. We have made the observation that by using a newly derived set of partial charges, although the overall changes seem to be small, a significantly better

TABLE I. Lennard-Jones parameters σ , ϵ (all taken from Ref. 16) and charges q (all newly calculated in this work) for all interaction sites of the $[\text{NTf}_2]$ anion.

Site	σ (Å)	ϵ (K)	q (e)
F	2.6550	8.00	-0.189
C	3.1500	9.96	0.494
S	4.0825	37.73	1.076
O	3.4632	31.70	-0.579
N	3.2500	25.66	-0.690

TABLE II. Bond length $r_{\kappa\lambda}^0$, angle $\phi_{\kappa\lambda\omega}^0$, and $k_{\kappa\lambda\omega}^a$ (all taken from Ref. 16) for the angle potential $V_{\kappa\lambda\omega}^a = \frac{1}{2}k_{\kappa\lambda\omega}^a(\phi_{\kappa\lambda\omega} - \phi_{\kappa\lambda\omega}^0)^2$ in the force field of the [NTf₂] anions.

Bond	$r_{\kappa\lambda}^0$ (Å)	Angle	$\phi_{\kappa\lambda\omega}^0$ (deg)	$k_{\kappa\lambda\omega}^a$ /kJ mol ⁻¹ rad ⁻²
C-F	1.323	F-C-F	107.1	781.0
C-S	1.818	S-C-F	111.8	694.0
S-O	1.442	C-S-O	102.6	870.0
N-S	1.570	O-S-O	118.5	969.0
		O-S-N	113.6	789.0
		C-S-N	100.2	816.0
		S-N-S	125.6	671.0

TABLE III. Parameters k_m^{dp} and ψ_m^0 for the torsion potential $V_{\kappa\lambda\omega\tau}^{\text{dp}} = \sum_n k_m^{\text{dp}} [1 + \cos(m_n\psi_m - \psi_m^0)]$ in the force field of the [NTf₂] anion.

	$n(\kappa\lambda\omega\tau)$	m_n	k_m^{dp} (kJ mol ⁻¹)	ψ_m^0 (deg)
F-C-S-N	1	3	2.0401	0.0
S-N-S-C	1	1	23.7647	0.0
	2	2	6.2081	0.0
	3	3	-2.3684	0.0
	4	4	-0.0298	0.0
	5	5	0.6905	0.0
	6	6	1.0165	0.0

representation of the energy landscape was feasible as compared to the previously employed charge model. Therefore we re-computed partial charges from the MP2-wavefunction using the method of Singh and Kollman as implemented in the GAUSSIAN 09 program.²⁴ The refined charges are listed in Table I.

Finally, employing new refined parameters for the dihedral potentials and partial charges, we re-calculated the energy surface as a function of the two dihedral angles ϕ_1 and ϕ_2 (see Fig. 4, bottom panel). The result is in much better agreement with the *ab initio* calculations and resolves the conformational mismatch issue for the force field of the [NTf₂] anion. In addition, we would like to emphasize that this procedure also leads to a proper description of the barrier height between the two adjacent *gauche* conformations, which is critical for properly describing the conformational interconversion of the molecule between the two global energy minimum states on the energy landscape located at $\phi_1 = 90^\circ$, $\phi_2 = 90^\circ$ and $\phi_1 = 270^\circ$, $\phi_2 = 270^\circ$, respectively.

All parameters for the new [NTf₂] anion force field are listed in Tables I–III. The original parameters as well as the parameters for the cations can be found in the publication of Köddermann *et al.*¹⁶

MOLECULAR DYNAMICS SIMULATIONS

We performed MD simulations for the two force fields KPL and NGOLP with GROMACS 5.0.6^{25–29} over a temperature range from $T = 273$ –483 K to calculate thermodynamical and dynamical properties and compare them with the original KPL force field. All simulations were carried out in the *NpT* ensemble. However, to compute viscosities, we performed

additional *NVT* simulations using starting configurations sampled along the *NpT*-trajectory. Periodic boundary conditions were applied using cubic simulation boxes containing 512 ion-pairs. We applied smooth particle mesh Ewald summation³⁰ for the electrostatic interactions with a real space cutoff of 0.9 nm, a mesh spacing of 0.12 nm, and 4th order interpolation. The Ewald convergence factor α was set to 3.38 nm⁻¹ (corresponding to a relative accuracy of the Ewald sum of 10⁻⁵). All simulations were carried out with a time step of 2.0 fs, while keeping bond lengths fixed using the LINCS algorithm.³¹

An initial equilibration was done for 2 ns at $T = 500$ K using the Berendsen thermostat as well as the Berendsen barostat with coupling times $\tau_T = \tau_p = 0.5$ ps.³² After this another equilibration was done for 2 ns at each of the desired temperatures. For each of the six temperatures 273 K, 303 K, 343 K, 383 K, 423 K, and 483 K, we performed production runs of 30 ns, keeping the pressure fixed at 1 bar applying Nosé-Hoover thermostats^{33,34} with $\tau_T = 1$ ps and Rahman-Parrinello barostats^{35,36} with $\tau_p = 2$ ps.

RESULTS AND DISCUSSION

Analogous to the publication of Köddermann *et al.* from 2007,¹⁶ we will compare densities, self-diffusion coefficients, and vaporization enthalpies for [C_nMIm][NTf₂] as a function of temperature and alkyl chain-length as well as viscosities and reorientational correlation times for [C₂MIm][NTf₂] as a function of temperature. It is important to keep in mind that the original force field was optimized to reproduce these properties and yields a good agreement between the experiment and simulation. By resolving the mismatch of the favored conformations of the [NTf₂] anion, we are able to describe these properties as good as the KPL force field or even better.

Structural features

Here we take a look at structural features of the liquid phase and how they are influenced by changes in the conformation-population of the [NTf₂] anion.

Before discussing the inter-ionic structural features of the ionic liquids, we would like to briefly elaborate on the conformational states adopted by the anion and their transitions in the condensed ionic liquid phase. From the energy landscape depicted in Fig. 4, it is evident that the anion possesses two dominant low energy states, both labeled *trans* located at $\phi_1 = 90^\circ$, $\phi_2 = 90^\circ$ and $\phi_1 = 270^\circ$, $\phi_2 = 270^\circ$, respectively. In Fig. 7, we illustrate the time evolution of the conformation adapted by a single anion in the ionic liquid at $T = 273$ K over a time period of 16 ns. As expected it is evident that the anion resides mostly in either of the two *trans* states with rather frequent changes between them due to rapid conformational interconversions. It is rarely observed being resting in a *gauche* state as indicated in Fig. 7. It is mostly passing through the *gauche* states as a transitional state. By counting the number of transitions, we estimate the average residence time in either of the distinct *trans* states to be in the range of about 1 ns. As pointed out by Pádúa *et al.*,⁶ the observed rapid conformational interconversions illustrate the importance of a proper description of the conformational energy landscape.

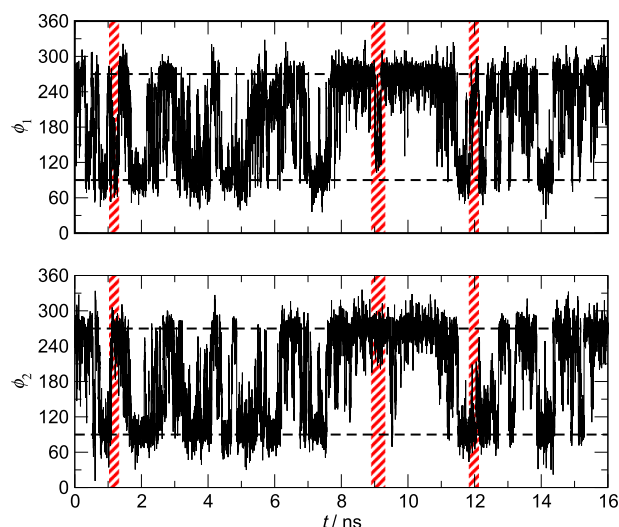


FIG. 7. Time evolution of the conformation-state of a single $[\text{NTf}_2]$ -anion over a time interval of 16 ns at $T = 273$ K indicated by the two dihedral angles $\phi_1(t)$ and $\phi_2(t)$. The red shaded regions indicate time intervals where one of the dihedral angles is resting in a *gauche* state.

First we inspect the three distinct center of mass pair distribution functions between the different ions computed for $[\text{C}_n\text{MIm}][\text{NTf}_2]$ with $n = 2$ at $T = 303$ K (shown in Fig. 8). It is quite apparent that these distribution functions are only slightly affected by the alterations in the force field. Most notable are the differences observed in the anion-anion pair distribution function depicted in Fig. 8(c) with the first peak being significantly broadened. It is quite obvious to assume that this behavior is related to the more distinct conformational states (*trans* and *gauche*) that the reparameterized $[\text{NTf}_2]$ anion is adopting as shown in Fig. 2. In the *trans* state, the molecule is more elongated along the molecular axis and more compact perpendicular to it. In addition, the *gauche*-state is generally more compact than the minimum energy conformations adopted by the original KPL force field model shown in Fig. 1. This leads to an enhanced population of both short and long anion-anion distances. This effect manifests itself also in the slight shift of the maximum of the first peak of the anion-cation pair distribution function towards smaller distances [see Fig. 8(a)]. Another interesting distribution function is the pair distribution function of the anion-oxygens surrounding the C(2)-hydrogen site on the cation. The C(2)-position is deemed to act as a hydrogen-bond donor.^{37,38} With changing conformations, we expect an effect on the hydrogen bonding situation between the anion and cation. Here we observe

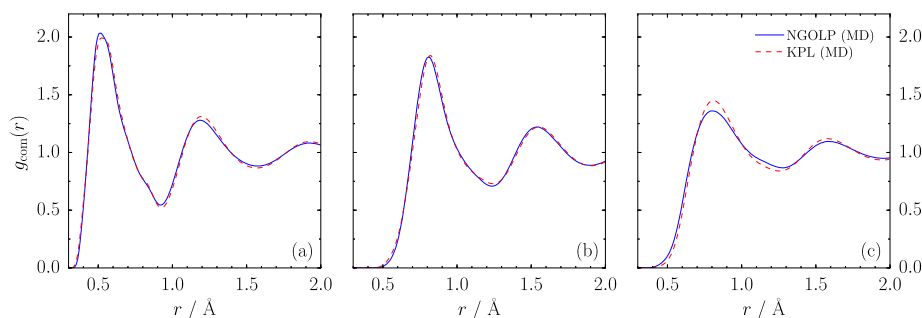


FIG. 8. Center of mass radial pair distribution functions for cation-anion (a), anion-anion (b), and cation-cation (c) for $[\text{C}_2\text{MIm}][\text{NTf}_2]$ at $T = 303$ K. The NGOLP-data are shown as blue lines, and the KPL-data force is shown as red dashed lines.

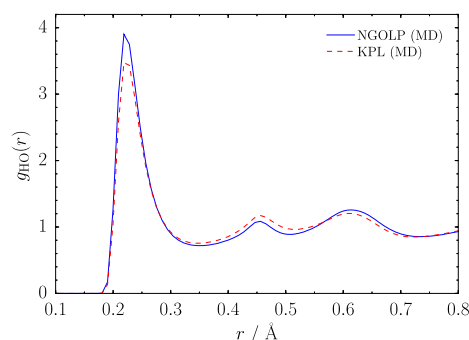


FIG. 9. Radial pair distribution function of the anion-oxygens around the C(2) hydrogen site on the cation for $[\text{C}_2\text{MIm}][\text{NTf}_2]$ at $T = 303$ K. The NGOLP force field is shown as the blue line, and the KPL force field as the red dashed line.

that the NGOLP force field promotes hydrogen bonds between anions and cations as indicated by an increased first peak of the O–H pair distribution function shown in Fig. 9. The computed number of hydrogen bonds increases throughout by about 4%, mostly unaffected by the alkyl chain-length and temperature (not shown). Taking into account the importance of more elongated *trans* configurations of the anion, it is also not surprising that the second peak is somewhat depleted, while the third peak is again enhanced (see Fig. 9). We further investigate the hydrogen-bond situation by not just looking at the distance between the oxygen and hydrogen but also at the angular distribution. Therefore we compute the probability density map of the anion-oxygens surrounding the C(2) hydrogen site on the cation. Again we focus on the C(2) hydrogen because its hydrogen-bond interaction with the anion is deemed the strongest and most important. To calculate this map, we compute both the O–H distance and the angle between the C–H bond-vector on the cation and the intermolecular C–O vector, where C is the C(2)-position of the cation and O represents the oxygen-sites on the anions. In addition, the computed probabilities are weighted by r_{OH}^{-2} . It is revealed that the maximum of this probability density map does not quite represent a linear hydrogen bond at a distance of 2.3 Å but is tilted by about 25° and is characterized by a rather broad angular distribution (Fig. 10).

Densities and self-diffusion coefficients

To get an idea on how the changing conformation-populations influence the properties of the imidazolium-based ionic liquids, we first take a look at the mass density of $[\text{C}_2\text{MIm}][\text{NTf}_2]$. In molecular simulations, the density has

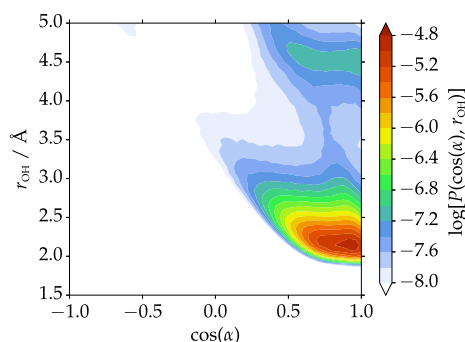


FIG. 10. Probability density of the anion-oxygens around the C(2) hydrogen sites as a function of the intermolecular distance r_{OH} and the angle between the C(2)–H bond-vector and the intermolecular C(cation)–O(anion) vector shown for the NGOLP force field at $T = 303$ K.

always been an important property for evaluating the force field. The enhanced conformational diversity of the $[NTf_2]$ anion leads to a slight increase in the density over the whole temperature range (see Fig. 11 and Table IV). This overall increase is in better agreement with the experimental data from the work of Tokuda *et al.*³⁹ For lower temperatures, the NGOLP force field even matches the experimental values. The thermal expansivity, however, is significantly overestimated, although at the highest temperatures the difference between the experiment and simulation is still within about 5%. Despite the overall density increase from KPL to NGOLP, the thermal expansivities of both models are practically identical.

With this increasing density, also slightly reduced self-diffusion coefficients for the $[NTf_2]$ anion are observed (see Fig. 12). We calculated the self-diffusion coefficient using the Einstein relation

$$D = \frac{1}{6} \lim_{t \rightarrow \infty} \frac{d}{dt} \langle |\vec{r}_i(t) - \vec{r}_i(0)|^2 \rangle \quad (2)$$

as a function of the temperature for $[C_2MIm][NTf_2]$ (Fig. 12) as well as a function of the alkyl chain-length of $[C_nMIm][NTf_2]$ at $T = 303$ K (Fig. 13 and Table V). As shown in 2007, the KPL force field is able to yield self-diffusion coefficients in good agreement with the experimental data. Nevertheless, using the new NGOLP parameters, we are able

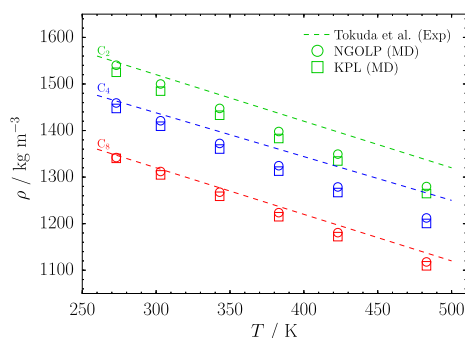


FIG. 11. Mass densities of $[C_nMIm][NTf_2]$ with $n = 2, 4, 8$ as a function of temperature. The experimental data of Tokuda *et al.* are given according to their fitted temperature dependence (dashed lines).³⁹ The results from our molecular dynamics simulation are shown as open symbols: NGOLP (open circles) and KPL (open squares). See also Table IV.

TABLE IV. Temperature dependence of the density ρ and the self-diffusion coefficients of the $[NTf_2]$ anion D_- in $[C_2MIm][NTf_2]$ according to the KPL and NGOLP force fields. See also Figs. 11 and 12.

T (K)	ρ (kg m ⁻³)		$D_-/10^{-11}$ (m ² s ⁻¹)	
	KPL	NGOLP	KPL	NGOLP
273	1525	1540	1.4	1.1
303	1485	1500	4.8	3.6
343	1433	1448	13.0	10.9
383	1383	1398	26.4	23.0
423	1335	1349	49.4	43.6
483	1265	1280	92.7	90.0

to describe the temperature dependence of the self-diffusion coefficient of the $[NTf_2]$ anion in $[C_2MIm][NTf_2]$ even better (Fig. 12 and Table IV). Taking a look at the alkyl chain-length dependence, we can support the findings for the $n = 2$ imidazolium ionic liquid. The NGOLP force field is able to reproduce the dependence better, especially for $n \leq 4$; for longer chains, the KPL force field is closer to the experiment (see Fig. 13). As observed for the temperature dependence, the general trend of the self-diffusion coefficient as a function of the alkyl chain-length is identical for the KPL and NGOLP force fields.

Vaporization enthalpies

The magnitude of the vaporization enthalpy of ionic liquids was studied extensively over the last few years and has been sometimes discussed quite emotionally.^{40–48} For the purpose of this study, we will compare our results with the more recent quartz-crystal microbalance (QCM) data of imidazolium-based ionic liquids of type $[C_nMIm][NTf_2]$ from the work of Verevkin *et al.* of 2013⁴⁷ as shown in Fig. 14. We would like to point out that an exhaustive overview of the huge amount of vaporization enthalpy data from different experiments as well as molecular simulation studies is provided in the supporting information in the work of Verevkin *et al.*⁴⁷ and in the COSMO-RS (conductor like screening model for real solvents) study by Schröder and Coutinho.⁴⁸ The vaporization enthalpies per mole of $[C_nMIm][NTf_2]$ were here calculated by assuming ideal gas behavior with

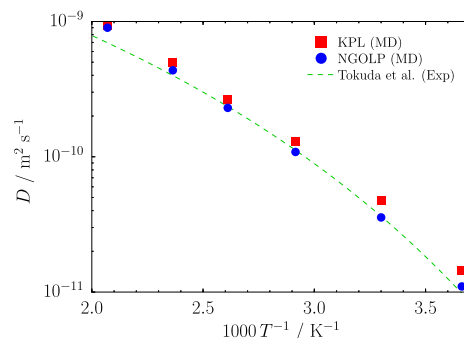


FIG. 12. Self-diffusion coefficients as a function of the temperature for $[C_2MIm][NTf_2]$. The experimental data of Tokuda *et al.* are represented according to their fitted temperature dependence (green dashed line).³⁹ The red squares (KPL) and blue dots (NGOLP) represent the results from our molecular dynamics simulations. See also Table IV.

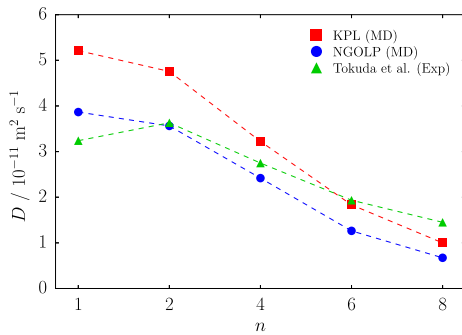


FIG. 13. Self-diffusion coefficients as a function of the alkyl chain-length for $[C_n\text{MIm}][\text{NTf}_2]$ at $T = 303$ K. The experimental data are shown as green triangles, the KPL force field is shown as red squares, and the NGOLP force field is shown as blue dots. The dashed lines are only guide to the eye. See also Table V.

$$\Delta_v H \approx \Delta_v U + RT, \quad (3)$$

which is a well-justified approximation, given the low vapor pressures of ionic liquids at low temperatures. The energy difference between the liquid and gas phases was computed via

$$\Delta_v U = U'_g - U'_l, \quad (4)$$

where U'_l and U'_g are the internal energies per mole ion-pairs of the liquid and gas phases, respectively. To determine U'_g , we performed gas phase simulations of individual ion-pairs without periodic boundary conditions. It has been shown in the literature that the gas phase of ionic liquids consists mostly of ion-pairs^{47,49–55} tied together by strong long-range electrostatic forces. Hence, simulating an isolated ion-pair instead of separated ions is the most realistic approximation of the gas phase. As it is standard practice, during the simulation of both the liquid phase and the isolated ion-pair, the total linear momentum was set to zero, thus eliminating the systems' center of mass translational motion. In addition, in the simulations of the isolated ion-pairs, also the total angular momentum was set to zero. However, when comparing the internal energy of the gas phase and the liquid phase, we have to correct for differences in the kinetic energy stored in the translational/rotation motion of either system by adding

$$U'_g = U_g + \frac{6}{2}RT, \quad (5)$$

$$U'_l = U_l + \frac{3}{2}RT \times \frac{1}{N_{\text{IP}}} \quad (6)$$

TABLE V. MD simulated self-diffusion coefficients of the $[\text{NTf}_2]$ anion D_- as a function of the alkyl chain-length n in $[C_n\text{MIm}][\text{NTf}_2]$ for the KPL and the new NGOLP force field as well as the experimental values by Tokuda *et al.*³⁹ at $T = 303$ K. See also Fig. 13.

n	$D_- / 10^{-11} \text{ (m}^2 \text{ s}^{-1})$		
	KPL	NGOLP	Expt.
1	5.21	3.87	3.24
2	4.76	3.56	3.63
4	3.22	2.42	2.75
6	1.83	1.26	1.93
8	1.00	0.67	1.45

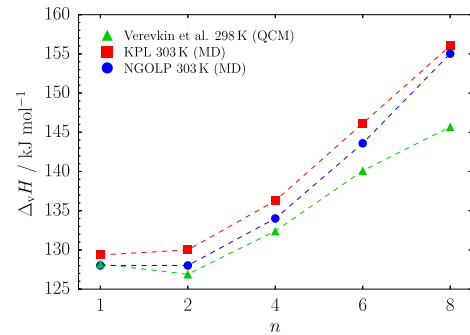


FIG. 14. Vaporization enthalpies as a function of the alkyl chain-length for NGOLP (blue dots) and KPL (red squares) at $T = 303$ K. For comparison, we also show the QCM data of Verevkin *et al.* for $T = 298$ K (green triangles).⁴⁷ See also Table VI.

per mole of ion-pairs, where $N_{\text{IP}} = 512$ is the number of ion-pairs used in the liquid simulation, and U_g and U_l are the total energies per ion-pair as computed directly from the MD simulations. With these corrected molar internal energies U'_g and U'_l , we compute the heat of vaporization $\Delta_v H$ using Eq. (3) for a temperature of $T = 303$ K shown in Fig. 14 and given in Table VI.

Both the data computed from the KPL and from the NGOLP force field as a function of alkyl chain-length are rather close to the experimental data of Verevkin *et al.*⁴⁷ However, we would like to point out that the optimized NGOLP force field is in even better agreement with the QCM experiments, particularly for chain-lengths up to $n = 4$. Not only are the data for $n = 2$ now in quantitative agreement with the experimental data but also the step from $n = 1$ to $n = 2$ is better captured by the new model, suggesting a significant influence of the enhanced conformational diversity of the $[\text{NTf}_2]$ anion.⁵⁶ Since the exact slope of $\Delta_v H$ as a function of the alkyl chain-length has been shown to be controlled by the counterbalance of electrostatic and van der Waals forces,⁵⁷ the increasing deviation for longer chain-length might indicate a slight misrepresentation of the size of the dispersion interaction introduced by increasing the alkyl chain-length.

Viscosities and reorientational correlation times

To further compare dynamical properties of the simulated ionic liquids with experimental data, the temperature dependence of the reorientational correlation times for the C(2)–H vector and viscosities for $[C_2\text{MIm}][\text{NTf}_2]$ were

TABLE VI. MD simulated vaporization enthalpies of the $[\text{NTf}_2]$ anion $\Delta_v H$ as a function of the alkyl chain-length n in $[C_n\text{MIm}][\text{NTf}_2]$ for the KPL and the new NGOLP force field as well as the experimental values by Verevkin *et al.*⁴⁷ at $T = 303$ K. See also Fig. 14.

n	$\Delta_v H \text{ (kJ mol}^{-1})$		
	KPL	NGOLP	Expt.
1	129.2	127.5	128.2
2	130.2	127.0	126.9
4	136.1	133.6	132.4
6	145.1	143.1	140.1
8	156.1	154.5	145.7

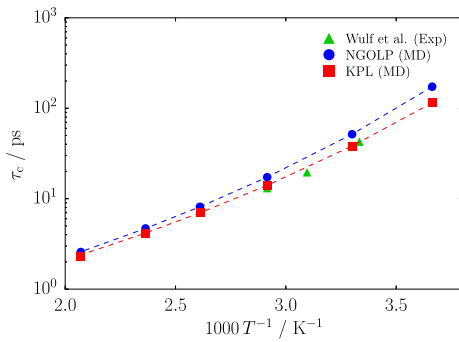


FIG. 15. Reorientational correlation time of the C(2)–H vector in $[\text{C}_2\text{MIm}][\text{NTf}_2]$ as a function of temperature. The experimental data of Wulf *et al.*⁵⁸ are shown as green triangles, the KPL-data are shown as red squares, and the NGOLP-data are shown as blue dots. The data are summarized in Table VII.

calculated. To compare with the quadrupolar relaxation experiments of Wulf *et al.*,⁵⁸ we computed reorientational correlation functions $R(t)$ of the C(2)–H bond-vector according to

$$R(t) = \langle P_2[\cos[\theta_{\text{CH}}(t)]] \rangle, \quad (7)$$

where P_2 is the second Legendre polynomial and

$$\cos[\theta_{\text{CH}}(t)] = \frac{\vec{r}_{\text{CH}}(0) \cdot \vec{r}_{\text{CH}}(t)}{|\vec{r}_{\text{CH}}|^2} \quad (8)$$

represents the angle-cosine between the CH-bond vector at times “0” and t and $|\vec{r}_{\text{CH}}|$ is the CH-bond length, which is kept fixed during the simulation. The reorientational correlation times τ_c are obtained as integral over the correlation function

$$\tau_c = \int_0^\infty R(t) dt. \quad (9)$$

Here, the long-time behavior is fitted to a stretched exponential function and the total correlation time is determined by numerical integration. Again we find that both force fields are in good agreement with the experimental values, albeit with the original KPL model being slightly closer to the experimental data (see Fig. 15 and Table VII).

To determine the viscosities, we used the approach of Zhang *et al.*⁵⁹ to compute viscosities from equilibrium-fluctuations of the off-diagonal elements of the pressure tensor via the Green-Kubo relation

TABLE VII. Viscosities η and reorientational correlation times of the C(2)–H vector τ_c as a function of temperature calculated from MD simulations of $[\text{C}_2\text{MIm}][\text{NTf}_2]$ employing the KPL and the NGOLP force fields. See also Figs. 15 and 16.

T/K	η (mPa s)		τ_c (ps)	
	KPL	NGOLP	KPL	NGOLP
273	67 ± 24	82 ± 22	173.1	114.7
303	26 ± 6	25 ± 4	51.6	38.2
343	8.6 ± 2.0	9.6 ± 2.4	17.3	14.1
383	4.4 ± 0.9	4.9 ± 0.9	8.1	7.0
423	2.9 ± 1.0	2.9 ± 0.6	4.7	4.1
483	1.6 ± 0.3	1.48 ± 0.21	2.6	2.3

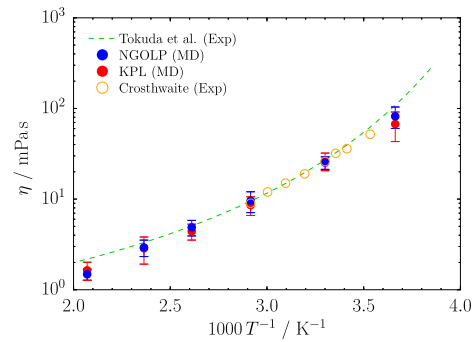


FIG. 16. Viscosities as a function of temperature for $[\text{C}_2\text{MIm}][\text{NTf}_2]$ for NGOLP (blue dots) and KPL (red squares). The experimental data were taken from the work of Tokuda *et al.* (green dashed line).³⁹ See also Table VII.

$$\eta = \frac{V}{k_B T} \int_0^\infty \langle P_{\alpha\beta}(0) \cdot P_{\alpha\beta}(t) \rangle dt. \quad (10)$$

For each temperature, we performed 15 independent NVT simulations, where the starting configurations were sampled from the earlier NpT simulations with a constant time interval of 2 ns. After a 1 ns equilibration, we computed 8 ns long production runs for each of the sampled configurations storing the pressure tensor data for each time step. Finally, the correlation function was calculated and integrated over a time-window of 1 ns for each of the 15 simulations. The average of the running integrals was calculated as well as standard deviation. The average over the running integrals as well as the standard deviation were handled as suggested by Zhang *et al.*⁵⁹ with a fitting cutoff t_{cut} at the point where $\sigma(t)$ is 40% of the calculated average viscosity.

We find that the differences between the KPL and NGOLP models to be rather small. Both are basically lying within the statistical errors of this method. However, both force field models yield viscosities very close to the experiment (Fig. 16 and Table VII).

CONCLUSIONS

We showed that the reparametrization of the dihedral potentials as well as charges of the $[\text{NTf}_2]$ anion leads to an improvement of the force field model of Köddermann *et al.* for imidazolium-based ionic liquids from 2007. The most prominent advantage of the new parameter set is that the minimum energy conformations (*trans* and *gauche*) of the anion, as demonstrated from *ab initio* calculations and Raman experiments, are now well reproduced.

The results obtained for $[\text{C}_n\text{MIm}][\text{NTf}_2]$ show that this correction leads to a slightly better agreement between experiment and molecular dynamics simulation for a variety of properties, such as densities, diffusion coefficients, vaporization enthalpies, reorientational correlation times, and viscosities. Even though we focused on optimizing the anion parameters, the alkyl chain-length dependence is found to be generally also closer to the experiment.

With this work, we want to point out that it is important to re-examine the established force field and, if necessary, to improve them. We highly recommend to use the new NGOLP force field for the $[\text{NTf}_2]$ anion instead of the original KPL force field. Especially for simulation aiming to

describe the thermodynamics, dynamics, and also structure of imidazolium-based ionic liquids.

ACKNOWLEDGMENTS

B.G. is thankful for financial support provided by COST Action CM 1206 (EXIL—Exchange on Ionic Liquids).

- ¹J. N. C. Lopes, J. Deschamps, and A. A. H. Pádua, *J. Phys. Chem. B* **108**, 2038 (2004).
- ²J. N. C. Lopes and A. A. H. Pádua, *J. Phys. Chem. B* **108**, 16893 (2004).
- ³J. N. A. C. Lopes and A. A. H. Pádua, *J. Phys. Chem. B* **110**, 7485 (2006).
- ⁴J. N. A. C. Lopes and A. A. H. Pádua, *J. Phys. Chem. B* **110**, 19586 (2006).
- ⁵J. N. A. C. Lopes, A. A. H. Pádua, and K. Shimizu, *J. Phys. Chem. B* **112**, 5039 (2008).
- ⁶J. N. A. C. Lopes, K. Shimizu, A. A. H. Pádua, Y. Umehayashi, S. Fukuda, K. Fujii, and S. I. Ishiguro, *J. Phys. Chem. B* **112**, 1465 (2008).
- ⁷J. N. A. C. Lopes, K. Shimizu, A. A. H. Pádua, Y. Umehayashi, S. Fukuda, K. Fujii, and S. I. Ishiguro, *J. Phys. Chem. B* **112**, 9449 (2008).
- ⁸T. Köddermann, K. Fumino, R. Ludwig, J. N. A. C. Lopes, and A. A. H. Pádua, *ChemPhysChem* **10**, 1181 (2009).
- ⁹K. Shimizu, D. Almantariotis, M. F. C. Gomes, A. A. H. Pádua, and J. N. A. C. Lopes, *J. Phys. Chem. B* **114**, 3592 (2010).
- ¹⁰J. N. A. C. Lopes and A. A. H. Pádua, *Theor. Chem. Acc.* **131**, 1129 (2012).
- ¹¹B. Guillot, *J. Mol. Liq.* **101**, 219 (2002).
- ¹²P. T. Kiss and A. Baranyai, *J. Chem. Phys.* **137**, 084506 (2012).
- ¹³J. F. Ouyang and R. P. Bettens, *CHIMIA Int. J. Chem.* **69**, 104 (2015).
- ¹⁴I. Shvab and R. J. Sadus, *Fluid Phase Equilib.* **407**, 7 (2015).
- ¹⁵G. A. Cisneros, K. T. Wikfeldt, L. Ojamäe, J. Lu, X. Xu, H. Torabifard, A. P. Bartok, G. Csanyi, V. Molinero, and F. Paesani, *Chem. Rev.* **116**, 7501 (2016).
- ¹⁶T. Köddermann, D. Paschek, and R. Ludwig, *ChemPhysChem* **8**, 2464 (2007).
- ¹⁷D. Kerlé, R. Ludwig, A. Geiger, and D. Paschek, *J. Phys. Chem. B* **113**, 12727 (2009).
- ¹⁸D. Kerlé, M. N. Jorabchi, R. Ludwig, S. Wohlrab, and D. Paschek, *Phys. Chem. Chem. Phys.* **19**, 1770 (2017).
- ¹⁹R. P. Daly, J. C. Araque, and C. J. Margulis, *J. Chem. Phys.* **147**, 061102 (2017).
- ²⁰R. Lynden-Bell and A. J. Stone, *J. Chem. Sci.* **129**, 883 (2017).
- ²¹M. M. Kazemi, M. Namboodiri, P. Donfack, A. Materny, D. Kerle, B. Rathke, and J. Kiefer, *Phys. Chem. Chem. Phys.* **19**, 15988 (2017).
- ²²K. Fujii, T. Fujimori, T. Takamuku, R. Kanzaki, Y. Umehayashi, and S. I. Ishiguro, *J. Phys. Chem. B* **110**, 8179 (2006).
- ²³M. J. Frisch, G. W. Trucks, H. B. Schlegel, G. E. Scuseria, M. A. Robb, J. R. Cheeseman, G. Scalmani, V. Barone, B. Mennucci, G. A. Petersson *et al.*, GAUSSIAN 09, Revision D.01, Gaussian, Inc., 2013.
- ²⁴U. C. Singh and P. A. Kollman, *J. Comput. Chem.* **5**, 129 (1984).
- ²⁵E. Lindahl, B. Hess, and D. van der Spoel, *J. Mol. Model.* **7**, 306 (2001).
- ²⁶H. J. C. Berendsen, D. van der Spoel, and R. van Drunen, *Comput. Phys. Commun.* **91**, 43 (1995).
- ²⁷B. Hess, C. Kutzer, D. van der Spoel, and E. Lindahl, *J. Chem. Theory Comput.* **4**, 435 (2008).
- ²⁸S. Pronk, S. Pall, R. Schulz, P. Larsson, P. Bjelkmar, R. Apostolov, M. R. Shirts, J. C. Smith, P. M. Kasson, D. van der Spoel *et al.*, *Bioinformatics* **29**, 845 (2013).
- ²⁹M. Abraham, B. Hess, D. van der Spoel, E. Lindahl, E. Apol, R. Apostolov, H. J. C. Berendsen, A. van Buuren, P. Bjelkmar, R. van Drunen *et al.*, GROMACS 5.0.6, 2015.
- ³⁰U. Essmann, L. Perera, M. L. Berkowitz, T. A. Darden, H. Lee, and L. G. Pedersen, *J. Chem. Phys.* **103**, 8577 (1995).
- ³¹B. Hess, H. Bekker, H. J. C. Berendsen, and J. G. E. M. Fraaije, *J. Comput. Chem.* **18**, 1463 (1997).
- ³²H. J. C. Berendsen, J. P. M. Postma, W. F. van Gunsteren, A. DiNola, and J. R. Haak, *J. Chem. Phys.* **81**, 3684 (1984).
- ³³S. Nosé, *Mol. Phys.* **52**, 255 (1984).
- ³⁴W. G. Hoover, *Phys. Rev. A* **31**, 1695 (1985).
- ³⁵M. Parrinello and A. Rahman, *J. Appl. Phys.* **52**, 7182 (1981).
- ³⁶S. Nosé and M. L. Klein, *Mol. Phys.* **50**, 1055 (1983).
- ³⁷K. Fumino, A. Wulf, and R. Ludwig, *Angew. Chem., Int. Ed.* **47**, 8731 (2008).
- ³⁸A. Wulf, K. Fumino, and R. Ludwig, *Angew. Chem., Int. Ed.* **49**, 449 (2010).
- ³⁹H. Tokuda, K. Hayamizu, K. Ishii, M. A. B. H. Susan, and M. Watanabe, *J. Phys. Chem. B* **109**, 6103 (2005).
- ⁴⁰D. H. Zaitsau, G. J. Kabo, A. A. Strechan, Y. U. Paulechka, A. Tschersich, S. P. Verevkin, and A. Heintz, *J. Phys. Chem. A* **110**, 7303 (2006).
- ⁴¹J. P. Armstrong, C. Hurst, R. G. Jones, P. Licence, K. R. J. Lovelock, C. J. Satterley, and I. J. Villar-Garcia, *Phys. Chem. Chem. Phys.* **9**, 982 (2007).
- ⁴²V. N. Emel'yanenko, S. P. Verevkin, and A. Heintz, *J. Am. Chem. Soc.* **129**, 3930 (2007).
- ⁴³L. M. N. B. F. Santos, J. N. C. Lopes, J. A. P. Coutinho, J. M. S. S. Esperanca, L. R. Gomes, I. M. Marrucho, and L. P. N. Rebelo, *J. Am. Chem. Soc.* **129**, 284 (2007).
- ⁴⁴H. Luo, G. A. Baker, and S. Dai, *J. Phys. Chem. B* **112**, 10077 (2008).
- ⁴⁵F. Heym, B. J. M. Etzold, C. Kern, and A. Jess, *Green Chem.* **13**, 1453 (2011).
- ⁴⁶M. A. A. Rocha, C. F. R. A. Lima, L. R. Gomes, B. Schröder, J. A. P. Coutinho, I. M. Marrucho, J. M. S. S. Esperanca, L. P. N. Rebelo, K. Shimizu, J. N. C. Lopes *et al.*, *J. Phys. Chem. B* **115**, 10919 (2011).
- ⁴⁷S. P. Verevkin, D. H. Zaitsau, V. N. Emel'yanenko, A. V. Yermalayeu, C. Schick, H. Liu, E. J. Maginn, S. Bulut, I. Krossing, and R. Kalb, *J. Phys. Chem. B* **117**, 6473 (2013).
- ⁴⁸B. Schröder and J. A. P. Coutinho, *Fluid Phase Equilib.* **370**, 24 (2014).
- ⁴⁹D. H. Zaitsau, V. Emel'yanenko, P. Stange, C. Schick, S. P. Verevkin, and R. Ludwig, *Angew. Chem., Int. Ed.* **55**, 11682 (2016).
- ⁵⁰S. P. Verevkin, D. H. Zaitsau, V. N. Emel'yanenko, and A. Heintz, *J. Phys. Chem. B* **115**, 12889 (2011).
- ⁵¹D. H. Zaitsau, K. Fumino, V. N. Emel'yanenko, A. V. Yermalayeu, R. Ludwig, and S. P. Verevkin, *ChemPhysChem* **13**, 1868 (2012).
- ⁵²S. P. Verevkin, R. V. Ralys, D. H. Zaitsau, V. N. Emel'yanenko, and C. Schick, *Thermochim. Acta* **538**, 55 (2012).
- ⁵³M. Ahrenberg, M. Brinckmann, J. W. P. Schmelzer, M. Beck, C. Schmidt, O. Kefler, U. Kragl, S. P. Verevkin, and C. Schick, *Phys. Chem. Chem. Phys.* **16**, 2971 (2014).
- ⁵⁴S. P. Verevkin, D. H. Zaitsau, V. N. Emel'yanenko, C. Schick, S. Jayaraman, and E. J. Maginn, *Chem. Commun.* **48**, 6915 (2012).
- ⁵⁵V. N. Emel'yanenko, G. Boeck, S. P. Verevkin, and R. Ludwig, *Chem. - Eur. J.* **20**, 11640 (2014).
- ⁵⁶K. Fumino, A. Wulf, S. Verevkin, A. Heintz, and R. Ludwig, *ChemPhysChem* **11**, 1623 (2010).
- ⁵⁷T. Köddermann, D. Paschek, and R. Ludwig, *ChemPhysChem* **9**, 549 (2008).
- ⁵⁸A. Wulf, R. Ludwig, P. Sasisanker, and H. Weingärtner, *Chem. Phys. Lett.* **439**, 323 (2007).
- ⁵⁹Y. Zhang, A. Otani, and E. J. Maginn, *J. Chem. Theory Comput.* **11**, 3537 (2015).

4.8 Publication VII

ForConX: A Forcefield Conversion Tool Based on XML

V. Lesch, D. Diddens, C. E. S. Bernardes, B. Golub, A. Dequidt, V. Zeindlhofer, M. Sega
and C. Schröder

J. Comp. Chem., 2017, **28**, 629-638

CRedit roles: Software (Gromacs part, equal), Writing - review & editing

Approximated contribution to the publication in percent: 20 %

Reprinted from V. Lesch, D. Diddens, C. E. S. Bernardes, B. Golub, A. Dequidt, V. Zeindlhofer, M. Sega and C. Schröder, *J. Comp. Chem.*, 2017, **148**, 193828/1-9, with the permission of John Wiley and Sons.

ForConX: A Forcefield Conversion Tool Based on XML

Volker Lesch,^[a] Diddo Diddens,^[a] Carlos E. S. Bernardes,^[b] Benjamin Golub,^[c]
Alain Dequidt,^[d] Veronika Zeindlhofer,^[e] Marcello Sega,^[e,f] and Christian Schröder^{*,[e]}

The force field conversion from one MD program to another one is exhausting and error-prone. Although single conversion tools from one MD program to another exist not every combination and both directions of conversion are available for the favorite MD programs AMBER, CHARMM, DL-POLY, GROMACS, and LAMMPS. We present here a general tool for the force field conversion on the basis of an XML document. The force field is converted to and from this XML structure facilitating the implementation of new MD programs for the conversion.

Furthermore, the XML structure is human readable and can be manipulated before continuing the conversion. We report, as testcases, the conversions of topologies for acetonitrile, dimethylformamide, and 1-ethyl-3-methylimidazolium trifluoromethanesulfonate comprising also Urey–Bradley and Ryckaert–Bellemans potentials. © 2017 Wiley Periodicals, Inc.

DOI: 10.1002/jcc.24708

Introduction

More than 40 years have passed since the pioneering work of Loup Verlet on Lennard–Jones fluids,^[1] and molecular dynamics (MD) simulations have become an irreplaceable tool in the investigation of the behavior of liquids at the atomic and molecular scale. During these decades, the scope of investigations performed via MD simulations has broadened to molecular liquids,^[2,3] proteins,^[4,5] lipid aggregates,^[6,7] synthetic polymers^[8,9] and polyelectrolytes and polymer electrolytes,^[10,11] nucleic acids^[12,13] and ionic liquids,^[14,15] to name but a few.

Since time scale and size of investigated systems is steadily increasing, many efforts have been made to optimize the MD program code to run simulations as fast as possible, exploiting parallel computing on different computer architectures. Not only simple trajectory production but also simulation techniques have been adapted, for example, nonequilibrium simulations,^[16] replica exchange,^[4] or free energy simulations,^[17] to answer particular questions. This development led to various MD simulation codes—the most prominent MD programs are AMBER,^[18] CHARMM,^[19] and GROMACS^[20]—that have several differences in the simulation tools and analysis techniques they put at disposal of the user. For a particular scientific problem, one of these programs, or another one not mentioned here, might be the best choice in terms of simulation speed, customization of the computational setup or simulation technique. Consequently, no MD program has gained an absolute monopoly.

The intermolecular and intramolecular interactions in most atomistic MD simulations (with the exception of deep-learning-based approaches^[21–23]) are calculated on a basis of a force field, that is, a collection of functional forms for the interaction potentials together with their parameters:

$$U(\{\vec{r}_i\}) = U_{\text{bonds}} + U_{\text{angles}} + U_{\text{dihedrals}} + U_{\text{impropers}} + U_{\text{vdWs}} + \sum_i \sum_{i < j} \frac{1}{4\pi\epsilon_0} \frac{q_i \cdot q_j}{|\vec{r}_{ij}|} \quad (1)$$

Intramolecular potentials are calculated from the position of atoms connected by bonds (U_{bonds}) or being involved in angles (U_{angles}), dihedral angles ($U_{\text{dihedrals}}$), or improper torsions ($U_{\text{impropers}}$), which usually describes the out-of-plane motions. Intermolecular potentials comprise van-der-Waals (U_{vdW}) and Coulomb interactions. In case of water, more than thirty models have been developed so far, without fully reaching the aim of reproducing all of its relevant static, dynamic and thermodynamic properties. Unfortunately both the functional forms of potentials as well as the file format for storing the parameters differ among MD programs. As a consequence, reproducing the results of a reported MD simulation is a tedious job at the moment.

[a] V. Lesch, D. Diddens

Westfälische Wilhelms-Universität Münster, Institut für physikalische Chemie, Corrensstraße 28/30, Münster 48149, Germany
E-mail: volkerlesch@uni-muenster.de, E-mail: christian.schroeder@univie.ac.at

[b] C. E. S. Bernardes

Centro de Química Estrutural, Instituto Superior Técnico, University Lisboa, Av. Rovisco Pais, Lisboa 1049-001, Portugal

[c] B. Golub

Institut für Chemie, Physikalische und Theoretische Chemie, Universität Rostock, Dr.-Lorenz-Weg 1, Rostock 18059, Germany

[d] A. Dequidt

Institut de Chimie de Clermont-Ferrand, CNRS UMR 6296, Université Blaise Pascal, Université Clermont Auvergne, Aubiere F-63178, France

[e] V. Zeindlhofer, M. Sega, C. Schröder

Faculty of Chemistry, Department of Computational Biological Chemistry, University of Vienna, Währingerstraße 19, Vienna 1090, Austria

[f] M. Sega

Faculty of Physics, University of Vienna, Boltzmanngasse 5, A-1090, Vienna, Austria

Contract grant sponsor: COST action; Contract grant number: CM1206; Contract grant sponsor: European Communitys Seventh Framework Programme (FP7-PEOPLE-2012-IEF; to M. S., C. S.); Contract grant number: 331932 SIDIS; Contract grant sponsor: SafeBatt project from BMBF; Contract grant number: 03X4631N; Contract grant sponsor: Fundação para a Ciência e a Tecnologia (FCT), Portugal (to C. B.); Contract grant number: SFRH/BPD/101505/2014

© 2017 Wiley Periodicals, Inc.

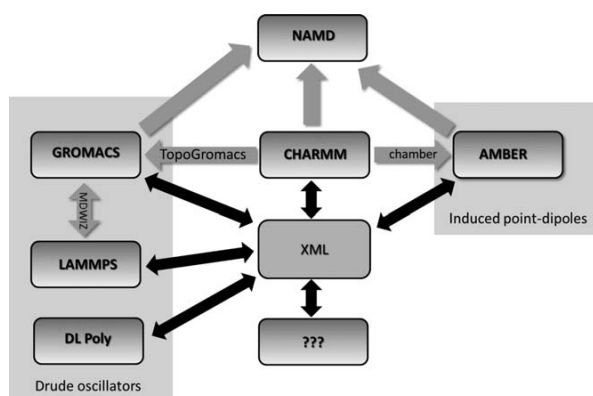


Figure 1. Current force field conversion tools exist between several pairs of MD programs and are often one directional. ForConX operates with an intermediate XML document. For each displayed MD program (as visible by the black arrows), it provides an `md2xml.py` to convert the force field file to the XML structure and a `xml2md.py` to write the force field files based on the XML structure. A complementary approach is used by NAMD which understands AMBER, CHARMM, and GROMACS force fields (gray arrows).

In this article, we present a novel tool “ForConX” for the conversion between several popular force field input formats. In essence, ForConX extracts the force field information from a particular MD program file and stores the information in a XML structure. This structure is used afterwards to convert the force field to the target MD program. This stepwise approach has several advantages: (1) The XML structure is human readable and can be edited manually. This way, the user is capable of intervening in the conversion by adding or removing interactions. (2) The conversion from or to new MD programs can be achieved by writing one interface of that MD program to the XML structure and not a plethora of routines for pairwise conversion of all already implemented MD programs to the new one.

The Conversion Tool

Manual conversion of force field parameters and topologies is tedious and error-prone, taking into account the amount of different available conventions, units and potentials in various MD programs. Furthermore, the large amount of defined potentials and tools for the automatic generation of angle and dihedral potentials—which may have additional generation rules—put one at risk to miss a particular potential or defining potentials twice.

Several conversion tools have been developed to reduce this burden, but they are mainly limited to uni-directional conversion between two MD packages: For example, Chamber^[24] converts CHARMM input including the force field parameters to AMBER input. Mdwiz^[25] converts force field files from GROMACS to LAMMPS and TopoGromacs from CHARMM to GROMACS.^[26] As visible in Figure 1 NAMD is able to use AMBER, CHARMM, and GROMACS force field files without any conversion and perform the molecular dynamics simulations. Unfortunately, not all force field features of the above mentioned programs are accessible in the current NAMD version 2.12b1. For example, the mixing rules of the GROMACS force field are disabled necessitating a rewriting of the force field file.

To overcome the limitations of uni-directional conversion we devised a FORce field CONVersion python tool using XML (ForConX) which is illustrated in Figure 1 and can be downloaded free of charge from our web page.^[27] The XML file also serves as log file since the information will be updated during the force field conversion. A ForConX run comprise three phases: in the first phase, the input force field is read, the second phase checks the sanity of the current XML structure and the last step is the conversion to the target force field file format. It is also possible to start from an XML structure (second phase) or to stop at an XML structure.

ForConX can also be used to format the force field file of a given MD program if the original and the target MD program coincide. This way, one may also change the van-der-Waals information from an atom-based description and mixing rules to a pairwise description where no mixing rules are needed anymore. This way, the drawback of the current NAMD version using the GROMACS force field can be overcome.

MD programs

The XML structure is decomposed into elements which are described separately in the next sections. The original and target MD program are defined in the element `<input>` and `<output>`, respectively and handled by the object `<mdElement>` of `input_outpy.py`.

```
<input md="XML">
  <energy unit="KCAL"/>
  <distance unit="ANGSTROM"/>
  <coordinates pdb="..." />
  <reference>
    <title>...</title>
    <author>...</author>
    ...
    <volume>...</volume>
    ...
    <pages>... </pages>
  </reference>
</input>

<output md="GROMACS">
  ...
  <energy unit="KJ"/>
  <distance unit="NM"/>
  ...
</output>
```

Consequently, there are two instances of `<mdElement>` as visible in Figure 2. Both instances read energy and distance units (which are defined for each MD program separately) and provide conversion factors. If these units are fixed in a MD program like in CHARMM, they are printed automatically, otherwise they are updated during the reading of the force field, for example, for DL-POLY.

In `<input>` one may also store the force field reference in a bibtext style. Although this information is not needed for the conversion process, it is still useful for sharing XML-based force field among several research groups.

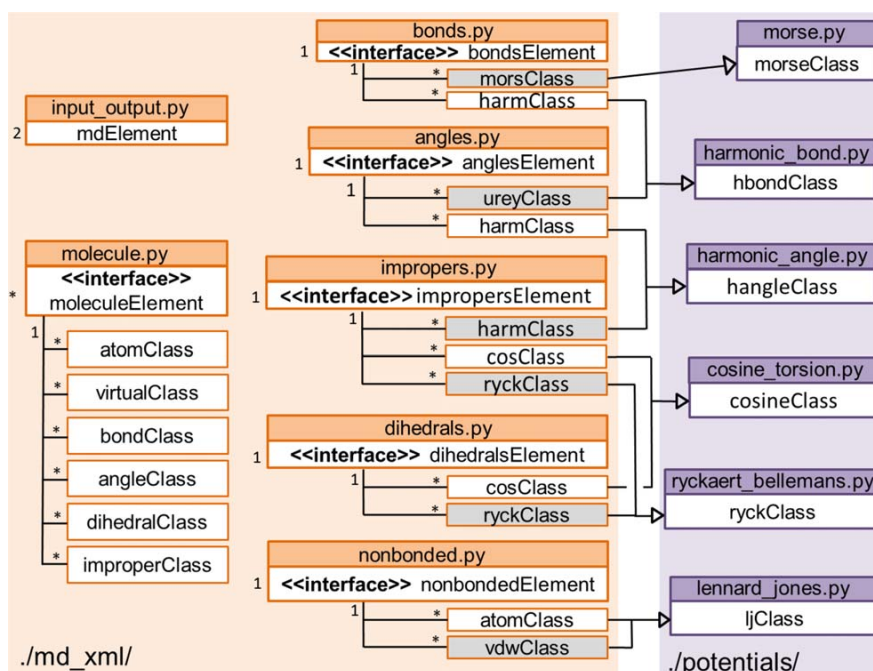


Figure 2. Overview of classes in ForConX: Inheritance is denoted by the arrows, lines show the association of classes. Here, the number denotes how many of a class interacts with the other, the asterisk stands for multiple instances. Python libraries in the orange area are stored in the relative directory ./md_xml/, whereas the parent classes of the potentials (violet area) are in ./potentials/. Classes in the orange area are used by the python scripts for the corresponding MD program to access the XML structure. [Color figure can be viewed at wileyonlinelibrary.com]

It is also possible to supply a coordinate file, which is mandatory for the conversion to LAMMPS as this program stores force field parameters in the very same file as the atomic positions. However, once defined, ForConX converts the MD program specific coordinate file to a file named `forconx.pdb`, which may result in a loss of accuracy when writing the coordinate file of the MD program defined in `<output>`.

During the development of ForConX the following version of the MD programs were used: AMBER 11, CHARMM c39a2, DL-POLY 4.07, GROMACS 5.0.7, and LAMMPS (February 3, 2016). In ForConX, to each MD program is associated a directory containing the `md2xml.py` and `xml2md.py` files, as well as some supporting libraries. However, all these python scripts use the objects defined in the ./md_xml and ./potentials directories, and represented schematically in Figure 2 for interfering with the XML document.

Force field

The force field information is divided into the topology and force field potentials describing bonds (`<bonds>`), angles (`<angles>`), dihedrals (`<dihedrals>`), impropers (`<impropers>`) and nonbonded (`<nonbonded>`) interactions for all molecules. As it is possible to convert the force-field and topology for various molecules at the same time, several instances of `<molecule>` are possible (denoted by the asterisk in Fig. 2). However, the force field sections for the bonds, angles, dihedrals, impropers, and nonbonded only occur once in the XML document and hence need only one

`<<interface>>` which gives access to all subelements of that section.

In the python modules (dark orange shaded areas in Fig. 2) the subelements are handled by objects. For example each harmonic angle in `<angles>` has its own object, that is, a `harmClass` object which inherits attributes and functions from its respective parent class `hangleClass` (violet area in Fig. 2). Please keep in mind that parent classes pass their functions on to various objects. The harmonic angle potential $k(\theta - \theta^0)^2$ may be used to describe the interaction between three atoms connected by two bonds or an improper torsion where θ is the angle between the plane defined by three atoms and a vector from the central atom to the atom moving out-of-plane.

Gray shaded classes denote “nonstandard” potentials, that is, not all MD programs have these functions and ForConX will try to convert them to standard potentials if possible and necessary. All class definition in the respective python modules are documented in an UML style.

Molecular topologies. Each molecular species is unambiguously defined by its name and may contain any number (denoted by an asterisk in Fig. 2) of atoms and virtual atoms also defined by their atom names which are stored in uppercase letters in the XML document. However, atoms may share an atom type, have the same mass or partial charge or polarizability alpha.

```
<molecule name="..." nmol="...">
<atom name="..." type="..."
mass="..."charge="..." alpha="..." />
```

```

...
<virtual name="..." type="..."
charge="..." zmatrix="..." r="..."
theta="..." phi="..." />
...
<bond name="..." />
...
<angle name="..." />
...
<dihedral name="..." />
...
<improper name="..." central="..." />
...
</molecule>
<molecule name="..." nmol="...">
<atom name="..." type="..."
mass="..." charge="..." alpha="..." />
<virtual name="..." type="..."
charge="..." zmatrix="..." r="..."
theta="..." phi="..." />
<bond name="..." />
...
<angle name="..." />
...
<dihedral name="..." />
...
<improper name="..." central="..." />
...
</molecule>

```

Some force fields make use of virtual atoms, for example, to introduce a charge center which is not located at the position of an atom. This is often done to model lone pairs of electrons, to separate the charge from the Lennard-Jones center of interaction, or to model rigid, linear molecules. As these virtual atoms have no mass, the resulting Coulombic forces on them cannot be translated into motion via Newton's equations. Therefore, the position of the virtual particle is fixed with respect to distinct atoms. For the position of the virtual particle ForConX uses a definition which is included in CHARMM, GROMACS, and LAMMPS and is based on the typical z-matrix known from quantum-mechanical calculations. The keyword *zmatrix* contains a sequence of atom names, *r*, *theta* and *phi* denote the distance of the virtual atom to the first atom in the *zmatrix*-sequence, the angle between the virtual atom and the first two atoms and the torsion defined by the virtual atom and the *zmatrix* sequence of atoms, respectively. This way, the position is uniquely defined and the virtual particle moves with its attached atoms, that is, it does not change the distance, angle and dihedral angle to the other atoms during the simulation. Unfortunately, the concept of virtual particles varies within MD programs, for example, DL-POLY has none. Therefore, the *zmatrix* offers the best opportunity to map the constraints described above on a common force field.

As visible in Figure 1, polarizable interactions based on atomic polarizabilities can be implemented by induced-point dipoles or Drude oscillators. The latter model is also called

"shell" or "charge-on-a-spring" model and models the induced dipole by a pair of particles. One is always located at the position of the polarizable atom whereas the second mobile Drude particle has the opposite charge and moves around responding to the local electric field. This corresponds to a physical picture of an induced dipole. In contrast, the induced-point dipole used in AMBER represents a mathematical dipole. On the one hand, this complicates the computation of interactions between the induced dipole and the atomic permanent charges but does not increase the number of particles. We already reported a comparison between the two models.^[28] For the sake of simplicity, no Thole functions are implemented in ForConX since only AMBER fully supports different functional forms. However, we noticed that 1-2, 1-3 exclusions as already used for Lennard-Jones and Coulomb interactions are sufficient to avoid the polarization catastrophe.^[29] Therefore, we use this alternative for the force field conversion instead of Thole functions.

The keywords *bond*, *angle*, *dihedral*, and *improper* are names. Here, the name is a string of corresponding atom names separated by one space and sorted alphabetically keeping the sequence of involved bonds. In other words, the sequence of atom names for bonds, angles and dihedrals is read forward or backward depending on the atom names of the first and last involved atom. However, since the sequence of atoms in an improper torsion differs in the MD programs, ForConX additionally stores the name of the central atom and does not perform the sorting of atom names.

The potentials present in *<molecule>* only describe the existence of a particular bond, angle, dihedral or improper within a distinct molecule but the actual functional form and the force field parameter are stored in *<bonds>*, *<angles>*, *<dihedrals>*, and *<impropers>*, as described in the next section. The interface object molecule Element in Figure 2 has functions to auto-generate angles, dihedrals and impropers based on the information of all molecular bonds. The interface to the classes depicted in Figure 2 is realized via functions to list all members of a particular class or to find a distinct one.

Intramolecular potentials. Of course, the conversion of a force field from one MD program to another is limited, that is, it is impossible to have 100% conversion accuracy, due to several reasons: natural constants are defined (within the MD codes) with different accuracy, potential parameters, and coordinates are stored in different precision and most importantly, functional forms of some interaction potentials are not available in all MD programs.

The current version of ForConX supports several functional forms for intramolecular potentials, which can be deduced from the following example XML code:

```

<bonds>
<harm type="..." k="..." r0="..." />
<mors type="..." D0="..." beta="..." r0="..." />
...
</bonds>
<angles>

```



```

<harm type="....." k="..." theta0="..."/>
<urey type="....." k="..." r0="..."/>
...
</angles>
<dihedrals>
<cos type="....."k="....." n="....."
delta="....."/>
<ryck type="....."c="....."/>
...
</dihedrals>
<impropers>
<cos type="....."k="....." n="....."
delta="....."/>
<harm type="....." k="..." theta0="..."/>
...
</impropers>

```

A particular bond potential U_{bonds} can be defined as harmonic bonds or Morse potentials (but not both):

$$U_{\text{bonds}} = \sum_{\xi} k_{\xi} (r - r_{\xi}^0)^2 + \sum_{\xi} D_{\xi}^0 (1 - e^{-\beta_{\xi}(r - r_{\xi}^0)})^2 \quad (2)$$

The factor of 1/2 used in the definition of an harmonic bond by some MD programs is automatically multiplied to the force constant k_{ξ} in the XML structure. ForConX also converts Morse potentials to harmonic bonds, that is, $k_{\xi} = D_{\xi}^0 \beta_{\xi}^2$, if the former potential is not available in that MD program. The harmonic bond potential is a Taylor series of the Morse potential at r_{ξ}^0 and only valid in the close proximity of the equilibrium distance as visible in Figure 3.

If a bond between two atoms is defined without a harmonic bond constant k_{ξ} , it is assumed that the interatomic distance should be constrained (this should be defined in the corresponding input script of the target MD program). However, a default value of 750 kcal/mol/Å² is stored in this case in the force field files of AMBER and CHARMM.

Angle potentials U_{angles} are harmonic angles and/or Urey–Bradley potentials:

$$U_{\text{angles}} = \sum_{\xi} k_{\xi} (\theta - \theta_{\xi}^0)^2 + K_{\xi} [r_{jk}(\theta) - r_{jk}^0]^2 \quad (3)$$

Urey–Bradley interactions are harmonic bonds between the first j and third atom k of an angle potential with a current distance $r_{jk}(\theta)$ and a fixed equilibrium value r_{jk}^0 which may be slightly shifted from $r_{jk}(\theta_{\xi}^0)$. Within all XML-potentials, the type is unique except for harmonic angles and Urey–Bradley's definition in <angles> which may share a type since sometimes they are used together for the very same angle, for example, for the angle of a terminal amid C=C=N in par_al-l36_cgenff.prm of the standard CHARMM force field. The harmonic force constant $k_{\xi} = 50$ kcal/mol/rad² and equilibrium angle $\theta_{\xi}^0 = 116.5^{\circ}$ is accompanied by a Urey–Bradley force constant of

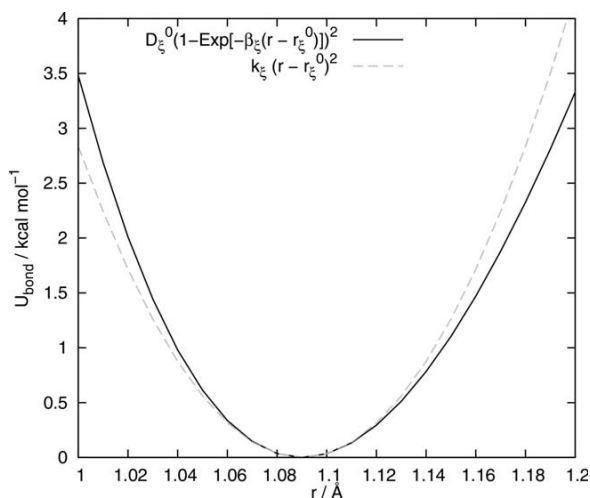


Figure 3. Morse potential of an aliphatic C–H bond in DREIDING force field^[30] (solid line) compared to the harmonic bond potential (dashed line) converted by ForConX.

$K_{\xi} = 50$ kcal/mol/Å² and an “equilibrium distance” of $r_{jk}^0 = 2.45$ Å which is 0.03 Å larger than $r_{jk}(\theta_{\xi}^0)$. This merged potential is depicted in Figure 4 as solid line. However, if Urey–Bradley potentials are not available in target MD program, one may add an harmonic angle potential with a force constant of Δk_{ξ}

$$\Delta k_{\xi} = \frac{r_{ij}^2 r_{ik}^2}{r_{jk}^2} \sin^2 [\theta(r_{jk}^0)] K_{\xi} \quad (4)$$

and a new equilibrium angle $\theta(r_{jk}^0)$ to the existing harmonic angle potential $k_{\xi}(\theta - \theta_{\xi}^0)^2$ which is shown as gray dashed line in Figure 4. However, if the MD program does not allow for two different harmonic angle potentials for the very same atoms, ForConX will use a single harmonic potential with a combined force constant of $k_{\xi} + \Delta k_{\xi}$ with a force constant weighted equilibrium angle of θ_{ξ}^0 and $\theta(r_{jk}^0)$ as shown by the dotted line in Figure 4. This potential is shifted since the Urey–Bradley contribution increases the potential if $\theta(r_{jk}^0)$ does not coincide with θ_{ξ}^0 . However, the discrepancy of both converted potentials (dashed and dotted lines in Fig. 4) from the original potential (solid line) is hardly discernible if meaningful r_{jk}^0 are used, that is, $\theta(r_{jk}^0) \simeq \theta_{\xi}^0$ or in other words, the overall potential has only small anharmonic character which suffices to reproduce the great majority of quantum-mechanical scans of angle potentials.

The quite uncommon angular harmonic cosine potentials

$$U_{\text{hcos}} = k_{\text{hcos}} (\cos \theta - \cos \theta^0)^2 \quad (5)$$

are not stored in the XML-structure since they are not available in all MD programs and can be converted to an harmonic angle potentials with $k_{\xi} = k_{\text{hcos}} (\sin \theta^0)^2$ for most purposes.^[31] The DREIDING potential for an angle H–C–H of a methyl group^[30] with a force constant of $k_{\text{hcos}} = 56.2$ kcal/mol/rad² is shown in Figure 5 as solid line. Its harmonic angle analogue (gray dashed line) starts to differ from the original potential for $\Delta \theta > 5^{\circ}$.

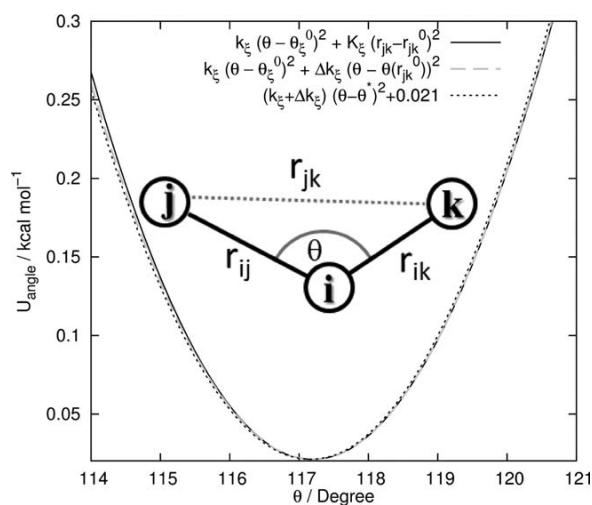


Figure 4. Conversion of an harmonic angle plus Urey-Bradley term (solid line) into two harmonic angle potentials with slightly different equilibrium angles θ_{ij}^0 and $\theta(r_{jk}^0)$ (gray dashed line) or a modified harmonic angle potential (dotted line) according to eq. (4). The angle θ^* is the force constant weighted average of θ_{ij}^0 and $\theta(r_{jk}^0)$.

Dihedral potentials $U_{\text{dihedrals}}$ are either cosine torsion or Ryckaert-Bellemans potentials (but not both):

$$U_{\text{dihedrals}} = \sum_{\xi}^{\text{dihedrals}} k_{\xi} [1 + \cos(n_{\xi} \phi - \delta_{\xi})] + \sum_{\xi}^{\text{dihedrals}} \sum_{\lambda=0}^5 c_{\xi\lambda} \cos^{\lambda}(\phi) \quad (6)$$

The latter potential is quite common in DL-POLY and GROMACS. Table 1 gives an overview on dihedral potentials used in the MD program under consideration here. The alternating sign in cos3 of DL-POLY can be mapped on the classical dihedral potential with a phase shift of $\delta_2 = \delta_4 = \delta_6 = 180^\circ$.

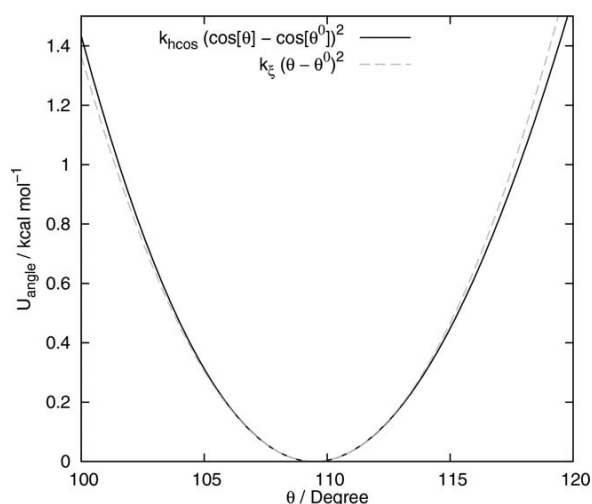


Figure 5. DREIDING potential of H-C-H of a methyl group (solid line) and its conversion to the common harmonic angle potential (dashed line).

Table 1. Dihedral potentials in various MD programs.

MD program	Dihedral potential
Amber	$\frac{1}{2} k [1 + \cos(n\phi - \delta)]$
Charmm	$k [1 + \cos(n\phi - \delta)]$
DL-Poly	$\frac{1}{2} \sum_{\lambda=1}^3 k_{\lambda} [1 - (-1)^{\lambda} \cos(\lambda\phi)]$
	$\sum_{\lambda=0}^5 c_{\lambda} \cos^{\lambda}(\phi)$
Gromacs	$k [1 + \cos(n\phi - \delta)]$
	$\sum_{\lambda=0}^5 c_{\lambda} \cos^{\lambda}(\phi)$
Lammps	$\frac{1}{2} \sum_{\lambda=1}^4 k_{\lambda} [1 - (-1)^{\lambda} \cos(\lambda\phi)]$
	$\sum_{\lambda=1}^5 k_{\lambda} \cos^{\lambda-1} \phi$
	$k [1 \pm \cos(n\phi)]$
	$k [1 + \cos(n\phi - \delta)]$

Ryckaert-Bellemans potentials can be converted to cosine torsion potential using the force constants displayed in Table 2 (all phase shifts δ_n equal 180°) and is performed by a function of the `ryckClass` of `dihedrals.py`. Please note, that depending on the Ryckaert-Bellemans parameters, there may be a constant shift of the potential as visible in Figure 6. However, this shift only affects the absolute energy of the torsion. All forces on the atoms are not changed. ForConX stores Ryckaert-Bellemans potentials in the XML structure, but they are immediately converted to cosine torsion in output force field files, if the corresponding MD program has no Ryckaert-Bellemans potentials like AMBER or CHARMM. For the sake of completeness, the conversion from a cosine torsion to a Ryckaert-Bellemans is also given in Table 2.

Improper torsion potentials $U_{\text{impropers}}$ are either cosine torsion potentials, Ryckaert-Bellemans or harmonic angle potentials which are mutually exclusive:

$$U_{\text{impropers}} = \sum_{\xi}^{\text{impropers}} k_{\xi} [1 + \cos(n_{\xi} \phi - \delta_{\xi})] + \sum_{\xi}^{\text{impropers}} \sum_{n=0}^5 c_{\xi n} \cos^n(\phi) + \sum_{\xi}^{\text{impropers}} k_{\xi} (\theta - \theta_{\xi}^0)^2 \quad (7)$$

Unfortunately, as one can notice from Table 3, not only the functional forms but also the sequence of atoms are defined in a different manner in the MD programs. Therefore, ForConX stores the central atom of an improper torsion in the corresponding improper sub element of `<molecule>`. Furthermore, the first atom type in the `<impropers/cos>` or `<impropers/harm>` is the central atom of the improper. However, the angle between the plane *i-j-k* and the vector *i-l* differ from that of the plane *i-j-k* and the angle from $(k+j)/2 - l$ as visible in Fig. 7. This results in two different energies

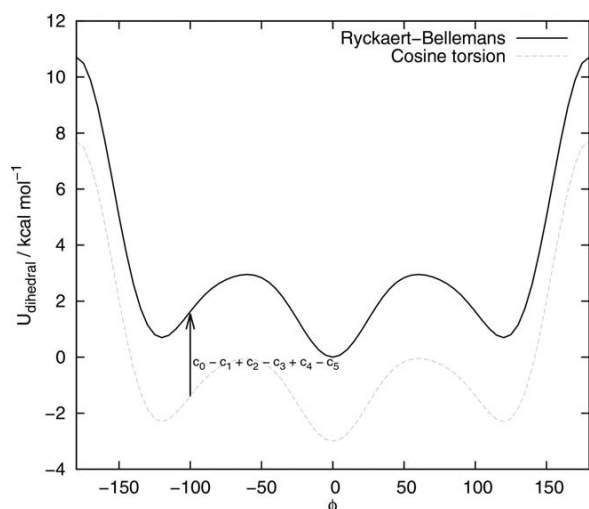


Figure 6. Dihedral torsion potential of alkanes^[32] parametrized by a Ryckaert-Bellemans potential (solid) and its conversion to a cosine torsion potential (dashed line). The potential shift only affects the energy but not the forces on the atoms.

for an improper torsion. Fortunately, both angles are quite small and consequently the energy difference since this potential is used for almost flat geometries.

If a force field contains a functional form that is not part of the potentials discussed here, ForConX will explicitly warn the user and omit the corresponding potential and continue the conversion. The user may manipulate manually the so-obtained XML file in order to achieve an agreement with the former force field as close as possible by mapping the unknown potential on a potential displayed in the violet of Figure 2 and restart the conversion.

Intermolecular potentials. The partial charges of the atoms were already defined in the atom-entries of `<molecule>`, thus only the van-der-Waals interactions U_{vdW} are parametrized in `<nonbonded>`. Due to limitations of some of our MD programs only standard Lennard-Jones potentials

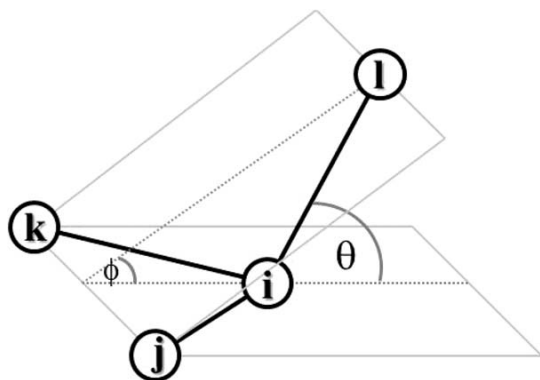


Figure 7. The improper angle θ (harmonic angle potential) and the dihedral angle ϕ for an improper torsion (defined by a dihedral torsion).

Table 2. Conversion from Ryckaert-Bellemans $\sum c_n \cos^n(\phi)$ to cosine torsion potentials $\sum k_n (1 + \cos(n\phi - \pi)) = \sum k_n (1 - \cos(n\phi))$ and vice versa.

n	k_n	c_n
0		$-k_1 + 2k_2 - k_3 - k_5$
1	$c_1 + \frac{3}{4}c_3 + \frac{5}{8}c_5$	$k_1 - 3k_3 + 5k_5$
2	$\frac{1}{2}(c_2 + c_4)$	$-2k_2 + 8k_4$
3	$\frac{1}{4}c_3 + \frac{5}{16}c_5$	$4k_3 - 20k_5$
4	$\frac{1}{8}c_4$	$-8k_4$
5	$\frac{1}{16}c_5$	$16k_5$

$$U_{vdWs} = \sum_{\xi} \sum_{\xi < \lambda} 4\epsilon_{\xi\lambda} \left[\left(\frac{\sigma_{\xi\lambda}}{r_{\xi\lambda}} \right)^{12} - \left(\frac{\sigma_{\xi\lambda}}{r_{\xi\lambda}} \right)^6 \right] \quad (8)$$

are available in the current version of our program, although this excludes many coarse-grained force fields from conversion^[33] using different exponents in eq. (8) or Buckingham potentials.

```
<nonbonded>
<mixing      rules      epsilon="geometric"
sigma="arithmetic"/>
<atom        type="..."      epsilon="..."
sigma="..."elec14="..." vdw14="...">
<vdw         type="..."      epsilon="..."
sigma="..."elec14="..." vdw14="...">
...
</nonbonded>
```

The mixing rules are identified by the `geometric` and `arithmetic` tags, which denote the method of averaging and affects only `<atom>` when computing the pairwise Lennard-Jones interactions. The keyword `<vdw>` already denotes a Lennard-Jones pair and hence the mixing rule is obsolete for them. In principle, the mixing rules can be varied for $\epsilon_{\xi\lambda}$ and $\sigma_{\xi\lambda}$ separately, however, Lorentz-Berthelot mixing rules as shown in the XML code fragment above are recommended.

Table 3. Improper torsions and atom ordering.

MD program	Potential	Atom ordering
Amber	$\frac{k}{2} [1 + \cos(n\phi - \delta)]$	j-k-i-l
Charmm	$k [1 + \cos(n\phi - \delta)]$	i-j-k-l
DL-Poly	$k(\theta - \theta^0)^2$	j-i-k-l
	$k(\theta - \theta^0)^2$	
Gromacs	$\frac{1}{2} k (\cos \theta - \cos \theta^0)^2$	i-j-k-l
	$\frac{1}{2} k (\theta - \theta^0)^2$	
Lammps	$\frac{1}{2} k [1 + \cos(n\phi - \delta)]$	i-j-k-l
	$\sum_{\lambda=0}^5 c_{\lambda} \cos^{\lambda}(\phi)$	
	$k [1 \pm \cos(n\phi)]$	
	$k(\theta - \theta^0)^2$	

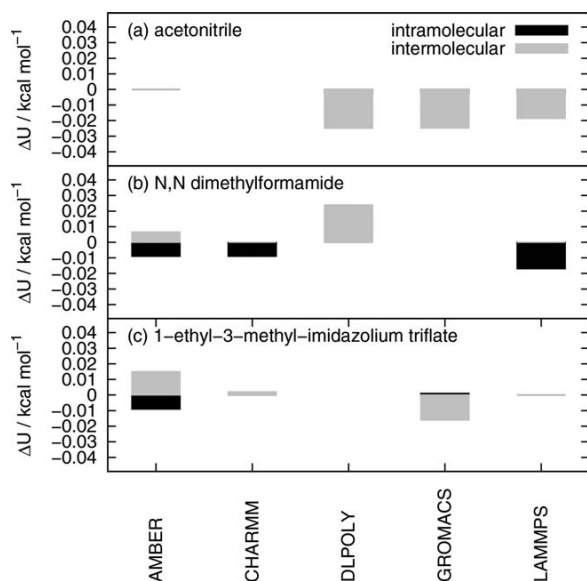


Figure 8. Energy discrepancies after the conversion of (a) acetonitrile from CHARMM par_all36_cgenff.prm, (b) *N,N*-dimethylformamide from GROMACS OPLS force field, and (c) 1-ethyl-3-methylimidazolium triflate from DL-POLY.

Another major source of energy discrepancies between different MD programs arises from the particular treatment of nonbonded interactions in case of atoms connected by a dihedral angle. 1-4 interactions are defined in several ways: AMBER and DL-POLY and GROMACS store this information in the topology, either where they define the dihedral angles or in a separate part of the topology, whereas CHARMM has a particular non-bonded section in the force field. However, DL-POLY, GROMACS, and CHARMM allow for values σ_{14} and ϵ_{14} of the Lennard-Jones 1-4 interaction, which may be completely different (not just rescaled) to the σ and ϵ between the very same atom types. AMBER restricts the 1-4 Lennard-Jones interaction to a scaling factor applied to ϵ , that is, $\sigma_{14} = \sigma$ and $\epsilon_{14} = \text{SCNB} \cdot \epsilon$.

In order to be flexible, the scaling factor for Coulomb (elec14) and Lennard-Jones (vdw14) interactions can be defined for each <atom> and <vdw> separately. However, <vdw> only affects the scaling of the $\epsilon_{\xi\lambda}$ but not $\sigma_{\xi\lambda}$ for an atom pair $\xi\lambda$ connected via a dihedral angle.

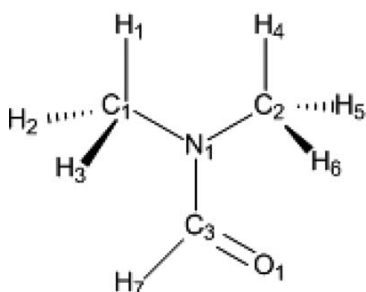


Figure 9. Atom numbering in *N,N*-dimethylformamide. Since unique atom names are mandatory for each atom in a particular <molecule>, the object moleculeElement (see Fig. 2) assigns a number to the chemical elements (or uses an additional letter).

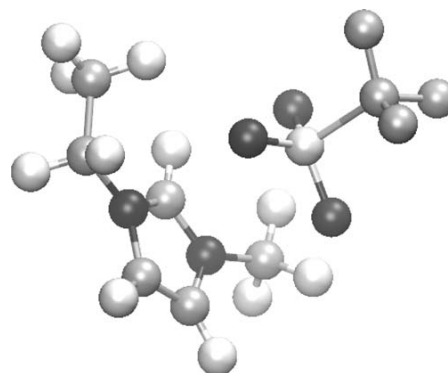


Figure 10. 1-ethyl-3-methyl-imidazolium trifluoromethanesulfonate [C₂mim][OTf].

Testing the Conversion

Since the most common protein force fields are available online in each MD force field format, for example for CHARMM^[34] and GROMACS^[35] including the torsional CMAP potentials, we focus on the conversion of solvent force fields in the present work. AMBER, CHARMM, and GROMACS force field files can be used in NAMD by using a Xplor-structure file (which may be gained from CHARMM or using genPSF.pl^[36]) and the .frcmod (AMBER), .top (GROMACS) or .prm (CHARMM) file. For the analysis of the trajectory data, MD analysis^[37] is capable of reading all trajectory formats of the MD programs used here.

All testcases described in the present work can be downloaded from the ForConX web site.^[27]

General Charmm force field

Our testcase from the general CHARMM force field par_all136_cgenff.prm is acetonitrile since all angles and dihedrals are not defined explicitly in the topology file but have to be generated automatically. Furthermore, the dihedral autogeneration in CHARMM takes into account the internal coordinate information. Since acetonitrile possess a linear angle, the corresponding dihedral torsion is problematic as the dihedral angle is computed by the angle between the vectors perpendicular to the involved two planes. Consequently, CHARMM skips that dihedral angle in the dihedral autogeneration process. ForConX will generate the dihedral since it is needed for 1-4 interactions in other MD programs but will set the force constant to zero. Additionally, the angle H—C—H is parametrized with an harmonic angle and an Urey-Bradley term making this molecule a perfect testcase for the conversion.

In Figure 8a the energy discrepancies of a single acetonitrile after the conversion to the other MD programs is displayed, decomposed into intramolecular and intermolecular errors. All these values are with respect to the computation in CHARMM using nonperiodic boundary conditions and an artificial cut-off radius $r_{\text{cut}} = 100 \text{ \AA}$. Overall, these errors are quite small taking into account that in AMBER and GROMACS the H—C—H Urey-Bradley potential was converted to an harmonic angle. The intermolecular energy discrepancies stem from the Coulomb

energy and may be (at least partially) due to the various pre-factors f_{elec} in

$$U_{\text{elec}}^{\xi\lambda} = f_{\text{elec}} \frac{q_{\xi}/e \cdot q_{\lambda}/e}{r_{\xi\lambda}/\text{\AA}} \quad (9)$$

which are 332.0777, 332.0716, 332.0641, 332.0636, and 332.0637 in AMBER, CHARMM, DL-POLY, GROMACS, and LAMMPS, respectively.

OPLS force field

The second testcase concerns *N,N*-dimethylformamide parametrized using the OPLS force field in GROMACS. Here, all dihedral angles are parametrized with Ryckaert–Bellemans potentials [cf. eq. (6)]. ForConX is able to detect the particular force field file format for OPLS in GROMACS which differs from the usual definitions of atom types.

The conversion of *N,N*-dimethylformamide (see Fig. 9 for labeling of the atoms) will stop in the second phase of ForConX where the sanity of the XML structure is checked noticing

```
<dihedral name="H7 N1 C3 O1" has no bond  
between H7 and N1!>
```

GROMACS does not discriminate between dihedral and improper torsions in the force field but for the conversion to the other MD programs a proper decomposition is mandatory. The XML sanity check of ForConX comprises that subsequent atoms in a dihedral angle have to be connected by a bond. Since the “dihedral” displayed above is not a dihedral but an improper, the user may modify the current XML document changing the dihedral to an improper and moving the corresponding force field parameters from the dihedrals to the improper section and rerun ForConX starting from the XML structure. This demonstrates the power of ForConX since the user is able to intervene in the conversion process.

As visible in Figure 8b the conversion from GROMACS only results in small energy deviations. The intramolecular energy differences do not stem from the Ryckaert–Bellemans potentials (as the respective parameter yield a zero shift in all dihedrals of dimethylformamide), but comes from the bond potentials which may be due to the high force constant value in $\text{kJ mol}^{-1} \text{ nm}^2$.

Ionic liquids

Ionic liquids are liquid salts at room temperature and gained interest to replace conventional organic solvents because of their low vapor pressure, low flammability and large temperature range of the liquid phase. The most common nonpolarizable ionic liquid force field of Canongia Lopes and Pádua^[38,39] was developed in DL-POLY. One ion pair of the ionic liquid 1-ethyl-3-methyl-imidazolium triflate (see Fig. 10 for the configuration) show the strongest intermolecular interactions of our testcases, in particular with respect to the electrostatic interactions. However, the energy deviations are small after the conversion to the other MD programs as visible in Figure 8c.

Conclusion

ForConX facilitates the force field conversion between MD programs, although 100% accuracy is not possible. However, uncommon potentials can be converted to the standard set of potentials without introducing large inaccuracies. The central XML structure produced during the conversion process is human readable and may be used as force field data base. The user is allowed then to modify the information and continue the conversion process.

ForConX provides object-oriented python code to handle various MD force field file formats which may be easily extended to additional MD program by writing an interface to the XML document. This way the conversion to all other MD program is realized at once without the need to write pairwise conversion tools.

Acknowledgments

The idea of this program emerged during the COST action CM1206 “Exchange on ionic liquids”. During the short term missions of V. Lesch, B. Golub, and C. Schröder the need for a force field conversion tool became obvious as each group used a different MD program. Consequently, the ForConX was augmented by each visiting student.

Keywords: force field · MD · force field conversion · XML

How to cite this article: V. Lesch, D. Diddens, C.E.S. Bernardes, B. Golub, A. Dequidt, V. Zeindlhofer, M. Sega, C. Schröder. *J. Comput. Chem.* **2017**, 38, 629–638. DOI: 10.1002/jcc.24708

- [1] D. Levesque, L. Verlet, *Phys. Rev. A* **1970**, 2, 2514.
- [2] M. P. Allen, D. Tildesley, *Computer Simulation of Liquids*; Oxford Science Publ (Clarendon Press), Oxford, **1989**.
- [3] D. Rapaport, *The Art of Molecular Dynamics Simulation*; Cambridge University Press, Bar-Ilan University, Israel, **2004**.
- [4] Y. Sugita, Y. Okamoto, *Chem. Phys. Lett.* **1999**, 314, 141.
- [5] D. H. de Jong, G. Singh, W. D. Bennett, C. Amarez, T. A. Wassenaar, L. V. Schafer, X. Periole, D. P. Tieleman, S. J. Marrink, *J. Chem. Theory Comput.* **2012**, 9, 687.
- [6] D. Tieleman, D. van der Spoel, H. Berendsen, *J. Phys. Chem. B* **2000**, 104, 6380.
- [7] D. Hakobyan, A. Heuer, *J. Phys. Chem. B* **2013**, 117, 3841.
- [8] K. Kremer, G. S. Grest, *J. Chem. Phys.* **1990**, 92, 5057.
- [9] S. Yang, S. Yu, W. Kyoung, D. S. Han, M. Cho, *Polymer* **2012**, 53, 623.
- [10] U. Micka, C. Holm, K. Kremer, *Langmuir* **1999**, 15, 4033.
- [11] D. Diddens, A. Heuer, *ACS Macro Lett.* **2013**, 2, 322.
- [12] W. D. Cornell, P. Cieplak, C. I. Bayly, I. R. Gould, K. M. Merz, D. M. Ferguson, D. C. Spellmeyer, T. Fox, J. W. Caldwell, P. A. Kollman, *J. Am. Chem. Soc.* **1995**, 117, 5179.
- [13] T. E. Cheatham, M. A. Young, *Biopolymers* **2000**, 56, 232.
- [14] T. Yan, C. J. Burnham, M. G. Del Pópolo, G. A. Voth, *J. Phys. Chem. B* **2004**, 108, 11877.
- [15] O. Borodin, *J. Phys. Chem. B* **2009**, 113, 12353.
- [16] O. Borodin, G. D. Smith, H. Kim, *J. Phys. Chem. B* **2009**, 113, 4771.
- [17] A. Laio, F. L. Gervasio, *Rep. Prog. Phys.* **2008**, 71, 126601.
- [18] Amber11. Available at: <http://www.ambermd.org>
- [19] Charmm: Chemistry at harvard macromolecular mechanics. Available at: <http://www.charmm.org/>
- [20] M. J. Abraham, T. Murtola, R. Schulz, S. Páll, J. C. Smith, B. Hess, E. Lindahl, *SoftwareX* **2015**, 1, 19.

- [21] J. Behler, M. Parrinello, *Phys. Rev. Lett.* **2007**, 98, 146401.
- [22] P. Geiger, C. Dellago, *J. Chem. Phys.* **2013**, 139, 164105.
- [23] T. Morawietz, A. Singraber, C. Dellago, J. Behler, *Proc. Natl. Acad. Sci. USA* **2016**, 113, 8368.
- [24] M. F. Crowley, M. J. Williamson, R. C. Walker, *Int. J. Quantum Chem.* **2009**, 109, 3767.
- [25] V. H. Rusu, V. A. C. Horta, B. A. C. Horta, R. D. Lins, R. Baron, *J. Mol. Graph. Model.* **2014**, 48, 80.
- [26] J. V. Vermaas, D. J. Hardy, J. E. Stone, E. Tajkhorshid, A. Kohlmeier, *J. Chem. Inf. Model.* **2016**, 56, 1112.
- [27] Force field conversion tool based on xml. Available at: <https://www.mdy.univie.ac.at/forconx/forconx.html>
- [28] M. Schmollngruber, V. Lesch, C. Schröder, A. Heuer, O. Steinhauser, *Phys. Chem. Chem. Phys.* **2015**, 17, 14297.
- [29] T. Taylor, M. Schmollngruber, C. Schröder, O. Steinhauser, *J. Chem. Phys.* **2013**, 138, 204119.
- [30] S. L. Mayo, B. D. Olafson, W. A. Goddard, III, *J. Phys. Chem.* **1990**, 94, 8897.
- [31] T. C. Lim, *J. Math. Chem.* **2002**, 32, 249.
- [32] J. P. Ryckaert, A. Bellemans, *Faraday Discuss. Chem. Soc.* **1978**, 66, 95.
- [33] D. H. de Jong, Ph.D. Thesis, University of Groningen, **2013**.
- [34] Charmm force field files. Available at: http://mackerell.umaryland.edu/charmm_ff.shtml
- [35] Gromacs force field files. Available at: http://www.gromacs.org/Downloads/User_contributions/Force_fields
- [36] Generating xplor psf from a pdb file. Available at: <http://blue11.bch.msu.edu/mmts/genPSF.pl>
- [37] N. Michaud-Agrawal, E. J. Denning, T. B. Woolf, O. Beckstein, *J. Comput. Chem.* **2011**, 32, 2319.
- [38] J. N. Canongia Lopes, J. Deschamps, A. A. H. Pádua, *J. Phys. Chem. B* **2004**, 108, 2038.
- [39] J. N. Canongia Lopes, A. A. H. Pádua, *J. Phys. Chem. B* **2004**, 108, 16893.

Received: 22 August 2016
Revised: 28 November 2016
Accepted: 30 November 2016
Published online in Wiley Online Library